

Master's Thesis

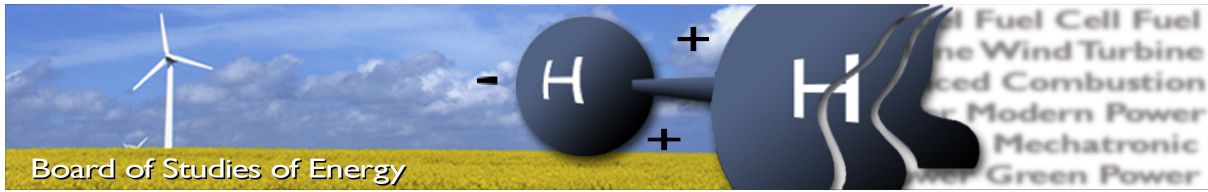
1st of February - 31st of May 2012

ADAPTIVE BACKSTEPPING CONTROL OF ASYMMETRIC ELECTRO-HYDRAULIC ACTUATOR SYSTEM



Thomas Schmidt

Mechatronic Control Engineering
under Study Board of Energy Technology



Title: Adaptive Backstepping Control of Asymmetric Electro-Hydraulic System
Semester: 10
Semester theme: Master's Thesis
Project period: 01.02.2012 to 31.05.2012
ECTS: 30
Supervisor: Torben O. Andersen & Lasse Schmidt
Project group: MCE4 - 1023

SYNOPSIS:

The objective of the project is to develop and evaluate controller designs based on backstepping technique, for an unmatched asymmetric electro-hydraulic system with highly nonlinear characteristics, large disturbances and parameter variations. To reach this objective a non-linear model of the system is developed and verified using experiments. The design and derivation of a robust adaptive backstepping controller with both nonlinear and linear parameter adaption is designed and proven globally uniformly asymptotically stable within a predefined constant tracking bound. A simplified backstepping controller is also proposed. This design is based on the larger and more complex backstepping controller but the inner control loop uses a simplified and linearized model for the pressure dynamics, to reduce the number of parameters and make the design realizable in the experimental setup. The robustness of this controller was shown both using simulations and experimental results, and is showed good tracking performance despite large parameter variations and disturbances in simulations.

Thomas Schmidt

Copies: 3
Pages, total: 160
Pages, Appendix: 38
Supplements: 1 CD

By signing this document, each member of the group confirms that all participated in the project work and thereby all members are collectively liable for the content of the report.

Dedicated to
Hanne and Arne Schmidt

And in memory of
Lene Schmidt

Contents

1	Nomenclature	13
1.1	General Naming Convention	13
1.2	Typesetting	13
1.3	Nomenclature List	14
2	Introduction	16
3	Hypothesis	18
I	System Model Development and Verification	20
4	System Model Development	21
4.1	System Parts	21
4.2	Mechanical System (Load)	23
4.3	Hydraulic System	26
4.4	Valve	28
4.5	Simulation Model Summary	30
5	Model Verification	31
5.1	Numerical Differentiation and Filtering	32
5.2	Verification of Mechanical Model	36
5.3	Verification of the Combined Hydraulic-Valve Model	43
6	Model Simplification and Linearization	49
6.1	Simplified Model	49
6.2	Linearized Model	50

II	Controller Design	55
7	Design of Robust Adaptive Backstepping Controller with Unknown Non-Linear Parameters	56
7.1	Principle of Backstepping	56
7.2	Neglected Valve Dynamics	56
7.3	System Form	57
7.4	Backstepping Controller Design	58
7.5	Summary of the Robust Adaptive Backstepping Controller with Non Linear Parameters .	70
8	Synthesis of Backstepping Control	73
8.1	Controller Structure	73
8.2	Error Dynamics	75
8.3	Practical Considerations and Complications	76
8.4	Improvements and Possible Solutions	77
9	Robust Adaptive Linear Backstepping Controller	79
9.1	Linear Controller Design	80
9.2	Damping Controller	80
9.3	Force Controller	84
9.4	Backstepping Position Controller	86
10	Reference Controller	88
10.1	Control System	88
10.2	Feedforward Controller Design	89
10.3	Feedback Controller Design	89
III	Controller Evaluation and Conclusion	93
11	Trajectory Planning	94
11.1	Trajectory Bounds	94
11.2	Trajectory Form	95
11.3	Parameter Variations of Reference Trajectory	97
11.4	PQ-Curve of Final Reference Trajectory	99
11.5	Force Bounds	100

11.6 Trajectory Summary	103
12 Simulation Results	104
12.1 Simulations Without Valve Dynamics	104
12.2 Simulations With Valve Dynamics	106
12.3 Critical Hydraulic Parameters	112
13 Experimental Results	114
13.1 Tracking Performance RABLIN	115
14 Conclusion	121
IV Appendix	122
A Simplified Model	123
A.1 Positive Spool Displacement	123
A.2 Negative Spool Displacement	125
A.3 Final Simplified Model	126
B Linearized Model	127
B.1 Linearization of Simplified Hydraulic Model	127
B.2 Block Diagram Representation	130
B.3 Transfer Function for Controller Design	131
B.4 System For Critical Operating Point	133
C Parameter Variations	135
C.1 Mechanical	135
C.2 Hydraulic	137
D Operating Point and Parameter Values	139
D.1 Choosing Critical Operating Point and Parameter Values	139
D.2 Parameter Values	140
D.3 Operating Point	143
D.4 Critical Point for RABLIN Control System	146
D.5 Final Remark	147
E Data for Verification	148

F	Stability Theorems and Lemmas	152
F.1	Lyapunov's Stability Theorem (Direct Method)	152
F.2	LaSalle's Invariance Theorem	153
F.3	Raffoul's Boundedness of Solutions Theorem	153
F.4	LaSalle-Yoshizawa Theorem	154
F.5	"Lyapunov-Like Lemma" (Based on Barbalat's Lemma)	156
G	System Forms	157
G.1	Strict Feedback Systems	157
G.2	Pure Feedback Systems	157
G.3	Assumption	158
	Bibliography	158

Preface

During the four month time frame of this project, research within the field of backstepping and various application specific articles have been studied mainly based on the first book written on the subject by Petar V. Kokotovic [Miroslav Krstic and Kokotovic, 1995] and the article [Guan and Pan, 2008] by Cheng Guan and Shuangxia Pan. Through this research the fundamental background knowledge for backstepping controller designs was developed. The theory was used to design an advanced robust adaptive backstepping controller with uncertain non-linear parameters.

The theory has been very challenging especially the large mathematical derivations needed in the control design. For help with this i would like to acknowledge Miroslav Krstic author of [Miroslav Krstic and Kokotovic, 1995] and associated Professor of mathematics Youssef N. Raffoul [Raffoul, 2012] for answering questions related to material presented in their work. I would also like to thank Bosch Rexroth for providing the test-facilities for the experiments and assistance with the control software.

A would like to thank my good friends Thomas Madsen, Dennis Bertelsen and Nicolaj Skafsgaard for providing assistance with proofreading and front page design, and a very special thanks to my girlfriend Stine for providing the best support you can possibly imagine through the four month of this project.

May 2012

Thomas Schmidt

Summary

The project hypothesis has been: *"It is possible to design a position tracking controller using adaptive backstepping control theory, for a nonlinear unmatched asymmetric electro-hydraulic system with good tracking performance and robustness towards disturbances and parameter variations."*

The work done to assess this hypothesis is summarized in three parts. The first part is concerned with **system modeling and verification**, the second part with **controller design** and the last part with **evaluation** of the developed backstepping controllers.

To summarize the content of the first part of the report it was concerned with three major objectives: System Model Development in Chapter 4, Model Verification in Chapter 5 and Model Simplification in Chapter 6.

In Chapter 4 the modeling was done with three main purposes:

1. Nonlinear controller design.
2. Evaluation of controller performance.
3. Determination of parameter variations and bounds.

and the system was split into three subsystems each modeled separately

1. Mechanical System (load)
2. Hydraulic System
3. Valve

The result was the so-called **Simulation Model**.

In Chapter 5 the Simulation Model was verified. The verification included determination of 11 tuning parameters and the verification yielded good correlation between measured and simulated data, which validated the hydraulic and mechanical parts of the simulation model. It was shown that the pump pressure was fluctuating which was assumed the cause for reduced valve performance in the test.

In Chapter 6 a simplified and a linearized model were introduced. The Linearized Model was verified to yield the same dynamic response as the Simulation Model close to the operating point, but reduced precision when moved a small range from the operating point.

To summarize the content of the second part of the report it was concerned with controller design of the three controllers:

RABNLP Robust Adaptive Backstepping Controller with Non-Linear Parameters in **Chapter 7**. First the principle of backstepping was defined. Then the system equations from the simulation model were simplified and put on the right form. After this, the actual backstepping-like controller design was presented proving global stability and convergence of the error states to within a pre-defined ball in the state space, resulting in bounded tracking error.

Chapter 8 was a synthesis of the RABNLP controller investigating the controller structure and the error dynamics of the two first intermediate control laws. It also contained a section describing the practical considerations and complications along with suggestions for improvements and possible solutions.

RABLIN Robust Adaptive Backstepping Linear Controller in **Chapter 9**. The RABNLP controller was simplified into the RABLIN controller. It is based on the 2^nd intermediate control law from the RABNLP controller, but uses a linear control structure for the inner force loop instead. This reduced the number of tuning parameters from 18 to 7 and made it possible to tune the controller using linear control theory.

LINREF Linear Reference Controller in **Chapter 10**. The chosen reference is a position controller structure with P-LEAD feedback and inverse steady state feedforward .

The last part of the report presented the evaluation of the controller design through simulations and experiments carried out on a test facility provided by Bosch Rexroth [Rexroth, 2012b]. Before the results was introduces two trajectories was defined.

The trajectories was designed so they revealed the tracking performance of the controllers while emphasizing the parameter variations of the system. This was achieved by planning trajectories that took the system through a large region in the state-space.

The controller design showed robustness towards parameter variations and disturbances in both simulations and experiments. The tracking performance was also evaluated but the experimental implementation was involved with uncertain problems resulting in reduced performance and a change of parameter values from the original design was required. The performance in the simulation model showed good tracking performance for both transient and steady state situations of sinusoidal and ramp trajectories. The adaption parameters did not converge although persistently excited, and dead-zone techniques were attempted. This, combined with final experimental verification of the simplified backstepping controller could not be solved within the limited time frame of the project.

At a theoretical level the hypothesis was confirmed by both the original and the simplified backstepping controller; They both used adaptive backstepping theory to achieve good tracking performance and robustness towards disturbances and parameter variations on a nonlinear unmatched asymmetric electro-hydraulic system. Moreover, the simplified controller proved robustness in the physical setup.

The hypothesis was therefore confirmed theoretically and partly confirmed experimentally, and the objective of this project have been met.

Chapter 1

Nomenclature

To make it easier to follow the mathematical derivations and expressions in this report a naming convention is established. The convention is chosen so it should be intuitively to understand the meaning of the quantities from the context in which they appear. However, if the following simple rules are memorized before reading through the heavier chapters it will probably make it easier to follow. For a full list of quantities see Table 1.3 later in this chapter.

1.1 General Naming Convention

1. The first letter indicates the type of the quantity e.g. L for length, m for mass and a for angle.
2. Constants and variables have distinct names to differentiate from one another without using the parameter parentheses e.g. a variable length is denoted x not $l(t)$, the same goes for variable angle which is denoted v instead of $a(t)$.
3. All suffixes are capitalized unless the meaning of the quantity by tradition is lower case like x_d for desired position reference. The suffixes are ordered alphabetically e.g. x_{CE} instead of x_{EC} ,

1.2 Typesetting

1. Expressions in computer-programs like Matlab are written in "type-writer" typography e.g. `solve()`.
2. Vectors and matrices are written in italic-bold-type, scalars are only italic-type e.g. a multi-state linear state-space SISO system is written as: $\dot{\mathbf{x}} = \mathbf{Ax} + \mathbf{Bu}$
3. The argument to a variable quantity (or function) is often omitted. It is included when it is important for the context.
4. English decimal separation are used hence a ',' indicates thousands and '.' is the decimal separator.

1.3 Nomenclature List

α	Piston area ratio	$[-]$
β_A	Parameter estimation	$[m]$
β_B	Parameter estimation	$[m]$
β	Bulk modulus	$[Pa]$
ϵ_{1-9}	Second parameter estimation	$[-]$
γ_1	Adaption gain	$[-]$
γ_2	Adaption gain	$[-]$
ν_X	Friction coefficient	$[-]$
ϕ_1	Parameter estimation	$[-]$
ϕ_2	Parameter estimation	$[-]$
ρ	Oil density	$[kg/m^3]$
τ	Time constant	$[s]$
θ_{1-7}	First parameter estimation	$[-]$
ζ	Damping ratio	$[-]$
a_1	Constant angle around rotating joint see figure 4.2	$[rad]$
a_2	Constant angle around rotating joint see figure 4.2	$[rad]$
a_3	Constant angle around rotating joint see figure 4.2	$[rad]$
A_A	Piston area side A	$[m^2]$
A_B	Piston area side B	$[m^2]$
B	Viscous damping coefficient	$[N \cdot s/m]$
C_D	Discharge coefficient	$[-]$
C_L	Leakage coefficient	$[m^3/s \cdot Pa]$
F_F	Friction force	$[N]$
F_L	Force from the hydraulic actuator system	$[N]$
g	Gravity	$[m/s^2]$
G_1	Oscillary variable	$[-]$
G_2	Oscillary variable	$[-]$
J_L	Moment of inertia af the link about joint A	$[kg \cdot m^2]$
k_1	Gain	$[-]$
k_2	Gain	$[-]$
k_3	Gain	$[-]$
K_A	Discharge coefficient	$[m^3/s \cdot \sqrt{Pa}]$
K_B	Discharge coefficient	$[m^3/s \cdot \sqrt{Pa}]$
K_{VA}	Area gradient	$[m]$
K_{VB}	Area gradient	$[m]$
L_{AB}	Length from the rotating point A to point B	$[m]$
L_{AC}	Length from the rotating point to point C	$[m]$
L_{AD}	Length from the rotating point A to point D	$[m]$
L_{BE}	Length from point B to point E	$[m]$
m	Mass	$[kg]$

M_A	Moments about point A	$[N \cdot m]$
p_A	Pressure piston side A	$[Pa]$
p_B	Pressure piston side B	$[Pa]$
p_P	Pump pressure	$[Pa]$
p_T	Tank pressure	$[Pa]$
Q_A	Flow chamber A	$[m^3/s]$
Q_B	Flow chamber B	$[m^3/s]$
Q_C	Leakage flow	$[m^3/s]$
Q_P	Pump flow	$[m^3/s]$
Q_T	Tank flow	$[m^3/s]$
R_A	A port driving pressure	$[Pa]$
R_B	B port driving pressure	$[Pa]$
v_1	Angle around rotating joint see figure 4.2	$[rad]$
v_2	Angle around rotating joint see figure 4.2	$[rad]$
v_3	Angle around rotating joint see figure 4.2	$[rad]$
V_{A0}	Initial volume of chamber A	$[m^3]$
V_A	Volume of chamber A	$[m^3]$
V_{B0}	Initial volume of chamber B	$[m^3]$
V_B	Volume of chamber B	$[m^3]$
x_1	Cylinder displacement	$[m]$
x_2	Cylinder velocity	$[m/s]$
x_3	Pressure in chamber A	$[Pa]$
x_4	Pressure in chamber B	$[Pa]$
x_{CE}	Cylinder displacemant	$[m]$
x_V	Valve position	$[m]$
z_1	Tracking error and error variable	$[-]$
z_2	Error variable	$[-]$
z_3	Error variable	$[-]$

Chapter 2

Introduction

Background

Hydraulic systems are used widely in the industry by virtue of a small size-to-power ratio and their ability to produce large forces and torques [Guan and Pan, 2008, p. 1]. When rapid and precise control of sizable loads is required an electro-hydraulic servo is often the best approach and the performance of such encompasses every industrial application [Rydberg, 2008, p. 2].

Both hydraulic and electric servo drive technologies are increasingly becoming the norm in machine automation, where the operators are demanding greater precision, faster operation and simpler adjustment but at a lower cost [Rydberg, 2008, p. 1]. Hydraulic systems are often involved with large parameter variations, uncertainties and non-linear disturbances causing difficulties in the control of such systems. In practice this may result in over-sized, conservative, low performing and expensive designs [Rexroth, 2012b].

Previous Work

Adaptive linear control theory has been used to deal with the parameter variations, like in [Plummer and Vaughan, 1996] and [Bobrow and Lum, 1996]. However, important dynamic informations are lost in the linearization process which favors non-linear control methods. This has encouraged designs such as adaptive sliding mode control [Alleyne and Hedrick, 1995], adaptive feedback linearization control [Garagic and Srinivasan, 2004] and nonlinear adaptive controllers based on **backstepping** techniques. These have been applied using force control in [Alleyne and Liu, 2000b] and [Alleyne and Liu, 2000a]. An applied robust adaptive controller has been presented in [Yao and Chiu, 1998] and [Yao and Chiu, 1999] for an *asymmetric* cylinder compensating for both parametric and nonlinear uncertainties.

In the article [Guan and Pan, 2008] a special novel-type Lyapunov function has been used to construct a Lyapunov-based controller and parameter update law for *nonlinear* parameters. The article combines the backstepping method to provide the whole system controller and all unknown parameters update laws. A simple robust method was used to solve the problem of unmodeled uncertainties. The system showed improved performance over controllers with only linear parameter adaption and the result was proven using an experimental setup.

The system considered had a **known spring constant** and did not include the **linear friction** in the model. The experiments were carried out using a **small-scale cylinder** with chamber pressures below 50 Bar and a cylinder travel length of 18 cm (the reference controller still yielded an error of 4 cm). Also, due to very small differences in chamber pressures the cylinder was *horizontal* meaning small gravitational disturbances.

Problem

In this report the results of [Guan and Pan, 2008] are extended with an adaption law to deal with the linear friction. Moreover, the design is constructed for a **full scale** cylinder attached to a mechanical body with loose joints. The hydraulic system considered apply a proportional valve instead of a fast **servo** valve. Furthermore, the size of the parameter variations and disturbances are significantly larger than in [Guan and Pan, 2008]. The system considered has mechanical parameters and gravitational forces changing during **operation**, and the gravitational disturbance is so large that it (due to unmatched cylinder and valve) increases the chamber pressure above pump pressure, and introduces large unwanted variations in pump pressure as a consequence. The valve is internally supplied by the pump pressure directly, meaning that varying pump pressure dramatically lowers the performance of the valve and the control task becomes even more challenging.

Report Structure

The report are structured in three parts

1. System Model Development and Verification
2. Controller Design
3. Controller Evaluation and Conclusion

In the first part a nonlinear simulation model is developed and verified. Then a simplified and a linearized model are developed and verified using the simulation model.

The second part presents the design of three controllers: A robust adaptive backstepping controller with non-linear parameter adaption, along with a simplified robust adaptive linear backstepping controller.

The last controller is a linear feedback controller with an added feedforward path used as a reference for the evaluation of the backstepping controllers in part 3. The evaluation part contains a chapter with trajectory planning followed by simulations and experimental results. The part ends with a conclusion based on the requirements and goals for the controllers which is used to settle the hypothesis.

The next chapter presents this hypothesis stating the objective of the project together with part objectives used to structure the work through the project.

Chapter 3

Hypothesis

"It is possible to design a position tracking controller using adaptive backstepping control theory, for a nonlinear unmatched asymmetric electro-hydraulic system with good tracking performance and robustness towards disturbances and parameter variations."

To assess the hypothesis an objective of the project is defined together with a set of part objectives in order to reach the main objective.

Objective

To use backstepping theory to develop and evaluate controller designs for an unmatched asymmetric electro-hydraulic system, provided by Bosch Rexroth [Rexroth, 2012b]. The designs must ensure robustness towards disturbances and parameter variations, using an adaptive backstepping approach, and the design must obtain good tracking performance.

Part Objectives

The part objectives is a break-down of the tasks that must be accomplished in order to reach the objective and the final assessment of the hypothesis.

Backstepping Research The advanced theories and concepts of the backstepping procedure must be researched and understood in order to develop the controller designs. The research must be continued to a level of application.

System Analysis and Modeling To apply backstepping theory a dynamic model of the system is required, and the main parts of the system must be analyzed.

Model Verification For the theory to be applicable in reality the model must be sufficiently accurate, and should therefore be verified using measurements obtained from the physical test setup.

Controller Designs The actual controller designs must be carried out using the obtained knowledge from the research and the verified system model.

Reference Controller In order to evaluate the controller designs a reference must be defined. The reference should be chosen so it corresponds to common industrial controller designs for similar systems.

Parameter Variations and Disturbances Bounds on the system parameters and disturbances are needed in order to obtain a robust design.

Simulation To theoretically verify and evaluate the controller designs a simulation model based on the verified system model is required. And the controllers must be implemented in this model.

Controller Implementation In order to experimentally verify the simulated performance a test setup must be configured and controllers, discretized and implemented. Configuration also involves research in the Bosch Rexroth software and control electronics.

Trajectory Planning To make a proper evaluation a trajectory revealing the controllers performance must be planned and programmed into both the simulation model and the control software in the physical test setup.

Experiments To finally make an assessment of the hypothesis the controllers must be implemented in the control software of the test setup and data for evaluation must be extracted, analyzed and compared.

With the hypothesis, objective and part objectives defined the first part of the project can be presented, concerning system model development and verification.

Part I

System Model Development and Verification

Chapter 4

System Model Development

To easier follow the derivation in this chapter a naming convention and a nomenclature list has been made in section 1 on page 13.

The system is modeled with the following purposes:

1. Nonlinear controller design.
2. Evaluation of controller performance.
3. Determination of parameter variations and bounds.

This chapter presents the derivation of the **Simulation Model** fulfilling the above objectives. Later the model is simplified with the following purposes:

1. Trajectory planning.
2. Linear controller designs.

The Simplified Model used for trajectory planning is derived in Chapter A and the Linearized Model used for linear controller design are derived in Chapter B. These are discussed in details later.

4.1 System Parts

An overview of the system and its parts are seen in Figure 4.1.

The system is analyzed and modeled in three separate parts, each having its own section in this chapter. The valve is also a part of the hydraulic circuit but it is modeled separately.

- Mechanical Part (load)
- Hydraulic Part
- Valve Part

Besides the three modeled parts, the system also includes a digital control unit. This unit works in discrete time steps and introduces sampling effects. However, the effect of sampling are ignored since it

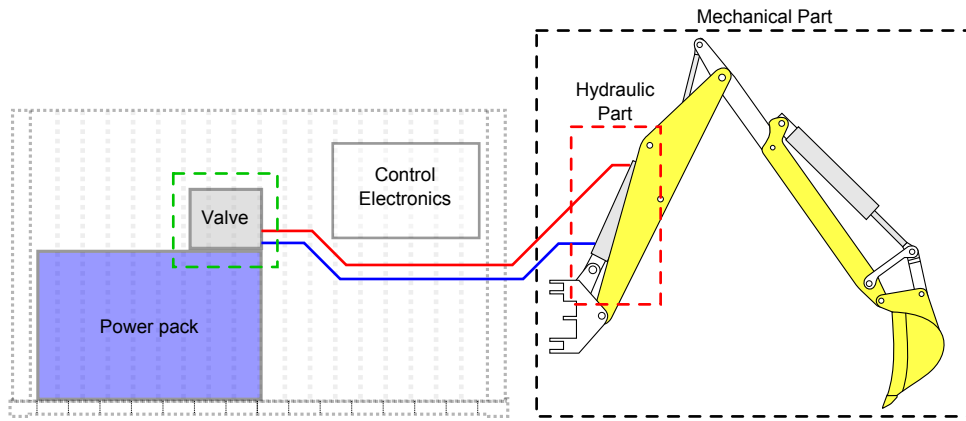


Figure 4.1: Overview of the system.

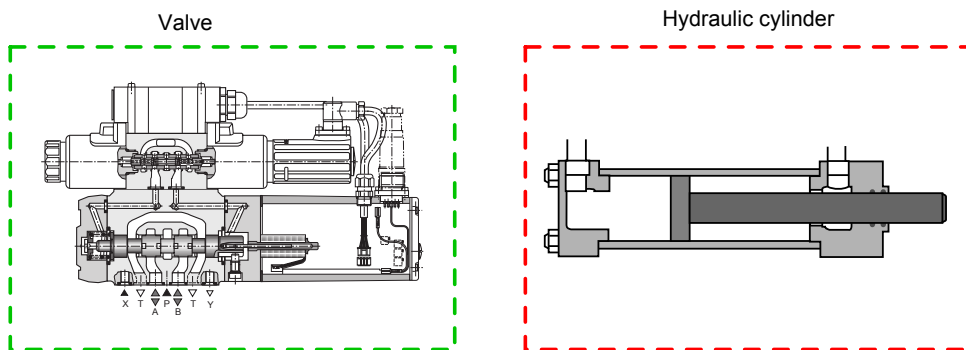


Figure 4.2: The valve and the hydraulic part of the system.

is assumed that the control period (sampling period) is small, and all modeling and analysis is therefore considered in continuous time.

The first part of the model to be presented is the Mechanical Part.

4.2 Mechanical System (Load)

The mechanical model is obtained using the *Euler-Lagrange* method for cylindrical coordinates. The method is based on the following equation [Mark W. Spong, 2005, Eq. 6.11, P. 190]:

$$\frac{d}{dt} \left(\frac{\partial \mathcal{L}}{\partial \dot{v}_2} \right) - \frac{\partial \mathcal{L}}{\partial v_2} = Q \quad (4.1)$$

Where the *Lagrangian*, \mathcal{L} , (also called action) is defined as $\mathcal{L} = T - V$. The quantities T and V are the total kinetic- and potential energy of the system, respectively. The Q represents all non-conservative moments such as friction and moments due to external forces. Considering the diagram of Figure 4.3 we are able to derive the expressions necessary to obtain the mechanical system equation.

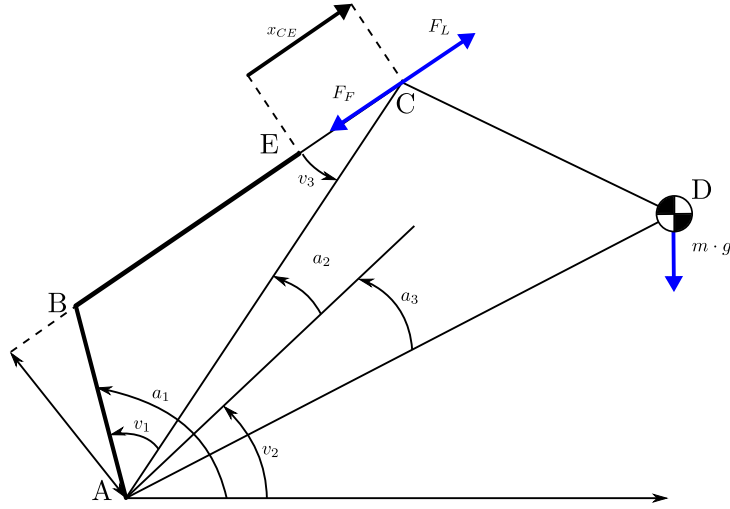


Figure 4.3: Illustration of the mechanical part of the system.

The link of the 1-degree-of-freedom (1-DoF) manipulator is assumed **uniformly rigid**, meaning that bending of the links are neglected. The moment of inertia of the link about point A is denoted J_L , and the total mass of the link is denoted m . The force F_F is a non-conservative friction force and F_L represents the force from the hydraulic actuator system. Seen from the mechanical system these are both external forces.

Kinetic energy:

$$T = \frac{1}{2} J_L \dot{v}_2^2 \quad (4.2)$$

Potential energy:

$$V = L_{AD} g m \sin(v_2 - a_3) \quad (4.3)$$

Lagrangian:

$$\mathcal{L} = \frac{1}{2} J_L \dot{v}_2^2 - L_{AD} g m \sin(v_2 - a_3) \quad (4.4)$$

Partial derivative of L wrt. \dot{v}_2 :

$$\frac{\partial \mathcal{L}}{\partial \dot{v}_2} = J_L \dot{v}_2 \quad (4.5)$$

Full derivative of $\frac{\partial \mathcal{L}}{\partial \dot{v}_2}$:

$$\frac{d}{dt} \left(\frac{\partial \mathcal{L}}{\partial \dot{v}_2} \right) = J_L \ddot{v}_2 \quad (4.6)$$

Partial derivative of L wrt. v_2 :

$$\frac{\partial \mathcal{L}}{\partial v_2} = -L_{AD} g m \cos(v_2 - a_3) \quad (4.7)$$

Non-conservative moments about point A:

$$Q = L_{AC} \sin(v_3) (F_F - F_L) \quad (4.8)$$

Substituting the results from Equation (4.6 - 4.8) into the Euler-Lagrange Formula (4.1) the differential equation governing the dynamics of the mechanical system is obtained:

$$\ddot{v}_2 = \frac{L_{AC} \sin(v_3) (F_F - F_L) - L_{AD} g m \cos(v_2 - a_3)}{J_L} \quad (4.9)$$

The same result could be obtained considering the sum of moments about point A, ΣM_A , and applying Newtons second law of motion:

$$\ddot{v}_2 = \frac{\Sigma M_A}{J_L} \quad (4.10)$$

$$\Sigma M_A = \underbrace{L_{AC} \sin(v_3) (F_F - F_L)}_{\text{Resulting actuator force}} - \underbrace{L_{AD} g m \cos(v_2 - a_3)}_{\text{Gravity force}} \quad (4.11)$$

The derivation based on Newtons second law is simpler because the system is only a 1-DoF system. However, for multiple DoF systems the Euler-Lagrange method is usually easier to apply.

As a final remark; the friction force F_F contains a linear friction (sometimes called viscous friction). This part of F_F is modeled separately as

$$F_F = \nu_X \cdot \dot{x}_{CE} + F_R \quad (4.12)$$

leaving the reminder of F_F in F_R . This reminder then contains the non-linear friction components Coulomb friction and stiction.

4.2.1 Cylinder Coordinates

The goal is an expression containing only the cylinder force F_L , the reminder of the non-conservative friction F_R , the cylinder displacement x_{CE} and derivatives hereof.

Therefore, the quantities v_2 and v_3 must be substituted from Equation (4.9). In order to do so, the following two cosine-relations are established:

$$v_2 = a_1 - a_2 - \arccos \left(\frac{L_{AB}^2 - (L_{BE} + x_{CE})^2 + L_{AC}^2}{2 L_{AB} L_{AC}} \right) \quad (4.13)$$

$$v_3 = \arccos\left(\frac{(L_{BE} + x_{CE})^2 - L_{AB}^2 + L_{AC}^2}{2 L_{AC} (L_{BE} + x_{CE})}\right) \quad (4.14)$$

Furthermore, the angular acceleration \ddot{v}_2 must also be expressed in terms of cylinder coordinates. The expression for v_2 is differentiated twice:

$$\dot{v}_2 = -\frac{\dot{x}_{CE} (2 L_{BE} + 2 x_{CE})}{2 L_{AB} L_{AC} \sqrt{1 - \frac{(L_{AB}^2 - (L_{BE} + x_{CE})^2 + L_{AC}^2)^2}{4 L_{AB}^2 L_{AC}^2}}} \quad (4.15)$$

$$\ddot{v}_2 = \frac{(2 L_{BE} + 2 x_{CE})^2 \left(L_{AB}^2 - (L_{BE} + x_{CE})^2 + L_{AC}^2 \right) G_1(x_{CE}) - 8 G_1(x_{CE})^3}{8 G_1(x_{CE})^4} \dot{x}_{CE}^2 - G_1(x_{CE}) \ddot{x}_{CE} \quad (4.16)$$

$$G_1(x_{CE}) = L_{AB} L_{AC} \sqrt{1 - \frac{(L_{AB}^2 - (L_{BE} + x_{CE})^2 + L_{AC}^2)^2}{4 L_{AB}^2 L_{AC}^2}} \quad (4.17)$$

Substituting the three expressions (4.13), (4.14) and (4.16) into Equation (4.9) reveals the final equation; the equation that describes the dynamics of the mechanical system in cylinder coordinates. The equation is too large to be presented here, but when put on the form of (4.18) we can present its coefficients which is seen in Equation (4.19) to (4.22).

$$M(x_{CE}) \ddot{x}_{CE} = F_L - B(x_{CE}, \dot{x}_{CE}) \dot{x}_{CE} - F(t), \quad (4.18)$$

The form of Equation (4.18) can be seen as a force equilibrium of a cylinder with a varying viscous damping coefficient B , varying mass M and a non-linear time-dependent disturbance $F(t)$.

$$M(x_{CE}) = \frac{J_L (L_{BE} + x_{CE})}{G_1(x_{CE}) G_2(x_{CE})} \quad (4.19)$$

$$B(x_{CE}, \dot{x}_{CE}) = \frac{J_L \dot{x}_{CE}}{G_1(x_{CE}) G_2(x_{CE})} - \frac{J_L \dot{x}_{CE} (2 L_{BE} + 2 x_{CE})^2 \left(L_{AB}^2 - (L_{BE} + x_{CE})^2 + L_{AC}^2 \right)}{8 G_1(x_{CE})^3 G_2(x_{CE})} + \nu_X \quad (4.20)$$

$$F(t) = F_R - \frac{L_{AD} g m}{G_2(x_{CE})} \cos \left[a_1 - a_2 - a_3 - \arccos \left(\frac{L_{AB}^2 - (L_{BE} + x_{CE})^2 + L_{AC}^2}{2 L_{AB} L_{AC}} \right) \right] \quad (4.21)$$

$$G_2(x_{CE}) = L_{AC} \sqrt{1 - \frac{\left((L_{BE} + x_{CE})^2 - L_{AB}^2 + L_{AC}^2 \right)^2}{4 L_{AC}^2 (L_{BE} + x_{CE})^2}} \quad (4.22)$$

The two terms in $B(x_{CE}, \dot{x}_{CE})$ are classified as *centrifugal terms*. According to [Mark W. Spong, 2005, p. 202], centrifugal terms are defined as terms in the force equilibrium that have the derivative of a generalized coordinate squared. The position x_{CE} is the generalized coordinate in the sense presented in [Mark W. Spong, 2005]. In our case B has two terms with \dot{x}_{CE} in the nominator, both terms are centrifugal terms as the product " $B x_{CE}$ " appear in the force equilibrium (4.18).

4.3 Hydraulic System

Considering only the main parts of the the hydraulic system it consists of an asymmetric cylinder, a 4/3-way proportional valve, a tank and a variable displacement pump. An illustration of the hydraulic system is seen in Figure 4.4.

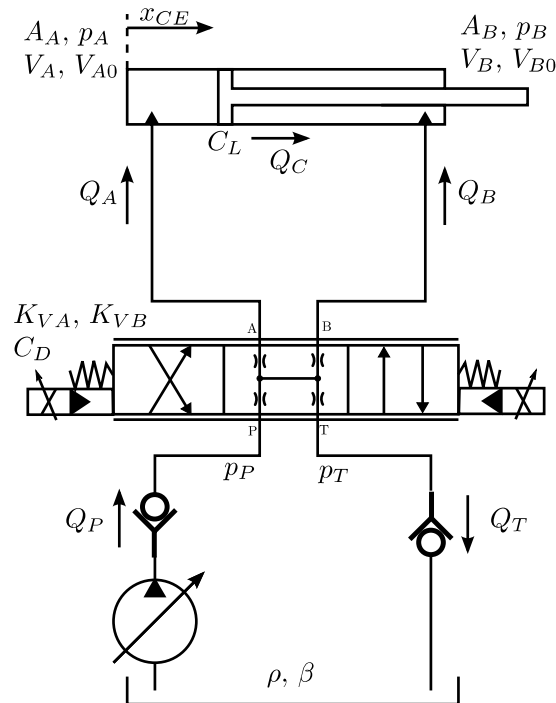


Figure 4.4: Illustration of the hydraulic part of the system.

Assumptions:

1. p_T and p_P are constant. This is reasonable if the pump is fast and the volume of the supply cavity is large.
2. p_T is the lowest pressure in the system. It is hence assumed that no cavitation occur and the flow Q_T is never negative.
3. p_P is the highest pressure occurring in the system and the flow Q_P is never negative.
4. Q_C is laminar and therefore affine/linear with respect to pressure.
5. Q_A and Q_B are turbulent over the valve, so the orifice equation can be used assuming a constant C_D value.
6. ρ is assumed constant i.e. invariant with respect to pressure and temperature changes.
7. Leakage flow from the valve is ignored.
8. Pressure drop across the check-valves are ignored.

Derivation:

The pressure build-up in cylinder chambers are described by the continuity equation.

$$\dot{p}_A = \frac{\beta}{V_{A0} + A_A x_{CE}} (Q_A - \dot{x}_{CE} A_A - Q_C) \quad (4.23)$$

$$\dot{p}_B = \frac{\beta}{V_{B0} - A_B x_{CE}} (Q_B + \dot{x}_{CE} A_B + Q_C) \quad (4.24)$$

Due to the assumption that p_P is the highest and p_T the lowest pressure in the system and because the flow is assumed turbulent through the valve we can express the flow using the orifice equation.

$$Q_A = C_D K_{VA} x_V \sqrt{\frac{2}{\rho}} (s(x_V) \sqrt{p_P - p_A} + s(-x_V) \sqrt{p_A - p_T}) \quad (4.25)$$

$$Q_B = -C_D K_{VB} x_V \sqrt{\frac{2}{\rho}} (s(x_V) \sqrt{p_B - p_T} + s(-x_V) \sqrt{p_P - p_B}) \quad (4.26)$$

$$Q_C = C_L(p_A - p_B) \quad (4.27)$$

With the function $s(*)$ defined as:

$$s(*) = \begin{cases} 1 & \text{if } * \geq 0 \\ 0 & \text{if } * < 0 \end{cases} \quad (4.28)$$

Introducing two functions $R_A(\mathbf{x})$, $R_B(\mathbf{x})$ and the two constants:

$$K_A = C_D K_{VA} \sqrt{\frac{2}{\rho}} \quad (4.29)$$

$$K_B = C_D K_{VB} \sqrt{\frac{2}{\rho}} \quad (4.30)$$

We can rewrite the orifice equations as:

$$Q_A = K_A x_V \underbrace{(s(x_V) \sqrt{p_P - p_A} + s(-x_V) \sqrt{p_A - p_T})}_{R_A(\mathbf{x})} \quad (4.31)$$

$$Q_B = -K_B x_V \underbrace{(s(x_V) \sqrt{p_B - p_T} + s(-x_V) \sqrt{p_P - p_B})}_{R_B(\mathbf{x})} \quad (4.32)$$

Substituting the expressions (4.27), (4.31) and (4.32) into the equations for the pressure build-up (4.23) and (4.24), we obtain the following two equations:

$$\dot{p}_A = \frac{\beta}{V_{A0} + A_A x_{CE}} (K_A x_V R_A(\mathbf{x}) - \dot{x}_{CE} A_A - C_L(p_A - p_B)) \quad (4.33)$$

$$\dot{p}_B = \frac{\beta}{V_{B0} - A_B x_{CE}} (-K_B x_V R_B(\mathbf{x}) + \dot{x}_{CE} A_B + C_L(p_A - p_B)) \quad (4.34)$$

The hydraulic model links the mechanical model through the cylinder force F_L which is defined as

$$F_L = A_A p_A - A_B p_B \quad (4.35)$$

This concludes the derivation of the hydraulic system.

4.4 Valve

A cross-sectional overview of the valve is given in Figure 4.5. The two-stage valve contains two spools: A pilot spool and a main spool. The pilot stage works as a hydraulic amplifier between the input signal and the main stage. The dynamics of the pilot stage is ignored as it is assumed much faster than the main stage, and when referring to *the valve* it is the main stage that is considered.

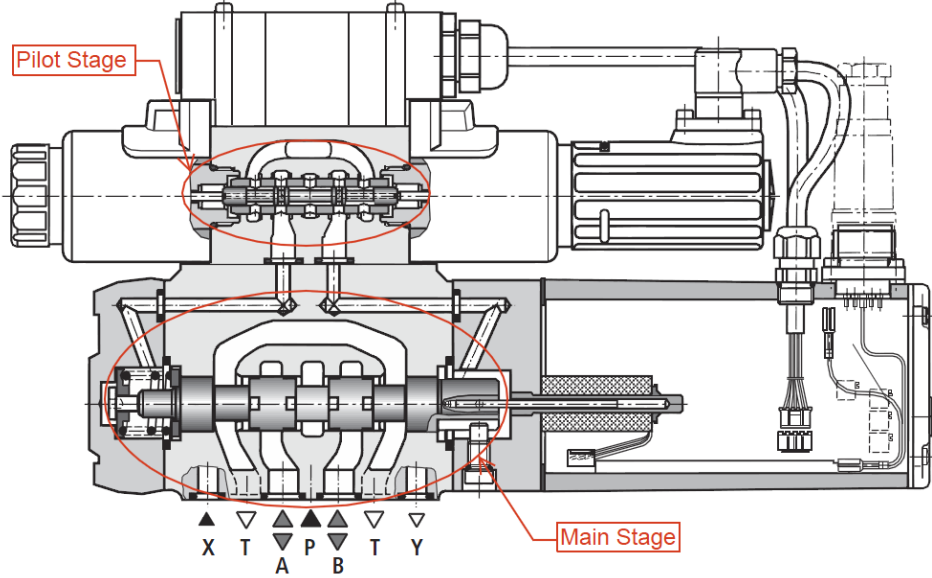


Figure 4.5: Cross sectional view of the valve used in the experimental setup. [Rexroth, 2006, p.11]

We have two different low-order linear ways to model the valve as a 1.-order or a 2.-order system. Combinations of these resulting in higher order systems is possible but the cost is a more complex model. In the time-domain the two simple models are given as:

$$\dot{x}_V = \frac{K_V}{\tau_V} u - \frac{1}{\tau_V} x_V \quad (4.36)$$

$$\ddot{x}_V = K_V \omega_V^2 u - 2\zeta \omega_V \dot{x}_V - \omega_V^2 x_V \quad (4.37)$$

Figure 4.6 shows a frequency response of the valve. It shows the *sinusoidal steady-state* behavior for sinusoidal input voltages ranging from 1-200Hz in frequency. As the phase transition of Figure 4.6 is very steep the valve is modeled as the 2-order system using Equation (4.37), and the first order is ignored.

Values for the equation is found using the Bode plot of figure 4.6 which makes it an empirical linear model approximating the *dynamic* behavior of the valve.

There is no magnitude peak in the amplitude characteristics of the frequency responses in Figure 4.6 so the damping ratio should be $\zeta_V \geq 1$. The phase shows highly nonlinear behavior, especially for large input values, but because the phase transition is steep the damping ratio is chosen as

$$\zeta_V = 1 \quad (4.38)$$

The cut-off frequency is also seen to vary with the input amplitude, which is a non-linear characteristic that cannot be modeled by a linear model. Therefore we have to choose an operating point for the input signal. A conservative choice would be the $\pm 100\%$ line and an optimistic choice would be the $\pm 10\%$. We choose a value so that the approximation lies in between those lines. For a critically damped system ($\zeta_V = 1$) we have a double pole at ω_V , resulting in a -6 dB attenuation at this point. We choose an

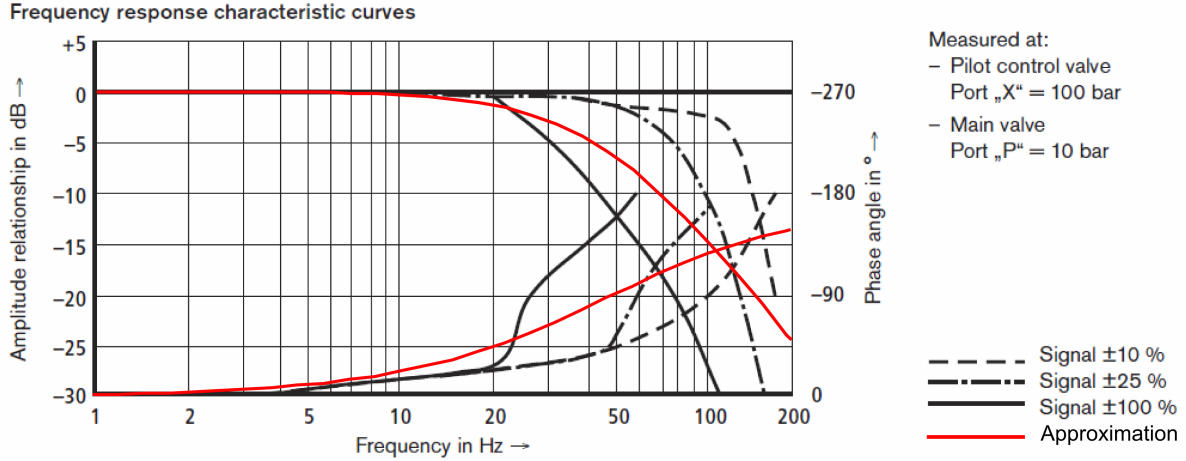


Figure 4.6: Bode plot illustrating the steady-state behavior of the valve for sinusoidal inputs. The red-line indicates the 2-order approximation [Rexroth, 2006].

eigenfrequency of 50 Hz, which corresponds to:

$$\omega_V = 314.16 \text{ rad/s} \quad (4.39)$$

The 2-order approximation is plotted with values of ζ_V and ω_V together with the empirical bode plots from [Rexroth, 2006, p.11] and the result is seen as the red line in Figure 4.6. As expected the model do not show as steep a characteristics as the empirical data, and a higher order model is necessary if a better result is needed. As both the damping ratio and the eigenfrequency have been defined the time-constant, as defined in [Phillips and Harbor, 2000, p. 125 eq. 4-27], of the critically damped system can be calculated:

$$\tau_V = \frac{1}{\zeta_V \omega_V} = 0.00318 \text{ s} \quad (4.40)$$

The last value that is to be determined is the DC-gain K_V . The magnitude of Figure 4.6 do not reveal this value as it is normalized so that $u = 1 \text{ V}$ corresponds to $x_V = 1 \text{ m}$. Instead, the value of K_V is found from the maximum values of u and x_V , as the data sheet states that $u = 100\%$ corresponds to $x_V = 100\%$. From [Rexroth, 2006, p. 6] we have $u_{MAX} = 10 \text{ V}$ and $x_{VMAX} = 3.5 \text{ mm}$.

$$K_V = \frac{x_{VMAX}}{u_{MAX}} = \frac{3.5e-3}{10} = 350e-6 \frac{\text{m}}{\text{V}} \quad (4.41)$$

This finalize the modeling of the valve, and as both the mechanical and hydraulic parts have been modeled, also the system as a whole. The next section is a summary of all the important equations derived in this chapter.

4.5 Simulation Model Summary

Mechanical System

$$M(x_{CE}) \ddot{x}_{CE} = F_L - B(x_{CE}, \dot{x}_{CE}) \dot{x}_{CE} - F(t), \quad (4.42)$$

With parameter variations described by:

$$M(x_{CE}) = \frac{J_L (L_{BE} + x_{CE})}{G_1(x_{CE}) G_2(x_{CE})} \quad (4.43)$$

$$B(x_{CE}, \dot{x}_{CE}) = \frac{J_L \dot{x}_{CE}}{G_1(x_{CE}) G_2(x_{CE})} \left(1 - \frac{(2L_{BE} + 2x_{CE})^2 (L_{AB}^2 - (L_{BE} + x_{CE})^2 + L_{AC}^2)}{8 G_1(x_{CE})^2} \right) + \nu_X \quad (4.44)$$

$$F(t) = F_R(t) - \frac{L_{AD} g m}{G_2(x_{CE})} \cos \left[a_1 - a_2 - a_3 - \arccos \left(\frac{L_{AB}^2 - (L_{BE} + x_{CE})^2 + L_{AC}^2}{2 L_{AB} L_{AC}} \right) \right] \quad (4.45)$$

$$G_1(x_{CE}) = L_{AB} L_{AC} \sqrt{1 - \frac{(L_{AB}^2 - (L_{BE} + x_{CE})^2 + L_{AC}^2)^2}{4 L_{AB}^2 L_{AC}^2}} \quad (4.46)$$

$$G_2(x_{CE}) = L_{AC} \sqrt{1 - \frac{((L_{BE} + x_{CE})^2 - L_{AB}^2 + L_{AC}^2)^2}{4 L_{AC}^2 (L_{BE} + x_{CE})^2}} \quad (4.47)$$

Hydraulic System

$$\dot{p}_A = \frac{\beta}{V_{A0} + A_A x_{CE}} (K_A x_V R_A - \dot{x}_{CE} A_A - C_L(p_A - p_B)) \quad (4.48)$$

$$\dot{p}_B = \frac{\beta}{V_{B0} - A_B x_{CE}} (-K_B x_V R_B + \dot{x}_{CE} A_B + C_L(p_A - p_B)) \quad (4.49)$$

With:

$$K_A = C_D K_{VA} \sqrt{\frac{2}{\rho}} \quad (4.50)$$

$$K_B = C_D K_{VB} \sqrt{\frac{2}{\rho}} \quad (4.51)$$

Valve

The valve dynamics is *included* in the Simulation Model so the driving pressure over port A and B in the valve are calculated using the following functions:

$$R_A(p_A, x_v) = s(x_V) \sqrt{p_P - p_A} + s(-x_V) \sqrt{p_A - p_T} \quad (4.52)$$

$$R_B(p_B, x_v) = s(x_V) \sqrt{p_B - p_T} + s(-x_V) \sqrt{p_P - p_B} \quad (4.53)$$

with:

$$s(*) = \begin{cases} 1 & \text{if } * \geq 0 \\ 0 & \text{if } * < 0 \end{cases} \quad (4.54)$$

and the valve is modeled as a 2.-order linear system:

$$\ddot{x}_V = K_V \omega_V^2 u - 2\zeta \omega_V \dot{x}_V - \omega_V^2 x_V \quad (4.55)$$

Chapter 5

Model Verification

This chapter presents the verification of the three parts of the model i.e. the Mechanical part, the Hydraulic part and the Valve. When referring to *the model* in this section it is the Simulation Model that is referenced.

An overview of the model and how the parts connect are given in Figure 5.1.

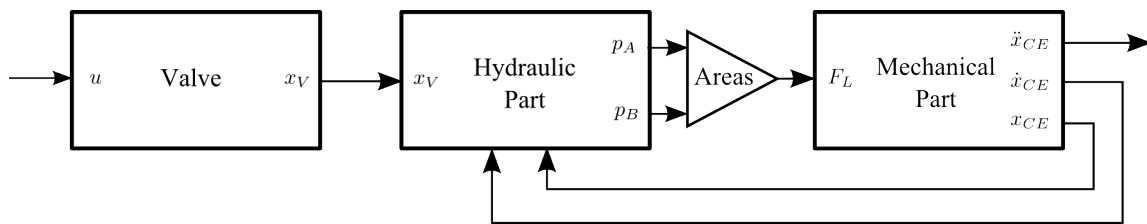


Figure 5.1: Overview of the three parts of the model and how they connect.

The mechanical model is verified when it is able to describe the motion of the cylinder (\ddot{x}_{CE} , \dot{x}_{CE} , x_{CE}), to a dynamic cylinder force F_L , sufficiently precise. The definition of "sufficient" is not exact, but it is based on intuition and experience. The model is primarily used for controller design purposes, hence it should be so precise that the controllers developed for the model show expected performance in the test setup.

The hydraulic part is verified when it predicts the pressure in the two cylinder chambers i.e. p_A and p_B , for a given spool position x_V . As for the mechanical part, this should be predicted sufficiently precise so that the model can be used for controller design and evaluation. The spool position x_V is not available for measurements, so the hydraulic part cannot be verified without considering the valve. The valve links the spool position x_V to the *known* control signal u .

Another challenge when verifying the model is that the velocity \dot{x}_{CE} and the acceleration \ddot{x}_{CE} are not available for measurements - at least not directly. However, the position x_{CE} is available, so velocity and acceleration data can be obtained through numeric differentiation, provided that the noise from the measurements can be removed.

How this is achieved is described in the first section of this chapter, 5.1 Numerical Differentiation and Filtering, and the result is used in the succeeding sections; 5.2 Verification of Mechanical Model and 5.3 Verification of the Combined Hydraulic-Valve Model.

5.1 Numerical Differentiation and Filtering

As described in the introduction to this chapter the purpose of differentiation of the position signal is to obtain precise velocity and acceleration signals to be used in the verification.

The position measurement is carried out using a draw-wire sensor from the company Way-Con. The measurements are analog but converted to a digital/discrete signal and therefore quantified into a fixed precision. It has a maximum precision of 0.01% of maximum displacement, 1000 mm [Way-Con, 2012], yielding a maximum resolution of 0.1 mm. Even though this is very precise it leads to quantification noise, which is amplified by differentiation. As the signal is originally analog it yields other noise factors like the 50 Hz noise from the utility grid, and good filtering is essential for the final result, especially as the signal are to be differentiated twice.

The signal is sampled with 1 ms sample period and exported from the PLC to the PC with 5 decimal digits, 0.01 mm precision, which is more precise than the sensor and therefore ensure that the main quantification error is from the sensor and not the data logging procedure.

5.1.1 Differentiation and Linear Filter

As an initial attempt two cascaded linear first order filters were chosen, see Figure 5.2. The bandwidth of the filters had to be very low in order to remove the noise and an initial value at around 20 rad/s were required to filter out the noise. The pressure measurements show that the system dynamics is significant around 15-20 rad/s, and as each filter introduces significant phase lag ($45^\circ/\text{dec}$) beginning approximately for frequencies at around one decade lower than the bandwidth of the filter, this filter arrangement could not be used without distorting the phase.

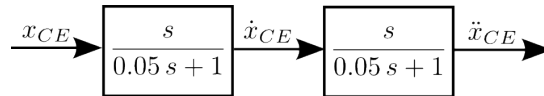


Figure 5.2: Block diagram of initial filters to obtain velocity and acceleration information from position measurements.

5.1.2 Butterworth Filter with Zero-Phase Filtering

By using a Butterworth filter we are able to make a maximum flat magnitude filter with approximately linear phase characteristics [Oppenheim and Willsky, 1998, p.704-705]. By using the butterworth filter with the Matlab routine `filtfilt(b,a,x)` we are applying so called "zero-phase" filtering to the data, as it runs the data through the filter both forward and backwards, resulting in a non distorted phase [Matlab, 2012a]. A Butterworth filter of 12'th order is designed to have a cut-off frequency of 4 Hz. Because of the high order it has a very steep magnitude characteristics after the cut-off frequency, but due to the flat magnitude of a Butterworth filter and the zero-phase filtering the data below of say 3.1 Hz is almost not distorted at all which is seen in Figure 5.3.

Three data-series is generated in the test setup to be used for validation. These are Stair, Sawtooth and Step. The result of applying the described differentiator and filter to the position signal for the "Sawtooth" trajectory is seen in Figure 5.5, and for the stair and step in Appendix E on page 148. The filtering is validated by integrating the resulting acceleration and comparing it to the original position signal. The result for the sawtooth trajectory is seen in figure 5.6 on page 35, and for the step and stair tests; in Appendix E on page 148 and 151.

As we now have velocity and acceleration "measurements" for the three test series: Stair, Sawtooth and Step, we know all the signals in both the mechanical and the hydraulic part of the model, and we are therefore able to proceed with the verification.

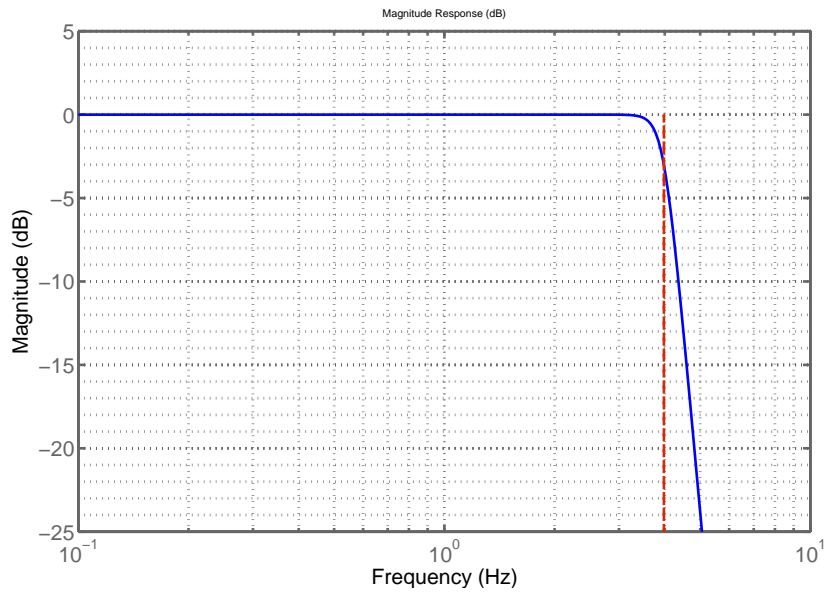


Figure 5.3: Magnitude characteristics of the 12'th order Butterworth filter.

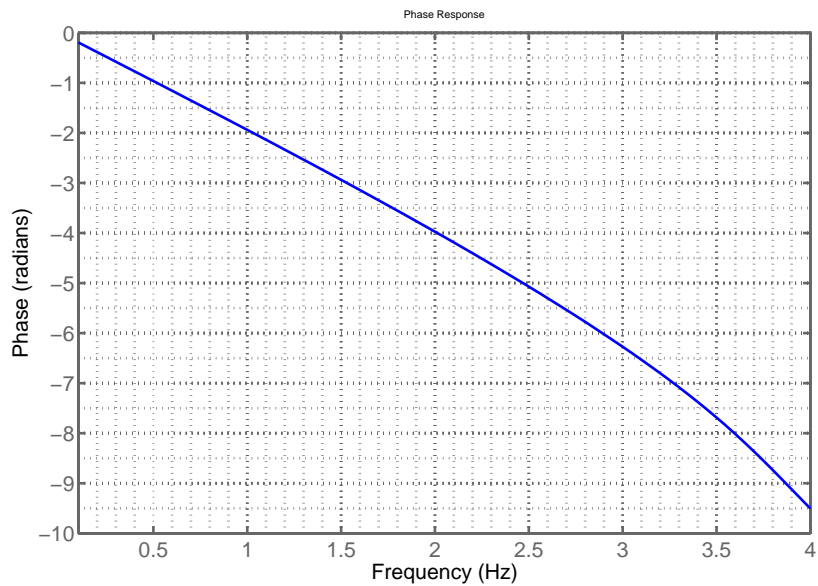


Figure 5.4: Phase characteristics of the 12'th order Butterworth filter. Even though the phase lag is very larger within the bandwidth of the filter, it does not affect the output as the input is applied both forward and backward through the filter, obtaining zero-phase filtering [Matlab, 2012a]

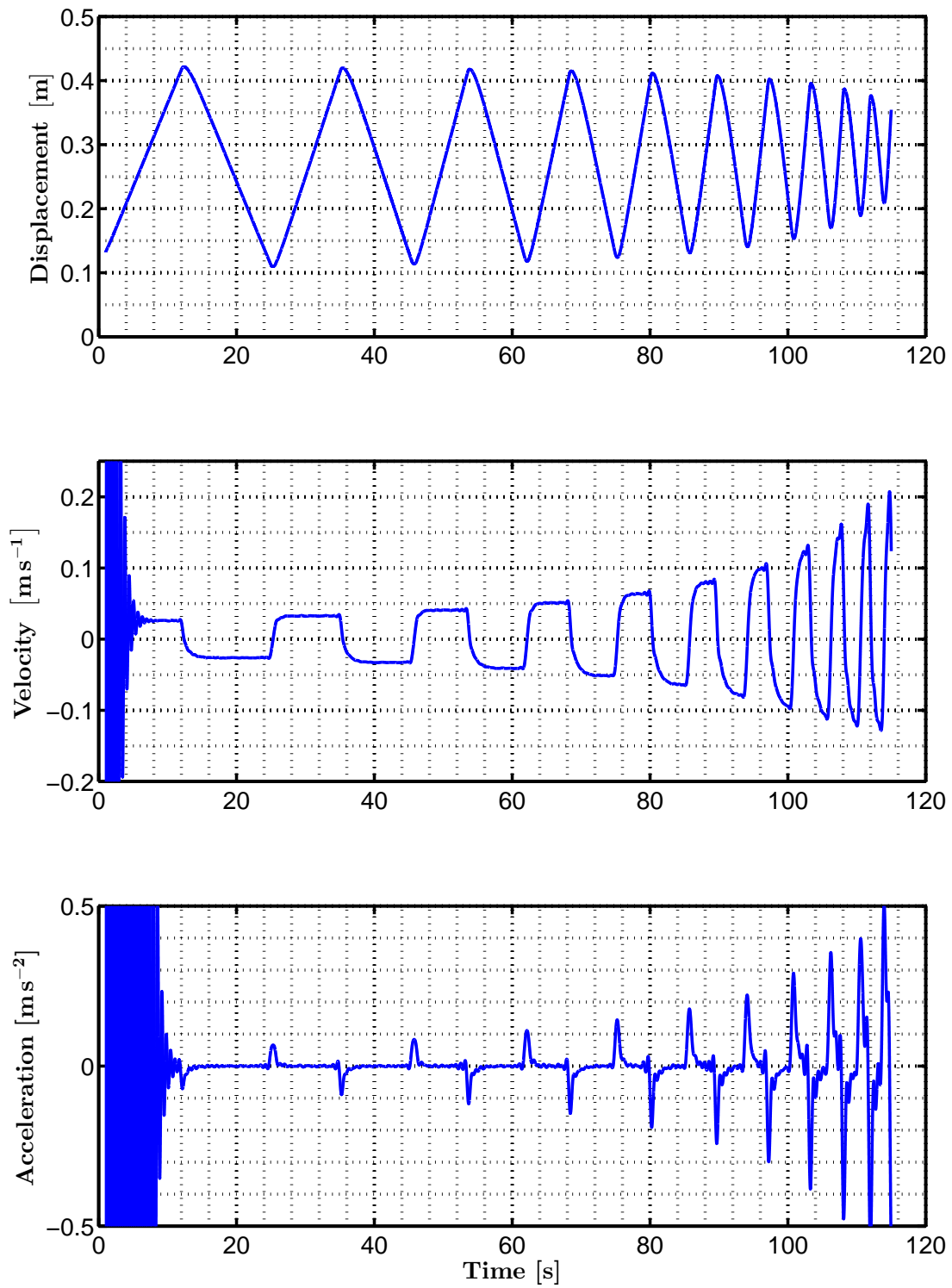


Figure 5.5: Result of filtering of the **Sawtooth** trajectory. The transient period in the beginning of the response is very significant and it is due to the high order of the filter. The acceleration and velocities in these regions is not correct, and therefore not used for validation.

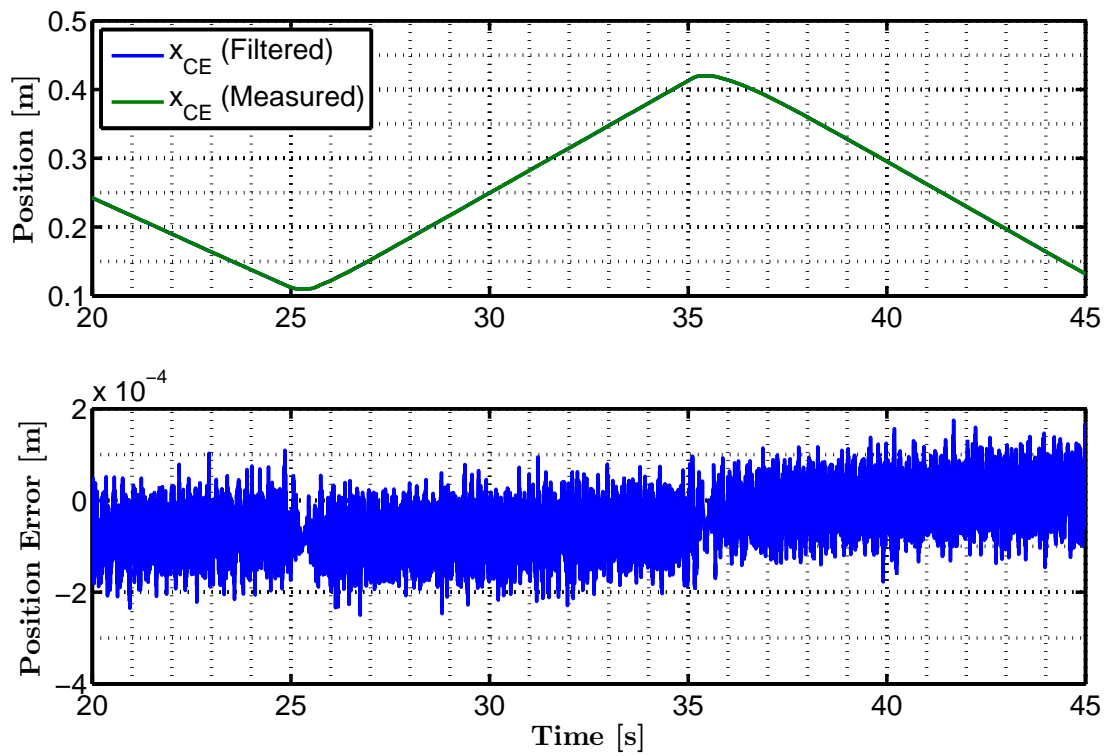


Figure 5.6: Position error of **Sawtooth** trajectory. The acceleration, obtained from differentiation and filtering, is integrated twice and compared to the original position signal.

5.2 Verification of Mechanical Model

The main equation of the mechanical model is from (4.42), and repeated here:

$$M(x_{CE}) \ddot{x}_{CE} = F_L - B(x_{CE}, \dot{x}_{CE}) \dot{x}_{CE} - F(t) \quad (5.1)$$

From the measurements of the two chamber pressure p_A and p_B we are able to obtain an expression for the cylinder force by using Equation (4.35), repeated below, if we assumed that we know the cylinder piston areas A_A and A_B precise.

$$F_L = A_A p_A - A_B p_B \quad (5.2)$$

As the position x_{CE} , the velocity \dot{x}_{CE} and the acceleration \ddot{x}_{CE} is known, we can solve for expressions of $M(x_{CE})$, $B(x_{CE}, \dot{x}_{CE})$ and $F(x_{CE})$ and compare them to expressions for these quantities seen in the system summary on page 30. Due to the complexity of the expressions and number of parameters it requires extensive tuning of the parameters to yield a satisfying result. The tuning parameters are listed in Table 5.1.

Name	Symbol	Unit
Equivalent Mass	m	[kg]
Distance to Center of Mass	L_{AD}	[m]
Angle to Center of Mass	a_3	[rad]
Viscous Friction Coefficient	ν_X	[kg/s]
Moment of Inertia	J_L	[kg m ²]

Table 5.1: Tuning parameters in the Mechanical part of the model.

Instead of tuning all parameters at once, we have chosen trajectories that allow them to be tuned in steps. First step is to find the parameters (m , L_{AD} , a_3) of the gravitation force $F(t)$.

5.2.1 Gravitation Force $F(t)$

The stair trajectory, as seen in Figure 5.7, have 10 periods of stationary position. In these positions the velocity \dot{x}_{CE} and the acceleration \ddot{x}_{CE} is zero, and the equation of (5.1) simplifies to:

$$F_L = F(t) \quad (5.3)$$

As we are able to measure the cylinder Force F_L we can determine the friction parameter $F(t)$ from (5.3). The friction parameter $F(t)$ is assumed to be dominated by the gravitation force as modeled by Equation (4.47), and repeated below:

$$F(t) = F_R - \underbrace{\frac{L_{AD} g m}{G_2(x_{CE})} \cos \left[a_1 - a_2 - a_3 - \arccos \left(\frac{L_{AB}^2 - (L_{BE} + x_{CE})^2 + L_{AC}^2}{2 L_{AB} L_{AC}} \right) \right]}_{F_T} \quad (5.4)$$

Therefore, the non-linear friction F_R containing e.g. Coulomb friction and Stiction is ignored for now.

For each stationary period a single point is chosen. The points are equally distributed and seen in Figure 5.7. Each point has a corresponding set of chamber pressure p_A and p_B , which is used to calculate a cylinder force using (5.2), which due to (5.3) and the assumption $F_R = 0$ equals the gravitational force F_T .

The initial value of the equivalent mass m , the distance to C.o.M. (Center of Mass), L_{AD} , and the angle to the C.o.M. a_3 is chosen as in (5.5). A figure illustrating the quantities on the system is seen in Figure

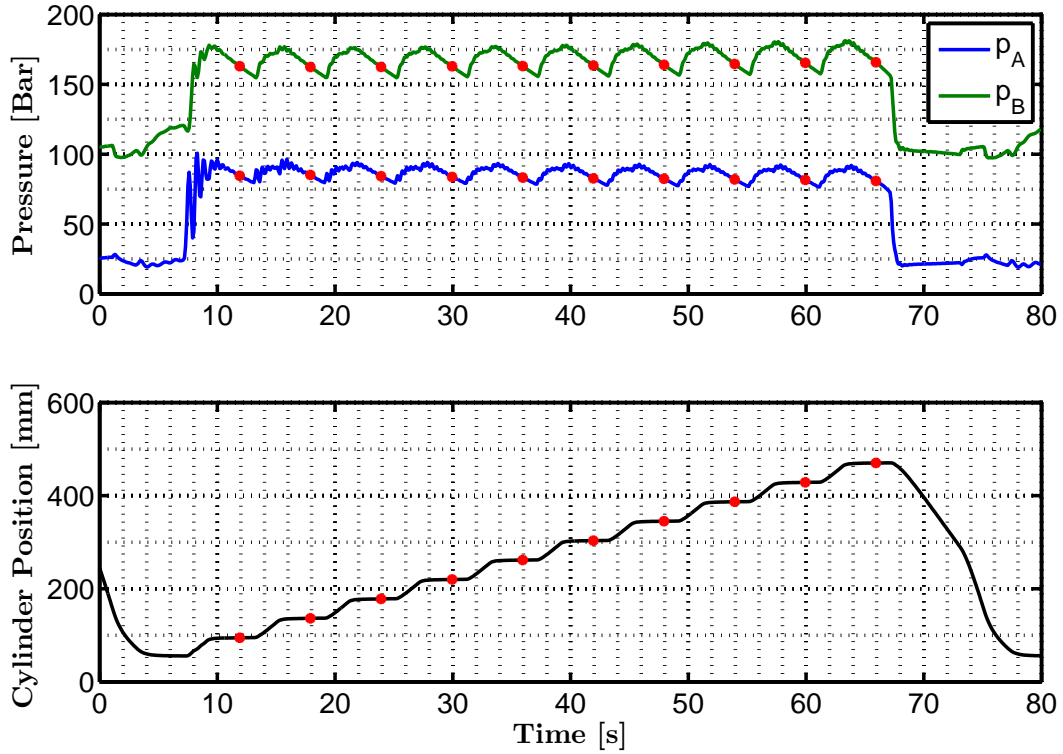


Figure 5.7: Measured values of chamber A and B pressure, (p_A p_B), along with cylinder position x_{CE} .

4.3 on page 23.

$$m = 1000 \text{ kg} \quad L_{AD} = 2.5 \text{ m} \quad a_3 = 0.2 \text{ rad} \quad (5.5)$$

A plot of the calculated gravitational force F_T using the values of (5.5) together with the "measured" values, calculated from the stationary points, are seen in Figure 5.8.

To obtain a better correlation between the two plots the parameters must be adjusted. How, is not very clear from the expression of (5.4) and therefore a numerical optimization algorithm is used instead. The cost function being the squared error between the two plots. Hence, the optimization algorithm is minimizing the squared distance between the two plots. The chosen algorithm is an unconstrained simplex method which has the advantage that it do not require derivative information like gradient based algorithms do [Matlab, 2012b]. The method is invoked through the Matlab command `fminsearch(x)`, and after 98 consecutive iterations the algorithm converges at the new values seen in (5.6).

$$m = 1288 \text{ kg} \quad L_{AD} = 2.08 \text{ m} \quad a_3 = 0.094 \text{ rad} \quad (5.6)$$

The gravitational force is calculated again, this time with the new parameter values, resulting in the adjusted plot seen in Figure 5.9.

If the assumption that F_R could be neglected is valid the plot in Figure 5.9 show a good correlation between the modeled and the measured values. This determines 3 of the 5 parameters in the mechanical model, see Table 5.1, and left are only the viscous friction ν_X and the moment of inertia J_L . First the viscous friction coefficient is determined.

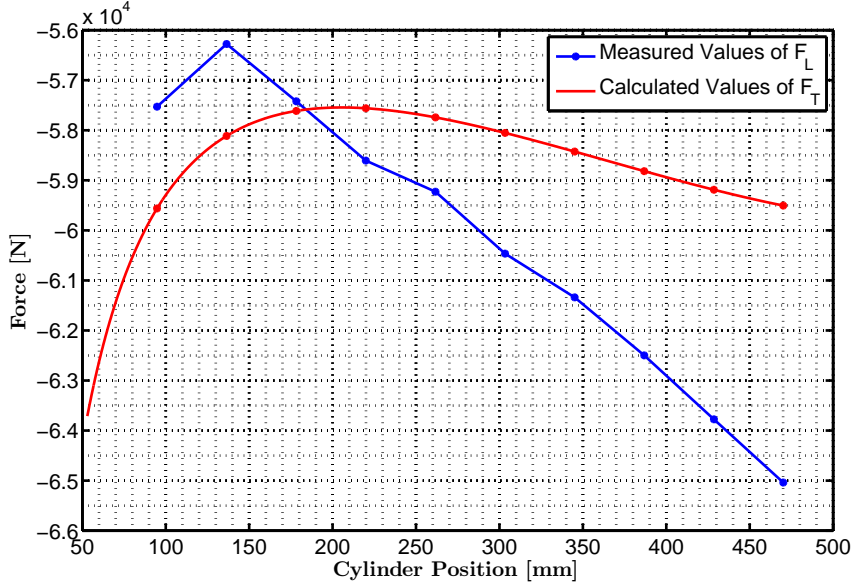


Figure 5.8: The cylinder force F_L calculated from the *measured* pressures, along with the gravity force F_T calculated using equation (4.45) of the mechanical model.

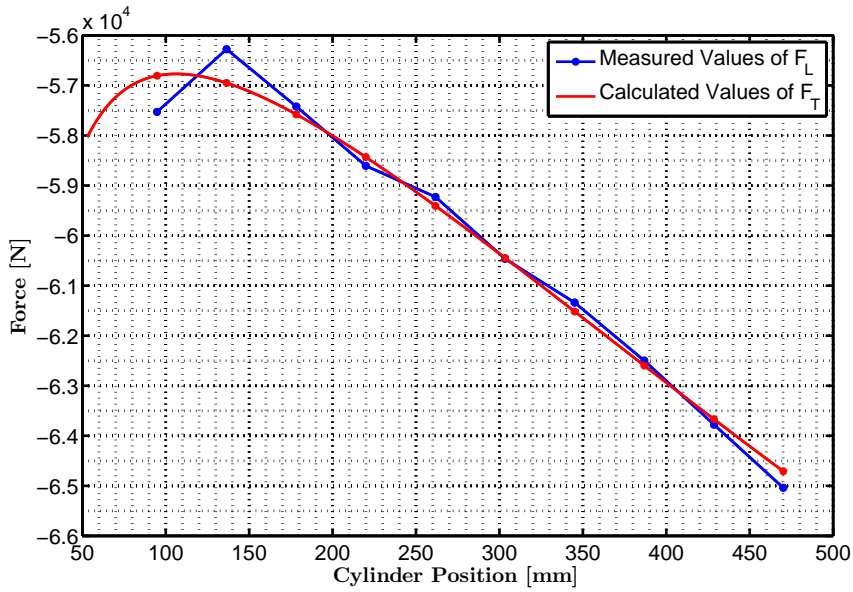


Figure 5.9: This figure show the cylinder force F_L calculated from the *measured* pressures, along with the gravity force F_T calculated using equation (4.45) of the mechanical model. The parameters m , a_3 and L_{AD} have been altered to the values found from optimization.

5.2.2 Viscous Friction B

The Sawtooth trajectory as seen in Figure 5.11 has 22 periods of approximately constant velocity. In these periods the acceleration is assumed zero, and the viscous friction force $B \dot{x}_{CE}$ is determined from Equation (5.1) as:

$$B \dot{x}_{CE} = F_L - F(t) \quad (5.7)$$

Like for the stair trajectory a point in each period is chosen. This time for a cylinder position at $x_{CE} = 0.3$ m. The cylinder force is calculated from the chamber pressure p_A and p_B using (5.2) and the data shown in Figure 5.11. The result is seen in the top figure of 5.10.

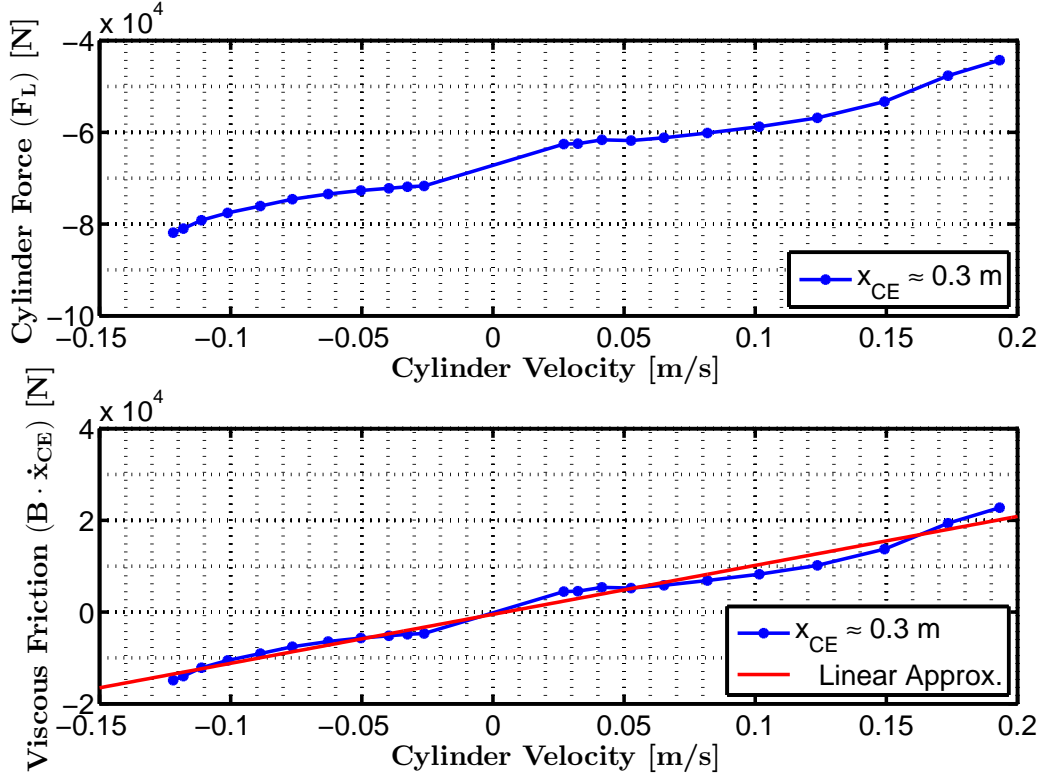


Figure 5.10: Top: Plot of the measured cylinder force, calculated using (5.2). Bottom: Viscous friction force and linear approximation. The slope of the linear approximation is the viscous friction coefficient B .

Besides the cylinder force F_L , in the expression (5.7), we also need the friction force $F(t) = F_R + F_T$. Again, the nonlinear friction F_R is neglected, and therefore we have $F(t) = F_T$. As all points of Figure 5.11 are chosen in $x_{CE} = 0.3$ m, the cylinder force F_T attains a single value as seen in Figure 5.9.

Plotting the viscous Friction $B\dot{x}_{CE}$ calculated from (5.7), using the cylinder force calculated from the red points seen in Figure 5.11, and the friction force for $x_{CE} = 0.3$ m in Figure 5.9 yields the result seen in the bottom of Figure 5.10. The parameter B is determined as the slope of the linear approximation shown as a red line. It is assumed that the parameter ν_X dominates in the expression for B , and therefore chosen as:

$$\nu_x \approx B \approx 106.8 \text{ kN s/m} \quad (5.8)$$

This assumption is asserted by considering the derived expression for B repeated in (5.9).

$$B = \frac{J_L \dot{x}_{CE}}{G_1(x_{CE}) G_2(x_{CE})} \left(1 - \frac{(2L_{BE} + 2x_{CE})^2 (L_{AB}^2 - (L_{BE} + x_{CE})^2 + L_{AC}^2)}{8G_1(x_{CE})^2} \right) + \nu_X \quad (5.9)$$

Assuming constant coefficients in (5.9) it only depends on the position x_{CE} and the velocity \dot{x}_{CE} , and for a fixed position; only velocity. In figure 5.10 we have a fixed position, at $x_{CE} = 0.3$ m and an approximately constant B , independent of the velocity \dot{x}_{CE} . The conclusion is therefore that the terms involving the velocity in (5.9) is neglectable, at least for a position of $x_{CE} = 0.3$ m, and the assumption that $\nu_X \approx B$ is asserted.

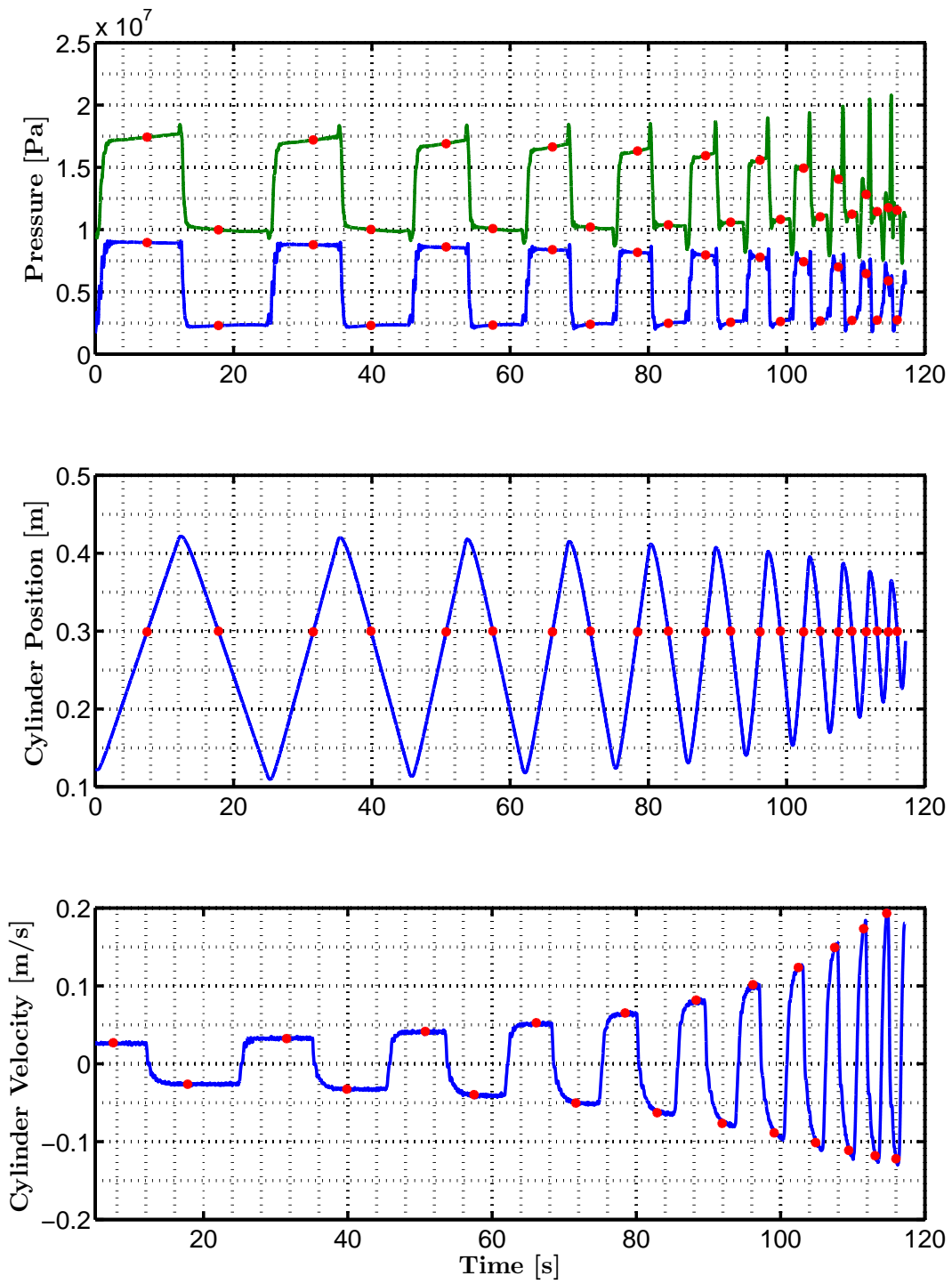


Figure 5.11: Top Figure: Measured values of A and B pressure. Mid Figure: Measured cylinder position. Bottom Figure: Measured Velocity. (Through differentiation and filtering of position).

5.2.3 Inertia M

All parameters, besides the moment of inertia J_L , have been determined systematically. To complete the tuning of the mechanical model 20s of the stair trajectory is considered. All trajectories yield inertia information and the reason for choosing the stair trajectory is that this is assumed to have the smallest error in the acceleration "measurement". This assumption is based on Figure E.1 on page 148 in Appendix E, which show a smaller error than for both the sawtooth trajectory in Figure 5.6 and the step trajectory in Figure E.4. However, all trajectories could be used for final validation and to find the moment of inertia J_L .

The chosen part of the stair trajectory is seen in Figure 5.13 on page 42, and the acceleration error after J_L has been tuned, is seen in Figure 5.12 below.

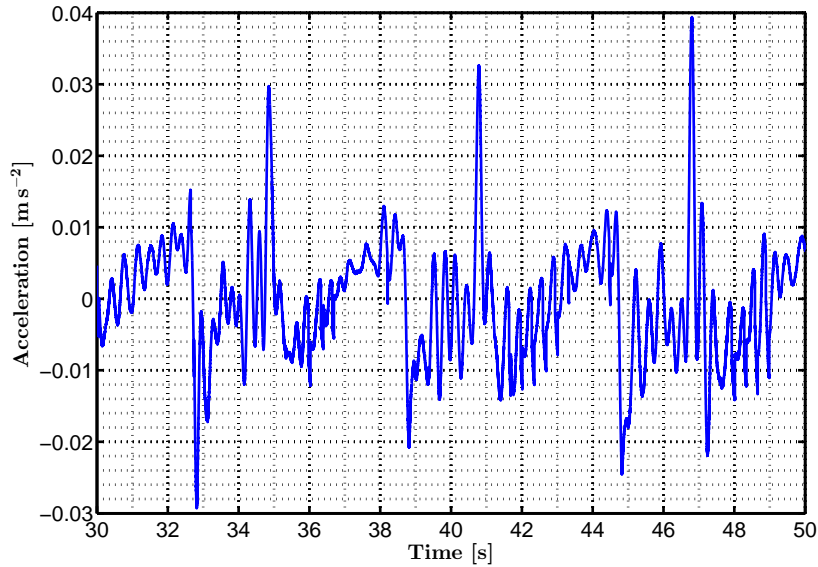


Figure 5.12: Difference in acceleration for the stair trajectory between simulated and measured values. See Figure 5.13.

The chosen value for the moment of inertia is:

$$J_L = 23404 \text{ kg m}^2 \quad (5.10)$$

The simulations for the two verification figures 5.12 and 5.13 uses the *measured* position and velocity to calculate the acceleration, so that the accumulated error in the simulated position and velocity do not alter the simulated value of the acceleration.

The model seems to correspond with the measurements, and it is therefore assumed to yield a sufficiently precise response for both controller design purposes and evaluation. All the values determined in the verification is listed in Table 5.3 on page 48 which concludes the verification of the mechanical model.

In the next section the hydraulic part is verified together with the valve.

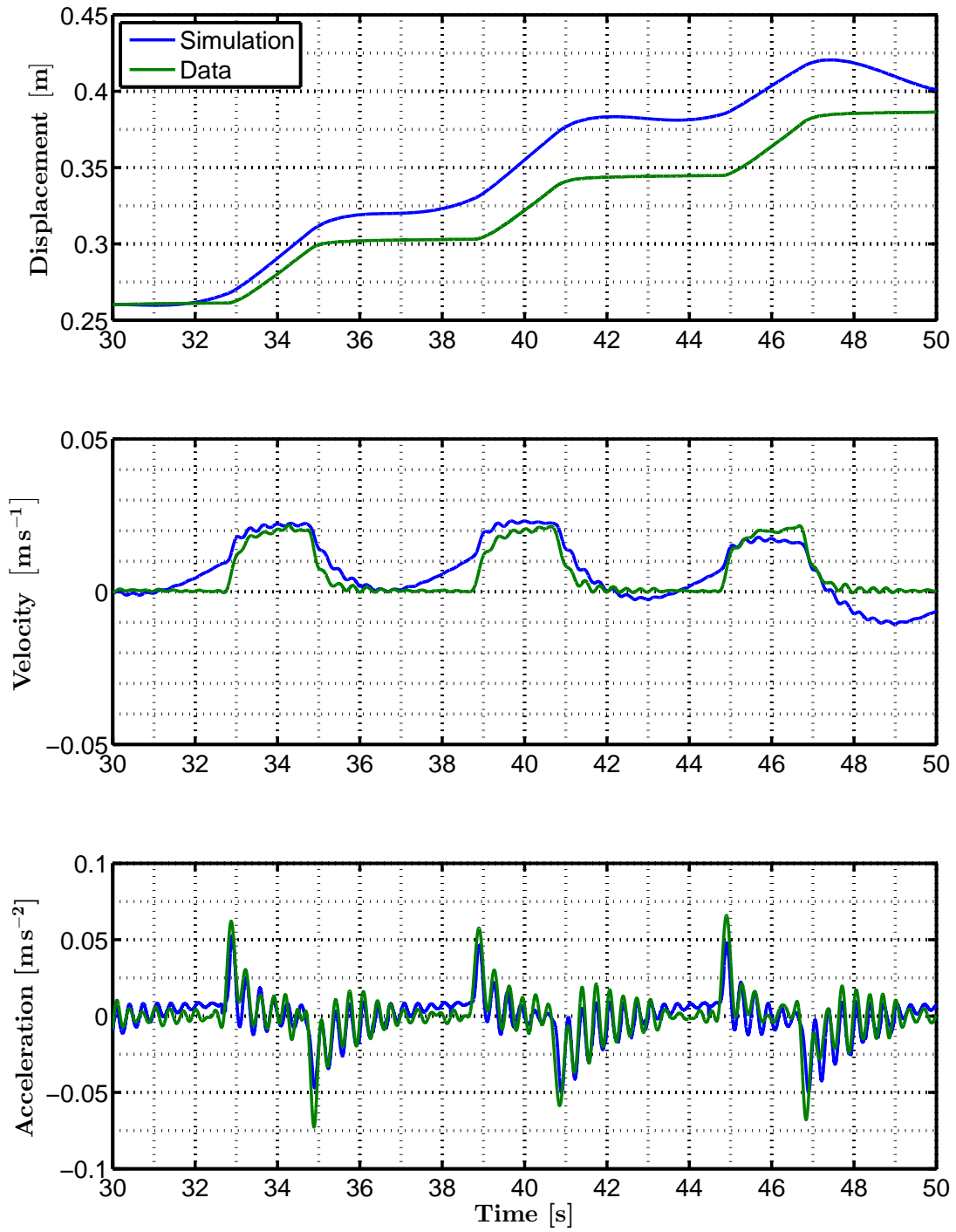


Figure 5.13: Final comparison of simulated and measured data for 20 seconds of the stair trajectory.

5.3 Verification of the Combined Hydraulic-Valve Model

The main equations in the hydraulic model are (4.48) and (4.49), seen on page 30 and repeated below:

$$\dot{p}_A = \frac{\beta}{V_{A0} + A_A x_{CE}} (K_A x_V R_A - \dot{x}_{CE} A_A - C_L(p_A - p_B)) \quad (5.11)$$

$$\dot{p}_B = \frac{\beta}{V_{B0} - A_B x_{CE}} (-K_B x_V R_B + \dot{x}_{CE} A_B + C_L(p_A - p_B)) \quad (5.12)$$

The cylinder piston areas A_A and A_B are known and assumed precise:

$$A_A = 0.0127 \text{ m}^2 \quad A_B = 0.0101 \text{ m}^2 \quad (5.13)$$

As there is no coefficients to determine in the functions R_A and R_B , the parameters to be tuned are the rest of the parameters seen in the two above equations. The parameters are listed in Table 5.2 below.

Name	Symbol	Unit
Initial Volume A	V_{A0}	$[m^3]$
Initial Volume B	V_{B0}	$[m^3]$
Flow Constant A	K_A	$[m^2/s\sqrt{Pa}]$
Flow Constant B	K_B	$[m^2/s\sqrt{Pa}]$
Bulk Modulus	β	$[Pa]$
Leakage Coefficient	C_L	$[m^3/sPa]$

Table 5.2: Tuning parameters in the hydraulic part of the model.

5.3.1 Initial Volumes V_{A0} and V_{B0}

The initial volumes are the volumes of chamber A and B where the cylinder is fully retracted i.e. $x_{CE} = 0$. By considering the geometry of the pipes and hoses connecting the hydraulic parts of the system, we are able to determine the volumes relatively precise. A sketch of the hydraulic system is seen in Figure 5.14. Both orifices on A and B port of the valve are shot, so the accumulators are neglected in the calculation.

The volumes are calculated using the values seen in the figure 5.14, and additionally assuming that the length of the *cylinder* B chamber is 80 cm when the piston is fully retracted, yielding a B volume inside the cylinder of: $A_B \cdot 0.8\text{m} = 8.08 \text{ L}$.

$$\begin{aligned} V_{A0} &= \pi \left(\frac{0.0159 \text{ m}}{2} \right)^2 (6 \text{ m} + 1 \text{ m} + 1 \text{ m} + 0.5 \text{ m}) \\ &= 1.688\text{e-}3 \text{ m}^3 = 1.688 \text{ L} \end{aligned} \quad (5.14)$$

$$\begin{aligned} V_{B0} &= \pi \left(\frac{0.0159 \text{ m}}{2} \right)^2 (6 \text{ m} + 1 \text{ m} + 1 \text{ m} + 1 \text{ m}) + A_B 0.8 \text{ m} \\ &= 9.867\text{e-}3 \text{ m}^3 = 9.867 \text{ L} \end{aligned} \quad (5.15)$$

o: Outer Diameter Black: Steel Pipe i:15.9 mm, o:20 mm
i: Inner Diameter Blue: Rubber Hose i:15.9 mm, o:26 mm
l: length Red: Rubber/Steel. i:20.0 mm, o:30 mm

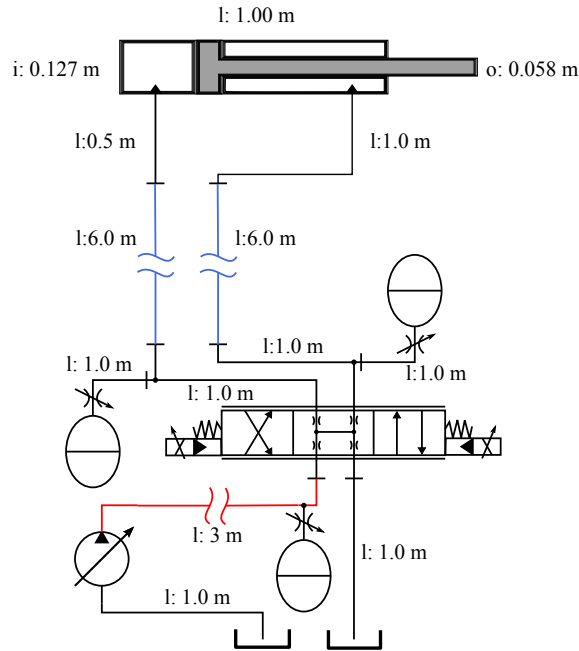


Figure 5.14: Overview of the main cavities and volumes in the hydraulic system.

5.3.2 Flow Constants K_A and K_B

The model has two flow constants but one is enough to model the valve this particular valve as from [Rexroth, 2006, p.2 (Type: V1)] the relationship between them are:

$$K_B = \frac{1}{2} K_A \quad (5.16)$$

The data for K_A is obtained from an internal simulation program from Bosch Rexroth called "D&C System Simulator" [Rexroth, 2012a]. The value of K_A is:

$$K_A = 6.4974e-4 \text{ m}^2 / s\sqrt{Pa} \quad (5.17)$$

As the four constants V_{A0} , V_{B0} , K_A , K_B have been determined, left are only the bulk modulus β and leakage coefficient C_L .

5.3.3 Bulk Modulus β and Leakage Coefficient C_L

Like for the verification of the mechanical model in the previous section we use the measured velocity and position so that the the simulated values do not introduce errors in the pressure calculations. As the pump-pressure has large variations, see Figure E.5 in Appendix E, this is fed into the simulations as well instead of just using a constant.

The chosen trajectory is the step trajectory. This trajectory is generated by making an open-loop step in u from 0 to +3V and from +3V to -3V, and then stepping up from -3V to 0V again. This is seen in the bottom plot of Figure 5.15 on the next page. The reason for choosing steps is to reveal the transient dynamics of the hydraulic system.

After tuning the values of bulk modulus β and the leakage coefficient C_L , the simulation show the pressures seen in the top two figures of Figure 5.15. The leakage coefficient is primarily responsible for the response where $u=0$ and bulk modulus adjusts most of the dynamic part of the response. The chosen values are:

$$\beta = 10000 \text{ Bar} = 1 \text{ GPa} \quad C_L = 1.1\text{e-}12 \text{ m}^3/\text{s Pa} \quad (5.18)$$

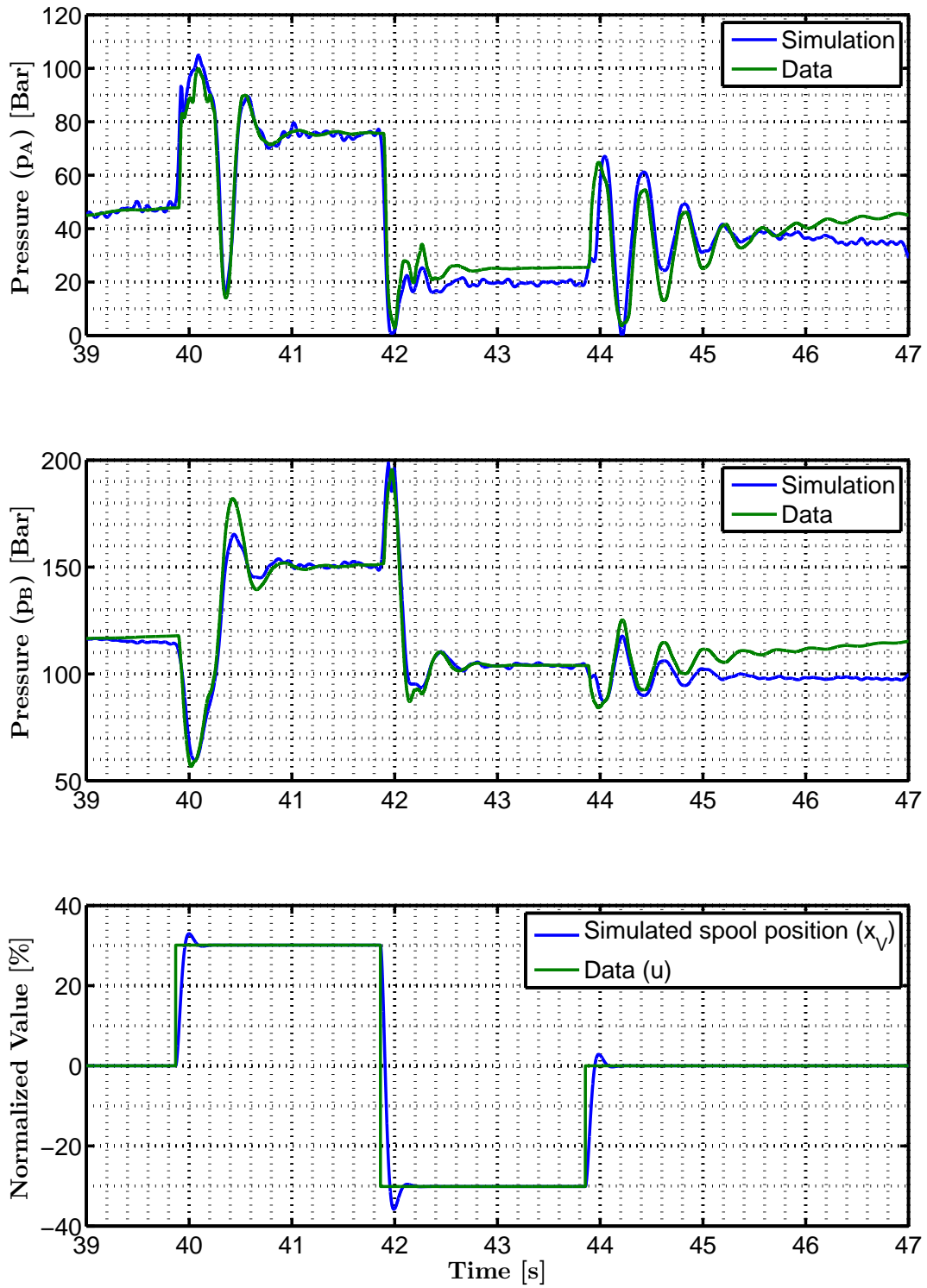


Figure 5.15: Comparison of simulated and measured data for verification of the hydraulic-valve part of the model. The data is the 8 active seconds of the **step** trajectory. Top: Chamber A pressure. Mid: Chamber B Pressure. Bottom: Normalized control signal and spool position.

Drifting occur in the pressure measurements of the last period in the graph (after 44s). Leakage between the two chambers defined by C_L cannot explain this. If it was leakage between the chambers the pressure change would be in opposite direction for each chamber. However, it might be explained by leakage flow through the critical center valve (null-lap). The model do not take this into account so for $u=0$ the valve have $Q_A = Q_B = 0$, and in reality there is a leakage flow. The datasheet has a figure showing this (see Figure 5.16). The amount of leakage flow is hard to state precise when the spool position is not exactly known and therefore the figure is only shown to state that a leakage flow probably exist when $u=0$.

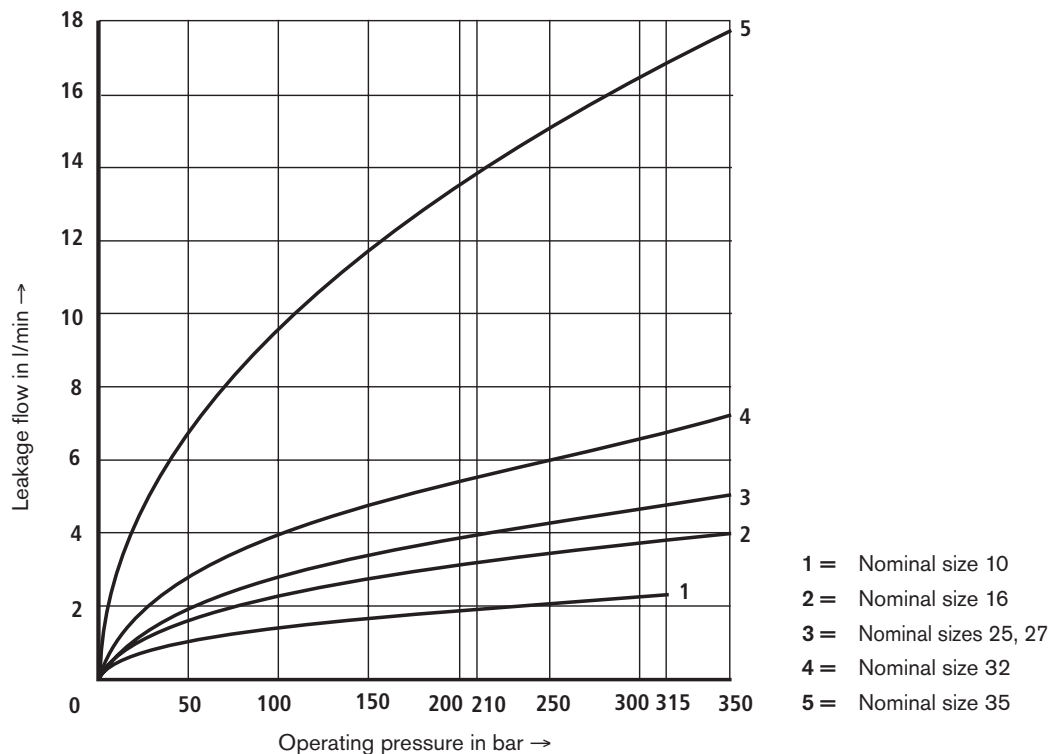


Figure 5.16: Leakage flow through the critical center valve. The nominal size of the valve is NS10 and it is therefore the bottom graph that are considered.

To obtain the result seen in 5.15 the valve parameters have also been tuned. In Section 4.4 the valve parameters were determined as:

$$\omega_V = 314.16 \text{ rad/s} \quad (5.19)$$

$$\zeta_V = 1 \quad (5.20)$$

But changing the parameters to $\zeta_V = 0.6$ and $\omega_V = 30 \text{ rad/s}$ makes a good correlation between the simulated and measured pressures as seen in Figure 5.15. The values are changed significantly from the expected based on data from [Rexroth, 2006]. The reason is probably that the pilot stage controlling the spool position has *internal* supply, meaning that it is supplied by the pump pressure directly. As the pump pressure fluctuates as seen in E.5 on page 151 the performance of the internal spool position control is reduced.

The valve parameters are not altered in the model, but the conclusion is that for the valve to be neglectable in the controller design, the pump pressure must be stabilized, or the pilot stage must have external supply, otherwise the reduced performance of the valve might influence the performance of the controllers as well.

As all parameters listed in Table 5.2 have been determined, and as the response of the simulations is assumed to correspond sufficiently precise with the measurements, the hydraulic model is now verified. The tuning parameters and their new values are listed in Table 5.4, on page 48.

Name	Symbol	Value	Unit
Equivalent Mass For Gravity	m	1288	[kg]
Distance to Center of Mass	L_{AD}	2.08	[m]
Angle to Center of Mass	a_3	0.094	[rad]
Viscous Friction Coefficient	ν_X	$106.8 \cdot e^3$	[kg/s]
Moment of Inertia	J_L	23404	[kg m^2]

Table 5.3: Final values of the parameters in the verified **mechanical** part of the model.

Name	Symbol	Value	Unit
Initial Volume A	V_{A0}	1.688 e-3	[m^3]
Initial Volume B	V_{B0}	9.867 e-3	[m^3]
Flow Constant A	K_A	6.4974e-4	[$m^2/s\sqrt{Pa}$]
Flow Constant B	K_B	2.1658 e-4	[$m^2/s\sqrt{Pa}$]
Bulk Modulus	β	1.000 e9	[Pa]
Leakage Coefficient	C_L	1.1e-12	[m^3/sPa]

Table 5.4: Final values of the parameters in the verified **hydraulic** part of the model.

Chapter 6

Model Simplification and Linearization

As mentioned in the introduction to Chapter 4 a Simplified Model and a Linearized Model have been developed. The two models have the following purposes and simplifications.

Simplified Model This model is used for trajectory planning in Chapter 11. It is equivalent to the Simulation Model except for neglected valve dynamics and a steady state simplification in the hydraulic part of the model. The model is derived in Appendix A.

Linearized Model The linearized model is a linearized version of the Simplified Model. All equations are linearized around an operating point using a first-order Taylor expansion. This is seen in Appendix B.

The result from the simplification in Appendix A and the linearization in Appendix B are summarized below. For a detailed discussion we refer to the respective chapters in appendix.

6.1 Simplified Model

Steady state flow relation:

$$\alpha Q_A = -Q_B \quad (6.1)$$

For **positive** control signal $u \geq 0$:

$$p_A = \frac{\alpha^3 p_P + \alpha \sigma^2 p_T + \sigma^2 p_L}{\sigma^2 + \alpha^3} \quad p_B = \frac{\alpha^2 p_P + \sigma^2 p_T - \alpha^2 p_L}{\sigma^2 + \alpha^3} \quad (6.2)$$

$$Q_A = K_L u \sqrt{p_P - \alpha p_T - p_L} \quad Q_B = -\alpha K_L u \sqrt{p_P - \alpha p_T - p_L} \quad (6.3)$$

For **negative** control signal $u < 0$:

$$p_A = \frac{\alpha^3 p_T + \alpha \sigma^2 p_P + \sigma^2 p_L}{\sigma^2 + \alpha^3} \quad p_B = \frac{\alpha^2 p_T + \sigma^2 p_P - \alpha^2 p_L}{\sigma^2 + \alpha^3} \quad (6.4)$$

$$Q_A = K_L u \sqrt{\alpha p_P - p_T + p_L} \quad Q_B = -\alpha K_L u \sqrt{\alpha p_P - p_T + p_L} \quad (6.5)$$

With:

$$K_L = \frac{\sigma K_A K_V}{\sqrt{\sigma^2 + \alpha^3}} \quad \alpha = \frac{A_B}{A_A} \quad \sigma = \frac{K_B}{K_A} \quad (6.6)$$

Virtual load pressure:

$$\dot{p}_L = \frac{\beta}{\gamma V_{AL}} [(\gamma + \alpha^2)Q_A - (\gamma + \alpha)C_{LF}p_L - (\gamma + \alpha^2)A_A\dot{x}_{CE}] \quad (6.7)$$

With:

$$\gamma(x_{CE}) = \frac{V_{BL}(x_{CE})}{V_{AL}(x_{CE})} \quad V_{AL}(x_{CE}) = V_{A0} + A_A x_{CE} \quad V_{BL}(x_{CE}) = V_{B0} - A_B x_{CE} \quad (6.8)$$

6.2 Linearized Model

The linearized system is re-arranged for controller design purposes into the system structure seen in Figure 6.1. The linearized model describes the system in an operating point. The most critical operating

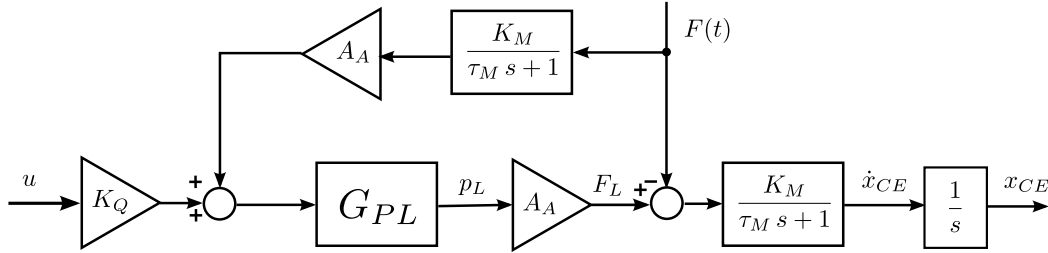


Figure 6.1: Block diagram of system used for controller design.

point with respect to stability is investigated in Section D. The parameter values also influence the stability margins of the system and the most critical value must be chosen in order to guarantee stability for all the values the parameters can attain. The parameter variations are seen and discussed in Section C. The chosen operating point and critical parameter values are summarized in Table D.2 and 6.2.

Name	Symbol	Symbolic Value	Value	Unit
Input Signal	u_0	-	0.00	[V]
Cylinder Position	x_{CE0}	x_{CEMIN}	0.0530	[m]
Cylinder Velocity	\dot{x}_{CE0}	-	0.00	[m/s]
Load Pressure	p_{L0}	p_{LMIN}	-119 e5	[Pa]

Table 6.1: Critical operating point for the linearized system.

6.2.1 Linearized Model Equations

A linearized model covering all operating points have been derived in Section B, but after investigating the critical operating point, presented in Section D, the model could be simplified. It is the simplified linearized model that is summarized here. This is the only linear model that is used for controller design and when referring to the "linearized model" it is the summarized here that is considered.

Name	Symbol	Symbolic Value	Value	Unit
Initial Volume A	V_{A0}	V_{A0MAX}	2.0256 e-3	$[m^3]$
Flow Constant A	K_A	K_{AMAX}	7.7969 e-4	$[m^2/s\sqrt{Pa}]$
Bulk Modulus	β	β_{MIN}	1000 e5	$[Pa]$
Leakage Coefficient	C_{LF}	C_{LFMIN}	0 e-12	$[m^3/sPa]$

Table 6.2: Critical parameter values for the linearized system.

The mechanical coefficients are independent of the control signal, and defined as:

$$K_M = \frac{1}{B} \quad \tau_M = \frac{M}{B} \quad (6.9)$$

In the operating point the parameters are:

$$M = 451.16e3 \text{ kg} \quad B = 478.74e3 \text{ s/m} \quad (6.10)$$

The parameters are for the upright position where the cylinder is almost parallel with the robot arm, which is the reasons for the large values as described in Appendix C on page 135. The parameters leads to:

$$K_M = 2.09 \text{ e-6 m/Ns} \quad \tau_M = 0.9424 \text{ s} \quad \Leftrightarrow \quad \omega_M = \frac{1}{\tau_M} = 1.06 \text{ rad/s} \quad (6.11)$$

When $u_0 = 0$ the *flow gain* is the only parameter that changes for positive and negative control signal / spool position. In the chosen critical point the cylinder force demands a $p_L = \frac{F_L}{A_A}$ that push $p_A = p_P$ and $p_B = p_T$, making the flow gain K_Q as high as possible. When considering negative displacement the critical value of p_L is when $p_L = p_P - \alpha p_T$.

$$K_Q = K_L \sqrt{(\alpha + 1)(p_P - p_T)} \quad u \geq 0 \quad (6.12)$$

The linearized Load-Pressure Model:

$$G_{PL}(s) = K_{PL} \frac{\omega_{PL}^2 (\tau_M s + 1)}{s^2 + 2\zeta_{PL} \omega_{PL} s + \omega_{PL}^2} \quad (6.13)$$

With the coefficients

$$K_{PL} = \frac{K_H}{A_A^2 K_M} \quad \omega_{PL} = \sqrt{\frac{A_A^2 K_M}{\tau_M}} \quad \zeta_{PL} = \sqrt{\frac{1}{4 A_A^2 K_M \tau_M}} \quad (6.14)$$

If the DC-gains (K_M , K_H) and the time constants (τ_M , τ_H) are substituted we get:

$$K_{PL} = \frac{B}{A_A^2} \quad \omega_{PL} = \sqrt{\frac{A_A^2 \beta (\gamma + \alpha^2)}{M \gamma V_{AL}}} \quad \zeta_{PL} = \frac{B}{2 A_A} \sqrt{\frac{\gamma V_{AL}}{M \beta (\gamma + \alpha^2)}} \quad (6.15)$$

And if the critical parameter values are inserted we obtain:

$$K_{PL} = 2.983 \text{ e9 Pa/V} \quad \omega_{PL} = 3.951 \text{ rad/s} \quad \zeta_{PL} = 0.1343 \quad (6.16)$$

6.2.2 Verification of Linearized Model

The linearized model are verified by comparing the velocity \dot{x}_{CE} output for a step input u to the response from the non-linear Simulation Model (without valve dynamics and disturbance F). To do this both systems are included in a single Simulink model, and the integrators of the Simulation model are initialized to the operating point of the linear system. Then a very small input step of $\Delta u = 0.001$ V is applied and the result is seen in Figure 6.2. The small step is to verify the equations in the linear model, and see if they are able to describe the dynamics in the operating point, which is positively confirmed by Figure 6.2.

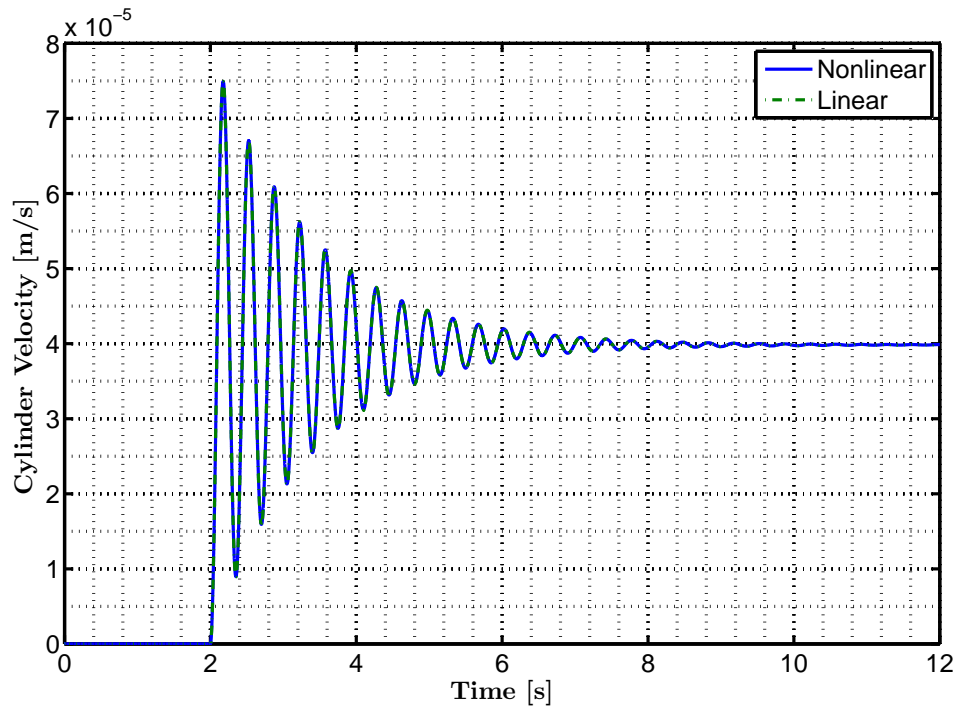


Figure 6.2: Response of the linear and the non-linear system to a very small step in input signal $\Delta u = 0.001$ V. This show that the linearization of the linear system is correct and therefore verifies the Linearized Model.

A larger step is also given $\Delta u = 0.5$ V and the result is seen in Figure 6.3. As the operating point of the linear system is the same as in Figure 6.2 the linear response is the same but scaled with the input amplitude i.e. $\frac{0.5}{0.001} = 500$ times larger. The parameters in the non-linear system changes as it gets further from the operating point which alter the response. The response have approximately the same frequency but is considerable more damped, and the steady state value is different as well. The change is only $\frac{0.5}{20} = 2.5\%$ of the whole input range, which indicates that the system is highly non-linear around the chosen operating point, and that a linear model describes the dynamics only in a narrow band.

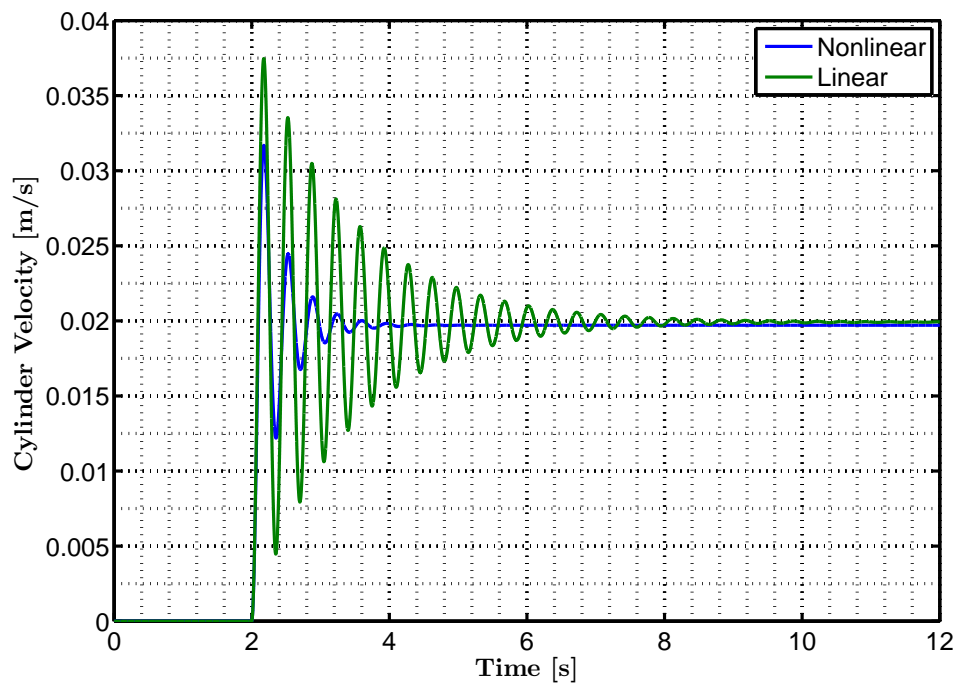


Figure 6.3: Response of the linear and the non-linear system to a step in input signal $\Delta u = 0.5$ V. This indicates that the linear system are having trouble describing the dynamics outside the operating point.

Part Conclusion and Summary

To summarize the content of the first part of the report it was concerned with three major objectives: System Model Development in Chapter 4, Model Verification in Chapter 5 and Model Simplification in Chapter 6.

In Chapter 4 the modeling was done with three main purposes:

1. Nonlinear controller design.
2. Evaluation of controller performance.
3. Determination of parameter variations and bounds.

and the system was split into three subsystems each modeled separately

1. Mechanical System (load)
2. Hydraulic System
3. Valve

The result was the so-called **Simulation Model**.

In Chapter 5 the Simulation Model was verified. The verification included determination of 11 tuning parameters and the verification yielded good correlation between measured and simulated data, which validated the hydraulic and mechanical parts of the simulation model. It was shown that the pump pressure was fluctuating which was assumed the cause for reduced valve performance in the test.

In Chapter 6 a simplified and a linearized model were introduced. The Linearized Model was verified to yield the same dynamic response as the Simulation Model close to the operating point, but reduced precision when moved a small range from the operating point.

To summarize, the following models have been used in the project:

Simulation Model A non-linear simulation model has been developed, this is used to evaluate the controller designs and to obtain the mechanical parameter variations. It is the foundation for the other models. The model (with ignored valve dynamics) is used for backstepping controller design in Chapter 7.

Simplified Model This model is equivalent to the Simulation Model except for neglected valve dynamics and a steady state simplification in the hydraulic part of the model, where the compression flow in each separate chamber is neglected. More about this in Section A. The model is used for trajectory planning in Chapter 11.

Linearized Model The linearized model is a linearized version of the Simplified Model. All equations are linearized around an operating point using a first-order Taylor expansion. See Section B. The model is used for linear controller design in Chapter 9 and 10.

This finalizes the part of the report concerned with system modeling and verification. All determined parameters are seen in tables 5.3 and 5.4. The equations used in the Simulation Model are summarized in Section 4.5 on page 30 and the equations used in the simplified and the linearized model are summarized in Section 6 on page 49. The next part of the report is concerned with *controller design*.

Part II

Controller Design

Chapter 7

Design of Robust Adaptive Backstepping Controller with Unknown Non-Linear Parameters

This chapter presents the backstepping controller that have been designed in the project. First the principle of backstepping is defined. Then the system equations are simplified and put on the right system form. After this, the actual backstepping-like controller design is presented and then some aspects of the controller is synthesized in order to give a better understanding of the developed control structure and to highlight some practical complications of the developed controller. Conclusively, the control law together with the parameter update law and parameter bounds are summarized.

7.1 Principle of Backstepping

In the backstepping procedure the designer obtains asymptotic stability for a set of error-variables \mathbf{z} , making $|\mathbf{z}| \rightarrow \mathbf{0}$ for $t \rightarrow \infty$, by recursively designing intermediate control laws for so-called "virtual controls". In each step the designer ensure that the sub-system considered is stable, often using a set of Lyapunov-like theories (See Chapter F). The method is used to obtain asymptotic tracking while guaranteeing global uniform stability of an equilibrium. [Zhou and Wen, 2008, p. 9].

7.2 Neglected Valve Dynamics

From the Model Summary Section 4.5, seen on page 30, we have all the equations describing the system. However, the need for spool position- and velocity feedback arises if a full-state-feedback controller is developed using the Simulation Model directly. To remove this demand and to reduce the dynamic order of the control system the valve-dynamics have been neglected in the derivation of the backstepping controller and the valve is modeled in steady state using

$$x_V = k_V u \quad (7.1)$$

As the spool position x_V is no longer a state in the model the control signal u can be used in the orifice equation instead

$$R_A(p_A, u) = s(u) \sqrt{p_P - p_A} + s(-u) \sqrt{p_A - p_T} \quad (7.2)$$

$$R_B(p_B, u) = s(u) \sqrt{p_B - p_T} + s(-u) \sqrt{p_P - p_B} \quad (7.3)$$

$$s(*) = \begin{cases} 1 & \text{if } * \geq 0 \\ 0 & \text{if } * < 0 \end{cases} \quad (7.4)$$

To summarize: The model used for the backstepping controller design is the Simulation Model with valve *dynamics* neglected, and the equations used are seen in the Simulation Model Summary Section 4.5 on page 30, but with the above equations describing the valve.

7.3 System Form

In order to apply the general backstepping control theory the system must be on a specific form called *pure-feedback-form* shown in Appendix G. The method is systematic if the system can be put on *strict-feedback-form* which is a sub-class of the pure feedback form. In our case we are only able to get a semi-strict-feedback system, which is shown later in this section. First

7.3.1 Semi-Strict Feedback Form

First the dynamic equations are put on state-space form by introducing the state-vector as:

$$\mathbf{x} = [x_{CE} \quad \dot{x}_{CE} \quad p_A \quad p_B]^T \quad (7.5)$$

$$\dot{x}_1 = x_2 \quad (7.6)$$

$$\dot{x}_2 = \frac{1}{M(x_1)} [A_A x_3 - A_B x_4 - B(x_1, x_2) x_2 - F(t)] \quad (7.7)$$

$$\dot{x}_3 = \frac{\beta}{V_{A0} + A_A x_1} [K_A x_V(u) R_A(\mathbf{x}, u) - A_A x_2 - C_L(x_3 - x_4)] \quad (7.8)$$

$$\dot{x}_4 = \frac{\beta}{V_{B0} - A_B x_1} [-K_B x_V(u) R_B(\mathbf{x}, u) + A_B x_2 + C_L(x_3 - x_4)] \quad (7.9)$$

By introducing the new state as the cylinder force $\bar{x}_3 = F_L = A_A x_3 - A_B x_4$ it is possible to put the first two state-equations (7.6) and (7.7) on (semi)-strict-feedback-form as in (7.10):

$$\begin{aligned} \dot{x}_1 &= x_2 \\ \dot{x}_2 &= \frac{1}{M(x_1)} [\bar{x}_3 - B(x_1, x_2) x_2 - F(t)] \\ \dot{\bar{x}}_3 &= \frac{\beta A_A}{V_{A0} + A_A x_1} [K_A K_V u R_A(\mathbf{x}, u) - A_A x_2 - C_L(x_3 - x_4)] \\ &\quad - \frac{\beta A_B}{V_{B0} - A_B x_1} [-K_B K_V u R_B(\mathbf{x}, u) + A_B x_2 + C_L(x_3 - x_4)] \end{aligned} \quad (7.10)$$

As the general form of strict-feedback systems do not allow for a term that is changing independent of the states, $d(t)$ is the reason why the second equation is only semi-strict-feedback, see Section G for a definition of strict-feedback-form. The system (7.10) can be represented in parameterized form as:

$$\begin{aligned}
\dot{x}_1 &= x_2 \\
\dot{x}_2 &= \theta_1 \bar{x}_3 - \theta_2 x_2 - d(t) \\
\dot{\bar{x}}_3 &= \frac{1}{\beta_A + x_1} [-\theta_3 x_2 - \theta_4 (x_3 - x_4) + \theta_5 u R_A(\mathbf{x}, u)] \\
&\quad - \frac{1}{\beta_B - x_1} [\theta_6 x_2 + \theta_4 (x_3 - x_4) - \theta_7 u R_B(\mathbf{x}, u)]
\end{aligned} \tag{7.11}$$

Where:

$$\begin{aligned}
\theta_1 &= \frac{1}{M(x_1)} & \theta_2 &= \frac{B(x_1, x_2)}{M(x_1)} & \theta_3 &= \beta A_A & \theta_4 &= \beta C_L & \theta_5 &= \beta K_A K_V \\
\theta_6 &= \beta A_B & \theta_7 &= \beta K_B K_V & \beta_A &= \frac{V_{A0}}{A_A} & \beta_B &= \frac{V_{B0}}{A_B} & d(t) &= \frac{F(t)}{M(x_1)}
\end{aligned}$$

$$\boldsymbol{\theta} = [\theta_1, \theta_2, \theta_3, \theta_4, \theta_5, \theta_6, \theta_7]^T \tag{7.12}$$

$$\begin{aligned}
R_A(x_3, u) &= s(u) \sqrt{p_P - x_3} + s(-u) \sqrt{x_3 - p_T} \\
R_B(x_4, u) &= s(u) \sqrt{x_4 - p_T} + s(-u) \sqrt{p_P - x_4}
\end{aligned} \tag{7.13}$$

The former states x_3 and x_4 are no longer a part of the new state-vector $\mathbf{x} = [x_1, x_2, \bar{x}_3]^T$. Therefore, the occurrence of the variables in the state-space model (7.11) *prevent* the last equation of the model from attending strict-feedback-form.

As a whole and in conclusion, the model (7.11) can be said to be on semi-strict-feedback form, which allows for a modified backstepping approach, this model is therefore used in the backstepping controller design presented next.

7.4 Backstepping Controller Design

The backstepping design procedure is *recursive*, meaning that it is divided into a number of steps determined by the order of the system. As the system (7.11) is 3. order we have 3 steps in the design procedure.

The first step describes a general step in the backstepping procedure, as the first equation in (7.11) involves no adaption nor disturbance terms. The second step is basic *adaptive* backstepping, but as the second term of (7.11) also includes a disturbance term $d(t)$ the choice of intermediate control law is more challenging and chosen in a special way to ensure robustness. The last step is again an altered form of the adaptive backstepping procedure as it involves non-linear parameters β_A and β_B .

The derivation will assume that the system is locally Lipschitz. This property is required in order to apply the Lasalle Yoshisawa Theorem F.4.2. Locally Lipschitz is described in Appendix F.4.3.

7.4.1 Step 1 - Basic Backstepping

First we define the error variable (z_1) for this first step as the tracking error:

$$z_1 = x_1 - x_d \tag{7.14}$$

with derivative:

$$\begin{aligned}
\dot{z}_1 &= \dot{x}_1 - \dot{x}_d \\
&= x_2 - \dot{x}_d
\end{aligned} \tag{7.15}$$

A standard quadratic, positive definite (PD) and radially unbounded Lyapunov function candidate is also defined:

$$V_1(z_1) = \frac{1}{2} z_1^2 \quad (7.16)$$

with derivative:

$$\begin{aligned} \dot{V}_1(z_1) &= z_1 \dot{z}_1 \\ &= z_1(x_2 - \dot{x}_d) \end{aligned} \quad (7.17)$$

Here we see x_2 as a virtual control variable and define for it an intermediate control law (x_{2d}) called a "*stabilizing function*". We choose x_{2d} , so that when $x_{2d} = x_2$ the derivative of the Lyapunov function candidate is negative definite (ND). According to Lyapunov's direct method (F.1) this will guarantee asymptotic stability of the equilibrium $z_1 = 0$ i.e. $|z_1| \rightarrow 0$ for $t \rightarrow \infty$. As z_1 is defined as the tracking error (7.14) asymptotic position tracking is achieved i.e. no error between the actual position x_1 and the desired position x_d when $t \rightarrow \infty$ and $x_{2d} = x_2$. The first intermediate control law is, from inspection of (7.17), chosen as:

$$x_{2d} = -k_1 z_1 + \dot{x}_d \quad k_1 > 0 \quad (7.18)$$

If $x_{2d} = x_2$ then this choice of intermediate control x_{2d} yields $\dot{V}_1(z_1) = -k_1 z_1^2$, which is clearly negative definite, however at this point we cannot guarantee that $x_{2d} = x_2$ and therefore introduce the second error variable as:

$$z_2 = x_2 - x_{2d} \quad (7.19)$$

If we are able to make this second error variable $|z_2| \rightarrow 0$ for $t \rightarrow \infty$ we will also make the first error variable $|z_1| \rightarrow 0$ for $t \rightarrow \infty$. This is seen if (7.19) is substituted into (7.17):

$$\begin{aligned} \dot{V}_1(z_1) &= z_1 (z_2 + x_{2d} - \dot{x}_d) \\ &= \underbrace{-k_1 z_1^2}_{\text{Negative Term}} + \underbrace{z_1 z_2}_{\text{Cross Term}} \end{aligned} \quad (7.20)$$

If the cross term disappear the function will be negative definite. According to Lyapunov's Stability Theorem (F.1) this means that the equilibrium $z_1 = 0$ is globally asymptotically stable, because we have defined a positive definite and radially unbounded Lyapunov function $V_1(z_1)$ with a negative definite derivative $\dot{V}_1(z_1)$.

7.4.2 Step 2 - Backstepping with Linear Parameter Adaption and Robustness

In this step we want to design an intermediate control law \bar{x}_{3d} for the virtual control variable \bar{x}_3 , appearing in the second equation of (7.11), so that the error variable $|z_2| \rightarrow 0$ for $t \rightarrow \infty$. The starting point is the error variables time-derivative:

$$\begin{aligned} \dot{z}_2 &= \dot{x}_2 - \dot{x}_{2d} \\ &= \theta_1 \bar{x}_3 - \theta_2 x_2 - d(t) - \dot{x}_{2d} \end{aligned} \quad (7.21)$$

Let the vector $\hat{\theta}$ denote the estimate of the parameter vector θ , defined in (7.12), and let the error between them be defined as:

$$\tilde{\theta} = \theta - \hat{\theta} \quad (7.22)$$

Define a standard quadratic positive definite and radially unbounded Lyapunov function candidate as:

$$V_2(z_1, z_2, \tilde{\theta}) = V_1 + \frac{1}{2} z_2^2 + \frac{1}{2} \tilde{\theta}^T \Gamma^{-1} \tilde{\theta} \quad (7.23)$$

with time derivative:

$$\dot{V}_2(z_1, z_2, \tilde{\theta}) = \underbrace{-k_1 z_1^2 + z_1 z_2}_{\dot{V}_1 \text{ see (7.20)}} + z_2 \underbrace{[\theta_1 \bar{x}_3 - \theta_2 x_2 - d(t) - \dot{x}_{2d}]}_{z_2 \text{ see (7.21)}} - \tilde{\theta}^T \Gamma_1^{-1} \dot{\tilde{\theta}} \quad (7.24)$$

Because the parameters (θ_1, θ_2) appear affine/linear we can design an intermediate control law directly from this function based on preconception: What should \bar{x}_3 be in order to render \dot{V}_2 negative semi-definite? One choice would be

$$\bar{x}_{3d} = \frac{1}{\hat{\theta}_1} \left[-z_1 - k_2 z_2 + \hat{\theta}_2 x_2 + \dot{x}_{2d} + \bar{x}_{3r} \right], \quad k_2 > 0 \quad (7.25)$$

Where the term \bar{x}_{3r} is designed to compensate for the disturbance $d(t)$. The parameter estimate $\hat{\theta}_1$ is assumed non-zero $\hat{\theta}_1 \neq 0$, which is assured in the last step of the backstepping procedure. A parameter update law can also be found from the equation as:

$$\dot{\tilde{\theta}} = \Gamma_1 z_2 [\bar{x}_{3d}, -x_2, 0, 0, 0, 0, 0]^T \quad (7.26)$$

If state \bar{x}_3 follows the intermediate control law \bar{x}_{3d} and the parameter estimations are correct i.e. $\hat{\theta}_1 = \theta_1$ and $\hat{\theta}_2 = \theta_2 \Leftrightarrow \tilde{\theta}^T = 0$, and lastly \bar{x}_{3r} successfully compensates the disturbance $d(t)$, then the intermediate control law render \dot{V}_2 negative semi-definite. *Semi*-definite because $\tilde{\theta}$ do not appear in the equation.

$$\dot{V}_2(z_1, z_2, \tilde{\theta}) = -k_1 z_1^2 - k_2 z_2^2 + z_2 [\bar{x}_{3r} - d(t)] \quad (7.27)$$

Even though the parameter estimations do not equal the real values, the preconceptive choice of control law still results in the same expression for \dot{V}_2 , because of the choice of parameter update law. The expression for \dot{V}_2 is expanded to clarify why.

First the error variable between the actual value of \bar{x}_3 and the intermediate control \bar{x}_{3d} is defined.

$$z_3 = \bar{x}_3 - \bar{x}_{3d} \quad (7.28)$$

From (7.22) we get that $\theta_1 = \hat{\theta}_1 + \tilde{\theta}_1$ and $\theta_2 = \hat{\theta}_2 + \tilde{\theta}_2$. Substituting this into the above equation for \dot{V}_2 together with the error variable ($\bar{x}_3 = \bar{x}_{3d} + z_3$), yields:

$$\dot{V}_2(z_1, z_2, \tilde{\theta}) = -k_1 z_1^2 + z_1 z_2 + z_2 \left[\underbrace{\tilde{\theta}_1 \bar{x}_{3d} + \hat{\theta}_1 \bar{x}_{3d} + \overbrace{\tilde{\theta}_1 z_3}^{\text{Cross Term}}}_{=\theta_1 \bar{x}_3} \underbrace{-\tilde{\theta}_2 x_2 - \hat{\theta}_2 x_2}_{=-\theta_2 x_2} - d(t) - \dot{x}_{2d} \right] - \tilde{\theta}^T \Gamma_1^{-1} \dot{\tilde{\theta}} \quad (7.29)$$

Substituting the choice of intermediate control (\bar{x}_{3d}) from Equation (7.25), into the expression for \dot{V}_2 (7.29), results in:

$$\dot{V}_2(z_1, z_2, \tilde{\theta}) = \underbrace{-k_1 z_1^2 - k_2 z_2^2}_{\text{Negative Terms}} + \underbrace{z_2 [\bar{x}_{3r} - d(t)]}_{\text{Robust Term}} + \underbrace{\tilde{\theta}_1 z_2 \bar{x}_{3d} - \tilde{\theta}_2 z_2 x_2 - \tilde{\theta}^T \Gamma_1^{-1} \dot{\tilde{\theta}}}_{\text{Adaption Terms}} + \underbrace{\theta_1 z_2 z_3}_{\text{Cross Term}} \quad (7.30)$$

As in step 1 the substitution of the intermediate control law ($\bar{x}_3 = \bar{x}_{3d} + z_3$) results in a cross-term from the error variable z_3 . Substituting the intermediate parameter update law of Equation (7.26) into expression (7.30) removes the Adaption Terms, leaving the same negative semi-definite function as in Equation (7.27), extended with the cross term, which is compensated in the succeeding step of the backstepping procedure i.e. $|z_3| \rightarrow 0$ for $t \rightarrow \infty$.

$$\dot{V}_2(z_1, z_2, \tilde{\theta}) = \underbrace{-k_1 z_1^2 - k_2 z_2^2}_{\text{Negative Terms}} + \underbrace{z_2 [\bar{x}_{3r} - d(t)]}_{\text{Robust Term}} + \underbrace{\theta_1 z_2 z_3}_{\text{Cross Term}} \quad (7.31)$$

Intermediate Robust Controller

The robust intermediate control, \bar{x}_{3r} , appearing in the Robust Term of Equation (7.31) are yet to be designed. One approach would be a Variable Structure Controller (VSC) like the sliding-mode control, but as the derivative of each intermediate control law is needed in the succeeding step of the backstepping procedure, this strategy cannot be applied. Instead the control law is chosen as [Guan and Pan, 2008]:

$$\bar{x}_{3r} = -z_2 \frac{D}{\delta}, \quad \delta > 0, \quad |d(t)| \leq D \quad (7.32)$$

where δ is an error bound on $|z_2|$ corresponding to $|z_1| < \frac{\delta}{k_1}$ for $t \rightarrow \infty$ as seen in [Guan and Pan, 2008]. D is the absolute maximum value the disturbance $d(t)$ can attain

Rewriting (7.30) with the update law, $\dot{\tilde{\theta}}$, (7.26) and the robust control law, \bar{x}_{3r} , (7.32):

$$\dot{V}_2(z_1, z_2, \tilde{\theta}) = -k_1 z_1^2 - k_2 z_2^2 - \underbrace{\left[\frac{D}{\delta} z_2^2 + d(t) z_2 \right]}_{\text{Robust Term}} + \underbrace{\theta_1 z_2 z_3}_{\text{Cross Term}} \quad (7.33)$$

For (7.33) to be negative semi definite, the robust term must fulfill:

$$\frac{D}{\delta} z_2^2 + d(t) z_2 \geq 0 \quad (7.34)$$

In the worst case the disturbance is of opposite sign of z_2 and at its maximum value. Mathematically this is the situation where $z_2 = |z_2|$ and $d(t) = -D$. Rewriting (7.34) to match this situation:

$$\frac{D}{\delta} |z_2|^2 - D |z_2| \geq 0 \quad (7.35)$$

If the equation (7.35) is reduced we get the condition that

$$\begin{aligned} \frac{|z_2|}{\delta} - 1 &\geq 0 \\ |z_2| &\geq \delta \end{aligned} \quad (7.36)$$

So, as long as $|z_2| \geq \delta$ the expression (7.33) will be negative semi-definite, provided that the cross term containing z_3 is eliminated i.e. $|z_3| \rightarrow 0$ for $t \rightarrow \infty$.

Step 2 - Conclusion

When $|z_2| \geq \delta$ one can see that \dot{V}_2 is upper bounded by a negative semi-definite function ($-W_2$) defined as:

$$\dot{V}_2(z_1, z_2, \tilde{\theta}) \leq -W_2 = -k_1 z_1^2 - k_2 z_2^2 \quad (7.37)$$

All states are guaranteed bounded. Which is evident from Lyapunov stability theorem F.1, as we have a positive definite Lyapunov function of the states with a negative semi-definite derivative. Convergence of z_1 and z_2 will be addressed further when the final control law is developed in step 3.

An important remark is that the demand: $|z_2| \rightarrow 0$ for $t \rightarrow \infty$ from step 1 on page 59 is annulled, as a new control Lyapunov function (V_2) is obtained covering both error variables (z_1, z_2), so the fact that $|z_2|$ is only converging to within a certain error bound δ and not to 0 is not a problem in that respect.

7.4.3 Step 3 - Robust Adaptive Backstepping with Non-Linear Parameters

In this step we want to design the *final control law* for the control variable u and not just an intermediate control law. This is possible because the control variable, u , now appears in the expression for the differentiated error variable z_3 :

$$\dot{z}_3 = \dot{\hat{x}}_3 - \dot{\hat{x}}_{3d} \quad (7.38)$$

with:

$$\dot{\hat{x}}_3 = \frac{1}{\beta_A + x_1} [-\theta_3 x_2 - \theta_4 (x_3 - x_4) + \theta_5 u R_A(\mathbf{x}, u)] - \frac{1}{\beta_B - x_1} [\theta_6 x_2 + \theta_4 (x_3 - x_4) - \theta_7 u R_B(\mathbf{x}, u)] \quad (7.39)$$

The equation is rewritten by first making a common denominator:

$$\dot{\hat{x}}_3 = \frac{(\beta_B - x_1)[- \theta_3 x_2 - \theta_4 (x_3 - x_4) + \theta_5 R_A u] - (\beta_A + x_1)[\theta_6 x_2 + \theta_4 (x_3 - x_4) - \theta_7 R_B u]}{(\beta_A + x_1)(\beta_B - x_1)} \quad (7.40)$$

then expanding:

$$\begin{aligned} \dot{\hat{x}}_3 = & \frac{-\beta_B \theta_3 x_2 + \theta_3 x_1 x_2 - \beta_B \theta_4 x_3 + \beta_B \theta_4 x_4 + \theta_4 x_1 x_3 - \theta_4 x_1 x_4 + \beta_B \theta_5 R_A u - x_1 \theta_5 R_A u}{\beta_A \beta_B + (\beta_B - \beta_A) x_1 - x_1^2} \\ & + \frac{-\beta_A \theta_6 x_2 - \theta_6 x_1 x_2 - \beta_A \theta_4 x_3 - \beta_A \theta_4 x_4 - \theta_4 x_1 x_3 + \theta_4 x_1 x_4 + \beta_A \theta_7 R_B u + x_1 \theta_7 R_B u}{\beta_A \beta_B + (\beta_B - \beta_A) x_1 - x_1^2} \end{aligned} \quad (7.41)$$

and then factoring:

$$\dot{\hat{x}}_3 = \frac{\overbrace{-\beta_B \theta_3 x_2 + \theta_3 x_1 x_2 - \beta_B \theta_4 x_3 + \beta_B \theta_4 x_4 + \theta_4 x_1 x_3 - \theta_4 x_1 x_4}^{f_n(\mathbf{x})} + \overbrace{\beta_B \theta_5 R_A u - x_1 \theta_5 R_A u}^{g_n(\mathbf{x})}}{\underbrace{\beta_A \beta_B + (\beta_B - \beta_A) x_1 - x_1^2}_{f_d(\mathbf{x})}} u \quad (7.42)$$

Auxiliary functions (f_n , g_n and f_d) are introduced, so that the expression becomes easier to handle in further derivation.

$$\dot{z}_3 = \frac{f_n(\mathbf{x}) + g_n(\mathbf{x}) u}{f_d(x_1)} - \dot{\hat{x}}_{3d} \quad (7.43)$$

The nominator of the equation can be handled using the same procedure as in step 2, however the denominator f_d contains unknown parameters β_A , β_B that now appear *non-linear* in the expression, and therefore a standard quadratic choice of Lyapunov function candidate $V_3 = \frac{1}{2} z_3^2$ will have non-linear parameters appearing in its derivative as well:

$$\begin{aligned} \dot{V}_3 &= z_3 \dot{z}_3 \\ &= z_3 \frac{f_n(\mathbf{x}) + g_n(\mathbf{x}) u}{f_d(x_1)} - z_3 \dot{\hat{x}}_{3d} \end{aligned} \quad (7.44)$$

Choosing a modified Lyapunov function candidate as in [Guan and Pan, 2008, p. 6]:

$$V_3 = \frac{1}{2} f_d(x_1) z_3^2, \quad f_d(x_1) > 0 \quad (7.45)$$

we are able to get a derivative (\dot{V}_3) without non-linear parameters:

$$\begin{aligned} \dot{V}_3 &= f_d(x_1) z_3 \dot{z}_3 + \frac{1}{2} \frac{\partial f_d(x_1)}{\partial x} \dot{x}_1 z_3^2 \\ &= f_d(x_1) z_3 \left(\frac{f_n(\mathbf{x}) + g_n(\mathbf{x}) u}{f_d(x_1)} - \dot{\hat{x}}_{3d} \right) + \frac{1}{2} (\beta_B - \beta_A - 2x_1) x_2 z_3^2 \\ &= [f_n(\mathbf{x}) + g_n(\mathbf{x}) u] z_3 - \dot{\hat{x}}_{3d} f_d(x_1) z_3 + \frac{1}{2} (\beta_B - \beta_A) x_2 z_3^2 - x_1 x_2 z_3^2 \end{aligned} \quad (7.46)$$

A Lyapunov function candidate (V_3) should *always* be positive definite (PD), and therefore we have the criterion $f_d(x_1) > 0$, $\forall x_1 \in \mathbb{R}$. Considering the physical nature of the system, and the expression for f_d this is easily verified.

$$\begin{aligned} f_d(x_1) &= (\beta_A + x_1)(\beta_B - x_1) \\ &= \left(\frac{V_{A0}}{A_A} + x_1 \right) \left(\frac{V_{B0}}{A_B} - x_1 \right) \\ &= \frac{V_A}{A_A} \cdot \frac{V_B}{A_B} \end{aligned} \quad (7.47)$$

V_A and V_B are physical volumes and therefore positive. This guarantees that $f_d(x_1) > 0$ which consequently makes $V_3(z_3)$, in (7.45), positive definite.

Doing initialization of the control algorithm on a physical setup, care must be taken so that the initial volumes V_{A0} and V_{B0} match the real volumes at $x_1 = 0$, so that V_A and V_B are maintained positive and *non-zero* for all values of $0 \leq x_{1min} \leq x_1 \leq x_{1max}$.

The derivative of the intermediate control law, \bar{x}_{3d} (developed in step 2) is needed in the expression for \dot{V}_3 of (7.46). So, from Equation (7.25) on page 60 we get:

$$\begin{aligned} \bar{x}_{3d} &= \frac{1}{\hat{\theta}_1} \left[-z_1 - k_2 z_2 + \hat{\theta}_2 x_2 \quad \underbrace{-\frac{D}{\delta} z_2}_{\bar{x}_{3r} \text{ see (7.32)}} \quad \underbrace{-k_1 \dot{z}_1 + \ddot{x}_d}_{\dot{x}_{2d} \text{ see (7.18)}} \right] \\ &= \frac{1}{\hat{\theta}_1} \left[\underbrace{-x_1 + x_d}_{-z_1} - \left(k_2 + \frac{D}{\delta} \right) \underbrace{(x_2 - x_{2d})}_{z_2} + \hat{\theta}_2 x_2 \underbrace{-k_1 x_2 + k_1 \dot{x}_d}_{-k_1 \dot{z}_1} + \ddot{x}_d \right] \\ &= \frac{1}{\hat{\theta}_1} \left[-x_1 + x_d - \left(k_2 + \frac{D}{\delta} \right) \left(x_2 + \underbrace{k_1(x_1 - x_d) - \dot{x}_d}_{-x_{2d} \text{ see (7.18)}} \right) + \hat{\theta}_2 x_2 - k_1 x_2 + k_1 \dot{x}_d + \ddot{x}_d \right] \end{aligned} \quad (7.48)$$

Now Equation (7.48) contains an expression for \bar{x}_{3d} as a function of $(x_1, x_2, \hat{\theta}_1, \hat{\theta}_2, x_d, \dot{x}_d, \ddot{x}_d)$, and therefore we can apply the chain-rule to obtain its derivative as:

$$\dot{\bar{x}}_{3d} = \frac{\partial \bar{x}_{3d}}{\partial x_1} \dot{x}_1 + \frac{\partial \bar{x}_{3d}}{\partial x_2} \dot{x}_2 + \frac{\partial \bar{x}_{3d}}{\partial \hat{\theta}_1} \dot{\hat{\theta}}_1 + \frac{\partial \bar{x}_{3d}}{\partial \hat{\theta}_2} \dot{\hat{\theta}}_2 + \frac{\partial \bar{x}_{3d}}{\partial x_d} \dot{x}_d + \frac{\partial \bar{x}_{3d}}{\partial \dot{x}_d} \ddot{x}_d + \frac{\partial \bar{x}_{3d}}{\partial \ddot{x}_d} \ddot{\ddot{x}}_d \quad (7.49)$$

The partial derivatives are solved term-wise:

$$\begin{aligned} \dot{\bar{x}}_{3d} &= \underbrace{-\frac{k_1 k_2 + k_1 \frac{D}{\delta} + 1}{\hat{\theta}_1} x_2}_{1. \text{ Term - certain}} + \underbrace{\frac{\hat{\theta}_2 - k_2 - \frac{D}{\delta} - k_1}{\hat{\theta}_1} (\theta_1 \bar{x}_3 - \theta_2 x_2 - d(t))}_{2. \text{ Term - uncertain}} \\ &\quad \underbrace{-\frac{\bar{x}_{3d} \dot{\hat{\theta}}_1}{\hat{\theta}_1}}_{3. \text{ Term - certain}} + \underbrace{\frac{x_2 \dot{\hat{\theta}}_2}{\hat{\theta}_1}}_{4. \text{ Term - certain}} + \underbrace{\frac{k_1 k_2 + k_1 \frac{D}{\delta} + 1}{\hat{\theta}_1} \dot{x}_d}_{5. \text{ Term - certain}} + \underbrace{\frac{k_1 + k_2 + \frac{D}{\delta}}{\hat{\theta}_1} \dot{x}_d}_{6. \text{ Term - certain}} + \underbrace{\frac{1}{\hat{\theta}_1} \ddot{x}_d}_{7. \text{ Term - certain}} \end{aligned} \quad (7.50)$$

Collecting all the terms in a certain part, $\dot{\bar{x}}_{3dc}$ and an uncertain part, $\dot{\bar{x}}_{3du}$:

$$\dot{\bar{x}}_{3d} = \dot{\bar{x}}_{3dc} + \dot{\bar{x}}_{3du} \quad (7.51)$$

$$\dot{\bar{x}}_{3dc} = \frac{1}{\hat{\theta}_1} \left[x_2 \dot{\hat{\theta}}_2 - \bar{x}_{3d} \dot{\hat{\theta}}_1 + \left(k_1 k_2 + k_2 \frac{D}{\delta} + 1 \right) (\dot{x}_d - x_2) + \left(k_1 + k_2 + \frac{D}{\delta} \right) \dot{x}_d + \ddot{x}_d \right] \quad (7.52)$$

$$\dot{\bar{x}}_{3du} = \underbrace{\frac{\hat{\theta}_2 - k_2 - \frac{D}{\delta} - k_1}{\hat{\theta}_1}}_{f_c(\hat{\theta}_1, \hat{\theta}_2)} \underbrace{(\theta_1 \bar{x}_3 - \theta_2 x_2 - d(t))}_{\dot{x}_2} \quad (7.53)$$

Furthermore, the partial derivative in the uncertain part is certain, and so we define it by a function f_c .

$$f_c(\hat{\theta}_1, \hat{\theta}_2) = \frac{\partial \bar{x}_{3d}}{\partial x_2} = \frac{1}{\hat{\theta}_1} \left(\hat{\theta}_2 - k_1 - k_2 - \frac{D}{\delta} \right) \quad (7.54)$$

Inserting (7.50) and (7.42) into (7.46) yields:

$$\dot{V}_3 = z_3 f_n + z_3 g_n u - \dot{\bar{x}}_{3d} f_d z_3 + \frac{1}{2} (\beta_B - \beta_A) x_2 z_3^2 - x_1 x_2 z_3^2 \quad (7.55)$$

$$= z_3 \left[f_n + g_n u + \dot{\bar{x}}_{3dc} f_d + -\dot{\bar{x}}_{3du} f_d + \frac{1}{2} (\beta_B - \beta_A) x_2 z_3 - x_1 x_2 z_3 \right] \quad (7.56)$$

$$= z_3 \left[\underbrace{-(\beta_B \theta_3 + \beta_A \theta_6) x_2 - \beta_B + \beta_A}_{f_n} \theta_4 (x_3 - x_4) + (\theta_3 - \theta_6) x_1 x_2 \right. \\ \left. + \underbrace{[\beta_B \theta_5 R_A + \beta_A \theta_7 R_B + (\theta_7 R_B - \theta_5 R_A) x_1]}_{g_n} u - \underbrace{(\beta_A \beta_B - (\beta_B - \beta_A) x_1 - x_1^2)}_{f_d} \dot{\bar{x}}_{3dc} \right. \\ \left. - \underbrace{f_c [\theta_1 \bar{x}_3 - \theta_2 x_2 - d(t)]}_{\dot{\bar{x}}_{3du}} \underbrace{[\beta_A \beta_B + (\beta_B - \beta_A) x_1 - x_1^2]}_{f_d} + \frac{1}{2} (\beta_B - \beta_A) x_2 z_3 - x_1 x_2 z_3 \right] \quad (7.57)$$

As just mentioned, the quantities f_c and $\dot{\bar{x}}_{3dc}$ are *certain* and so all uncertain quantities now appear in the expression (7.57). It is therefore possible to parameterize it so an adaptive controller can be derived using Lyapunov theory.

$$\dot{V}_3 = z_3 \left[-\epsilon_1 x_2 - \epsilon_2 (x_3 - x_4) + \epsilon_3 x_1 x_2 - (\phi_1 + \phi_2 x_1 - x_1^2) \dot{\bar{x}}_{3dc} \right. \\ \left. + [\epsilon_4 R_A + \epsilon_5 R_B + (\theta_7 R_B - \theta_5 R_A) x_1] u + \frac{1}{2} \phi_2 x_2 z_3 - x_1 x_2 z_3 \right. \\ \left. + f_c (\phi_1 + \phi_2 x_1 - x_1^2) d(t) - f_c (\epsilon_6 + \epsilon_7 x_1) \bar{x}_3 \right. \\ \left. + f_c (\theta_1 \bar{x}_3 - \theta_2 x_2) x_1^2 + f_c (\epsilon_8 + \epsilon_9 x_1) x_2 \right] \quad (7.58)$$

where:

$$\begin{aligned} \epsilon_1 = \beta_B \theta_3 + \beta_A \theta_6 & \quad \epsilon_2 = (\beta_A + \beta_B) \theta_4 & \quad \epsilon_3 = \theta_3 - \theta_6 & \quad \epsilon_4 = \beta_B \theta_5 & \quad \epsilon_5 = \beta_A \theta_7 & \quad \epsilon_6 = \theta_1 \beta_A \beta_B \\ \epsilon_7 = \theta_1 (\beta_B - \beta_A) & \quad \epsilon_8 = \theta_2 \beta_A \beta_B & \quad \epsilon_9 = \theta_2 (\beta_B - \beta_A) & \quad \phi_1 = \beta_A \beta_B & \quad \phi_2 = \beta_B - \beta_A \end{aligned}$$

The parameters are arranged in vectors, just as for the first parameterization of θ seen on page 58.

$$\epsilon = [\epsilon_1, \epsilon_2, \epsilon_3, \epsilon_4, \epsilon_5, \epsilon_6, \epsilon_7, \epsilon_8, \epsilon_9]^T, \quad \phi = [\phi_1, \phi_2]^T \quad (7.59)$$

with estimation vectors

$$\hat{\epsilon} = [\hat{\epsilon}_1, \hat{\epsilon}_2, \hat{\epsilon}_3, \hat{\epsilon}_4, \hat{\epsilon}_5, \hat{\epsilon}_6, \hat{\epsilon}_7, \hat{\epsilon}_8, \hat{\epsilon}_9]^T, \quad \hat{\phi} = [\hat{\phi}_1, \hat{\phi}_2]^T \quad (7.60)$$

and adaption error vectors

$$\tilde{\epsilon} = \epsilon - \hat{\epsilon}, \quad \tilde{\phi} = \phi - \hat{\phi} \quad (7.61)$$

As the system is parameterized and the necessary quantities defined, we are now able to establish the final Lyapunov function candidate for the whole system. This is done using the previously defined Lyapunov function candidates $V_2(z_1, z_2, \tilde{\theta})$ and $V_3(z_3)$ including quadratic terms for the new parameterization $(\tilde{\epsilon}, \tilde{\phi})$. The final Lyapunov function candidate is chosen as:

$$V(z_1, z_2, z_3, \tilde{\theta}, \tilde{\epsilon}, \tilde{\phi}) = V_2(z_1, z_2, \tilde{\theta}) + V_3(z_3) + \frac{1}{2} \tilde{\epsilon}^T \Gamma_2^{-1} \tilde{\epsilon} + \frac{1}{2} \tilde{\phi}^T \Gamma_3^{-1} \tilde{\phi} \quad (7.62)$$

with time derivative from (7.30) and (7.58):

$$\begin{aligned}
\dot{V}(z_1, z_2, z_3, \tilde{\theta}, \tilde{\epsilon}, \tilde{\phi}) &= \overbrace{-k_1 z_1^2 - k_2 z_2^2 - \left[\frac{D}{\delta} z_2^2 + d(t) z_2 \right] + \theta_1 z_2 z_3 - \tilde{\theta}^T \Gamma_1^{-1} \dot{\tilde{\theta}} - \tilde{\epsilon}^T \Gamma_2^{-1} \dot{\tilde{\epsilon}} - \tilde{\phi}^T \Gamma_3^{-1} \dot{\tilde{\phi}}}_{\dot{V}_2 \text{ From (7.30)}} \\
&+ z_3 \left[-\epsilon_1 x_2 - \epsilon_2 (x_3 - x_4) + \epsilon_3 x_1 x_2 - (\phi_1 + \phi_2 x_1 - x_1^2) \dot{\tilde{x}}_{3dc} \right. \\
&\quad + [\epsilon_4 R_A + \epsilon_5 R_B + (\theta_7 R_B - \theta_5 R_A) x_1] u + \frac{1}{2} \phi_2 x_2 z_3 - x_1 x_2 z_3 \\
&\quad + \underbrace{f_c(\phi_1 + \phi_2 x_1 - x_1^2) d(t)}_{\text{Disturbance Term}} - f_c(\epsilon_6 + \epsilon_7 x_1) \bar{x}_3 \\
&\quad \left. + f_c(\theta_1 \bar{x}_3 - \theta_2 x_2) x_1^2 + f_c(\epsilon_8 + \epsilon_9 x_1) x_2 \right] \tag{7.63}
\end{aligned}$$

The expression is now in a form that allow us to choose a control law u .

Control Law

As in [Guan and Pan, 2008] we choose to split the controller into 3 parts, where u_1 is a *certain* controller compensating for known dynamics, u_2 an *adaptive* controller compensating for the unknown parameters, and finally u_3 which is a *robust* controller compensating for the disturbance $d(t)$.

$$u = \frac{u_1 + u_2 + u_3}{\hat{\epsilon}_4 R_A + \hat{\epsilon}_5 R_B + (\hat{\theta}_7 R_B - \hat{\theta}_5 R_A) x_1} \tag{7.64}$$

The estimates: $\hat{\epsilon}_4, \hat{\epsilon}_5, \hat{\theta}_7, \hat{\theta}_5$ are all kept positive, so for the denominator to become zero it requires that $R_A = R_B = 0$. Referring to the definition of R_A and R_B , Equation (7.13) on page 58, it is seen that $R_A = R_B = 0$ corresponds to P_A and P_B having the same values as P_P and P_T , which is not a feasible operating situation. However, it could happen in rare cases or if the signals are noisy, and therefore the denominator (7.64) is limited above zero with a small positive number ζ_3 .

$$\hat{\epsilon}_4 R_A + \hat{\epsilon}_5 R_B + (\hat{\theta}_7 R_B - \hat{\theta}_5 R_A) x_1 \geq \zeta_3 > 0 \tag{7.65}$$

From inspection of (7.63) we choose the **certain** controller as

$$u_1 = x_1 x_2 z_3 - \dot{\tilde{x}}_{3dc} x_1^2 - k_3 z_3 = -k_3 z_3 + x_1 (x_2 z_3 - x_1 \dot{\tilde{x}}_{3dc}) \tag{7.66}$$

and the **adaptive** controller as

$$\begin{aligned}
u_2 &= -\hat{\theta}_1 z_2 + \hat{\epsilon}_1 x_2 + \hat{\epsilon}_2 (x_3 - x_4) - \hat{\epsilon}_3 x_1 x_2 + (\hat{\epsilon}_6 + \hat{\epsilon}_7 x_1) f_c \bar{x}_3 - (\hat{\epsilon}_8 + \hat{\epsilon}_9 x_1) f_c x_2 \\
&\quad + (\hat{\phi}_1 + \hat{\phi}_2 x_1) \dot{\tilde{x}}_{3dc} - \frac{1}{2} \hat{\phi}_2 x_2 z_3 - (\hat{\theta}_1 \bar{x}_3 - \hat{\theta}_2 x_2) f_c x_1^2 \tag{7.67}
\end{aligned}$$

This choice of u_1 and u_2 cancels the indefinite terms in (7.63) and adds a negative term $-k_3 z_3^2$.

To compensate the disturbance term in (7.63), we have to design the **robust** controller u_3 so that

$$[f_c(\phi_1 + \phi_2 x_1 - x_1^2) d(t) + u_3] z_3 \leq 0 \tag{7.68}$$

To make sure that the controller is always working opposite z_3 , in (7.68), with an amplitude of D , the first step is to choose

$$u_3 = -D \text{sign}(z_3) u_{3h} \tag{7.69}$$

Which due to $z_3 \text{sign}(z_3) = |z_3|$ makes it possible to rewrite (7.68) to:

$$(\phi_1 + \phi_2 x_1 - x_1^2) f_c z_3 d(t) - |z_3| D u_{3h} \leq 0 \quad (7.70)$$

$$\phi_1 + \phi_2 x_1 - x_1^2) f_c z_3 d(t) \leq |z_3| D u_{3h} \quad (7.71)$$

We know that $d(t) \leq D$ and so the above inequality is satisfied, no matter the sign of z_3 , if

$$(\phi_1 + \phi_2 x_1 - x_1^2) f_c \leq u_{3h} \quad (7.72)$$

For positive x_1 , the worst case of (7.72) is when ϕ_1 and ϕ_2 are as large as possible, and if we assume that we know the bounds of $\beta_A \leq B_A$ and $\beta_B \leq B_B$, the largest values are

$$|\phi_1| = \beta_A \beta_B \leq B_A B_B \quad \text{and} \quad |\phi_2| = |\beta_B - \beta_A| < \max(B_A, B_B) \quad (7.73)$$

The term containing $-x_1^2$ can be ignored since it will only ease the choice of u_{3h} as it is negative $\forall x_1 \in \mathbb{R}$. As in [Guan and Pan, 2008] the appearance of x_1 in (7.72) is substituted by $\sqrt{x_1^2 + \zeta_1}$, which can be toughed of as ensuring that $x_1 \geq 0$ in the expression.

$$\left(B_A B_B + \max(B_A, B_B) \sqrt{x_1^2 + \zeta_1} \right) f_c \leq u_{3h}, \quad \zeta_1 > 0 \quad (7.74)$$

The constant ζ_1 is introduced to make the controller less sensitive to noise in x_1 , and the same "trick" is used on f_c , and the final robust controller is obtained

$$u_3 = -D \text{sign}(z_3) \left[B_A B_B + \max(B_A, B_B) \sqrt{x_1^2 + \zeta_2} \right] \sqrt{f_c^2 + \zeta_2}. \quad (7.75)$$

All the controllers of the control law (7.64) have now been determined; the certain u_1 , the adaptive u_2 and the robust u_3 . Now the parameter update law should be designed so it effectively compensates for the parameter variations $(\tilde{\theta}, \tilde{\epsilon}, \tilde{\phi})$.

Parameter Update Law

The expression (7.63) for \dot{V} , can be written with all its parameters (θ, ϵ, ϕ) extended: $\theta = \hat{\theta} + \tilde{\theta}$, $\epsilon = \hat{\epsilon} + \tilde{\epsilon}$, $\phi = \hat{\phi} + \tilde{\phi}$. If this is done and the controller, u , (7.64) is substituted into the expression, it leaves us with an expression where the parameters (θ, ϵ, ϕ) have been substituted with the parameter errors $(\tilde{\theta}, \tilde{\epsilon}, \tilde{\phi})$. The certain terms have been removed by u_1 and the negative term $-k_3 z_3^2$ is now appearing together with $-k_1 z_1^2$ and $-k_2 z_2^2$.

$$\begin{aligned} \dot{V}(z_1, z_2, z_3, \tilde{\theta}, \tilde{\epsilon}, \tilde{\phi}) = & -k_1 z_1^2 - k_2 z_2^2 - k_3 z_3^2 - \tilde{\theta}^T \Gamma_1^{-1} \dot{\tilde{\theta}} - \tilde{\epsilon}^T \Gamma_2^{-1} \dot{\tilde{\epsilon}} - \tilde{\phi}^T \Gamma_3^{-1} \dot{\tilde{\phi}} \\ & + z_3 \left[\tilde{\theta}_1 z_2 - \tilde{\epsilon}_1 x_2 - \tilde{\epsilon}_2 (x_3 - x_4) + \tilde{\epsilon}_3 x_1 x_2 - (\tilde{\phi}_1 + \tilde{\phi}_2 x_1) \dot{x}_{3dc} \right. \\ & + \left[\tilde{\epsilon}_4 R_A + \tilde{\epsilon}_5 R_B + (\tilde{\theta}_7 R_B - \tilde{\theta}_5 R_A) x_1 \right] u + \frac{1}{2} \tilde{\phi}_2 x_2 z_3 \\ & + f_c (\tilde{\theta}_1 \bar{x}_3 - \tilde{\theta}_2 x_2) x_1^2 + f_c (\tilde{\epsilon}_8 + \tilde{\epsilon}_9 x_1) x_2 - f_c (\tilde{\epsilon}_6 + \tilde{\epsilon}_7 x_1) \bar{x}_3 \\ & \left. + f_c (\phi_1 + \phi_2 x_1 - x_1^2) d(t) + u_3 \right] - \underbrace{\left[\frac{D}{\delta} z_2^2 + d(t) z_2 \right]}_{\text{Robust part}} \end{aligned} \quad (7.76)$$

The parameter update laws are chosen so that the terms in (7.76) that involves a parameter estimation error $(\tilde{\theta}, \tilde{\epsilon}, \tilde{\phi})$, are cancelled.

$$\dot{\hat{\theta}} = \mathbf{\Gamma}_1 z_3 [z_2 + f_c x_1^2 \bar{x}_3, -f_c x_1^2 x_2, 0, 0, -x_1 R_A u, 0, x_1 R_B u] \quad (7.77)$$

$$\dot{\hat{e}} = \mathbf{\Gamma}_2 z_3 [-x_2, x_4 - x_3, x_1 x_2, R_A u, R_B u, -f_c \bar{x}_3, -f_c x_1 \bar{x}_3, f_c x_2, f_c x_1 x_2] \quad (7.78)$$

$$\dot{\hat{\phi}} = \mathbf{\Gamma}_3 z_3 [-\dot{\bar{x}}_{3dc}, \frac{1}{2} x_2 z_3 - x_1 \dot{\bar{x}}_{3dc}] \quad (7.79)$$

By inserting these update laws into (7.76) it is seen that the expression no longer contains parameter estimation errors:

$$\dot{V} = -k_1 z_1^2 - k_2 z_2^2 - k_3 z_3^2 - \left[\frac{D}{\delta} z_2^2 + z_2 d(t) \right] + [f_c(\phi_1 + \phi_2 x_2 - x_1^2) d(t) + u_3] z_3 \quad (7.80)$$

However, the parameter update laws allow for the denominator of (7.64) to become zero. An assumption was made for this not to happen in (7.65). It states that the parameter estimates $\hat{e}_4, \hat{e}_5, \hat{\theta}_7, \hat{\theta}_5$ should all be kept positive. Also parameter $\hat{\theta}_1$, appearing in the denominator of the intermediate control law (7.25), should be maintained positive. In order to comply with this, the estimates are limited to its max. and min. values by the following function.

$$\text{proj}_{\theta}(\ast) = \begin{cases} 0, & \text{if } \hat{\theta} \geq \theta_{max} \text{ and } \ast > 0 \\ 0, & \text{if } \hat{\theta} \leq \theta_{min} \text{ and } \ast < 0 \\ \ast, & \text{otherwise} \end{cases} \quad (7.81)$$

The function is chosen so that the limitation of the estimates $\hat{\theta}_1, \hat{\theta}_5, \hat{\theta}_7, \hat{e}_4, \hat{e}_5$ to their bounds never alter $\dot{V} > 0$. This is best explained by an example. If the terms involving $\hat{\theta}_1$ from the adaptive part of, \dot{V} , (7.76) is collected we get

$$\underbrace{(\theta_1 - \hat{\theta}_1)}_{\tilde{\theta}_1} \underbrace{(z_2 z_3 + f_c x_1^2 \bar{x}_3 z_3)}_{=\ast} - \underbrace{(\theta_1 - \hat{\theta}_1)}_{\tilde{\theta}_1} \underbrace{\text{proj}_{\theta_1}(z_2 z_3 + f_c x_1^2 \bar{x}_3 z_3)}_{\Gamma_{1(1,1)} \dot{\hat{\theta}}_1} \leq 0 \quad (7.82)$$

and if the expression is evaluated in the three scenarios of (7.81):

Upper Bound The proj function saturates making $\text{proj}_{\theta_1}(\ast) = 0$ and $\hat{\theta}_1 = \theta_{1max}$. This render (7.82)

$$\underbrace{\tilde{\theta}_1}_{\leq 0} \underbrace{(z_2 z_3 + f_c x_1^2 \bar{x}_3 z_3)}_{\ast \geq 0} \leq 0 \quad (7.83)$$

, as $\text{proj}_{\theta_1}(\ast) = 0$ removes the term on the right of (7.82) and $\hat{\theta}_1 = \theta_{1max}$ makes $\tilde{\theta}_1 = \theta_1 - \theta_{1max} \leq 0$. The argument to the $\text{proj}_{\theta_1}(\ast)$ function is represented by a (\ast) , and for the estimate to reach the upper limit the argument must be positive as it represent the gradient.

Between Bounds When no limitation occur, $\text{proj}_{\theta_1}(\ast) = \ast$, and the two terms of (7.82) are equal.

Lower Bound The proj function saturates making $\text{proj}_{\theta_1}(\ast) = 0$ and $\hat{\theta}_1 = \theta_{1min}$. This is the same situation as for the upper bound, but with opposite sign of $\tilde{\theta}_1 = \theta_1 - \theta_{1min} \geq 0$, making (7.82):

$$\underbrace{\tilde{\theta}_1}_{\geq 0} \underbrace{(z_2 z_3 + f_c x_1^2 \bar{x}_3 z_3)}_{\ast \leq 0} \leq 0 \quad (7.84)$$

we see that even though θ_1 reaches its limits (θ_{1min} and θ_{1max}) it does not render $\dot{V} > 0$.

The final update laws are the same as (7.77), (7.78) and (7.79), but with the $\text{proj}(\cdot)$ function on the parameters $\hat{\theta}_1, \hat{\theta}_5, \hat{\theta}_7, \hat{\epsilon}_4, \hat{\epsilon}_5$.

$$\begin{aligned}\dot{\hat{\theta}} &= \Gamma_1 [\text{proj}_{\theta_1}(z_2 z_3 + f_c x_1^2 \bar{x}_3 z_3), -f_c x_1^2 x_2 z_3, 0, 0, \text{proj}_{\theta_5}(-x_1 R_A z_3 u), 0, \text{proj}_{\theta_7}(x_1 R_B z_3 u)] \\ \dot{\hat{\epsilon}} &= \Gamma_2 [-x_2 z_3, x_4 z_3 - x_3 z_3, x_1 x_2 z_3, \text{proj}_{\epsilon_4}(R_A z_3 u), \text{proj}_{\epsilon_5}(R_B z_3 u), -f_c \bar{x}_3 z_3, -f_c x_1 \bar{x}_3 z_3, f_c x_2 z_3, f_c x_1 x_2 z_3] \\ \dot{\hat{\phi}} &= \Gamma_3 [-\dot{\bar{x}}_{3dc} z_3, \frac{1}{2} x_2 z_3^2 - x_1 \dot{\bar{x}}_{3dc} z_3]\end{aligned}\quad (7.85)$$

If these parameter update laws are used instead, the *equality* of (7.80) is changed to an *inequality* as the terms involving a parameter estimation error are negative but not necessarily canceled if the proj -function saturates.

$$\dot{V} \leq -k_1 z_1^2 - k_2 z_2^2 - k_3 z_3^2 - \left[\frac{D}{\delta} z_2^2 + z_2 d(t) \right] + [f_c(\phi_1 + \phi_2 x_2 - x_1^2) d(t) + u_3] z_3 \quad (7.86)$$

and from (7.68) we know that:

$$[f_c(\phi_1 + \phi_2 x_1 - x_1^2) d(t) + u_3] z_3 \leq 0 \quad (7.87)$$

so therefore it can be further reduced to

$$\dot{V} \leq -k_1 z_1^2 - k_2 z_2^2 - k_3 z_3^2 - \left[\frac{D}{\delta} z_2^2 + z_2 d(t) \right] \quad (7.88)$$

Conclusion

When $|z_2| \geq \delta$ or when $d(t) = 0$ we know that (7.88) is negative semi-definite and as (7.62) is continuously differentiable, radially unbounded and positive definite we know that $(z_1, z_2, z_3, \tilde{\theta}, \tilde{\epsilon}, \tilde{\phi})$ is bounded. Furthermore, as the system is assumed locally Lipschitz and (7.88) is upper bounded by a continuous time-invariant semi-negative definite function

$$\dot{V}(z_1, z_2, z_3, \tilde{\theta}, \tilde{\epsilon}, \tilde{\phi}) \leq -W = -k_1 z_1^2 - k_2 z_2^2 - k_3 z_3^2 \quad (7.89)$$

we know from LaSalle-Yoshizawa's theorem F.4.2 that

$$\lim_{t \rightarrow \infty} W = \lim_{t \rightarrow \infty} (-k_1 z_1^2 - k_2 z_2^2 - k_3 z_3^2) = 0 \quad \Leftrightarrow \quad \lim_{t \rightarrow \infty} (|z_1|, |z_2|, |z_3|) = (0, 0, 0). \quad (7.90)$$

as z_1 is defined as the tracking error (7.14) we have shown that using the robust adaptive backstepping controller derived in this chapter, global asymptotic tracking when $d(t) = 0$ or $|z_2| \geq \delta$ is achieved together with boundedness of all signals in the system $(z_1, z_2, z_3, \tilde{\theta}, \tilde{\epsilon}, \tilde{\phi})$.

Conclusion with Disturbances

The situation changes when $d(t) \neq 0$ and $|z_2| < \delta$ because the expression (7.88) becomes indefinite as the disturbance might render the equation positive for some values of z_1, z_2 and z_3 .

Considering the last part of (7.88) we defined the indefinite term $F(z_2, t)$ as:

$$F(z_2, t) = -\frac{D}{\delta} z_2^2 - z_2 d(t) \quad (7.91)$$

At a time-instant, t , the disturbance $d(t)$ is constant, this function is therefore a second order polynomial in z_2 . A second order polynomial is convex and has a single global extreme point. As the dominating

term $(-z_2^2)$ is negative, this point is a global maximum. Taking a partial derivative of $F(z_2, t)$ and equating this to zero we obtain the value of z_2 that maximizes the term $F(z_2, t)$.

$$\frac{\partial F(z_2, t)}{\partial z_2} = -2\frac{D}{\delta}z_2 - d(t) = 0 \quad \Leftrightarrow \quad z_2 = -\frac{\delta d(t)}{2D} \quad (7.92)$$

Inserting this value of z_2 into (7.91) the maximum value of $F(z_2, t)$ is found

$$\begin{aligned} F(z_2, t) &\leq -\frac{D}{\delta} \left(\frac{\delta d(t)}{2D} \right)^2 + \frac{\delta d(t)^2}{2D} \\ &\leq -\frac{\delta d(t)^2}{4D} + \frac{\delta d(t)^2}{2D} \\ &\leq \frac{-2D\delta d(t)^2 + 4D\delta d(t)^2}{8D^2} \\ &\leq \frac{2D\delta d(t)^2}{8D^2} \\ &\leq \frac{\delta d(t)^2}{4D} \end{aligned} \quad (7.93)$$

In the worst case the disturbance is of its maximum value $|d(t)| = D$, so the maximum value of $F(z_2, t)$ is:

$$F(z_2, t) \leq \frac{\delta D}{4} \quad (7.94)$$

Inserting this *constant* in (7.88) we obtain:

$$\dot{V} \leq -k_1 z_1^2 - k_2 z_2^2 - k_3 z_3^2 + \frac{\delta D}{4} \quad (7.95)$$

As the derivative of the positive definite Lyapunov function V contains only negative terms and a positive constant we are able to guarantee that all the system states $(z_1, z_2, z_3, \tilde{\theta}, \tilde{\epsilon}, \tilde{\phi})$ are bounded due to Raffoul's Theorem F.3, seen on page 153.

When $-k_1 z_1^2 - k_2 z_2^2 - k_3 z_3^2 + \frac{\delta D}{4} \leq 0$, the equation becomes negative semi-definite and convergence is guaranteed with the same arguments as in the case of no disturbances.

The final conclusion with disturbances ($d(t) \neq 0$) can be visualized as a ball of radius $\frac{\delta D}{4}$, in the state-space, where the states z_1, z_2 and z_3 converge within, while all states of the system $(z_1, z_2, z_3, \tilde{\theta}, \tilde{\epsilon}, \tilde{\phi})$ remains bounded.

From Equation (7.14), (7.19) and (7.28) we obtain that the system states x_1, x_2 and \bar{x}_3 are bounded as well. We cannot mathematically guarantee that the two pressures x_3 and x_4 are bounded as we only know that the load pressure $\bar{x}_3 = A_A x_3 - A_B x_4$ is bounded. However, we assume that the individual pressures are always larger than the tank pressure and smaller than the pump pressure, which is realistic if the system is operating smoothly. Thus, all states of the system are bounded and the system is globally stable.

7.5 Summary of the Robust Adaptive Backstepping Controller with Non Lienar Parameters

This section is the summary of the controller design. It is the result of the design and it summarizes all equations, signals and parameters needed for the controller to be implemented in either a physical setup or a simulation model.

7.5.1 Controller Equations

Control law:

$$u = \frac{u_1 + u_2 + u_3}{\hat{\epsilon}_4 R_A + \hat{\epsilon}_5 R_B + (\hat{\theta}_7 R_B - \hat{\theta}_5 R_A) x_1} \quad (7.96)$$

The certain part:

$$u_1 = x_1 x_2 z_3 - \dot{\bar{x}}_{3dc} x_1^2 - k_3 z_3 = -k_3 z_3 + x_1 (x_2 z_3 - x_1 \dot{\bar{x}}_{3dc}) \quad (7.97)$$

The adaptive part:

$$\begin{aligned} u_2 = & -\hat{\theta}_1 z_2 + \hat{\epsilon}_1 x_2 + \hat{\epsilon}_2 (x_3 - x_4) - \hat{\epsilon}_3 x_1 x_2 + (\hat{\epsilon}_6 + \hat{\epsilon}_7 x_1) f_c \bar{x}_3 - (\hat{\epsilon}_8 + \hat{\epsilon}_9 x_1) f_c x_2 \\ & + (\hat{\phi}_1 + \hat{\phi}_2 x_1) \dot{\bar{x}}_{3dc} - \frac{1}{2} \hat{\phi}_2 x_2 z_3 - (\hat{\theta}_1 \bar{x}_3 - \hat{\theta}_2 x_2) f_c x_1^2 \end{aligned} \quad (7.98)$$

The robust part:

$$u_3 = -D \text{sign}(z_3) \left[B_A B_B + \max(B_A, B_B) \sqrt{x_1^2 + \zeta_2} \right] \sqrt{f_c^2 + \zeta_2}. \quad (7.99)$$

Parameter update law:

$$\begin{aligned} \dot{\hat{\theta}} &= \Gamma_1 [\text{proj}_{\theta_1}(z_2 z_3 + f_c x_1^2 \bar{x}_3 z_3), -f_c x_1^2 x_2 z_3, 0, 0, \text{proj}_{\theta_5}(-x_1 R_A z_3 u), 0, \text{proj}_{\theta_7}(x_1 R_B z_3 u)] \\ \dot{\hat{\epsilon}} &= \Gamma_2 [-x_2 z_3, x_4 z_3 - x_3 z_3, x_1 x_2 z_3, \text{proj}_{\epsilon_4}(R_A z_3 u), \text{proj}_{\epsilon_5}(R_B z_3 u), -f_c \bar{x}_3 z_3, -f_c x_1 \bar{x}_3 z_3, f_c x_2 z_3, f_c x_1 x_2 z_3] \\ \dot{\hat{\phi}} &= \Gamma_3 [-\dot{\bar{x}}_{3dc} z_3, \frac{1}{2} x_2 z_3^2 - x_1 \dot{\bar{x}}_{3dc} z_3] \end{aligned} \quad (7.100)$$

7.5.2 Signals

Independent Signals	
Position reference	x_d
Velocity reference	\dot{x}_d
Acceleration reference	\ddot{x}_d
Yerk reference	\dddot{x}_d
Cylinder displacement	$x_1 = x_{CE}$
Cylinder velocity	$x_2 = \dot{x}_{CE}$
Pressure in chamber A	$x_3 = p_A$
Pressure in chamber B	$x_4 = p_B$

Derived Signals Without Parameter Estimates	
New state variable	$\bar{x}_3 = A_A x_3 - A_B x_4$
Tracking error and error variable in first intermediate controller	$z_1 = x_1 - x_d$
Error variable in the second intermediate controller	$z_2 = x_2 - \dot{x}_d + k_1 z_1$
Driving pressure of valve port A	$R_A = s(u)\sqrt{p_p - x_3} + s(-u)\sqrt{x_3 - p_T}$
Driving pressure of valve port B	$R_B = s(u)\sqrt{x_4 - p_T} + s(-u)\sqrt{p_p - x_4}$
With the function $s(*)$ defined as:	$s(*) = \begin{cases} 1 & \text{if } * \geq 0 \\ 0 & \text{if } * < 0 \end{cases}$

Derived Signals With Estimates	
Error variable in the last controller	$z_3 = \bar{x}_3 - \bar{x}_{3d}$
Second intermediate control law	$\bar{x}_{3d} = \frac{1}{\hat{\theta}_1} \left[-z_1 - \left(k_2 + \frac{D}{\delta} \right) z_2 + \hat{\theta}_2 x_2 - k_1 x_2 + k_1 \dot{x}_d + \ddot{x}_d \right]$
Certain part of 2. int. controller	$\hat{x}_{3dc} = \frac{1}{\hat{\theta}_1} \left[x_2 \hat{\theta}_2 - \bar{x}_{3d} \hat{\theta}_1 + \left(k_1 k_2 + k_1 \frac{D}{\delta} + 1 \right) (\dot{x}_d - x_2) + \left(k_1 + k_2 + \frac{D}{\delta} \right) \dot{x}_d + \ddot{x}_d \right]$
Certain part of uncertain controller	$f_c = \frac{1}{\hat{\theta}_1} \left(\hat{\theta}_2 - k_1 - k_2 - \frac{D}{\delta} \right)$

7.5.3 Controller Parameters

Parameters from first parameterization:

$$\begin{aligned} \theta_1 &= \frac{1}{M(x_1)} & \theta_2 &= \frac{B(x_1, x_2)}{M(x_1)} & \theta_3 &= \beta A_A & \theta_4 &= \beta C_L & \theta_5 &= \beta K_A K_V \\ \theta_6 &= \beta A_B & \theta_7 &= \beta K_B K_V & \beta_A &= \frac{V_{A0}}{A_A} & \beta_B &= \frac{V_{B0}}{A_B} \end{aligned}$$

Parameters from second parameterization:

$$\begin{aligned} \epsilon_1 &= \beta_B \theta_3 + \beta_A \theta_6 & \epsilon_2 &= (\beta_A + \beta_B) \theta_4 & \epsilon_3 &= \theta_3 - \theta_6 & \epsilon_4 &= \beta_B \theta_5 & \epsilon_5 &= \beta_A \theta_7 & \epsilon_6 &= \theta_1 \beta_A \beta_B \\ \epsilon_7 &= \theta_1 (\beta_B - \beta_A) & \epsilon_8 &= \theta_2 \beta_A \beta_B & \epsilon_9 &= \theta_2 (\beta_B - \beta_A) & \phi_1 &= \beta_A \beta_B & \phi_2 &= \beta_B - \beta_A \end{aligned}$$

Tuneable Parameters

Converging Gains:

$$k_1 = 10 \quad k_2 = 10 \quad k_3 = 10 \quad (7.101)$$

Adaption Gains:

$$\Gamma_1, \Gamma_2, \Gamma_3 \quad (7.102)$$

7.5.4 Bounds

The parameters and disturbance bounds are calculated using the equations on the previous page and the parameter variations seen in Appendix C. The results are seen below.

Disturbance Bound

$$\delta = 0.01 \text{ m/s} \quad (7.103)$$

$$\frac{F(t)}{M(x_1)} = d(t) \leq D = 0.75 \text{ N/kg} \quad (7.104)$$

Parameter Bounds

Parameter	Minimum	Estimate	Maximum
θ_1	1.8519e-6	2.2165e-6	9.6154e-6
θ_2	0.2778	1.0611	3.6000
θ_3	1266770	12667700	15201240
θ_4	0	0.0011	0.0026
θ_5	18.0877	151.6063	327.4698
θ_6	1010250	10102500	12123000
θ_7	9.0438	75.8031	163.7349
ϵ_1	1.3719e6	1.3719e7	1.6462e7
ϵ_2	0	0.0012	0.0029
ϵ_3	256520	2565200	3078240
ϵ_4	17.6660	148.0722	319.8361
ϵ_5	1.2051	10.1009	21.8180
ϵ_6	2.4101e-7	2.8847e-7	1.2514e-6
ϵ_7	1.5619e-6	1.8695e-6	8.1100e-6
ϵ_8	0.0362	0.1381	0.4685
ϵ_9	0.2343	0.8950	3.0364
β_A	0.1066	0.1333	0.1599
β_B	0.7814	0.9767	1.1720
ϕ_1	0.1301	0.1301	0.1562
ϕ_2	0.6747	0.8434	1.0121

Table 7.1: List of the 20 parameters with minimum and maximum values. The estimate is calculated using the verified system parameters. To calculate values for M and B, used in the estimate, the operating point $x_{CE} = x_{CEMIN}$, $\dot{x}_{CE} = 0$ is chosen.

Chapter 8

Synthesis of Backstepping Control

This section elaborate on the developed controller. The obtained controller structures are investigated and the error dynamics for the 2^{nd} intermediate control law is determined. Then a discussion about practical considerations and complications follows. Conclusively, some improvements and possible solutions to the complications are introduced.

8.1 Controller Structure

Through the backstepping procedure we obtain a control law. This law is too complex to visualize in a block diagram but the 1. and 2. Intermediate control laws can, which is seen in the following subsections. The reason for this section is to give an idea about what type of control law the backstepping procedure produce, and then get a better understanding of how it can be tuned to obtain desired performance.

8.1.1 First Intermediate Control Law

The first intermediate control is a P-controller with an inverse dynamics feedforward, see Equation (8.1). The feed-forward provide perfect tracking if the model is perfect/exact. Models are never perfect, and the P-controller account for the imperfections.

$$x_{2d} = -k_1 z_1 + \dot{x}_d \quad k_1 > 0 \quad (8.1)$$

Provided that the 2^{nd} intermediate control law obtains $x_2 = x_{2d}$, the 1. control law can be visualized, in the system, as in Figure 8.1.

8.1.2 Second Intermediate Control Law

The 2^{nd} intermediate control law is seen in (8.2).

$$\bar{x}_{3d} = \frac{1}{\hat{\theta}_1} \left[\underbrace{-x_1 + x_d}_{-z_1} + \bar{x}_{3r} - k_2 \left(x_2 + \underbrace{k_1(x_1 - x_d) - \dot{x}_d}_{-x_{2d} \text{ see (7.18)}} \right) + \hat{\theta}_2 x_2 - k_1 x_2 + k_1 \dot{x}_d + \ddot{x}_d \right] \quad (8.2)$$

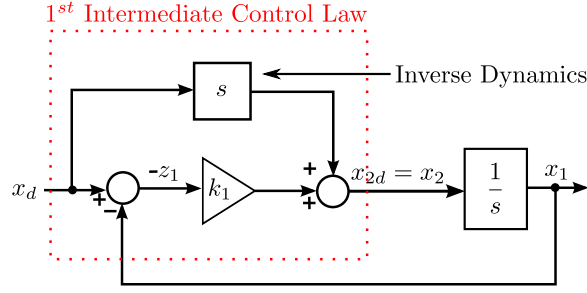


Figure 8.1: The first intermediate control law in block diagram realization.

Provided that the 3rd (and final) control law obtains $\bar{x}_3 = \bar{x}_{3d}$ the 2nd intermediate control can be visualized, in the system, as seen in Figure 8.2.

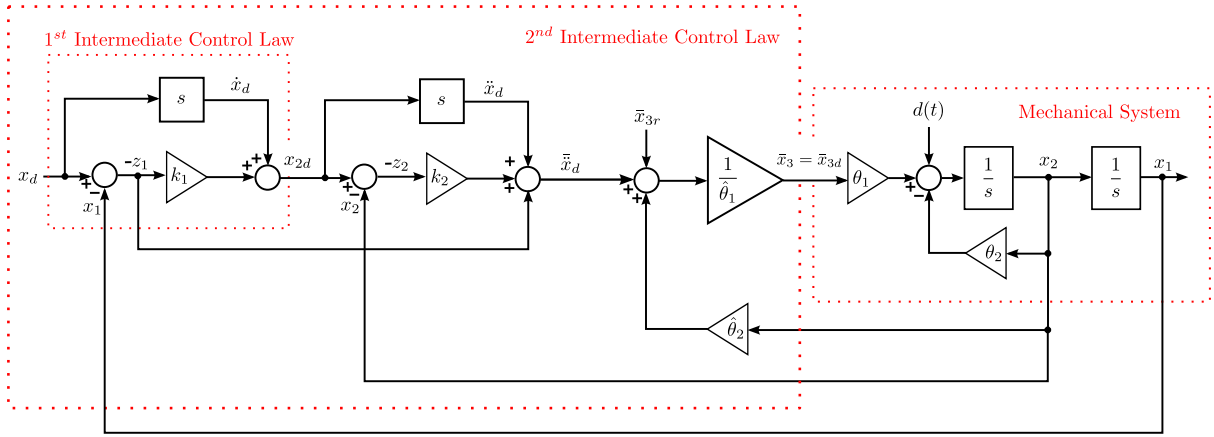


Figure 8.2: The second intermediate control law in block diagram realization. It is seen that the adaptive part of the controller cancels the system parameters if they adapt the correct values.

The second intermediate control provides yet another P-controller for the second error variable z_2 , and again tries to cancel out the dynamics of the system. This time based on the system parameter estimates $\hat{\theta}_1$ and $\hat{\theta}_2$, updated by (8.5). The robust controller \bar{x}_{3r} is designed so the system remains stable despite the disturbance $|d(t)| \leq D$.

It is seen that the backstepping procedure also created a cross-link from $-z_1$ directly to \bar{x}_d . The reason for this is clear when the error dynamics are inspected later, but before this is done the control law (8.2) can be rewritten to reveal a familiar control structure.

First the tracking error is denoted $e = -z_1 = x_d - x_1$, with derivatives $\dot{e} = \dot{x}_d - \dot{x}_2$ and $\ddot{e} = \ddot{x}_d - \ddot{x}_2$. Equation (8.2) is then factored:

$$\bar{x}_{3d} = \frac{1}{\hat{\theta}_1} \left[\underbrace{-x_1 + x_d}_e + \underbrace{(\hat{\theta}_2 - k_1 - k_2)x_2 + (k_1 + k_2)\dot{x}_d}_{(k_1 + k_2)\dot{e}} + \underbrace{k_1 k_2 x_d - k_1 k_2 x_1}_{k_1 k_2 e} + \ddot{x}_d + \bar{x}_{3r} \right] \quad (8.3)$$

and the tracking error e , with its derivatives, are substituted:

$$\bar{x}_{3d} = \frac{1}{\hat{\theta}_1} \left[(1 + k_1 k_2)e + (k_1 + k_2)\dot{e} + \hat{\theta}_2 x_2 + \ddot{x}_d + \bar{x}_{3r} \right] \quad (8.4)$$

This show that the cascaded P controllers can in fact be seen as a PD controller with an acceleration

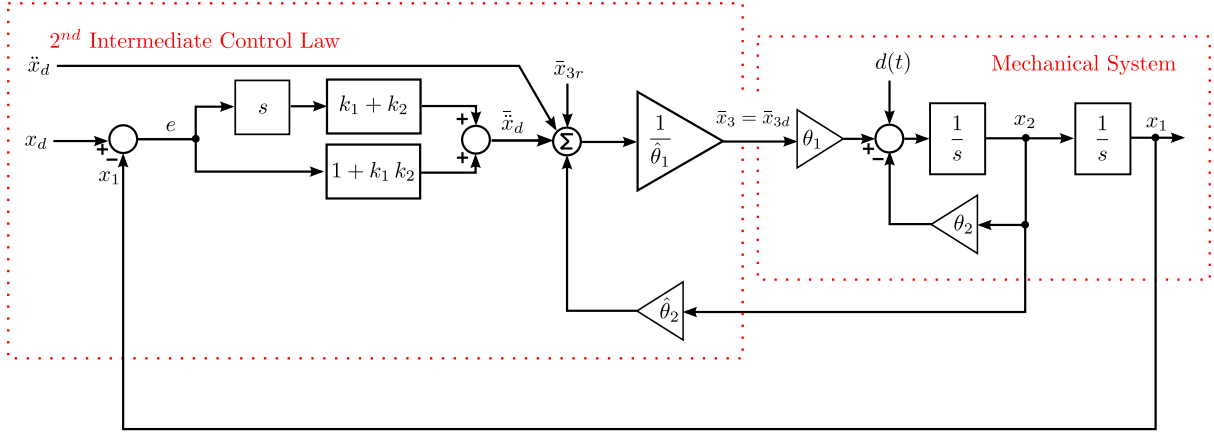


Figure 8.3: The second intermediate control law in block diagram realization. It is seen that the backstepping procedure produced two adaption gains to cancel out the dynamics of the mechanical system and then provided a PD controller to reduce the tracking error.

feed-forward, which has the advantages of making k_1 and k_2 tunable using classic linear control theory. It is mentioned that when the controller is implemented the derivative error \dot{e} is obtained from the velocity signal x_2 and the velocity reference \dot{x}_d instead of differentiating the error signal.

The adaption laws for the 2^{nd} intermediate control are seen in Equation (8.5) below:

$$\begin{aligned}\dot{\hat{\theta}}_1 &= \gamma_1 z_2 \bar{x}_{3d} \\ \dot{\hat{\theta}}_2 &= -\gamma_2 z_2 x_2\end{aligned}\quad (8.5)$$

All we know is that the parameter estimates are bounded, not that they converge to the right values. The adaption is a *direct* structure as the parameters that are estimated are parameters of the control law directly. Contradicting, the parameters are also *plant* parameters which usually indicates an in-direct adaption. However, since there is no translation of the estimated plant parameters before they are used in the control law the adaption is, pr. definition, direct [Slotine and Li, 1991, p. 320].

8.2 Error Dynamics

Combining Equation (8.4) with the system equation for the mechanical system, seen in Equation (8.6), reveals the error dynamics when $\bar{x}_3 = \bar{x}_{3d}$.

$$\dot{x}_2 = \theta_1 \bar{x}_3 - \theta_2 x_2 - d(t) \quad (8.6)$$

Inserting (8.4) into (8.6):

$$\dot{x}_2 = \frac{\theta_1}{\hat{\theta}_1} \left[(1 + k_1 k_2)e + (k_1 + k_2)\dot{e} + \hat{\theta}_2 x_2 + \dot{x}_d + \bar{x}_{3r} \right] - \theta_2 x_2 - d(t) \quad (8.7)$$

Recognizing $\ddot{e} = \dot{x}_d - \dot{x}_2$ and assuming correct parameter estimations i.e. $\hat{\theta}_1 = \theta_1$ and $\hat{\theta}_2 = \theta_2$:

$$(1 + k_1 k_2)e + (k_1 + k_2)\dot{e} + \ddot{e} = d(t) - \bar{x}_{3r} \quad (8.8)$$

Laplace transforming the equation and ignoring initial conditions yields:

$$e = \frac{d(t) - \bar{x}_{3r}}{(1 + k_1 k_2) + (k_1 + k_2)s + s^2} \quad (8.9)$$

This equation is also seen in block diagram representation in Figure 8.4. If \bar{x}_{3r} successfully compensate the disturbance $d(t)$ the tracking error converges to the equilibrium point $e = 0$ making the error dynamics exponentially stable.

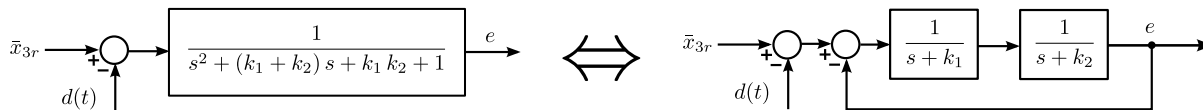


Figure 8.4: The error dynamics visualized in block diagrams.

It is possible to reduce the tuning variables by requiring that the error dynamics should be critically damped, which is when $k_1 = k_2$. This is, in the ideal case of correct parameter estimation and perfect force tracking the fastest response without overshoot for a given eigenfrequency ω_e . However, the controller is tuned using loop shaping and root locus design techniques instead, as the extra degree of freedom is wanted in our case.

8.3 Practical Considerations and Complications

The discussion so far has only been focusing on the 2^{nd} intermediate control law. The final control law is far more complex and consists of three parts; a certain part, an uncertain adaption part and a robust part which together forms the final control law. Besides the control law, also 15 parameter update laws have been designed.

The practical considerations of having a large complex controller with many parameters are discussed here. The discussion are based on the information listed in the 7.5 Controller Summary on page 70.

8.3.1 Number of Signals

The controller require position, velocity and pressure measurements. Compared to simple linear controllers (requiring only position measurements) the controller needs 3 extra sensors or has to utilize observers to obtain the required signals.

The controller also require extensive reference information: Position, velocity, acceleration and even jerk are required. One would assume that the higher derivatives could be left without when they are not available, and they probably can, but the stability of the controllers are not guaranteed in this case. The stability prove is derived on the assumption that these signals are correct and available.

8.3.2 Large and Complex Equations

The equations are cumbersome to implement and debug, which require programming time and experience. Positively, once they are programmed correctly the software can be used for similar systems, as long as enough computing power is available. This is therefore not considered as a remarkable concern in most applications.

8.3.3 Amount of System and Disturbance Parameters

Considering Table 7.1 on page 72 we see that there is 20 system parameters that require a lower and an upper bound together with an initial estimate. The performance depend on the estimate and the robustness on the bounds.

The parameter bounds are derived quantities and may be calculated from the 7 parameters of θ plus the two parameters ϕ_1 and ϕ_2 seen in 7.5.3. If this is taken into account the $3 \times 20 = 60$ quantities in Table 7.1 can be determined by $3 \times 9 = 27$ quantities. Besides these quantities one also has to determine the disturbance bound D , to be used in the robust part of the controller. In total it is a minimum of 28 system parameters.

The parameters are different from each system, and therefore must be determined every time a new controller is initialized. The increased cost of doing this must be outweighed by improved performance for the controller to be cost-effective.

8.3.4 Tuning Parameters

Each control law and parameter update law require a constant to be determined. The three controllers have k_1 , k_2 and k_3 , and the 15 adaption parameters are collected in the matrices $\Gamma_1, \Gamma_2, \Gamma_3$. How to determine the parameters are not obvious, and varies from system to system. The parameters cannot be determined individually as the optimal value of each depend on the value of all the other parameters. This is considered the largest drawback of the controller.

8.3.5 Input Saturation, Fluctuating Pump Pressure and Unmatched Cylinder-Valve

The controller has been derived based on the assumption that the pump pressure is constant. In a practical situation this is never the case, and in many systems it is far from constant.

The derivation also required that the pump-pressure is the highest pressure in the system. If the cylinder and valve are unmatched this requirement can sometimes be hard to fulfill.

All physical actuators is limited but the stability proof do not take this into account. The controllers should therefore be tuned so they do not saturate the actuator which consequently leads to conservative designs.

8.3.6 Conclusion

The test setup available in this project has shown to have **highly fluctuating pump pressure** as seen in Figure E.5 on page 151. It also has to maintain a large pressure differential across the cylinder just to compensate the gravitational force resulting from the weight of the arm. This, combined with **unmatched valve and cylinder** result in p_B being higher than the pump pressure p_P , a situation which cannot be avoided. This claim is documented in section 11.

It is concluded that the RABNLP controller is too comprehensive and that it has too many drawbacks to be used in a practical setup as it is. Considering the time spend on tuning the controller in the simulations and due to the practical complications just mentioned, the evaluation of the controller is carried out based on simulations instead of tests, see Section 13.

In the next section, some improvements to the controller along with possible solutions to the mentioned complications are addressed.

8.4 Improvements and Possible Solutions

A simplified backstepping controller has been developed, so that a controller derived using backstepping could be tested on the experimental setup despite the practical complications. The rest of this section

can be seen as a section of future work. It is included at this point in the report, as it relates to the complications just discussed.

8.4.1 Input Saturation

To be able to overcome the problem of conservative tuning one would have to take the input saturation into account. In [Zhou and Wen, 2008, p. 173-181] the author presents a new scheme to design adaptive backstepping controllers for a class of uncertain nonlinear systems when input saturation is present.

8.4.2 Extended Stability Proof

To overcome the problem of fluctuating pump pressure and too high chamber pressure one would have to carry out the backstepping procedure again, this time without the hydraulic assumptions and simplifications. The controller should either be robust towards, or adapt, the variations. The leakage flow is not modeled either, but it is always present. An extended stability proof could take this into account as well.

8.4.3 Tuning Functions

To avoid the over-parameterization that follows from adaptive backstepping control one could make adaptive design based on tuning functions. Using these, a parameter update law of minimum order is achieved, meaning that the number of adaption parameters equal the number of physical parameters. The method is presented in Chapter 4 of [Miroslav Krstic and Kokotovic, 1995, p. 123-183].

8.4.4 Simplified Controller

Considering the developed RABNLP controller it is clear that most of the complexity arises from the third step of the backstepping procedure. The idea is to use the 2^{nd} intermediate control law developed in 7.4.2, but replace the inner loop with a linear controller. The requirement for the 2^{nd} intermediate control law is that the inner controller obtain the desired cylinder force in finite time. That is $z_3 = \bar{x}_3 - \bar{x}_{3d} \rightarrow 0$ for $t \rightarrow \infty$.

The next chapter concerns the development of this inner controller resulting in the new hybrid control structure referenced as the RABLIN controller for Robust Adaptive Backstepping Linear Controller.

$\zeta_{PL} \leq 1$ to remove the resonance but maintain a fast response.

The block C_{PL} is a force controller. It is designed so the closed loop bandwidth is as high as the actuator limits allow. High loop gain is also preferable to suppress the disturbances $F(t)$ and plant variations.

The block **Backstepping Controller** is an adaptive position feedback controller with acceleration feed-forward, as seen in Section 8. It is described by the 2^{nd} intermediate control law, repeated in Equation (9.1), along with the adaption law seen in (7.26) and repeated in (9.2).

From Equation (8.4) on page 74 we have:

$$\bar{x}_{3d} = \frac{1}{\hat{\theta}_1} \left[(1 + k_1 k_2)e + (k_1 + k_2)\dot{e} + \hat{\theta}_2 x_2 + \ddot{x}_d + \bar{x}_{3r} \right], \quad k_1, k_2 > 0 \quad (9.1)$$

The feed back part of the controller is a PD controller which is tuned assuming $\hat{\theta}_1 = \theta_1$, $\hat{\theta}_2 = \theta_2$. It is tuned to have high open loop gain and closed loop bandwidth. The limitation is the stability margin and actuator saturation.

As the 3. step in the backstepping procedure is not used the two parameter update laws, in this controller, can be written more conveniently as:

$$\begin{aligned} \dot{\hat{\theta}}_1 &= \gamma_1 z_2 \bar{x}_{3d} \\ \dot{\hat{\theta}}_2 &= -\gamma_2 z_2 x_2 \end{aligned} \quad (9.2)$$

9.1 Linear Controller Design

The overall objective in the controller design (besides stability) is to have as small tracking error $e = x_d - x_1$ as possible. How the controller should be designed to accomplish this depends on the reference signal x_d , but in general it is achieved by having a large loop gain over a wide frequency band. The actual tracking accuracy is affected by plant parameter variations and disturbances, therefore also good disturbance rejection and low sensitivity is important design goals. Fortunately, low sensitivity and good disturbance rejection is also achieved by a high loop gain within a wide frequency band. [Phillips and Harbor, 2000, p.356].

9.2 Damping Controller

Before elaborating on the actual design of the damping controller the result is shown, so the reason for the damping control is clear. The open-loop transfer function from u to p_L is plotted *without* the damping controller H_{FB} . This is the plant that the *force controller* C_{PL} would have to control if *no damping* controller was used. There are two curves as there are two critical operating points for G_{PL} , one with lowest eigenfrequency and one with highest resonance peak. This is discussed further in Appendix D.4 on page 146.

From Figure 9.1 we get the plant transfer function for the force loop by multiplying $K_Q G_{PL} A_A$. The bodeplot is seen in Figure 9.2. The design specifications for the force controller require it to have a high loop gain over a wide frequency band as possible. The resonance peak makes it hard to accomplish without violating the stability margins of the system. By designing a damping controller H_{FB} we are able to design a plant for the force controller C_{PL} with the frequency response seen in Figure 9.3.

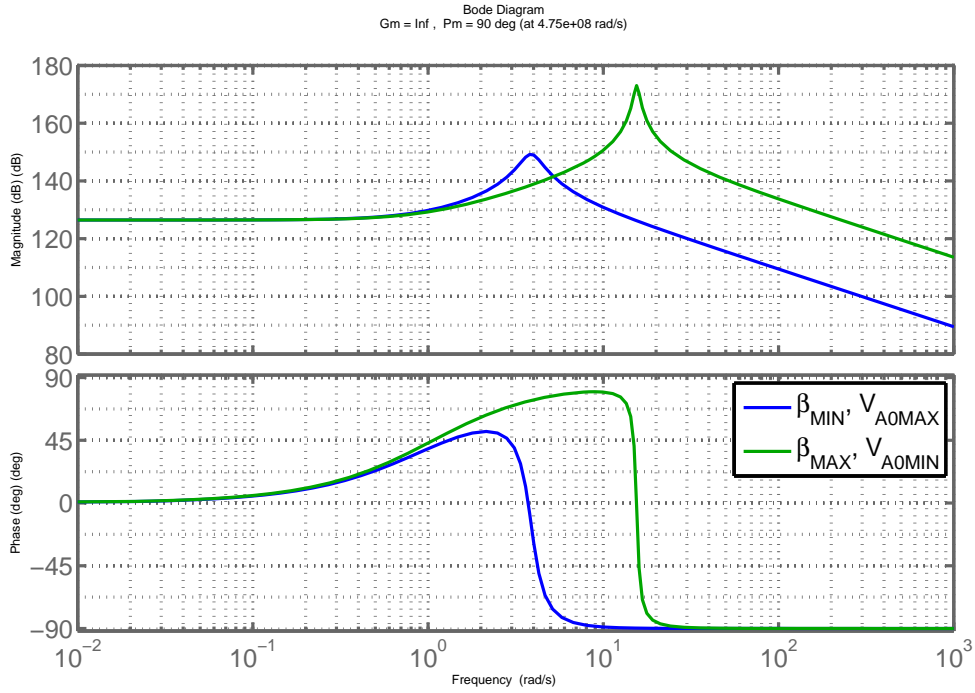


Figure 9.2: Bode plot of the plant for the **force** controller C_{PL} *without* damping controller H_{FB} . The diagram shows curves for both critical operating points.

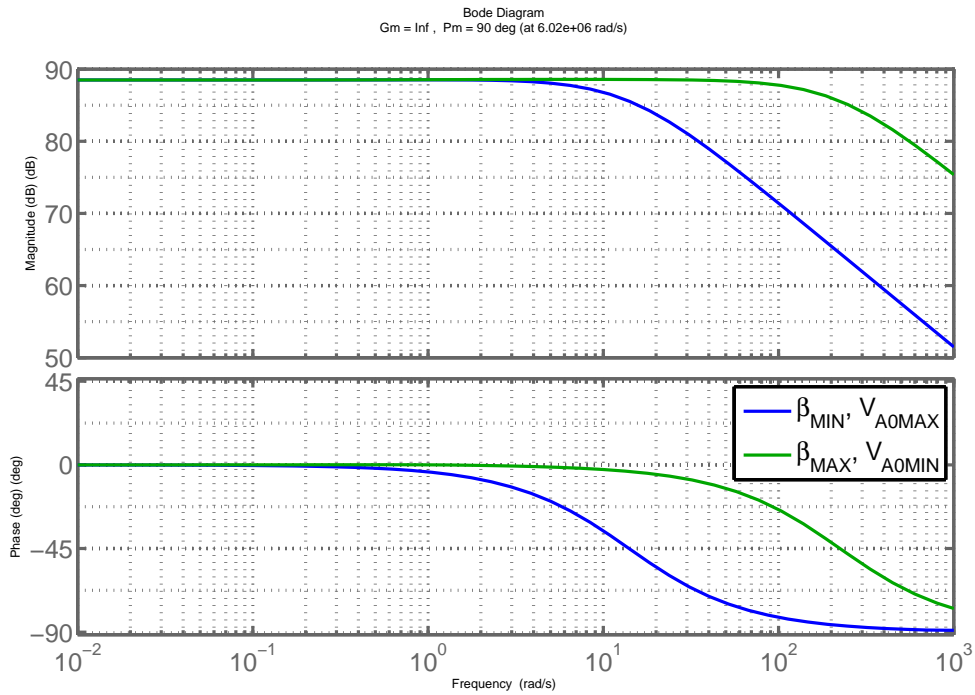


Figure 9.3: Bode plot of the plant for the **force** controller C_{PL} *with* damping controller H_{FB} . The diagram shows curves for both critical operating points.

9.2.1 Design of Damping Controller H_{FB}

At this point, the reason for the damping controller should be clear, how it is designed is shown in this subsection. From the main block diagram of Figure 9.1 the block diagram seen in Figure 9.4 is obtained.

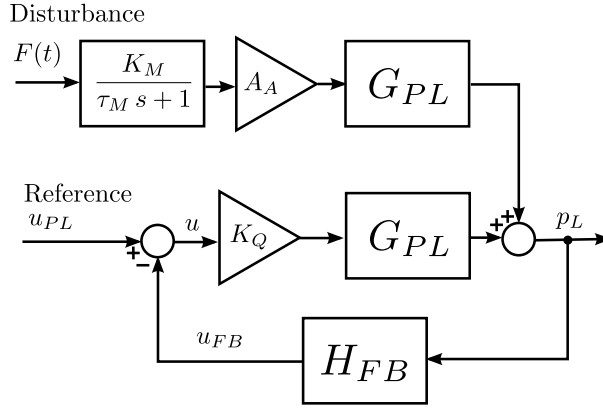


Figure 9.4: Block diagram representation of the **damping** control system

Multiplying the transfer functions in the disturbance path we find the disturbance transfer function which describes the influence in the output p_L for disturbance input F . The transfer function expressions are from the summary of the linearized model in section 6.2 on page 50. The disturbance transfer function is derived in (9.3) and shown in block diagram of Figure 9.5.

$$\begin{aligned}
 D_{PL}(s) &= \frac{K_M}{\tau_M s + 1} A_A G_{PL}(s) \\
 &= A_A K_{PL} \frac{K_M}{\tau_M s + 1} \frac{\omega_{PL}^2 (\tau_M s + 1)}{s^2 + 2\zeta_{PL} \omega_{PL} s + \omega_{PL}^2} \\
 &= A_A \frac{B}{A_A^2} \frac{\frac{1}{B}}{\tau_M s + 1} \frac{\omega_{PL}^2 (\tau_M s + 1)}{s^2 + 2\zeta_{PL} \omega_{PL} s + \omega_{PL}^2} \\
 &= \frac{1}{A_A} \frac{\omega_{PL}^2}{s^2 + 2\zeta_{PL} \omega_{PL} s + \omega_{PL}^2}
 \end{aligned} \tag{9.3}$$

The transfer function tells us that the disturbance (in this loop) is most significant below the eigenfrequency of the plant ω_{PL} .

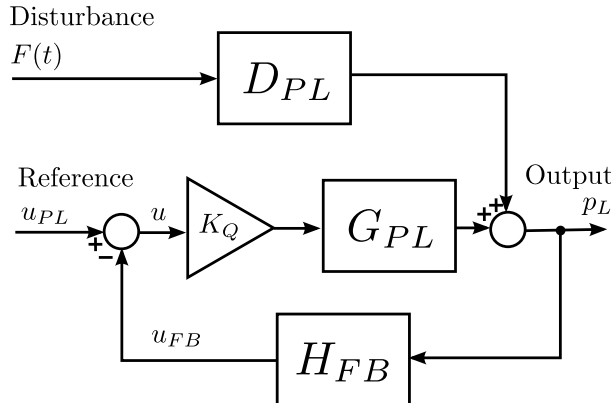


Figure 9.5: Block diagram representation of the **damping** control system, with disturbance transfer function.

Disturbance Rejection As the controller is positioned in the feedback loop of the control system, increased open-loop gain do not result in disturbance rejection. This is seen by inspecting the expression for the output $p_L(s)$.

$$\begin{aligned} p_L &= K_Q G_{PL} u_{PL} + D_{PL} F - K_Q G_{PL} H_{FB} p_L \\ &= \frac{K_Q G_{PL}}{1 + K_Q G_{PL} H_{FB}} u_{PL} + \frac{D_{PL}}{1 + K_Q G_{PL} H_{FB}} F \end{aligned} \quad (9.4)$$

The controller H_{FB} appears in the denominator of both the closed loop disturbance transfer function and the closed loop reference transfer function, which show that the damping controller has the same influence on both the reference and the disturbance output, thus no disturbance rejection is provided. If the controller was positioned in the forward path we would have gained disturbance rejection for increased controller gain as the expression for the output would have been:

$$(H_{FB} \text{ in forwardpath}) \quad p_L = \frac{K_Q G_{PL} H_{FB}}{1 + K_Q G_{PL} H_{FB}} p_{Ld} + \frac{D_{PL}}{1 + K_Q G_{PL} H_{FB}} F \quad (9.5)$$

Obtaining Increased Damping Two ways of increasing the damping have been considered. One is a pure gain, and the other is a differentiator with a real pole, resulting in a high-pass filter. They both yield similar performance but the P-controller has a larger low frequency gain, due to the discussion regarding disturbance rejection, this is not seen as a benefit and the one presented here is the high-pass filter.

$$H_{FB} = \frac{K_{FB} s}{s + \omega_{FB}} = \frac{4.718e-7 s}{s + 1.061} \quad (9.6)$$

The pole is chosen slightly lower than the mechanical cut-off frequency $\frac{1}{T_M}$. The analysis in D should make sure that the frequency do not get lower for any other operating point. The gain K_{FB} is adjusted so it yields the closed loop response seen in (9.3). The root locus of the system with compensator is seen

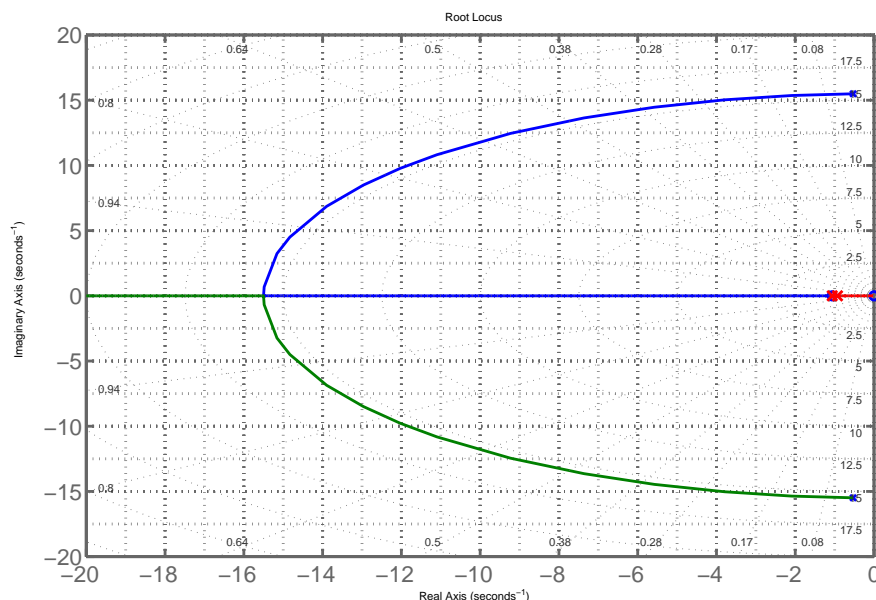


Figure 9.6: An equal axis root locus of the compensated **damping** system. The red branch is added by the compensator.

in (9.6). The two complex conjugated poles travels in opposite directions on the real-axis, one towards $-\infty$ and the other towards the mechanical cut-off frequency at -1.0611 rad/s. The pole traveling

in positive direction is the dominating of the two. The red branch is added by the compensator, where a new closed loop pole originates at the mechanical cut-off frequency, and travels towards the origin.

The gain is chosen so that the two dominating poles are placed as close to each other as possible. The limitation is the eigenfrequency of *the valve* at 314.16 rad/s. The gain is adjusted so the closed loop bandwidth of the faster system, (operating point where $\beta = \beta_{MAX}$) seen in Figure 9.3, is approximately 200 rad/s, about 100 rad/s lower than the valve dynamics. Having a pole close to the critical damped valve poles is clear when the force controller is discussed. The adjusted gain places the dominating closed loop poles at the locations of the red X's in Figure 9.6.

9.3 Force Controller

The force controller C_{PL} is designed so the closed loop bandwidth is as high as the actuator limits allow, therefore we include the valve in the closed loop expression for T_{FB} and the block diagram changes from 9.7 to 9.8.

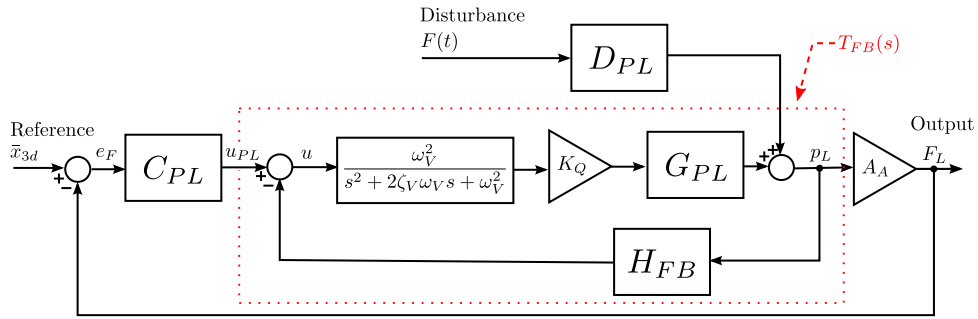


Figure 9.7: Block diagram representation of the **force** control system.

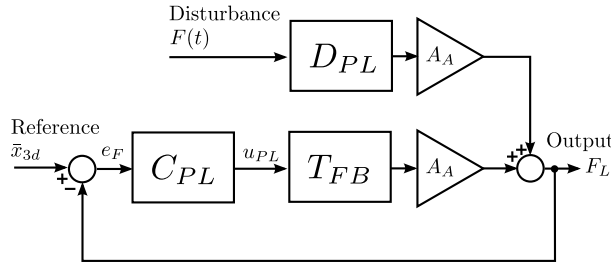


Figure 9.8: Reduced block diagram representation of the **force** control system.

In the ideal case an integrator should be added in order to increase the type of the control system. An increase would make the steady state error for a step-change, in force reference, zero. Thus, it rejects the DC-component of the noise $F(t)$, which is shown to be quite significant in the measurements. However, this controller is an intermediate control between the damping controller and the backstepping controller, and its closed loop system will work as the plant of the backstepping controller.

The backstepping controller already has two free-integrators (assuming $\hat{\theta}_2 = \theta_2$), so the last thing it needs is additional phase-lag. The compromise is a simple P-controller and the gain is adjusted using the root locus design plot seen in Figure 9.9. The plot is for the critical operating point which is $\beta = \beta_{MAX}$ $V_{A0} = V_{A0MIN}$, because this yields the smallest gain-margin.

The fast "insignificant" pole from the damping controller is seen to have a large effect on the valve dynamics, changing it from a double pole to a set of complex conjugated poles with lower damping and frequency. The design prioritizes a well damped hydraulic system because its dynamics happens at a lower frequency and therefore dominates the final response.

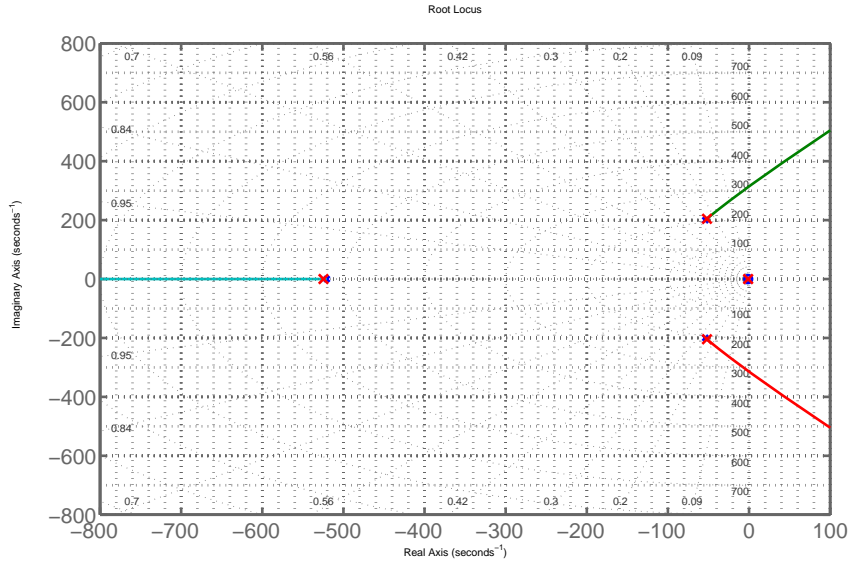


Figure 9.9: A root locus of the compensated **force** control system. The red branch is added by the compensator.

The chosen proportional gain of the Force controller is

$$C_{PL} = K_{PL} = 1.8062e-6 \text{ V/N} \quad (9.7)$$

Resulting in the closed loop bodeplots seen in Figure 9.10, and the following closed loop poles for the critical operating point $\beta = \beta_{MAX}$ $V_{A0} = V_{A0MIN}$.

$$\text{eig}(T_{PL}) = [-1.064, -51.88 \pm i204.5, -524.56] \quad (9.8)$$

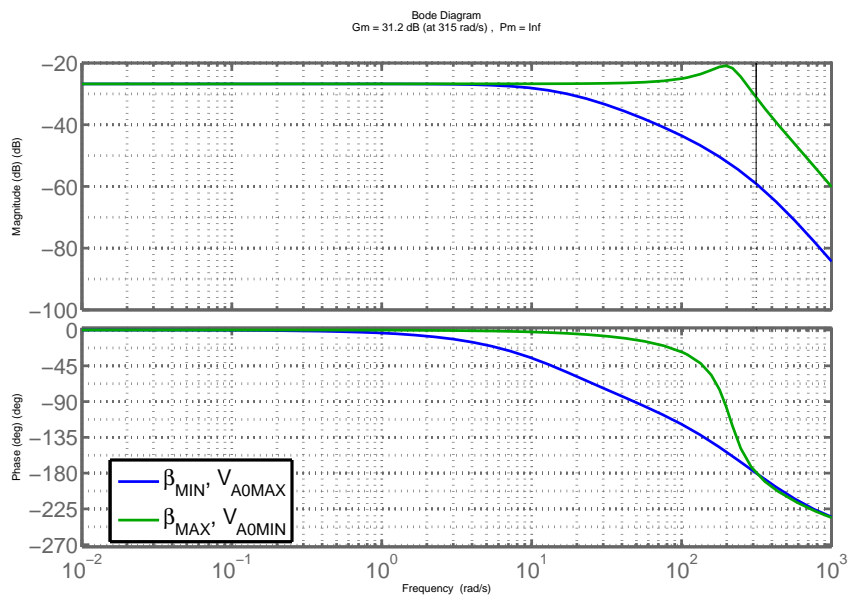


Figure 9.10: Closed loop bodeplot of the **force** control system. The diagram shows curves for both critical operating points.

9.4 Backstepping Position Controller

The backstepping controller is an adaptive PD position controller with acceleration feed-forward. The design task is to determine the values of K_P and K_D in the controller:

$$C_{BS} = K_P + K_D s \quad (9.9)$$

and then obtain values of k_1 and k_2 from the following expressions:

$$k_1 = K_D - k_2 \quad k_2 = \frac{K_P}{2} + \frac{\sqrt{K_D^2 - 4K_P + 4}}{2} \quad (9.10)$$

The control system is seen in block diagram representation in Figure 9.11.

The design is carried out with the critical values of the parameter estimates $\hat{\theta}_1$ and $\hat{\theta}_2$. The gain $\frac{1}{\hat{\theta}_1} = \hat{M}$ is critical when $\hat{\theta}_1 = \theta_{1MIN}$, as this is where the loop gain is highest. For the parameter $\theta_2 = \frac{B}{M}$, we choose $\hat{\theta}_2 = \theta_2$, as this is where the damping is completely compensated, resulting in a second free integrator.

Ignoring the disturbance, the block diagram of Figure 9.11 can be re-arranged into Figure 9.12.

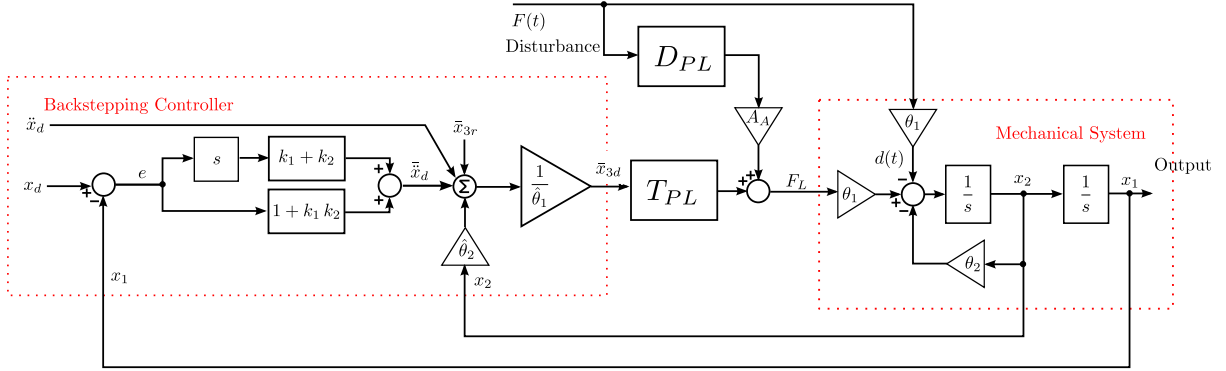


Figure 9.11: Block diagram representation of the **backstepping** control system.

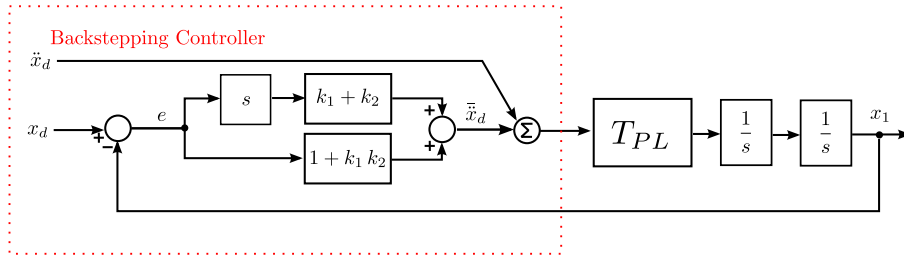


Figure 9.12: Reduced block diagram of the **backstepping** control system.

The controller is tuned so the system has as high open loop gain and closed loop bandwidth as the stability margins allow. This means that the controller is tuned aggressive for: ($\beta = \beta_{MIN}$, $V_{A0} = V_{A0MAX}$), and a bit conservative for ($\beta = \beta_{MAX}$, $V_{A0} = V_{A0MIN}$). The smallest phase margin is for ($\beta = \beta_{MIN}$, $V_{A0} = V_{A0MAX}$) and the smallest gain margin is for ($\beta = \beta_{MAX}$, $V_{A0} = V_{A0MIN}$):

$$\phi_M = 30^\circ \quad G_M = 20.5 \text{ dB} \quad (9.11)$$

The chosen compensator values are:

$$K_P = 1200 \text{ s}^{-2} \quad K_D = 200 \text{ s}^{-1} \quad (9.12)$$

and from (9.10) we get:

$$k_1 = 6.186 \text{ s}^{-1} \quad k_2 = 193.81 \text{ s}^{-1} \quad (9.13)$$

The compensated open loop bodeplot is seen in Figure 9.13 and the resulting closed loop system is seen in Figure 9.14.

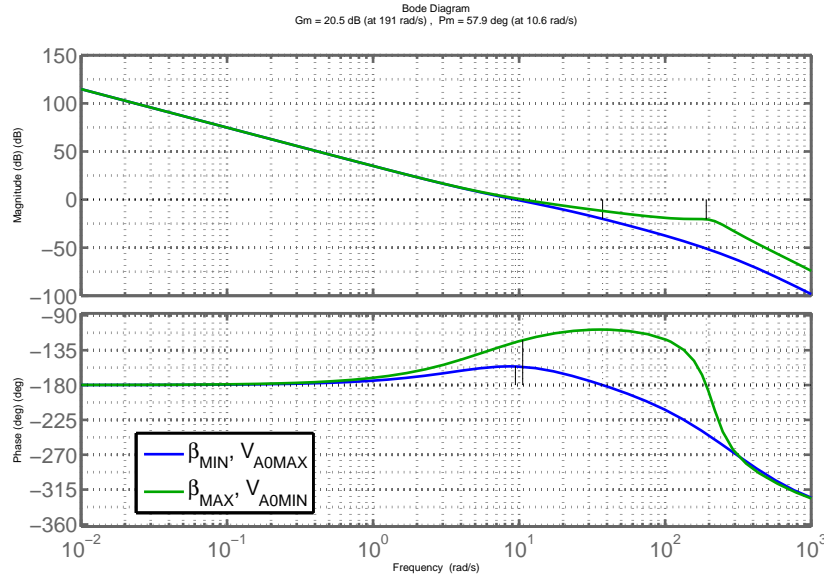


Figure 9.13: Open loop bodeplot of **backstepping** control system with PD position feedback controller, including valve dynamics. The diagram shows curves for both critical operating points.

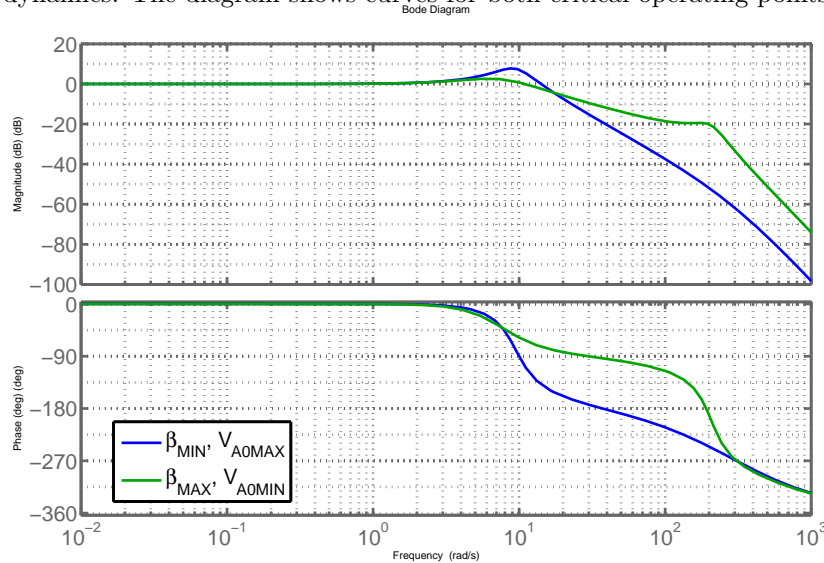


Figure 9.14: Closed loop bode plot of the **backstepping** control system including valve dynamics. The diagram shows curves for both critical operating points.

This concludes the feedback controller design of the backstepping controller. The feed-forward require no parameters and the adaption gains γ_1 and γ_2 are adjusted based on simulations to the following values:

$$\gamma_1 = 1e-13 \frac{1}{\text{kg m Pa}} \quad \gamma_2 = 10 \frac{\text{s}^3}{\text{kg m}^3} \quad (9.14)$$

Therefore, the controller design of the RABLIN controller is finished. The next chapter concerns the design of a reference controller.

Chapter 10

Reference Controller

To be able to evaluate the developed backstepping controllers a reference controller is designed. The controller chosen as a reference is a simple yet powerful P-LEAD feed-forward structure. The controller have a feed-forward path which provide the flow needed for the steady state motion of the cylinder. It is calculated in an operating point, so it is only in this point it provides the modeled steady state flow exact. The operating point should not be the most critical but the one that provides the best flow estimate.

The feed-forward is able to deliver a large flow without the risk of destabilizing the system, which is an extensive advantage over controllers with only feedback control e.g. a traditional PID, especially in systems with low damping as the feedback controller must be tuned very conservative to ensure responsible stability margins.

The P-LEAD controller accounts for the compression flow and the variations from the operating point. Compared to a pure P controller the LEAD part adds phase around the gain crossover frequency (where phase margin is calculated). This increases the stability margins and makes it possible to increase the open-loop gain further.

Unlike the controller design for the RABLIN controller in the previous chapter, this control system has only one critical operating point, as described in Appendix D.

10.1 Control System

The transfer function used in the design of the LINREF controller is the transfer function from Δu to Δx_{CE} . It is derived in Section B on page 133, and repeated in Equation(10.1).

$$G_{UX} = \frac{K_Q}{A_A} \frac{\omega_{PL}^2}{s(s^2 + 2\zeta_{PL}\omega_{PL}s + \omega_{PL}^2)} \quad (10.1)$$

Ignoring the disturbances the position control system for the reference controller can be visualized in block diagram as in Figure 10.1.

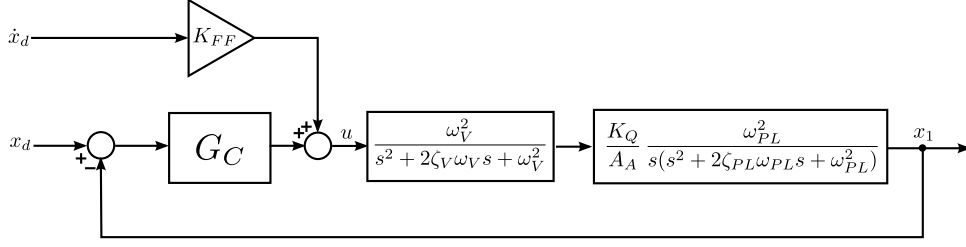


Figure 10.1: Block diagram of the reference controller and the linearized system.

10.2 Feedforward Controller Design

The Feed-forward gain are designed as the steady-state inverse of the plant, which is:

$$K_{FF} = \frac{A_A}{K_Q} \quad (10.2)$$

Where K_Q depend on the sign of the reference velocity and an operating point for the load-pressure p_{L0} . From (B.12) on page 128:

$$K_Q = \begin{cases} K_L \sqrt{p_P - \alpha p_T - p_{L0}} & \dot{x}_d \geq 0 \\ K_L \sqrt{\alpha p_P - p_T + p_{L0}} & \dot{x}_d < 0 \end{cases} \quad (10.3)$$

10.3 Feedback Controller Design

As the structure of the feedback controller is determined the design task is to choose the amount of gain together with the location of the zero and the pole of the filter. The transfer function of the feedback controller is

$$C_{BS} = K_{BS} \frac{s + \omega_0}{s + \omega_p} \quad \omega_0 < \omega_p \quad (10.4)$$

A, open-loop bode plot of the uncompensated system is seen in Figure 10.2. The lead filter provides a phase boost which is placed around the phase crossover frequency, allowing a further increase of the open loop gain. The locations of the pole and zero are chosen as

$$\omega_0 = 1.309 \text{ rad/s} \quad \omega_p = 1000 \text{ rad/s} \quad (10.5)$$

The gain K_{BS} is adjusted to yield the following stability margins

$$K_{BS} = 4509 \text{ V/m} \quad \Rightarrow \quad G_M = 16 \text{ dB} \quad \text{and} \quad \phi_m = 49.8^\circ \quad (10.6)$$

The compensated bodeplot with and without valve dynamics are seen in 10.3. We know from the choice of operating point that we are designing for the most critical situation, meaning that the phase cross-over frequency happens at higher frequencies and the open-loop gain only gets lower, resulting in increased gain and phase margin.

By inspecting the bodeplot of the valve from the datasheet, seen in Figure 4.6 on page 29, we know that the approximated model has more phase-lag up to ≈ 20 Hz than the worst case shown. As the gain cross-over frequency happens at ≈ 4 rad/s the valve model is more conservative than the worst case from the data-sheet. The step response is seen in Figure 10.4. It show a risetime of $T_R = 6.11$ s, a 2% settling time of $T_S = 11.98$ s, no overshoot but it is very oscillatory, which is a result of the low damping in the system.

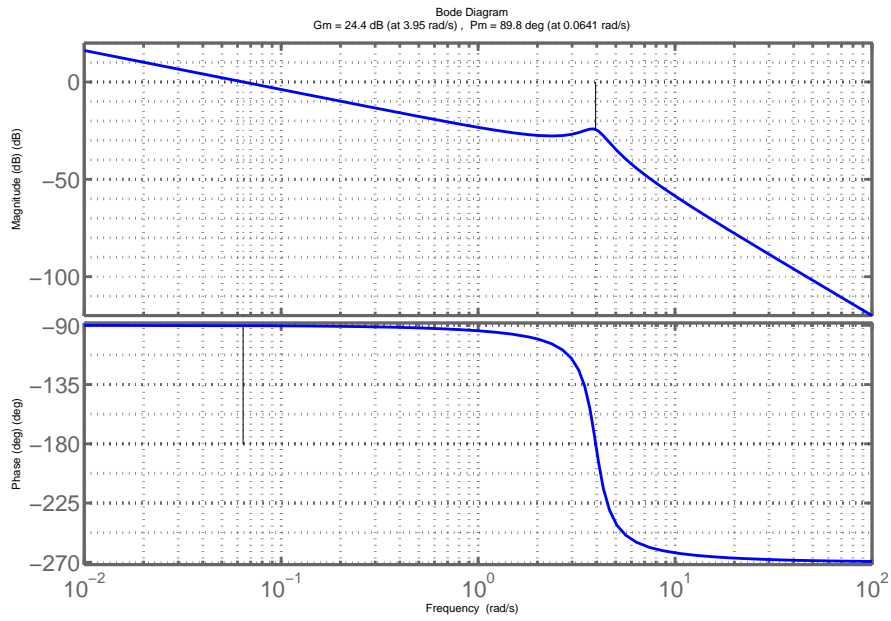


Figure 10.2: Open-loop bode plot of the linearized system.

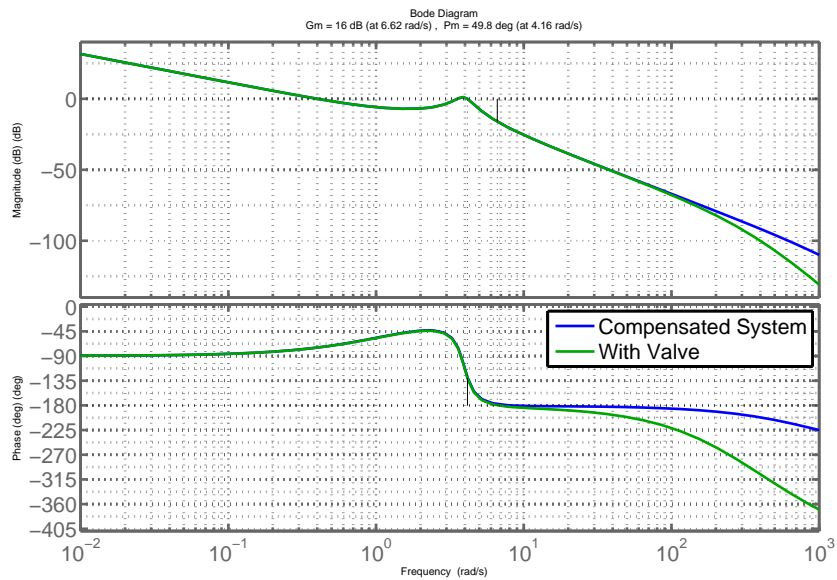


Figure 10.3: Open-loop bode plot of the feedback-compensated linearized system, with and without valve dynamics.

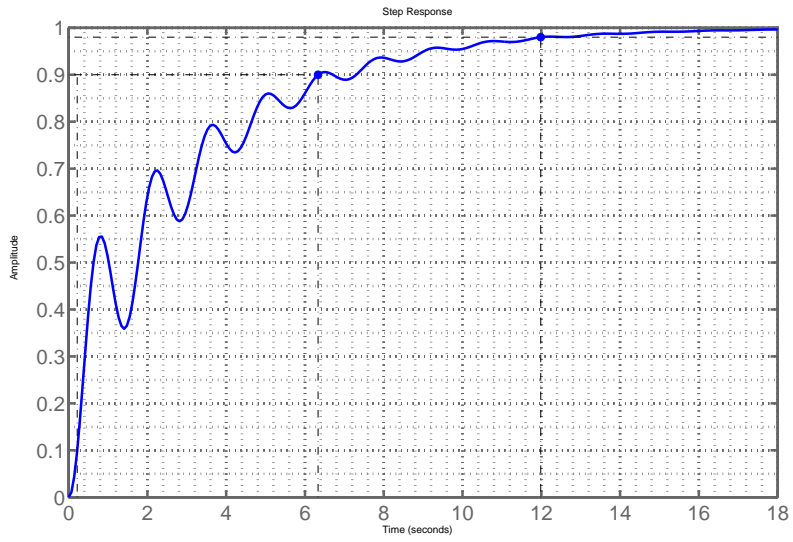


Figure 10.4: Step response of the feedback-compensated closed loop system.

Controller Design Part Conclusion

To summarize the content of the second part of the report it was concerned with controller design of the three controllers:

RABNLP Robust Adaptive Backstepping Controller with Non-Linear Parameters in Chapter 7. First the principle of backstepping was defined. Then the system equations from the simulation model were simplified and put on the right form. After this, the actual backstepping-like controller design was presented proving global stability and convergence of the error states to within a pre-defined ball in the state space, resulting in bounded tracking error.

Chapter 8 was a synthesis of the RABNLP controller investigating the controller structure and the error dynamics of the two first intermediate control laws. It also contained a section describing the practical considerations and complications along with suggestions for improvements and possible solutions.

RABLIN Robust Adaptive Backstepping Linear Controller in Chapter 9. The RABNLP controller was simplified into the RABLIN controller. It is based on the 2^nd intermediate control law from the RABNLP controller, but uses a linear control structure for the inner force loop instead. This reduced the number of tuning parameters from 18 to 7 and made it possible to tune the controller using linear control theory.

LINREF Linear Reference Controller in Chapter 10. The chosen reference is a position controller structure with P-LEAD feedback and inverse steady state feedforward .

This concludes the part concerned with *controller design*. Next part deals with the evaluation of tracking performance of the the two backstepping controllers RABNLP and RABLIN using the LINREF controller as a reference.

Part III

Controller Evaluation and Conclusion

Chapter 11

Trajectory Planning

The trajectories are designed so they reveal the tracking performance of the controllers while emphasizing the parameter variations of the system. This is achieved by planning trajectories that takes the system through a large region in the state-space, which results in parameter variations of both mass M , friction coefficient B and changing disturbances in form of gravitational force $F_T(t)$. Hydraulic parameter variations also occur from changing volumes V_A and V_B .

The mentioned parameter variations and disturbances are parameterized in the model, but there are several other factors that have not been considered. So besides the known disturbances and plant variations, the system also experience non-linear stiction and coulomb friction along with changing pump pressure p_P and oil parameters bulk modulus β and density ρ . This is described in Chapter C on page 135.

11.1 Trajectory Bounds

11.1.1 Position Bounds

As mentioned we want large parameter variations in the trajectories, and therefore we have to find the trajectory position bounds, this is done by carefully controlling the system to its end-positions which are found as:

$$x_{CEMIN} = 0.053 \text{ m} \quad x_{CEMAX} = 0.47 \text{ m} \quad (11.1)$$

A flow limiting safety algorithm has been programmed into the control system so that when the position reaches within 10% of the working range:

$$\text{Working Range} = x_{CEMAX} - x_{CEMIN} = 0.417 \text{ m} \quad (11.2)$$

the control signal is ramped down to zero while it approaches the limits x_{CEMIN} or x_{CEMAX} . If a controller is under evaluation we do not want it to end within this limit as it is not the controller that controls the system here. Therefore a safety margin of 20% of the working range is chosen in both ends. This yield a safety margin to the ends of 8.34 cm, and 4.17 cm from the safety region. The position trajectory x_d is therefore defined within:

$$0.1364 \text{ m} \leq x_d \leq 0.3866 \text{ m} \quad (11.3)$$

11.1.2 Velocity Bounds

The maximum velocity is determined from the nominal flow of the valves A port which according to the data sheet [Rexroth, 2006, p. 6] is:

$$Q_N = 100 \text{ L/min} = 0.001667 \text{ m}^3/\text{s} \quad (11.4)$$

In steady state we have

$$Q_A = A_A \cdot \dot{x} \quad (11.5)$$

So if the nominal flow is divided by the cylinder area, the corresponding nominal cylinder velocity is obtained:

$$\dot{x}_{NA} = \frac{Q_N}{A_A} = 0.1315 \text{ m/s} \quad (11.6)$$

The flow in B is half the size of A

$$\dot{x}_{NB} = \frac{Q_N}{2 A_B} = 0.0824 \text{ m/s} \quad (11.7)$$

but as the nominal flow is indicated for a pressure differential of 10 Bar the nominal flow of A is chosen.

$$-0.1315 \text{ m/s} \leq \dot{x}_d \leq 0.1315 \text{ m/s} \quad (11.8)$$

11.2 Trajectory Form

Two trajectories are chosen, see Figure 11.1 and 11.2.

1. Sine Trajectory
2. Ramp and Step Trajectory

Both trajectories are designed to reveal the tracking performance of the controllers, but they emphasize two different characteristics. The purpose of the sine is to reveal the steady state tracking performance, and the purpose of the ramp trajectory is to *also* reveal the transient performance.

The **ramp** has steps in its derivative (\dot{x}_d), which is a discontinuity that cannot be tracked perfectly and results in an error. How well the controller is able to recover from this is characterized as the transient performance. It also reveals steady state tracking performance after the transient period.

The **sine** trajectory reflects a situation where the system performs a *continuous* task of tracking a reference, thus it is not to reveal the controllers transient performance, but its *steady state* tracking performance in spite of plant variations and disturbances. The RABNLP backstepping controller require position (x_d), velocity (\dot{x}_d), acceleration (\ddot{x}_d) and jerk (\dddot{x}_d) information, and as the sine function is \mathcal{C}^∞ (all derivatives defined) the RABNLP benefits from this information in the sine trajectory.

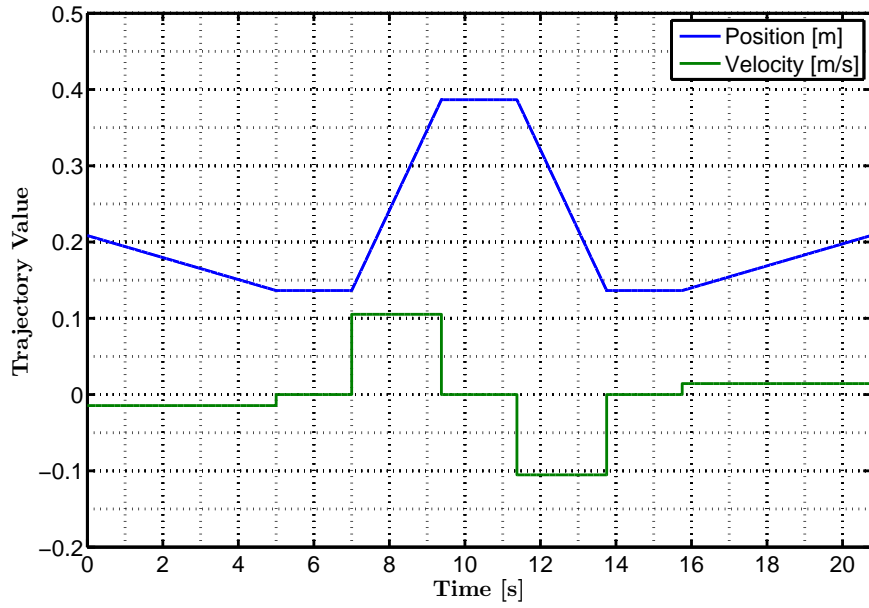


Figure 11.1: The Ramp Trajectory with its first derivative. It has *no* acceleration nor jerk information, but this trajectory reveals the controllers transient performance.

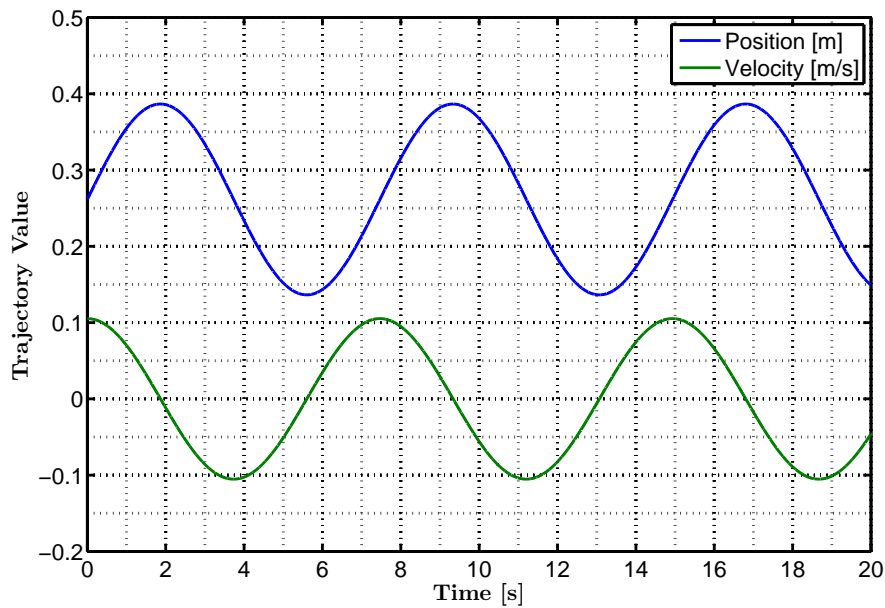


Figure 11.2: The Sine Trajectory with its first derivative. It also has acceleration and jerk information but these are not illustrated.

The ramp trajectory is ramped up to the starting position in both ends so that it can be used repeatedly without having steps in the position reference. The sine trajectory is continuous by definition.

11.3 Parameter Variations of Reference Trajectory

The parameter variations of the two chosen trajectories are seen in Figure 11.3 and 11.4.

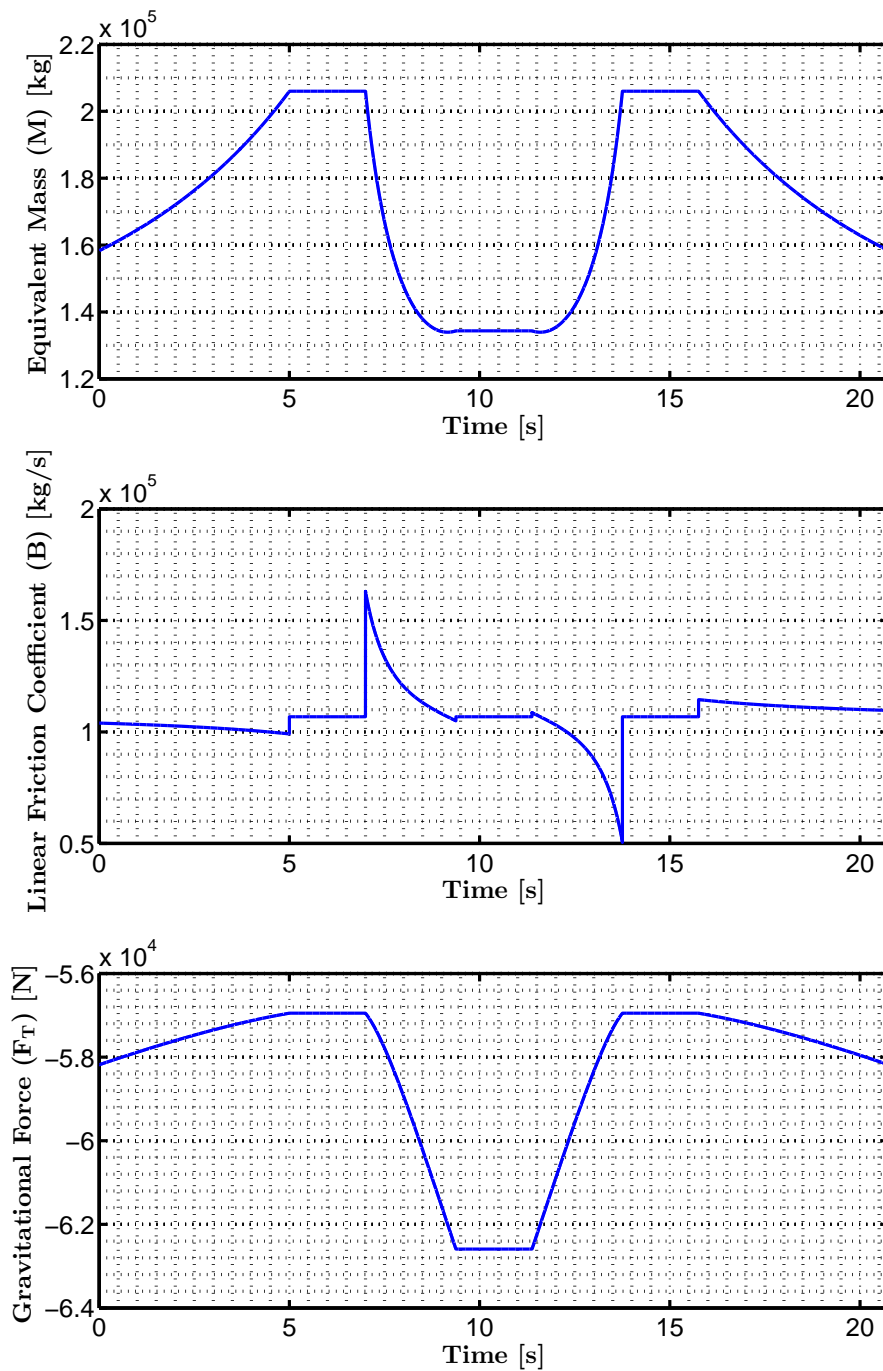


Figure 11.3: Mechanical parameter variations of ramp trajectory.

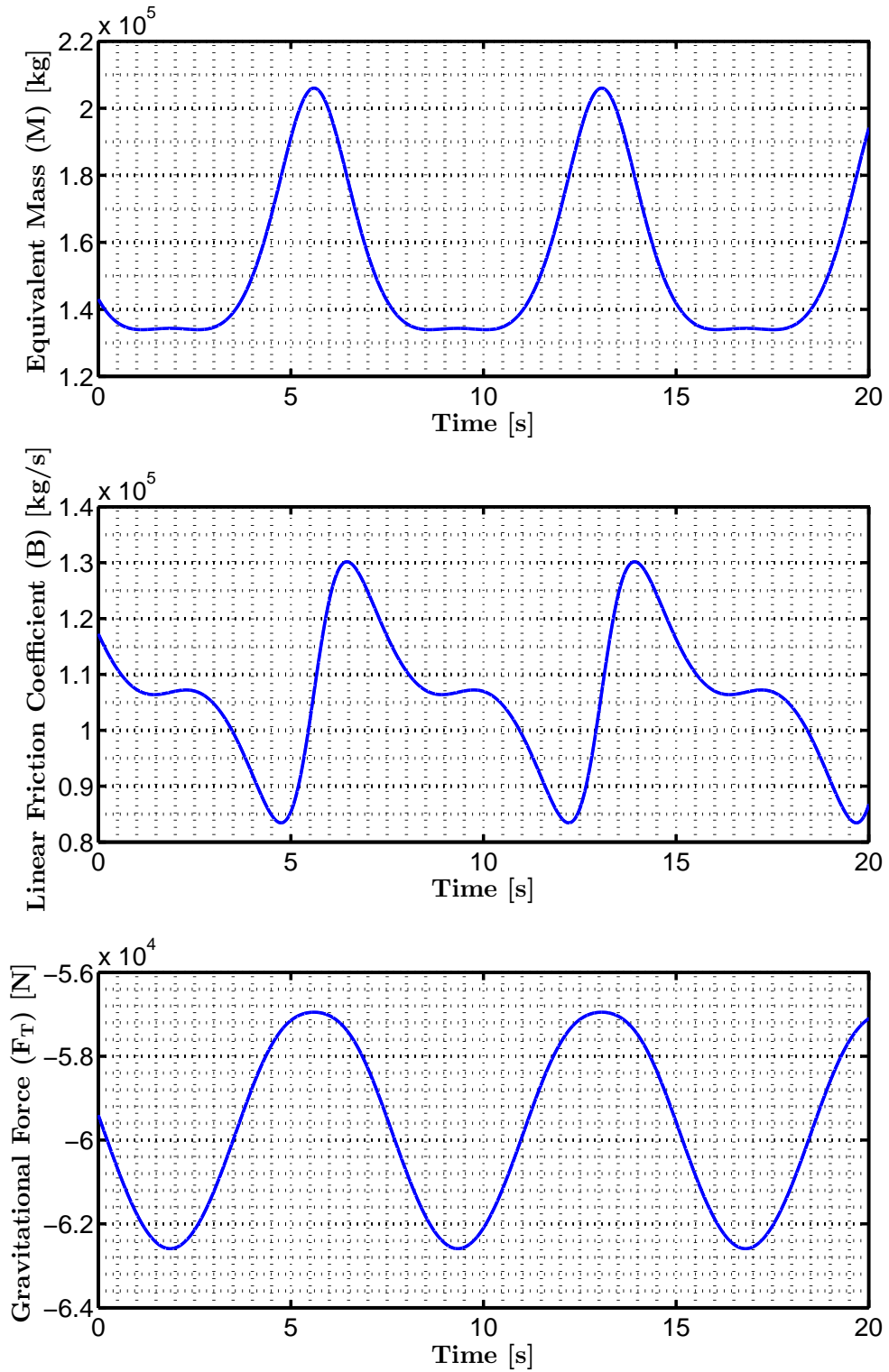


Figure 11.4: Mechanical parameter variations of sine trajectory.

11.4 PQ-Curve of Final Reference Trajectory

To evaluate if the chosen trajectory can be realized by the valve the Simulation Model is used to find a corresponding cylinder force. From Equation (4.42) in the summary of the simulation model on page 30 we get:

$$M(x_d) \ddot{x}_d = F_L - B(x_d, \dot{x}_d) \dot{x}_d - F(x_d), \quad (11.9)$$

The simplified model, derived in Appendix A and summarized in Section 6.1, is then used to calculate the required chamber pressures which due to the steady state assumption translates directly. This is clear from Equation (A.12) and (A.13) on page 124. The two equations are repeated here:

$$p_A = \frac{\alpha^3 p_P + \alpha \sigma^2 p_T + \sigma^2 \frac{F_L}{A_A}}{\sigma^2 + \alpha^3} \quad (11.10)$$

$$p_B = \frac{\alpha^2 p_P + \sigma^2 p_T - \alpha^2 \frac{F_L}{A_A}}{\sigma^2 + \alpha^3} \quad (11.11)$$

Also from the steady state assumption the A and B flow is proportional to the cylinder velocity. From Equation (A.2) on page 123 we get:

$$\dot{x}_d = \frac{Q_A}{A_A} = -\frac{Q_B}{A_B} \quad (11.12)$$

Plotting the flows Q_A and Q_B together with the pressure differentials over each port of the valve reveals whether the trajectory can be realized by the valve. The result is seen in Figure 11.5 and 11.6.

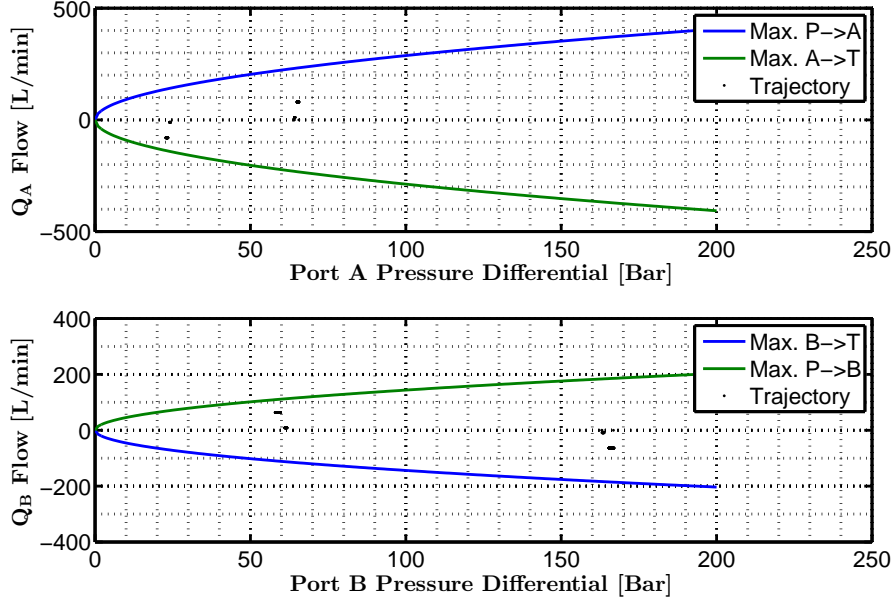


Figure 11.5: The Ramp Trajectory shown in QP plot to check for valve bounds.

At first the trajectories stays fine within the boundaries of the valve, however the pump pressure is only defined to 150 Bar in the calculations, and to realize the trajectory the B port pressure differential is larger than this. This is not a problem for the valve as long as the B port is connected to tank (when the arm is lowering), but when the port connects to the pump the pressure on the B side is larger than the pump side pressure.

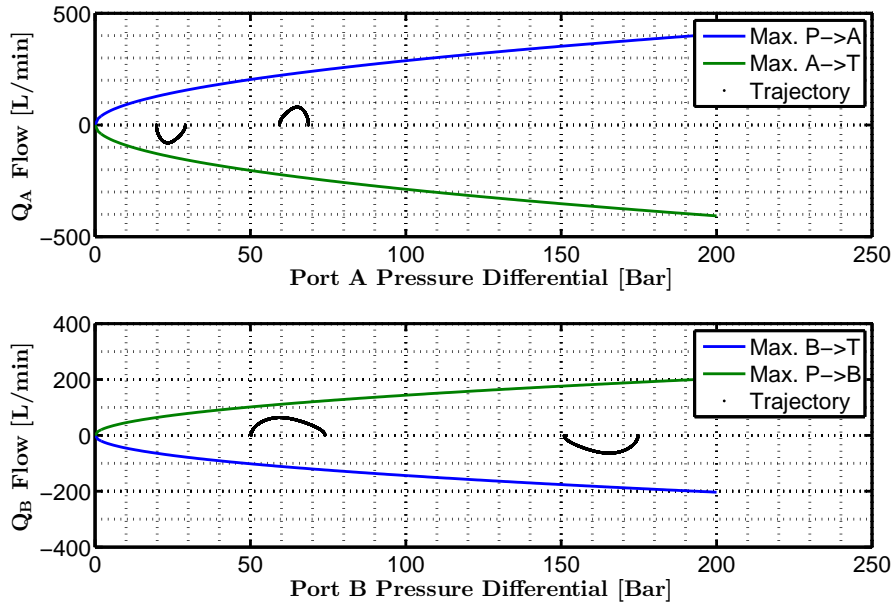


Figure 11.6: The Sine Trajectory shown in QP plot to check for valve bounds.

11.5 Force Bounds

By examining the hydraulic circuit seen in Figure 11.7 we see that the flow is prevented from entering the pump by the check-valve. What happens when the arm start lifting is that the pressure in A starts to drop as it gets connected to tank, and as the pressure in A drops the piston starts to move expanding the volume in B which then lower the pressure $p_B < p_P$, and the pump starts delivering flow again. This usually happens quite fast as only a little expansion of B makes a large pressure drop due to the large stiffness of the oil.

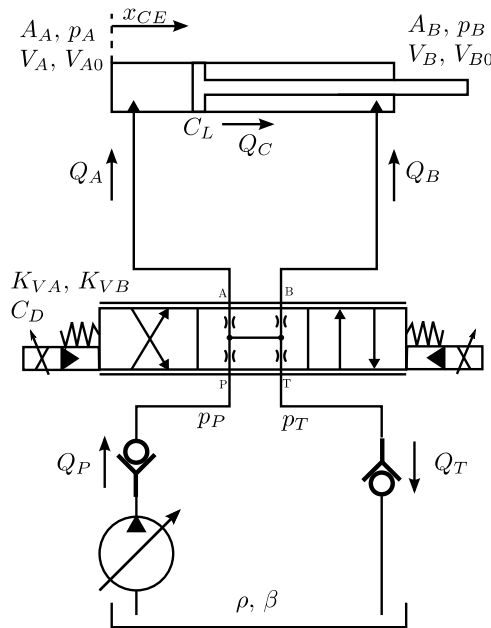


Figure 11.7: Illustration of the hydraulic part of the system.

Still, this is of course not an ideal operating situation but we cannot plan a trajectory to avoid it. It is a consequence of the unmatched valve and cylinder.

To assert this statement we use the equations (11.9), (11.10) and (11.11) on page 99 in the beginning of this section. By equating (11.10) and (11.11) to the pump pressure we can solve for the force expressions that will make $p_A = p_P$ and $p_B = p_P$:

$$F_{APP}(p_P) = A_A p_P - A_A \alpha p_T \quad (11.13)$$

$$F_{BPP}(\sigma, p_P) = \frac{A_A \alpha^2 p_P - A_A \alpha^3 p_P - A_A \sigma^2 p_P + A_A \sigma^2 p_T}{\alpha^2} \quad (11.14)$$

And to complete the picture we calculate the bound for cavitation $p_A = p_T$, $p_B = p_T$ as well:

$$F_{APT}(\sigma, p_P) = \frac{A_A \alpha^3 p_T + A_A \sigma^2 p_T - A_A \alpha \sigma^2 p_T - A_A \alpha^3 p_P}{\sigma^2} \quad (11.15)$$

$$F_{BPT}(p_P) = A_A p_P - A_A \alpha p_T \quad (11.16)$$

Here we do an observation: The force that will make $p_A = p_P$ is the same that will make $p_B = p_T$, and this force is independent of the valve ratio. Hence the maximum force for "pushing" i.e. downward action of the arm is determined solely by the pump-pressure.

From the force equilibrium (11.9) we get that for a stationary "trajectory" ($\dot{x}_d = \ddot{x}_d = 0$) that the cylinder force F_L must equal the gravity force F . From the parameter variations section C we have a figure C.1 illustrating the variations of F for different positions. We see that the smallest value it can attain is $F_{MIN} = -56700$ N.

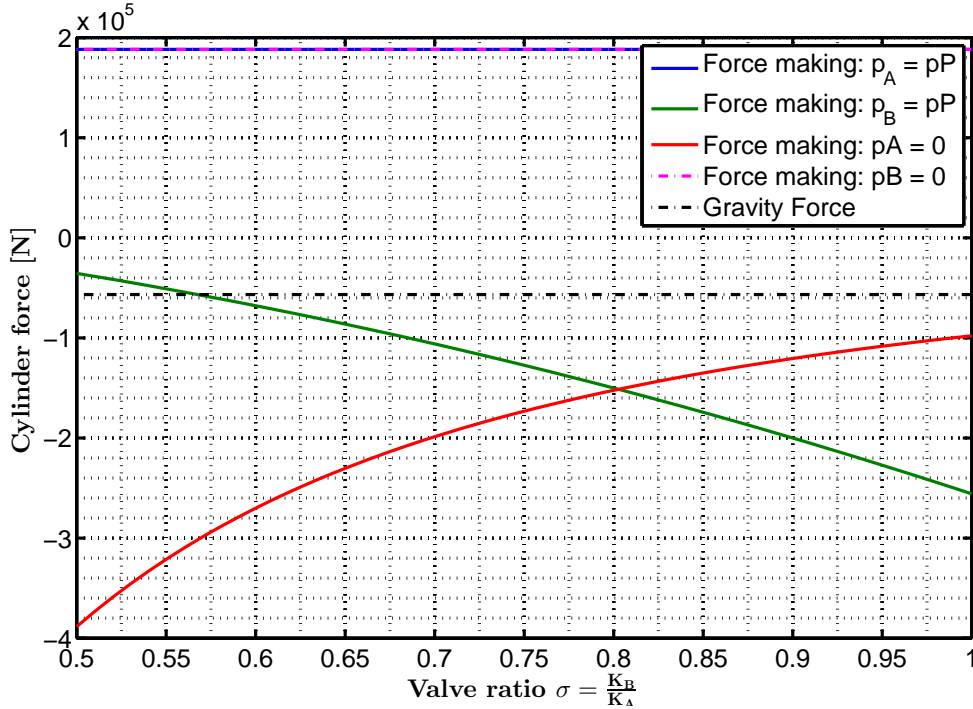


Figure 11.8: Illustration of the maximum and minimum force that the valve can handle without reaching pressures above pump pressure (150 Bar) or cavitation.

In figure 11.8 the bounds for reaching tank and pump pressure is shown as a function of the valve ratio $\sigma = \frac{K_B}{K_A}$. The minimum force for keeping the arm in stationary position is plotted as well.

It is seen that the maximum force for lifting is where the area ratio is $\sigma = 0.8$ which is when the cylinder and valve is matched. When they are unmatched the force for lifting is lowered severely. The valve used in our case has a ratio of $\sigma = 0.5$. For this ratio it is seen that the bound $p_B \leq p_P$ is violated as the PQ plots 11.5, 11.6 and all measurements (e.g. Figure 5.7) show as well.

Turning the valve around only makes things worse, which is equivalent of having $\sigma = 2$. To avoid it we could turn the cylinder around so that the gravity force acts in positive direction. This is however not possible in the time-frame available. The plot in Figure 11.8 are for a pump pressure of only 150 Bar. Increasing the pump pressure increases the bounds, allowing a more negative force. Plotting the bound for $p_B = p_P$ we see that a pump pressure of about 238 Bar is needed just to keep the arm in stationary position. To be able to operate without $p_B = p_P$ it should be even higher.

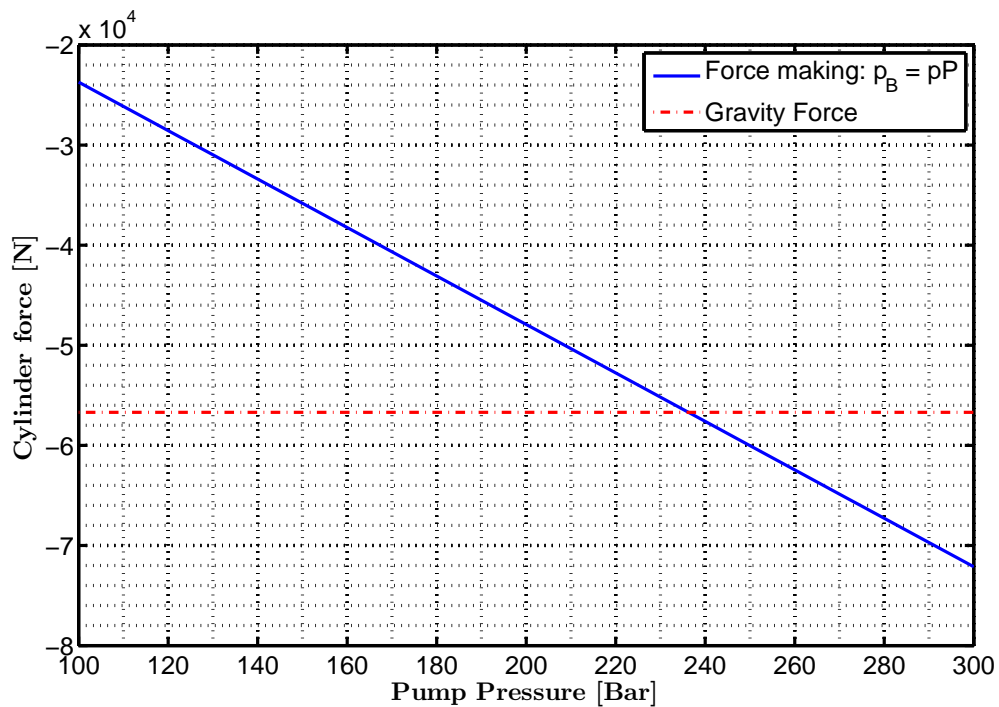


Figure 11.9: Cylinder force that will make $p_B = p_P$ as a function of the pump pressure p_P . The bound $p_B = p_P$ is violated for cylinder force below the blue line.

The pump pressure cannot be changed above approximately 150 Bar as it is now, and the system are to be used like it is.

11.6 Trajectory Summary

Trajectory Bounds

The minimum and maximum position and velocity for the trajectories have been defined.

Tajjectory Form

Two trajectories have been chosen. The trajectories are seen in Figure 11.1 and 11.2 on page 96.

1. Sine Trajectory
2. Ramp Trajectory

The Ramp trajectory is used to evaluate the controllers transient response and steady state response when only position and velocity reference are defined. The Sine trajectory is to evaluate the controllers steady state response when the acceleration and yerk is defined as well. The points used for the ramp trajectory is:

$$\mathbf{X}_{ramp} = [0.2085, 0.1364, 0.1364, 0.3866, 0.3866, 0.1364, 0.1364, 0.2085] \quad (11.17)$$

$$\mathbf{T}_{ramp} = [0, 5.0000, 7.0000, 9.3771, 11.3771, 13.7542, 15.7542, 20.7542,] \quad (11.18)$$

$$\dot{\mathbf{X}}_{ramp} = [-0.0144, 0.0000, 0.1053, 0.0000, -0.1053, 0.0000, 0.0144] \quad (11.19)$$

The points starts and end at the same value to avoid steps in the position signal if it is used cyclic. The position points are interpolated and the velocity points are held between time-values.

The amplitude A_{sine} , the offset B_{sine} and the frequency ω_{sine} of the sine trajectory are:

$$A_{sine} = 0.1251 \text{ m} \quad B_{sine} = 0.2615 \text{ m} \quad \omega_{sine} = 0.8414 \text{ rad/s} \quad (11.20)$$

Parameter Variations

The trajectories were chosen so they result in large parameter variations, as seen in Figure 11.3 and 11.4 on 97 and 98.

Force Bounds

The trajectories steady state flow and pressure were calculated to evaluate if they respects the valve bounds. The calculations showed that the rod side (B) pressure increases above pump pressure, and when the control signal changes direction the result was a negative pressure differential over port B. However, a negative flow was prevented by the pump-side check valve.

The low bound was a consequence of unmatched valve and cylinder. A trajectory that does not violate the bound could not be designed, as the pump pressure is limited to 150 Bar and the cylinder cannot be turned around.

Because of the check valve the trajectories designed are realizable in the real system but with a small delay when the valve switches from $p_T - > p_B$ to $p_P - > p_B$.

QP Plot

As seen in Figure 11.5 and 11.6 on page 99 and 100, the trajectories respect the other valve bounds.

This concludes the trajectory planning. In the next section the controllers will be evaluated using the described trajectories.

Chapter 12

Simulation Results

This chapter presents the simulation results used to evaluate controller performance. All simulations are carried out with either the Ramp or the Sine trajectory as a reference (Chapter 11), which yields the mechanical parameter variations and disturbances seen in Figure 11.3 and 11.4 on page 97 and 98. Besides the dynamics described in 4 the simulations also include the check-valves on the pump and tank side of the hydraulic part, see Figure 4.4 on 26.

Non of the controller designs consider the effect of the check-valve, as it was assumed that the pump pressure and tank pressure were always the highest and the lowest pressures in the system respectively. However, as the experiments (e.g. Figure 5.7) and calculations (11.5) showed that this could not be realized in the real system, the check-valves have been *included* in the simulations. This means that all figures and data presented in this chapter include the check-valves.

Results with and without valve dynamics are presented in section 12.1 and 12.2. The RABNLP controller are unstable if the valve dynamics are included so it is only evaluated without.

12.1 Simulations Without Valve Dynamics

Considering the tracking *accuracy* of the three controllers seen in Figure 12.1 the RABNLP controller is superior, having an RMS tracking error of only 0.1742 mm and a maximum error of 0.2633 mm. The values of the other controllers are more than 8 times larger as seen in table 12.1 on page 106. However, this performance comes at the cost of unrealistic control activity which is seen in Figure 12.2 and in Table 12.1. As a result, the controller is not implemented in the test setup, as the valve simply cannot realize the flow demand of this signal. Furthermore, the simulations show that the controller becomes unstable when this happens and therefore the controller evaluation of the RABNLP controller is based on the simulation results seen in this section.

Tracking Performance RABNLP

Considering the results of Figure 12.1-12.2 the RABNLP performs as expected; It is globally asymptotically stable in the three system states $x_1 = \text{Position}$, $x_2 = \text{Velocity}$ and $\bar{x}_3 = \text{Force}$, within a tracking bound of $e_{max} = \frac{\delta}{k_1} = \frac{0.01}{10} = 1 \text{ mm}$, despite mechanical parameter variations in M and B and disturbance from gravity F . Even though the check valves were not included in the stability analysis.

The next section presents simulation results *including* valve dynamics for the RABLIN and the LINREF controllers.

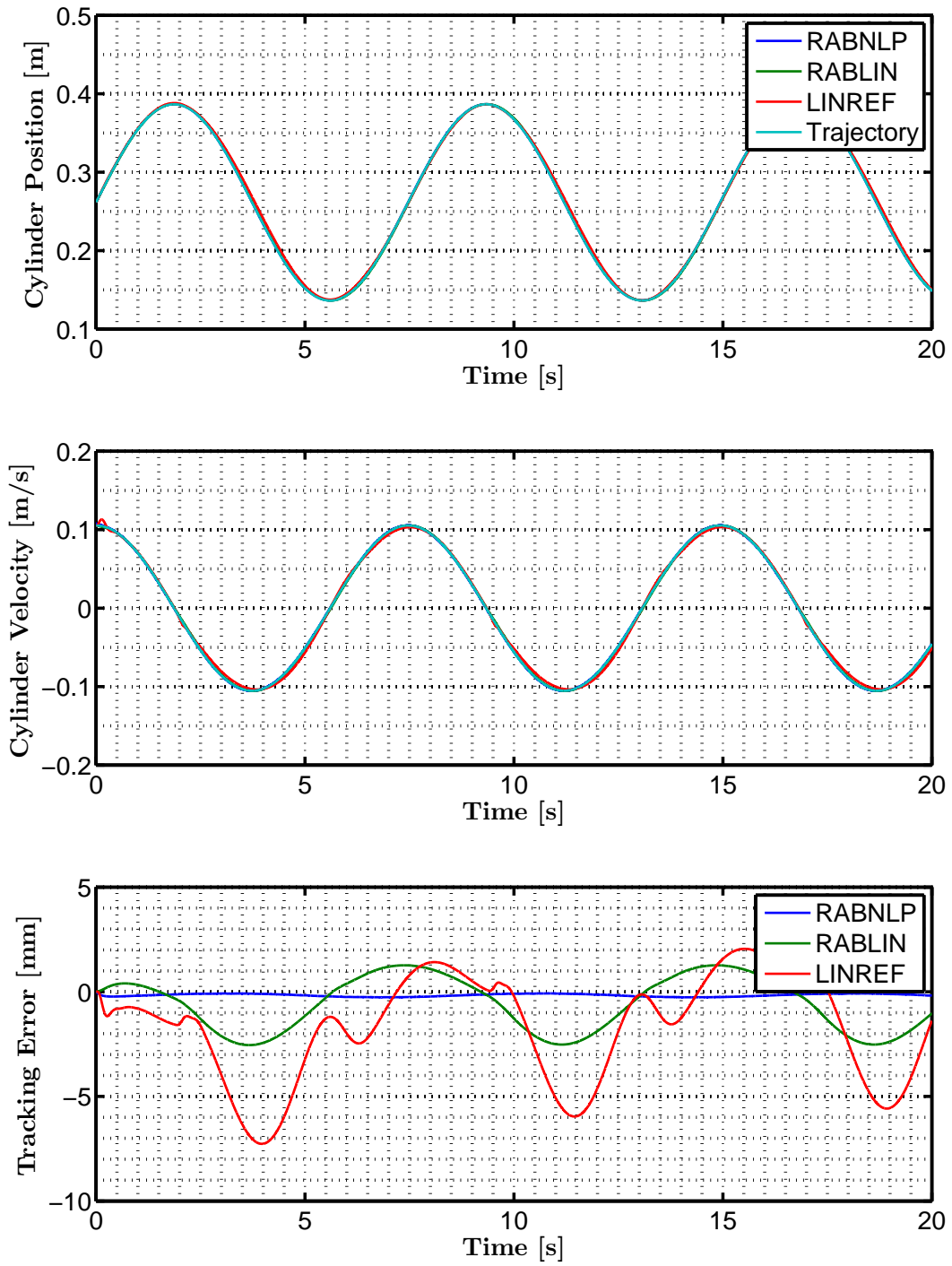


Figure 12.1: **Tracking accuracy** of the RABNLP (Section 7), RABLIN (Section 9) and the LINREF (Section 10) controller from simulations **without valve dynamics**.

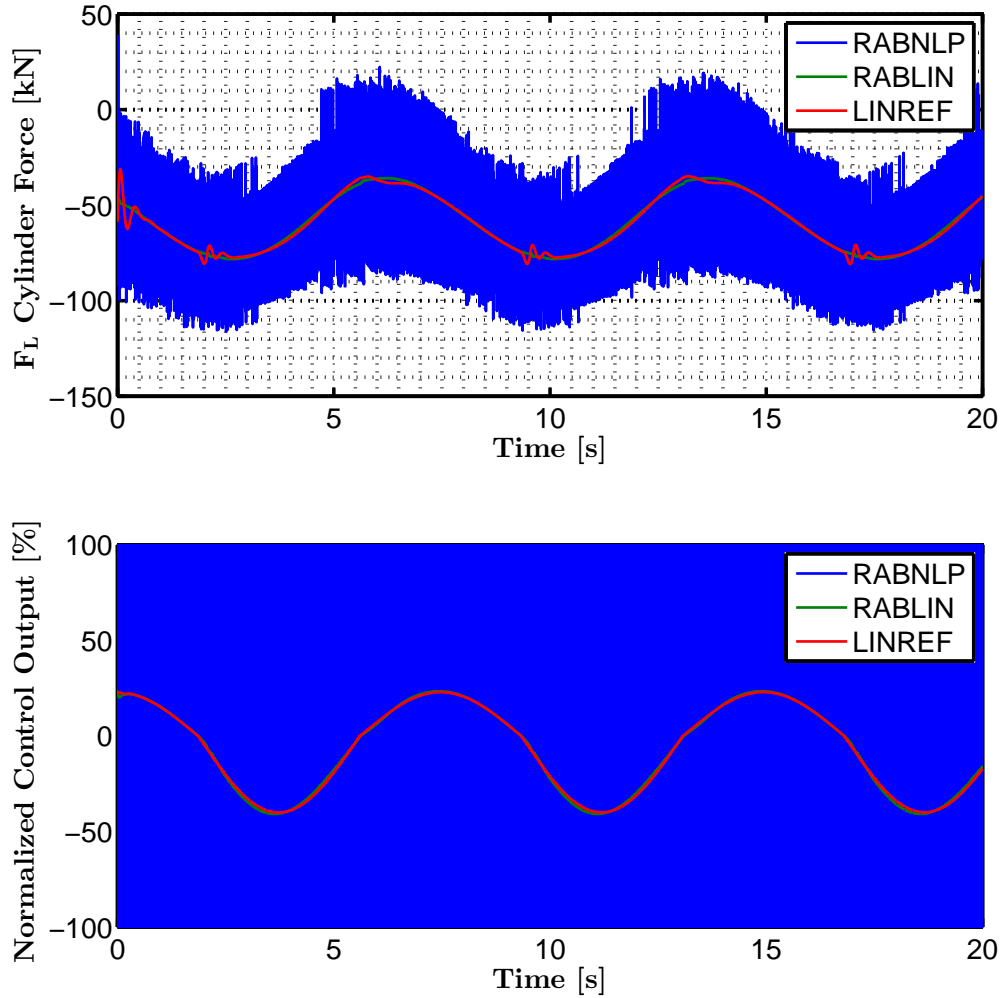


Figure 12.2: **Control effort** of the RABNLP (Section 7), RABLIN (Section 9) and the LINREF (Section 10) controller from simulations **without valve dynamics**.

Controller	RMS Error [mm]	Max. Error [mm]
RABNLP	0.1742	0.2633
RABLIN	1.4213	2.5475
LINREF	3.0132	7.2685

Table 12.1: Tracking Performance of RABNLP, RABLIN and LINREF controllers in simulation using the Sine trajectory (11), with **neglected valve dynamics**.

12.2 Simulations With Valve Dynamics

This section presents the simulated results including valve dynamics of the RABLIN and LINREF controllers. The results are used to theoretically evaluate the design of the RABLIN controller. Results for both the Ramp and the Sine trajectory are presented in Figure 12.4-12.6 and the result is summarized in Table 12.2.

12.2.1 General Observations

Before the evaluation of the tracking performance some general observations are highlighted. Considering first the result of the Sine trajectory seen in Figure 12.4 it is seen that it is very similar to the result without valve dynamics.

Valve Dynamics Calculating the RMS and maximum error of the response, as seen in Table 12.2, the error increases with only $20\ \mu\text{m}$ indicating that the valve dynamics have little influence on the final response as expected; Since the sine trajectory do not excite the transient response of the valve it is operating in *sinusoidal* steady state most of the time, which, if seen as a linear system, yields only a small phase lag and attenuation in its input-output relation. As the bandwidth of the valve is approximately $\omega_V = 314.16\ \text{rad/s}$ a sinusoid of $\omega_{sine} = 0.8414\ \text{rad/s}$ do not experience any noticeable phase lag or attenuation from the valve.

Check-Valves The periodic abrupt disturbances in the sinusoidal cylinder force happens at the time-instants when the control signal changes sign, and it is worst when the arm switches from lowering to lifting, which indicates that it is the check-valves that is the cause. The effect is described in 11.5, and is due to the unmatched asymmetry of the valve-cylinder combination.

12.2.2 Tracking Performance RABLIN

Transient Performance The transient period are visible in both trajectories. In the Sine trajectory is seen to be much longer for the LINREF controller as the tracking error continue to decrease between the three sinusoidal periods. The RABLIN controller attenuates the transient before the start of the second period. Inspecting the Ramp trajectory of 12.5 a more clear view of the transient performance are seen.

The controller has everything from position to force under complete control despite large disturbances and parameter variations. The transient performance of the RABLIN controller are superior in every aspect when evaluating for tracking accuracy. The control effort is larger, but only in very short time periods and it is not oscillatory. Considering the RMS tracking error of the RABLIN controller doing the Ramp trajectory it is seen that it is only 21.40% of the LINREF RMS error.

Constant Position The response of the LINREF controller is very oscillatory especially in periods of constant position. The oscillations are due to the low damping in the system which the P-LEAD controller do not handle very well. The RABLIN controller do not have these oscillations which indicates that the damping controller successfully increase the damping ratio of the control system. The steady state position cannot be evaluated for the LINREF controller as it is not reaching steady state. The steady state position error for the RABLIN is less than 0.1 mm (and decreasing towards zero), for all three periods of constant position, which is expected for a type 1 control system (one free integrator).

Constant Velocity In periods of constant velocity the feed-forward part of the LINREF controller is mostly responsible for the response. Due to the oscillations doing constant position the P LEAD controller could seem to have been tuned too aggressive, but considering the last part of constant velocity it is seen how little effect the feedback part has on the response as the transient is removed only very slowly. The steady state error for constant velocity is largest when the cylinder is retracting i.e. lifting. For the small slopes in each end of the trajectories the steady state velocity error is less than 0.4 mm, and for the steep slopes it is less than 2.5 mm.

Sinusoidal Performance The sinusoidal performance of the RABLIN controller is still superior compared to the LINREF controller, but the difference is not as striking as for the transient response. The RABLIN controller has an RMS error of only 42.92% of the LINREF controller.

Robustness towards the mechanical parameter variations and disturbances are confirmed as the RABLIN controller do not show any signs of low stability margins for the responses. To evaluate robustness for the hydraulic parameters the two critical operating point are evaluated using the Ramp trajectory. This is presented in the following section.

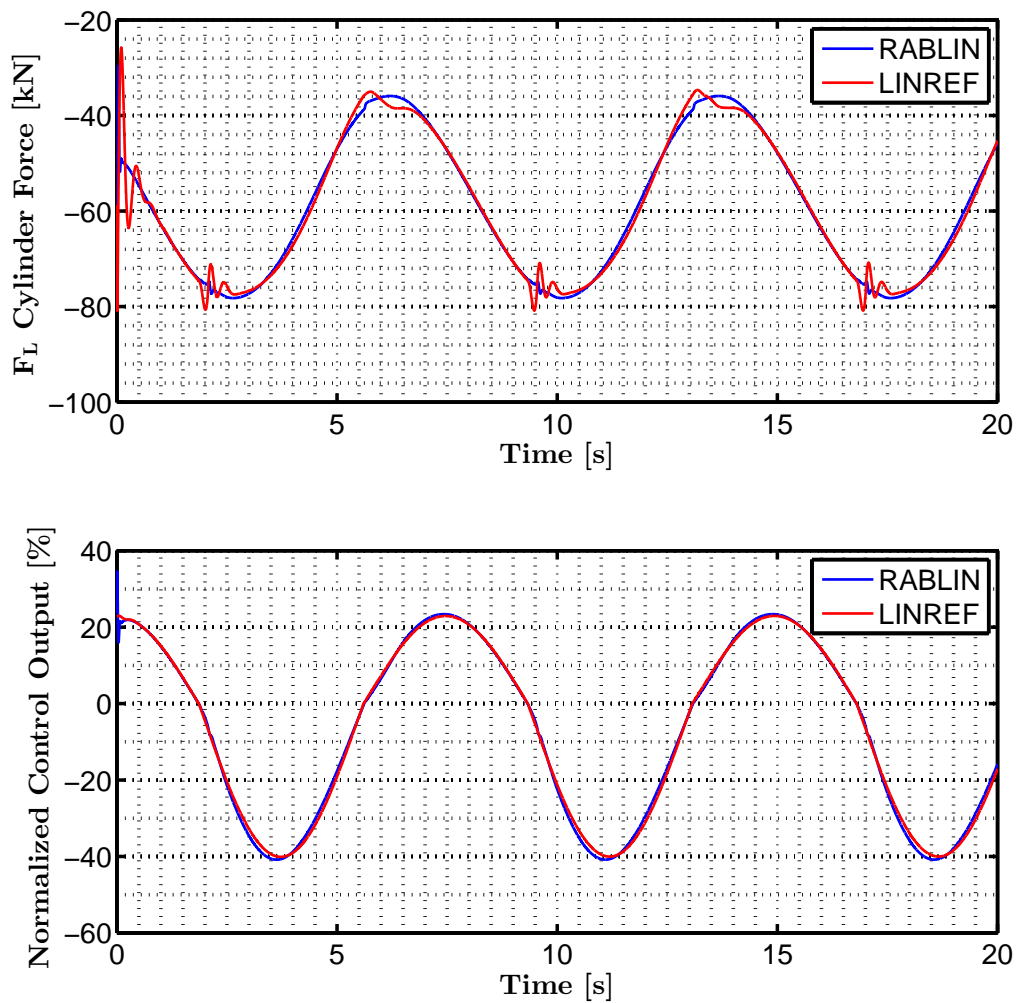


Figure 12.3: **Control effort** of the RABLIN (Section 9) and the LINREF (Section 10) controller from simulations **including** valve dynamics when tracking a sine trajectory.

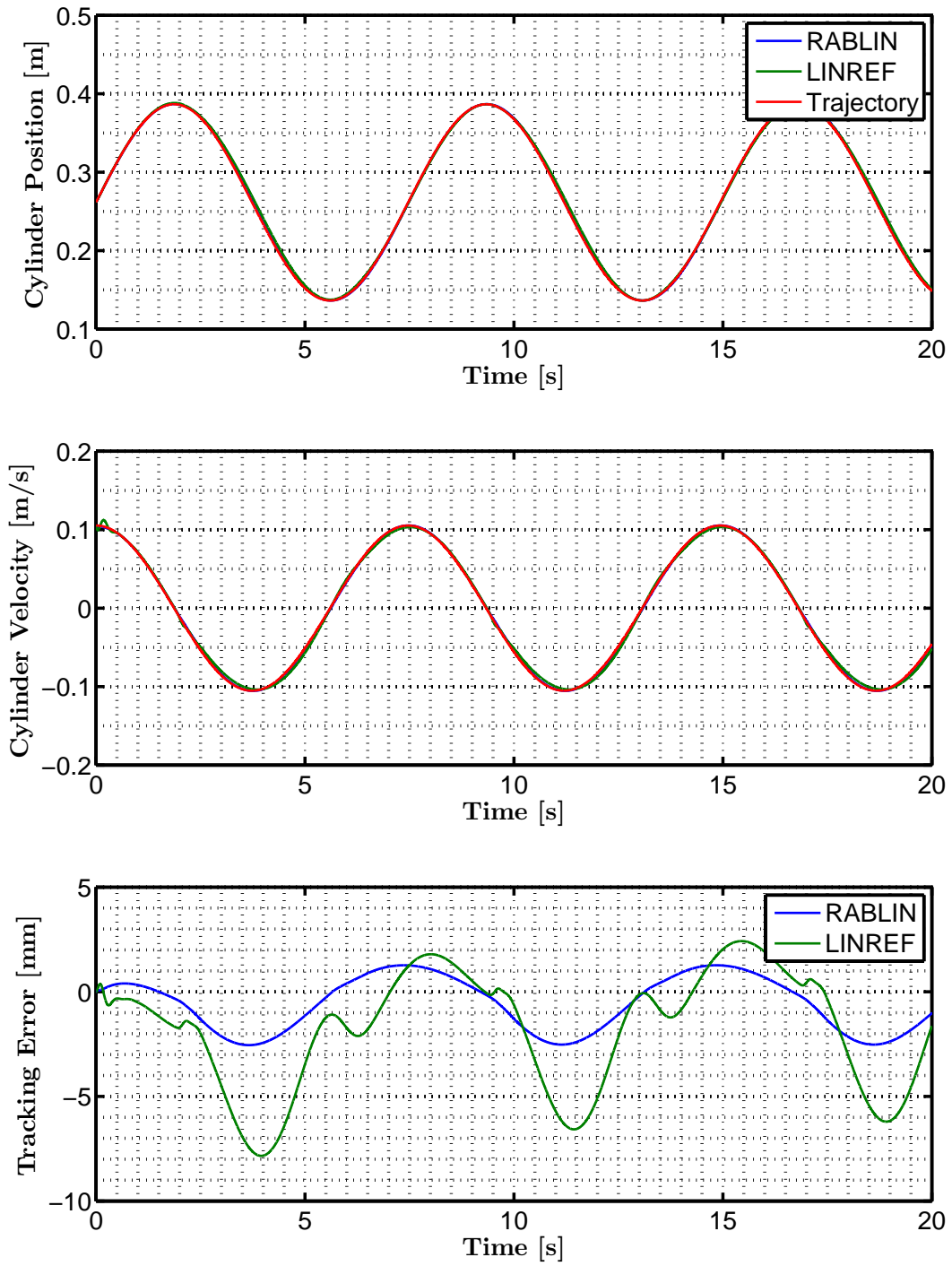


Figure 12.4: **Tracking accuracy** of the RABLIN (Section 9) and the LINREF (Section 10) controller from simulations **including** valve dynamics when tracking a sine trajectory.

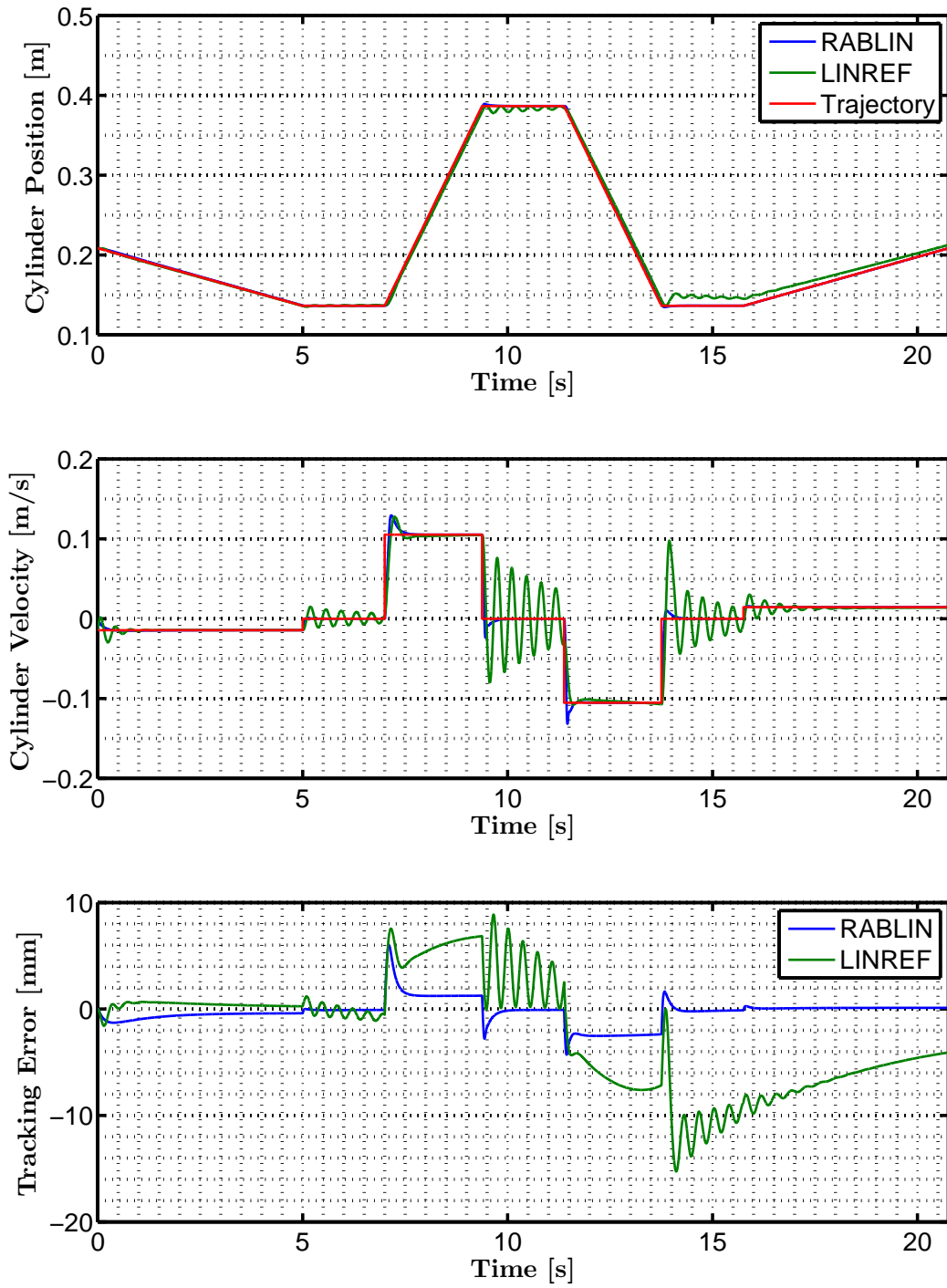


Figure 12.5: **Tracking accuracy** of the RABLIN (Section 9) and the LINREF (Section 10) controller from simulations **including** valve dynamics when tracking a ramp trajectory.

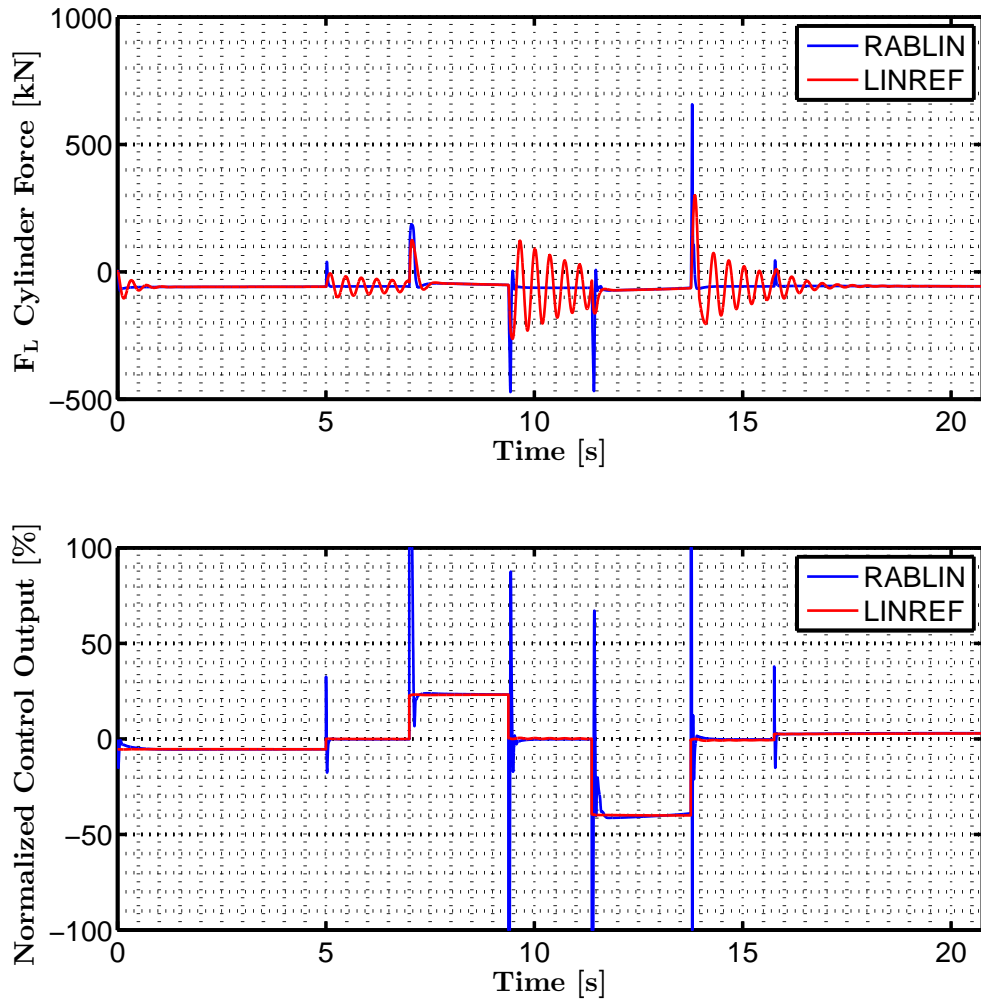


Figure 12.6: **Control effort** of the RABLIN (Section 9) and the LINREF (Section 10) controller from simulations **including** valve dynamics when tracking a ramp trajectory.

Controller	RMS Error [mm]	Max. Error [mm]
RABLIN SINE	1.4226	2.5495
LINREF SINE	3.3144	7.8416
RABLIN RAMP	1.1718	5.9951
LINREF RAMP	5.4762	20.3185

Table 12.2: Tracking Performance of RABLIN and LINREF controllers in simulation **including** valve dynamics, for both the Sine and the Ramp Trajectory.

12.3 Critical Hydraulic Parameters

The RABLIN controller is designed so it yields a phase margin of 30° for the low stiffness hydraulic bound of $\beta = \beta_{MIN}$ and $V_{A0} = V_{A0MIN}$, and a gain margin of 20.5 dB for the high stiffness hydraulic bound of $\beta = \beta_{MAX}$ and $V_{A0} = V_{A0MAX}$, see (9.11) on page 86. To evaluate that the system is stable within these bounds the controller have been simulated in both situations using the Ramp trajectory.

The result are seen in Figure 12.7-12.8. From the figures it is seen that the controller is stable, but due to the low phase-margin for the lower bound the response is quite oscillatory. The upper bound show increased performance, which is expected from a slightly higher closed loop bandwidth.

This concludes the tracking performance evaluation for the RABLIN controller based on *simulations*. The next chapter presents a similar discussion, but based on experimental results instead.

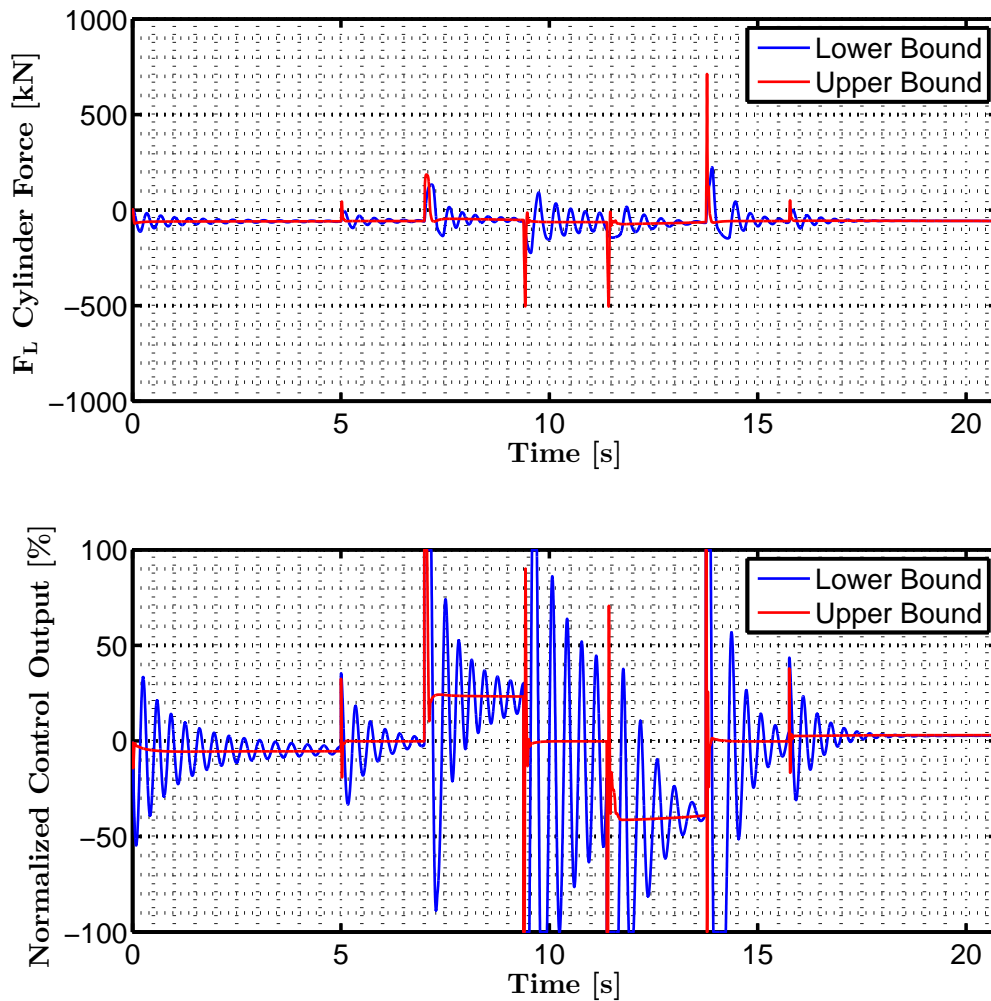


Figure 12.7: **Control effort** of the RABLIN (chapter 9) controller from simulations **including** valve dynamics for the two critical operating points. Lower bound is when $\beta = \beta_{MIN}$ and $V_{A0} = V_{A0MIN}$ and upper bound is when $\beta = \beta_{MAX}$ and $V_{A0} = V_{A0MAX}$, as described in appendix D.4.

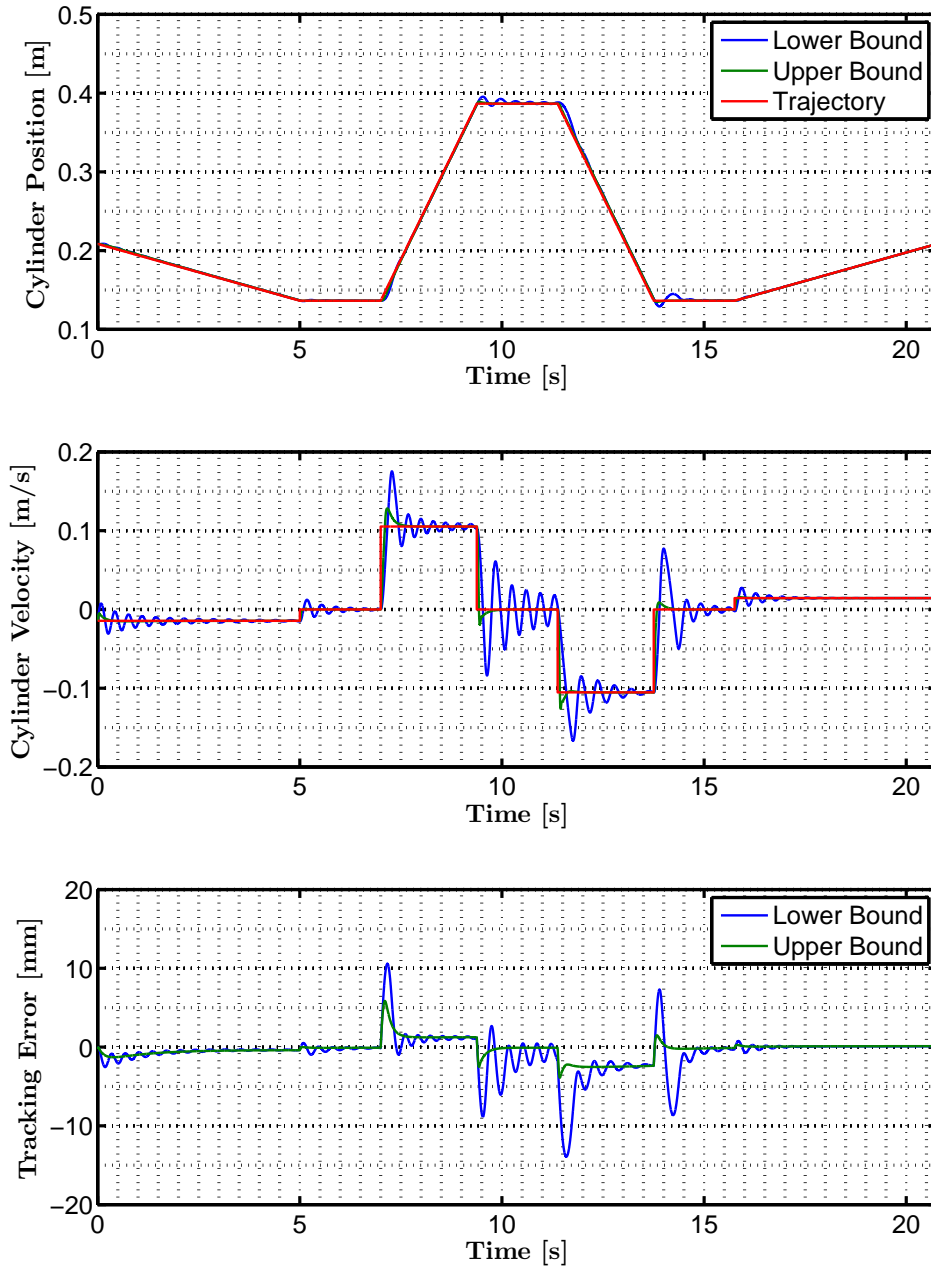


Figure 12.8: **Tracking accuracy** of the RABLIN (chapter 9) controller from simulations **including** valve dynamics for the two critical operating points. Lower bound is when $\beta = \beta_{MIN}$ and $V_{A0} = V_{A0MIN}$ and upper bound is when $\beta = \beta_{MAX}$ and $V_{A0} = V_{A0MAX}$, as described in appendix D.4.

Chapter 13

Experimental Results

This chapter presents the experimental results used to evaluate the controller performance. The RABNLP controller has some practical complications which makes the controller unfeasible for implementation as discussed in Section 8.3. The RABLIN controller and the LINREF controller have been implemented. The LINREF controller was performing as planned, but the RABLIN controller did not show the expected performance using the design presented in Chapter 9.

In order to evaluate the controller *structure* in the experimental setup the parameters of the controller have been changed as shown in Table 13.1. By doing this the evaluation changes from an analytically tuned controller to the evaluation of a controller structure tuned on-site. To make a fair comparison the LINREF controller have been tuned on-site as well. Tuning of the LINREF controller only involved changing the feedforward gain, rendering the stability margins for this controller unchanged. No general robustness conclusions can be drawn for the RABLIN controller for the parameter variations presented in C, but as the controller is proven stable in the experiments the RABLIN controller is concluded stable for the disturbances and parameter variations present during the experiments.

Parameter	Symbol	Previous Value	Adjusted Value	Unit
Maximum Tracking Error	e_{MAX}	0.001	10	m
Inverse Mass Estimate	θ_1	2.2165 e-6	0.22165 e-6	1/kg
Damping Controller Gain	K_{FB}	4.7184e-7	0.4718 e-7	V/Pa
Force Controller Gain	K_{PL}	1.8062e-6	18.062e-6	V/N

Table 13.1: Table of previous parameter values and adjusted values, used in experiments, for the RABLIN controller.

Parameter	Symbol	Previous Value	Adjusted Value	Unit
Positive Feed-Forward Gain	K_{FFP}	21.608	16.833	s / m V
Negative Feed-Forward Gain	K_{FFN}	37.588	39.333	s / m V

Table 13.2: Table of previous parameter values and adjusted values, used in experiments, for the LINREF controller.

The Feed-Forward gain of the LINREF controller depends on the load pressure in the chosen operating point and as the operating point changes it is not surprising that a better result can be obtained by tuning the values, especially as it is responsible for most of the control signal and the resulting response.

The parameter adjustments for the RABLIN controller are harder to explain. Most of them are changed by a factor of 10 and it may indicate an implementation error, either in signal scaling or other programming errors. The parameters have been insufficiently tuned as the two parameters in the Backstepping

part of the controller yielded strange result while tuning them. At the point in the project time-frame the controller was ready for implementation no further time was available for debugging the code, so further tuning and debugging is left for future work.

General Observations

Before the evaluation of the tracking performance some general observations are highlighted. First the *observed* velocity in Figure 13.1 are seen to yield a considerable amount of noise compared to the simulations, but not more than expected. However, for the fast velocity change in the Ramp trajectory of Figure 13.3 the observer cannot track the velocity accurately and the velocity estimation experience a transient period of reduced estimation accuracy. Hence, the shown velocities in these periods are not the actual velocities of the cylinder but it is the observed velocity, which reflects the signals that the controllers use in the calculations but it cannot be used to evaluate the velocity tracking performance in these situations.

Varying Pump Pressure In the simulations and in the model designs the pump pressure was assumed constant. As seen in bottom of Figure 13.3 and Figure 13.1, this is far from the reality. However, the adjusted controllers showed robustness towards the amount of variations seen in the figures, but it is assumed to have a major influence on the performance.

Valve Dynamics To make things worse; The valve is internally supplied which means that the pilot stage of the valve experience fluctuating supply pressure as well resulting in reduced performance. Doing the verification of the model, in Chapter 5, this seemed to degrade the performance from having a bandwidth and damping ratio of $\omega_V = 314.15$ rad/s and $\zeta_V = 1$ to the remarkable lower values of $\omega_V = 30$ rad/s and $\zeta_V = 0.6$. Such a performance change also affect the performance of the controllers.

Check-Valves Again some periodic disturbances happens in the cylinder forces around the time-instants when the control signal changes sign, and it is worst when the arm switches from lowering to lifting i.e. from positive to negative u . The force trajectory is far from the smooth sine response in the simulations for both controllers. This is probably caused by a combination of closing check-valves, fluctuating pump pressure and resulting lower valve performance.

13.1 Tracking Performance RABLIN

Delayed and Offset Response Both the Ramp and Sine response has a delay and a offset compared to the reference. This offset was seen to depend heavily on the Inverse Mass Parameter θ_1 and the cause have not been found within the time frame of the project. It might be explained by wrong scaling of signals in the code.

Transient Performance The transient performance are only visible in the Ramp trajectory, and from inspection of the curve for the tracking error it is seen that the RABLIN controller have significant slower transient performance than in the simulations and when compared to the LINREF controller. The response attains the form of a first order step-response instead of the higher order response expected. This indicates conservative tuning of the position controller.

Constant Position Again, the response of the LINREF controller is very oscillatory especially in periods of constant position, but also for periods of constant velocity which might be due to noise in the velocity signal. The steady state position error of the RABLIN controller is about 20 mm - a significant

increase over the simulations, and the cause is assumed to be an error in the position signal or the position control law.

Constant Velocity A large tracking error is experienced especially for negative velocity (lifting), where it attains a value of up to -80 mm and "only" 20 mm in the positive direction. The difference might be explained by the direction of the gravity disturbance which is working against the cylinder force when lifting, but also due to the offset and delayed position. For a positive motion the delay cancels the positive offset resulting in a lower tracking error than when they are both working to increase the error when the cylinder retracts.

Sinusoidal Performance Ignoring the delay and offset the sinusoidal tracking seems accurate, more interesting, considering the circumstances, are the robustness towards the mechanical parameter variations and disturbances. They are confirmed as the RABLIN controller do not show any signs of low stability margins in any of the figures. The force is fluctuating heavily in some situations, but this is partly due to fluctuating pump pressure, and it therefore do not contradict the robustness result.

Conclusion In conclusion; the evaluation of the RABLIN controller do not yield a very clear picture of the performance due to possible implementation errors, resulting in a delayed and offset response, and a lower tracking accuracy than the reference controller.

When the experiments were carried out, the motion of the RABLIN controller seemed very steady and without as much noise and clatter as the LINREF controller. This is also evident from the control signal as it involves less controller activity than the LINREF controller. To be able to make a qualitative assessment from experiments, the implementation of the RABLIN controller must be debugged and new experiments carried out. This has unfortunately not been possible within the time frame of the project, and is left for future work. The conclusion and assessment of the hypothesis is therefore based on a combination of simulation results and experiments.

As all important results obtained in the project have been presented, the next chapter is a conclusion with an assessment of the hypothesis stated in 3.

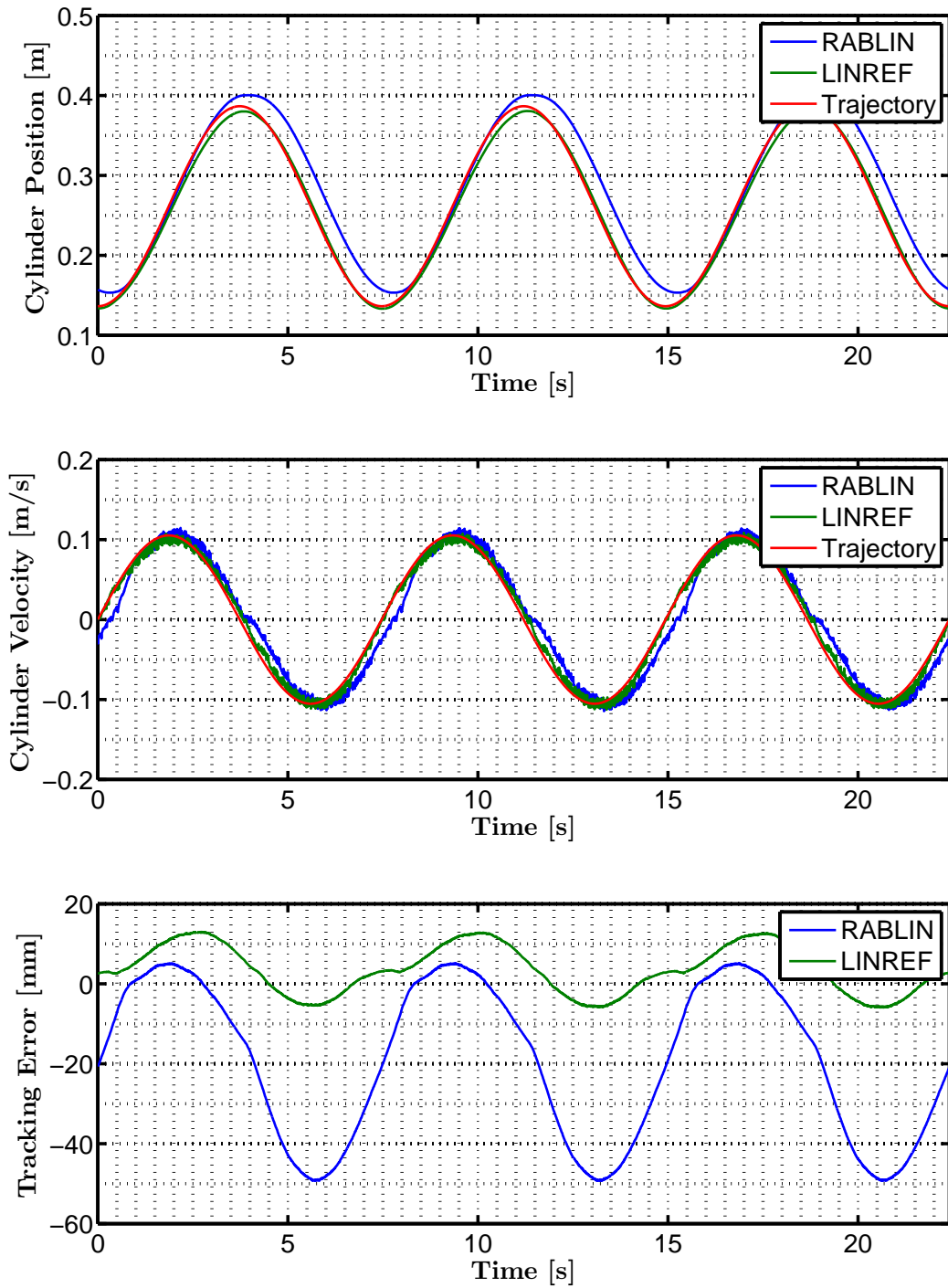


Figure 13.1: **Tracking accuracy** of the RABLIN (Section 9) and the LINREF (Section 10) controller from experimental results.

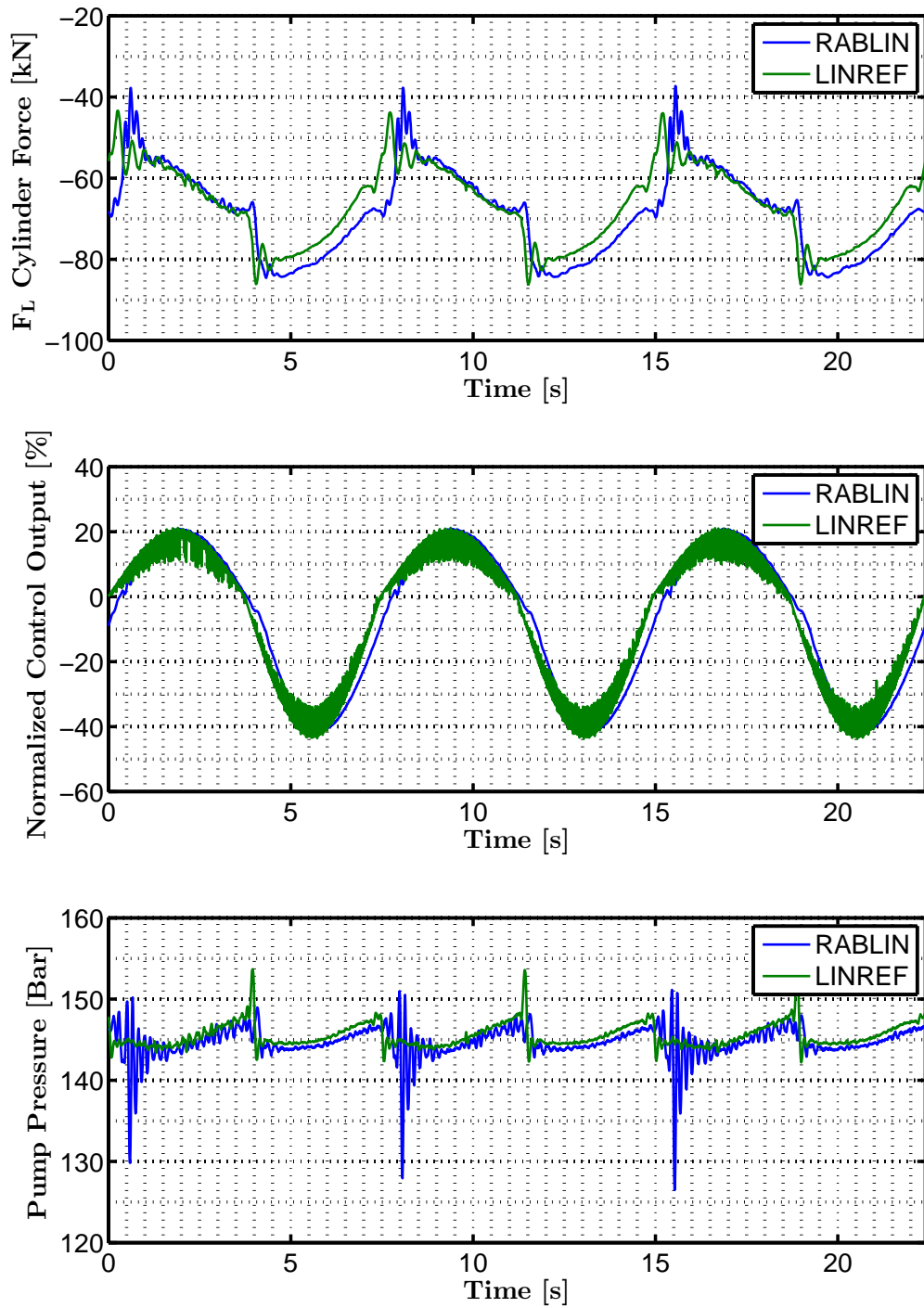


Figure 13.2: **Control effort** of the RABLIN (Section 9) and the LINREF (Section 10) controller from experimental results.

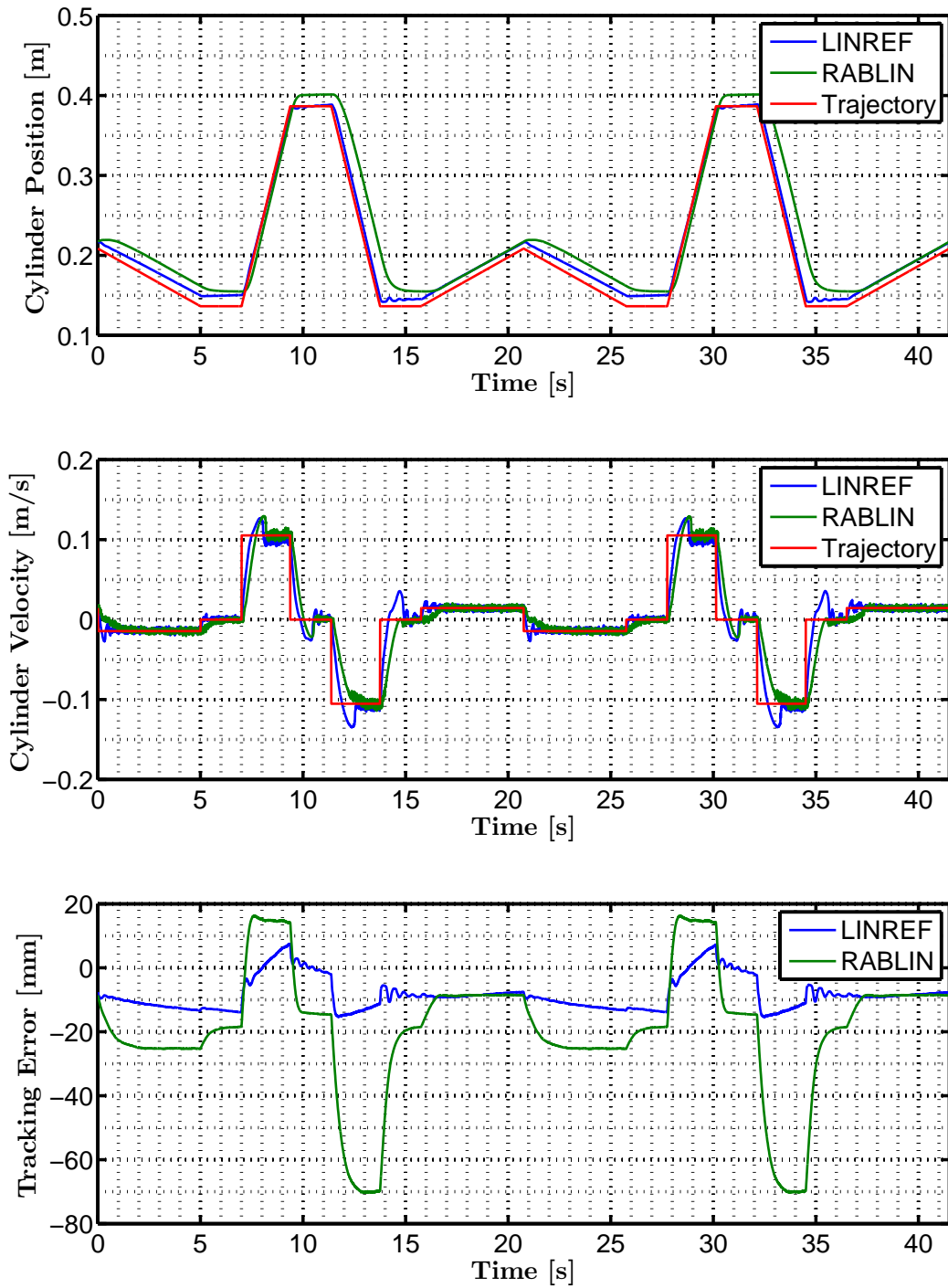


Figure 13.3: **Tracking accuracy** of the RABLIN (Section 9) and the LINREF (Section 10) controller from experimental results.

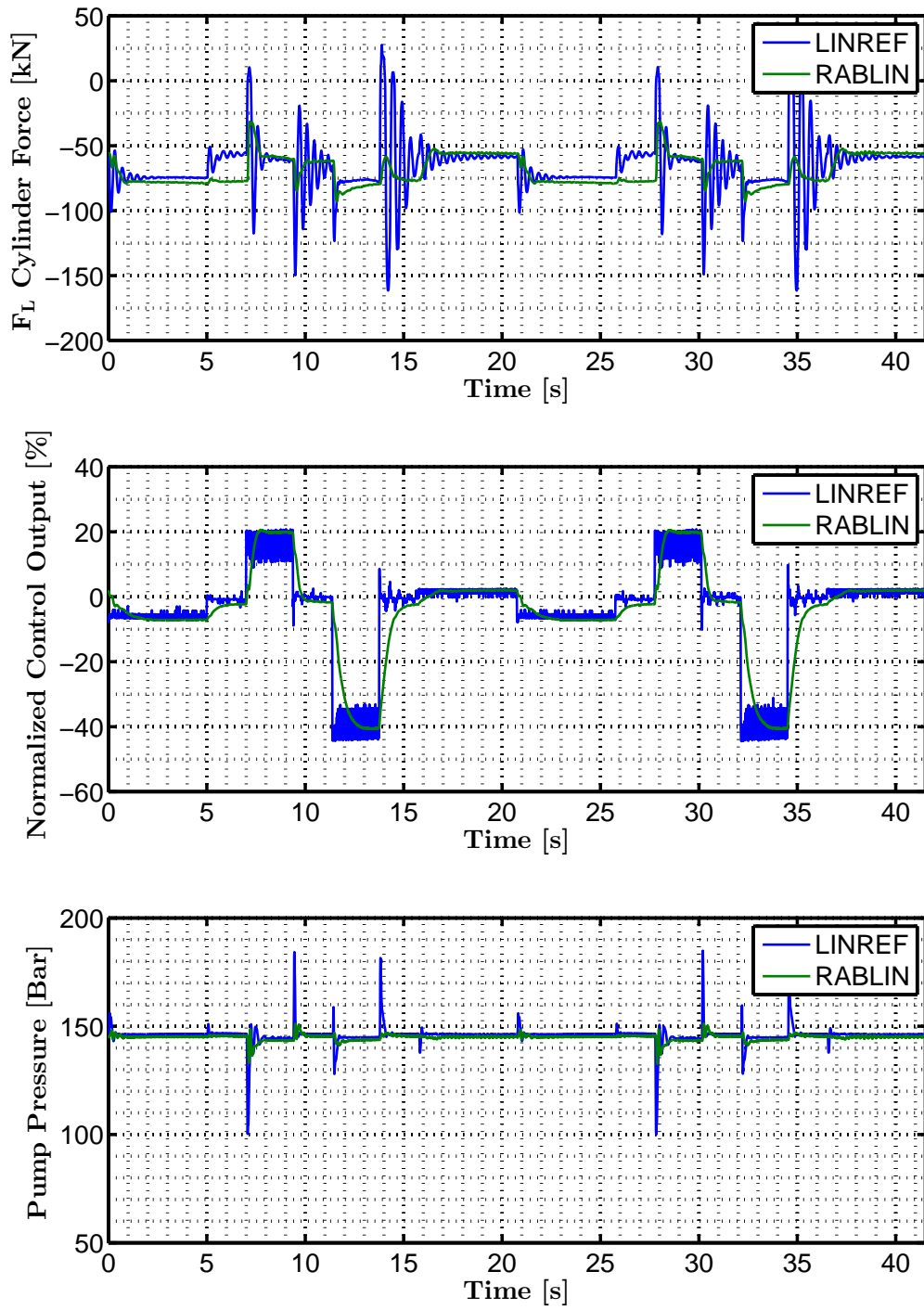


Figure 13.4: **Control effort** of the RABLIN (Section 9) and the LINREF (Section 10) controller from experimental results.

Chapter 14

Conclusion

The project hypothesis has been: *"It is possible to design a position tracking controller using adaptive backstepping control theory, for a nonlinear unmatched asymmetric electro-hydraulic system with good tracking performance and robustness towards disturbances and parameter variations."*

During the four month time frame of this project, research within the field of backstepping and various application specific articles have been studied mainly based on the first book written on the subject by Petar V. Kokotovic [Miroslav Krstic and Kokotovic, 1995] and the article [Guan and Pan, 2008] by Cheng Guan and Shuangxia Pan. Through this research the fundamental background knowledge for backstepping controller designs was developed.

The theory was used to design a robust adaptive backstepping controller with uncertain non-linear parameters, referenced as the RABNLP controller through the report. The controller obtained globally uniformly asymptotically stable states to within a predefined constant error bound, while guaranteeing bounded adaption parameters. The control law was implemented in a simulation model and the asymptotic tracking, despite large parameter variations and disturbances was confirmed. However, the parameter update laws did not converge and due to the large number of parameters the tuning was difficult. This, combined with other practical complications such as unrealizable flow demands, prevented experimental results from being obtained.

To overcome this a new control structure was proposed. The new controller was based on the original with the most complicated part of the controller replaced with a linear force controller, but otherwise maintaining the intermediate control law from the original design. This simplification reduced the number of adaption parameters from 15 to 2 and the control structure could be realized in the practical setup.

The new controller design showed robustness towards parameter variations and disturbances in both simulations and experiments. The tracking performance was also evaluated but the experimental implementation was involved with uncertain problems resulting in reduced performance and a change of parameter values from the original design was required. The performance in the simulation model showed good tracking performance for both transient and steady state situations of sinusoidal and ramp trajectories. The adaption parameters did not converge although persistently excited, and dead-zone techniques were attempted. This, combined with final experimental verification of the simplified backstepping controller could not be solved within the limited time frame of the project.

At a theoretical level the hypothesis has been confirmed by both the original backstepping controller and the simplified; They both used adaptive backstepping theory to achieve good tracking performance and robustness towards disturbances and parameter variations on a nonlinear unmatched asymmetric electro-hydraulic system. Moreover, the simplified controller proved robustness in the physical setup.

The hypothesis is therefore confirmed theoretically and partly confirmed experimentally, and the objective of this project have been met.

Part IV

Appendix

Appendix A

Simplified Model

A reduced order model of the Simulation Model is derived in this Chapter. The mechanical part is the same, but the hydraulic part is simplified and the valve-dynamics is neglected. Neglecting the valve dynamics yields the following steady state relation, with the same DC-Gain k_V as in the 2.-order valve equation (4.55).

$$x_V = k_V u \quad (\text{A.1})$$

The simplified hydraulic part is derived using the same assumptions as in the derivation for the Simulation Model, page 26, together with the following steady state assumption:

$$\dot{x}_{CE} = \frac{Q_A}{A_A} = -\frac{Q_B}{A_B} \quad (\text{A.2})$$

A corresponding hydraulic diagram can be seen on page 26.

Applying assumption (A.2) is equivalent of ignoring the compression flow in the system, saying that a flow Q_A into chamber A is proportional to a cylinder velocity x_{CE} and a flow in Q_B .

To make the expressions more compact the *cylinder area ratio*, α and *valve gradient ratio*, σ , is introduced:

$$\alpha = \frac{A_B}{A_A} \quad \sigma = \frac{K_B}{K_A} \quad (\text{A.3})$$

Using this we can rewrite (A.2):

$$\alpha Q_A = -Q_B \quad (\text{A.4})$$

A.1 Positive Spool Displacement

The simplified model derivation start for positive spool displacement $x_V \geq 0$, yielding the flows seen in (A.5).

$$\begin{aligned} Q_A &= K_A x_V \sqrt{p_P - p_A} \\ Q_B &= -\sigma K_A x_V \sqrt{p_B - p_T} \end{aligned} \quad (\text{A.5})$$

Substituting the flows from (A.5) into (A.4)

$$\begin{aligned} \alpha Q_A &= -Q_B \\ \alpha K_A x_V \sqrt{p_P - p_A} &= \sigma K_A x_V \sqrt{p_B - p_T} \end{aligned} \quad (\text{A.6})$$

and isolating p_A and p_B yields:

$$p_A = p_P - \frac{\sigma^2(p_B - p_T)}{\alpha^2} \quad p_B = p_T - \frac{\alpha^2(p_A - p_P)}{\sigma^2} \quad (\text{A.7})$$

From Equation (4.35) we have:

$$F_L = A_A p_A - A_B p_B \quad (\text{A.8})$$

this can be rewritten to an expression for a *virtual load pressure*, if it is divided by A_A :

$$p_L = \frac{F_L}{A_A} = p_A - \alpha p_B \quad (\text{A.9})$$

The pressure in each chamber of the cylinder can be expressed by the virtual load pressure p_L by substituting (A.7) into (A.9)

$$p_L = p_A - \alpha \underbrace{\left(p_T - \frac{\alpha^2(p_A - p_P)}{\sigma^2} \right)}_{p_B} \quad (\text{A.10})$$

$$p_L = p_P - \underbrace{\frac{\sigma^2(p_B - p_T)}{\alpha^2}}_{p_A} - \alpha p_B \quad (\text{A.11})$$

and isolating p_A in (A.10), and p_B in (A.11):

$$p_A = \frac{\alpha^3 p_P + \alpha \sigma^2 p_T + \sigma^2 p_L}{\sigma^2 + \alpha^3} \quad (\text{A.12})$$

$$p_B = \frac{\alpha^2 p_P + \sigma^2 p_T - \alpha^2 p_L}{\sigma^2 + \alpha^3} \quad (\text{A.13})$$

It is important to note that (A.12) and (A.13) defines p_A and p_B uniquely from p_L and therefore also uniquely from the force $F_L = A_A p_L$. This is not true in general, but it is a result of the steady-state assumption of (A.2), and therefore only true when the compression flow is ignored.

Substituting the expressions from (A.12) and (A.13) into (A.5) yields the final flow equations for positive spool displacement.

$$\begin{aligned} Q_A &= K_A x_V \sqrt{p_P - \underbrace{\frac{\alpha^3 p_P + \alpha \sigma^2 p_T + \sigma^2 p_L}{\sigma^2 + \alpha^3}}_{p_A}} \\ Q_B &= -\sigma K_A x_V \sqrt{\underbrace{\frac{\alpha^2 p_P + \sigma^2 p_T - \alpha^2 p_L}{\sigma^2 + \alpha^3}}_{p_B} - p_T} \end{aligned} \quad (\text{A.14})$$

Which can be rewritten into:

$$\begin{aligned} Q_A &= \sigma K_A x_V \sqrt{\frac{p_P - \alpha p_T - p_L}{\sigma^2 + \alpha^3}} \\ Q_B &= -\sigma \alpha K_A x_V \sqrt{\frac{p_P - \alpha p_T - p_L}{\sigma^2 + \alpha^3}} \end{aligned} \quad (\text{A.15})$$

Which is seen to correspond with (A.4).

A.2 Negative Spool Displacement

This derivation is similar to the derivation for positive spool displacement carried, but here $x_V < 0$, and the derivation start with the following flow equations instead of (A.5).

$$\begin{aligned} Q_A &= K_A x_V \sqrt{p_A - p_T} \\ Q_B &= -\sigma K_A x_V \sqrt{p_P - p_B} \end{aligned} \quad (\text{A.16})$$

Substituting the flows from (A.16) into (A.4), which is seen on 123 and repeated in (A.17):

$$\alpha Q_A = -Q_B \quad (\text{A.17})$$

$$\alpha K_A x_V \sqrt{p_A - p_T} = \sigma K_A x_V \sqrt{p_P - p_B} \quad (\text{A.18})$$

Isolating p_A and p_B :

$$p_A = p_T - \frac{\sigma^2(p_B - p_P)}{\alpha^2} \quad p_B = p_P - \frac{\alpha^2(p_A - p_T)}{\sigma^2} \quad (\text{A.19})$$

From Equation (A.9), seen on 124 we have:

$$p_L = p_A - \alpha p_B \quad (\text{A.20})$$

The pressure in each chamber of the cylinder can be expressed by the virtual load pressure p_L by substituting (A.19) into (A.20)

$$p_L = p_A - \alpha \underbrace{\left(p_P - \frac{\alpha^2(p_A - p_T)}{\sigma^2} \right)}_{p_B} \quad (\text{A.21})$$

$$p_L = p_T - \underbrace{\frac{\sigma^2(p_B - p_P)}{\alpha^2}}_{p_A} - \alpha p_B \quad (\text{A.22})$$

and isolating p_A in (A.21), and p_B in (A.22):

$$p_A = \frac{\alpha^3 p_T + \alpha \sigma^2 p_P + \sigma^2 p_L}{\sigma^2 + \alpha^3} \quad (\text{A.23})$$

$$p_B = \frac{\alpha^2 p_T + \sigma^2 p_P - \alpha^2 p_L}{\sigma^2 + \alpha^3} \quad (\text{A.24})$$

Substituting the expressions from (A.23) and (A.24) into (A.16) yields the final flow equations for negative spool displacement.

$$\begin{aligned} Q_A &= K_A x_V \sqrt{\underbrace{\frac{\alpha^3 p_T + \alpha \sigma^2 p_P + \sigma^2 p_L}{\sigma^2 + \alpha^3}}_{p_A} - p_T} \\ Q_B &= -\sigma K_A x_V \sqrt{p_P - \underbrace{\frac{\alpha^2 p_T + \sigma^2 p_P - \alpha^2 p_L}{\sigma^2 + \alpha^3}}_{p_B}} \end{aligned} \quad (\text{A.25})$$

Which can be rewritten into:

$$\begin{aligned} Q_A &= \sigma K_A x_V \sqrt{\frac{p_L - p_T + \alpha p_P}{\sigma^2 + \alpha^3}} \\ Q_B &= -\sigma \alpha K_A x_V \sqrt{\frac{p_L - p_T + \alpha p_P}{\sigma^2 + \alpha^3}} \end{aligned} \quad (\text{A.26})$$

Which is seen to correspond with (A.17).

A.3 Final Simplified Model

A virtual spool area gradient K_L is defined as

$$K_L = \frac{\sigma K_A K_V}{\sqrt{\sigma^2 + \alpha^3}} \quad (\text{A.27})$$

and if this is used together with Equation (A.15) and (A.26) the flow equations for the simplified model is obtained.

For **positive** spool displacement $x_V \geq 0$:

$$Q_A = K_L u \sqrt{p_P - \alpha p_T - p_L} \quad Q_B = -\alpha K_L u \sqrt{p_P - \alpha p_T - p_L} \quad (\text{A.28})$$

For **negative** spool displacement $x_V < 0$:

$$Q_A = K_L u \sqrt{\alpha p_P - p_T + p_L} \quad Q_B = -\alpha K_L u \sqrt{\alpha p_P - p_T + p_L} \quad (\text{A.29})$$

The pressure build-up for the virtual load pressure \dot{p}_L is obtained by differentiating (A.9) and then substituting expressions for \dot{p}_A and \dot{p}_B .

$$\dot{p}_L = \dot{p}_A - \alpha \dot{p}_B \quad (\text{A.30})$$

We already derived equations for \dot{p}_A and \dot{p}_B in (4.33-4.34), but this derivation is altered as we now want the leakage flow to be a function of the *virtual* load pressure p_L instead of the real load pressure ($p_A - p_B$). This is however a simplification and it is the same as saying that the leakage flow is proportional to the cylinder force $F_L = A_A p_L$ and not the pressure difference, which do not follow the general gab theory for a laminar flow where $Q_L \propto \Delta p$ [Linköping University, 2008, p. 14].

The pressure build up in each chamber is modeled using the continuity equation as for (4.33-4.34), but with the above assumption for the leakage flow using the leakage coefficient C_{LF} .

$$\dot{p}_A = \frac{\beta}{V_{A0} + A_A x_{CE}} (Q_A - C_{LF} p_L - A_A \dot{x}_{CE}) \quad (\text{A.31})$$

$$\dot{p}_B = \frac{\beta}{V_{B0} - A_B x_{CE}} (\underbrace{-\alpha Q_A}_{=Q_B} + C_{LF} p_L + A_B \dot{x}_{CE}) \quad (\text{A.32})$$

Substituting into (A.30) yields:

$$\dot{p}_L = \frac{\beta}{V_{A0} + A_A x_{CE}} (Q_A - C_{LF} p_L - A_A \dot{x}_{CE}) - \frac{\alpha \beta}{V_{B0} - A_B x_{CE}} (-\alpha Q_A + C_{LF} p_L + A_B \dot{x}_{CE}) \quad (\text{A.33})$$

The following functions are introduced

$$V_{AL}(x_1) = V_{A0} + A_A x_1 \quad V_{BL}(x_1) = V_{B0} - A_B x_1 \quad \gamma(x_1) = \frac{V_{BL}(x_1)}{V_{AL}(x_1)} \quad (\text{A.34})$$

and the expression (A.33) for \dot{p}_L can be reduced to

$$\begin{aligned} \dot{p}_L &= \frac{\beta}{V_{AL}} (Q_A - C_{LF} p_L - A_A \dot{x}_{CE}) - \frac{\alpha \beta}{\gamma V_{AL}} (-\alpha Q_A + C_{LF} p_L + A_B \dot{x}_{CE}) \\ &= \frac{\beta}{V_{AL}} \left[Q_A - C_{LF} p_L - A_A \dot{x}_{CE} + \frac{\alpha}{\gamma} (\alpha Q_A - C_{LF} p_L - \alpha A_A \dot{x}_{CE}) \right] \\ &= \frac{\beta}{\gamma V_{AL}} [(\gamma + \alpha^2) Q_A - (\gamma + \alpha) C_{LF} p_L - (\gamma + \alpha^2) A_A \dot{x}_{CE}] \end{aligned} \quad (\text{A.35})$$

This concludes the derivation of the simplified model.

Appendix B

Linearized Model

To carry out designs using classical control theory a linear model of the system dynamics is required. From the model summary section 4.5 we have a mechanical system described as:

$$M(x_{CE}) \ddot{x}_{CE} = F_L - B(x_{CE}, \dot{x}_{CE}) \dot{x}_{CE} - F(t), \quad (\text{B.1})$$

This equation is already linear if an operating point for x_{CE} and \dot{x}_{CE} is chosen, as it makes $M(x_{CE})$ and $B(x_{CE}, \dot{x}_{CE})$ constants.

Let Δ depict a change of variable from its operating point e.g. $\Delta x_{CE} = x_{CE} - x_{CE0}$. Due to (B.1) being linear the superposition property can then be used to rewrite it as:

$$M \Delta \ddot{x}_{CE} = \Delta F_L - B \Delta \dot{x}_{CE} - \Delta F(t), \quad (\text{B.2})$$

Laplace transforming this equation, ignoring initial conditions, yields

$$M \Delta x_{CE} s^2 = \Delta F_L - B \Delta x_{CE} s - \Delta F, \quad (\text{B.3})$$

which result in the following transfer function for the mechanical part of the linear model:

$$\Delta x_{CE} = \frac{1}{s} \cdot \frac{1}{M s + B} (\Delta F_L - \Delta F) \quad (\text{B.4})$$

And in standard first-order form with a free integrator:

$$\Delta x_{CE} = \frac{1}{s} \cdot \frac{K_M}{\tau_M s + 1} (\Delta F_L - \Delta F) \quad (\text{B.5})$$

where:

$$K_M = \frac{1}{B} \quad \tau_M = \frac{M}{B} \quad (\text{B.6})$$

B.1 Linearization of Simplified Hydraulic Model

The simplified hydraulic model derived in Section A, is used in the linear model. Therefore, it also neglects the valve dynamics and the compression flow. The simple model is, in spite of the name, still highly non-linear and therefore require linearization before linear control theory can be applied.

Linearizations are carried out using first-order Taylor expansions. The flow equations are seen in (6.3) and (6.5) and repeated below in (B.7):

$$Q_A = \begin{cases} K_L u \sqrt{p_P - \alpha p_T - p_L} & \text{for } u \geq 0 \\ K_L u \sqrt{\alpha p_P - p_T + p_L} & \text{for } u < 0 \end{cases} \quad (\text{B.7})$$

With:

$$K_L = \frac{\sigma K_A K_V}{\sqrt{\sigma^2 + \alpha^3}} \quad \alpha = \frac{A_B}{A_A} \quad \sigma = \frac{K_B}{K_A} \quad (\text{B.8})$$

The first order Taylor expansion of (B.7) is seen below in (B.9).

$$Q_A(u, p_L) = Q_A(u_0, p_{L0}) + \left. \frac{\partial Q_A}{\partial u} \right|_{p_{L0}} (u - u_0) + \left. \frac{\partial Q_A}{\partial p_L} \right|_{u_0, p_{L0}} (p_L - p_{L0}) \quad (\text{B.9})$$

Again, we let the symbol Δ denote a change of a variable from its operating point e.g. $\Delta u = u - u_0$. Then we can rewrite (B.9) into:

$$\Delta Q_A = \underbrace{\left. \frac{\partial Q_A}{\partial u} \right|_{p_{L0}}}_{K_Q} \Delta u - \underbrace{\left. \frac{\partial Q_A}{\partial p_L} \right|_{u_0, p_{L0}}}_{K_C} \Delta p_L \quad (\text{B.10})$$

The structure of the flow equation (B.10) is the same for both positive and negative control signal u , but the coefficients K_Q and K_C varies. Note the minus on K_C which follows the terminology in [Merritt, 1967, p. 83]. To indicate whether a coefficient is for a positive or a negative control signal, a P or an N is added to the suffix.

$$\Delta Q_A = \begin{cases} K_{QP} \Delta u - K_{CP} \Delta p_L & \text{for } u \geq 0 \\ K_{QN} \Delta u - K_{CN} \Delta p_L & \text{for } u < 0 \end{cases} \quad (\text{B.11})$$

Taking the partial derivatives of the flow equations (6.3) and (6.5), on page 49, we get the *flow gains* defined as:

$$K_{QP} = K_L \sqrt{p_P - \alpha p_T - p_{L0}} \quad K_{QN} = K_L \sqrt{\alpha p_P - p_T + p_{L0}} \quad (\text{B.12})$$

and *flow pressure coefficients* (in some literature denoted K_{QP} instead of K_C):

$$K_{CP} = \frac{K_L u_0}{2 \sqrt{p_P - \alpha p_T - p_{L0}}} \quad K_{CN} = -\frac{K_L u_0}{2 \sqrt{\alpha p_P - p_T + p_{L0}}} \quad (\text{B.13})$$

From these, also the *pressure sensitivities* of the valve can be calculated as [Merritt, 1967, p. 84]:

$$K_{PP} = \frac{K_{QP}}{K_{CP}} = \frac{2(p_P - \alpha p_T - p_{L0})}{u_0} \quad K_{PN} = \frac{K_{QN}}{K_{CN}} = \frac{2(p_T - p_{L0} - \alpha p_P)}{u_0} \quad (\text{B.14})$$

The flow in the other chamber, ΔQ_B , is related to ΔQ_A through the steady-state assumption seen in (6.1) and repeated here:

$$\alpha \Delta Q_A = -\Delta Q_B \quad (\text{B.15})$$

The equation for the virtual load pressure is seen in (6.7), on page 50, and repeated in (B.16):

$$\dot{p}_L = \frac{\beta}{\gamma V_{AL}} [(\gamma + \alpha^2) Q_A - (\gamma + \alpha) C_{LF} p_L - (\gamma + \alpha^2) A_A \dot{x}_{CE}] \quad (\text{B.16})$$

With:

$$\gamma(x_{CE}) = \frac{V_{BL}(x_{CE})}{V_{AL}(x_{CE})} \quad V_{AL}(x_{CE}) = V_{A0} + A_A x_{CE} \quad V_{BL}(x_{CE}) = V_{B0} - A_B x_{CE} \quad (\text{B.17})$$

Equation (B.16) is nonlinear as $\gamma(x_{CE})$ and $V_{AL}(x_{CE})$ is changing with the cylinder position, but if the cylinder position is assumed constant, then γ and V_{AL} will be constants and Equation (B.16) is linear.

As (B.16) is linear (when γ and V_{AL} is assumed constant) it poses the superposition property:

$$f(x) - f(x_0) = f(x - x_0) \quad (\text{B.18})$$

Applying the superposition property (B.18) to (B.16) allow us to write:

$$\dot{p}_L(Q_A, p_L, \dot{x}_{CE}) - \dot{p}_L(Q_{A0}, p_{L0}, \dot{x}_{CE0}) = \dot{p}_L(Q_A - Q_{A0}, p_L - p_{L0}, \dot{x}_{CE} - \dot{x}_{CE0}) \quad (\text{B.19})$$

which simplifies to:

$$\Delta \dot{p}_L = \dot{p}_L(\Delta Q_A, \Delta p_L, \Delta \dot{x}_{CE}) \quad (\text{B.20})$$

Using (B.20) allow us to rewrite (B.16) into:

$$\Delta \dot{p}_L = \frac{\beta}{\gamma V_{AL}} [(\gamma + \alpha^2)\Delta Q_A - (\gamma + \alpha)C_{LF} \Delta p_L - (\gamma + \alpha^2)A_A \Delta \dot{x}_{CE}] \quad (\text{B.21})$$

Now Laplace transforming yields:

$$s \Delta p_L(s) - \underbrace{\Delta p_L(t=0)}_{=0} = \frac{\beta}{\gamma V_{AL}} [(\gamma + \alpha^2)\Delta Q_A(s) - (\gamma + \alpha)C_{LF} \Delta p_L(s) - (\gamma + \alpha^2)A_A \Delta \dot{x}_{CE}(s)] \quad (\text{B.22})$$

Substituting ΔQ_A with (B.10), and omitting the parameter lists (s) on Laplace variables:

$$s \Delta p_L = \frac{\beta}{\gamma V_{AL}} [(\gamma + \alpha^2)(K_Q \Delta u - K_C \Delta p_L) - (\gamma + \alpha)C_{LF} \Delta p_L - (\gamma + \alpha^2)A_A \Delta \dot{x}_{CE}] \quad (\text{B.23})$$

Rewriting to match a standard first-order transfer function:

$$\begin{aligned} \Delta p_L &= \frac{\frac{\beta}{\gamma V_{AL}} [(\gamma + \alpha^2)K_Q \Delta u - (\gamma + \alpha^2)A_A \Delta \dot{x}_{CE}]}{s + \frac{\beta}{\gamma V_{AL}}(\gamma + \alpha)C_{LF} + \frac{\beta}{\gamma V_{AL}}(\gamma + \alpha^2)K_C} \\ &= \frac{K_Q \Delta u - A_A \Delta \dot{x}_{CE}}{\frac{\gamma V_{AL}}{\beta(\gamma + \alpha^2)}s + \frac{\gamma + \alpha}{\gamma + \alpha^2}C_{LF} + K_C} \\ &= \frac{K_Q \Delta u - A_A \Delta \dot{x}_{CE}}{\frac{\gamma V_{AL}}{\beta(\gamma + \alpha^2)}s + \frac{(\gamma + \alpha)C_{LF} + (\gamma + \alpha^2)K_C}{\gamma + \alpha^2}} \\ &= \frac{\gamma + \alpha^2}{(\gamma + \alpha)C_{LF} + (\gamma + \alpha^2)K_C} \cdot \frac{K_Q \Delta u - A_A \Delta \dot{x}_{CE}}{\frac{\gamma + \alpha^2}{(\gamma + \alpha)C_{LF} + (\gamma + \alpha^2)K_C} \frac{\gamma V_{AL}}{\beta(\gamma + \alpha^2)}s + 1} \\ &= \frac{\gamma + \alpha^2}{\underbrace{K_C \alpha^2 + C_{LF}\alpha + \gamma C_{LF} + \gamma K_C}_{K_H}} \cdot \frac{K_Q \Delta u - A_A \Delta \dot{x}_{CE}}{\underbrace{\frac{\gamma V_{AL}}{\beta(K_C \alpha^2 + C_{LF}\alpha + \gamma C_{LF} + \gamma K_C)}}_{\tau_H} s + 1} \end{aligned} \quad (\text{B.24})$$

Which leads to a SISO first order system with $(K_Q \Delta u - A_A \Delta \dot{x}_{CE})$ as input and Δp_L as output.

$$\Delta p_L = G_H(s) (K_Q \Delta u - A_A \Delta \dot{x}_{CE}) \quad (\text{B.25})$$

$$G_H(s) = \frac{K_H}{\tau_H s + 1} \quad (\text{B.26})$$

This first order system will be referred to as the linearized *hydraulic* system.

As mentioned before the coefficient K_C changes for positive and negative control signal u , so this leads to two different DC-gains and two different hydraulic time-constants.

$$K_{HP} = \frac{\gamma + \alpha^2}{K_{CP} \alpha^2 + C_{LF} \alpha + \gamma C_{LF} + \gamma K_{CP}} \quad \text{for } u \geq 0 \quad (\text{B.27})$$

$$K_{HN} = \frac{\gamma + \alpha^2}{K_{CN} \alpha^2 + C_{LF} \alpha + \gamma C_{LF} + \gamma K_{CN}} \quad \text{for } u < 0 \quad (\text{B.28})$$

$$\tau_{HP} = \frac{\gamma V_{AL}}{\beta (K_{CP} \alpha^2 + C_{LF} \alpha + \gamma C_{LF} + \gamma K_{CP})} \quad \text{for } u \geq 0 \quad (\text{B.29})$$

$$\tau_{HN} = \frac{\gamma V_{AL}}{\beta (K_{CN} \alpha^2 + C_{LF} \alpha + \gamma C_{LF} + \gamma K_{CN})} \quad \text{for } u < 0 \quad (\text{B.30})$$

B.2 Block Diagram Representation

The system equations are visualized in block diagrams in Figure B.1 and Figure B.2.

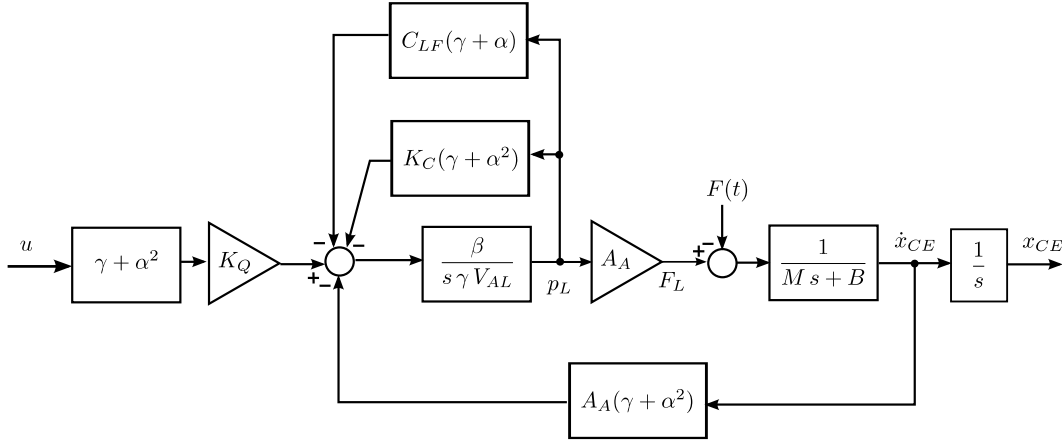


Figure B.1: Block diagram representation of the linearized system. From Equation (B.4) and (B.23).

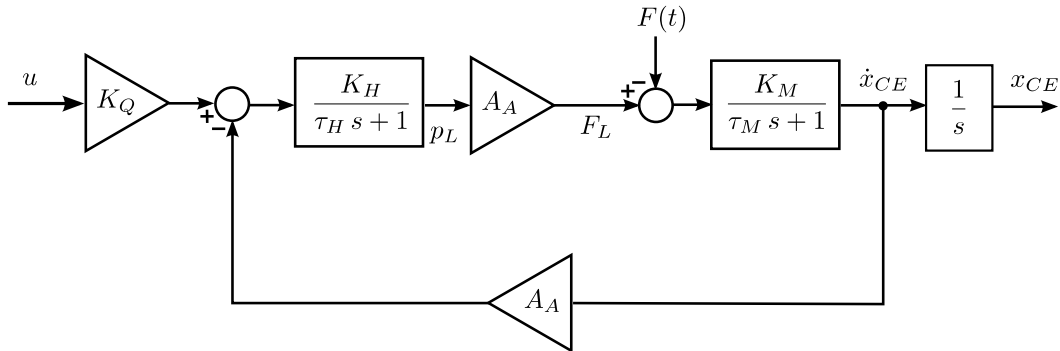


Figure B.2: Block diagram representation of the linearized system. Hydraulic and Mechanical systems are expressed in standard-form. From Equation (B.5) and (B.25).

B.3 Transfer Function for Controller Design

Two different systems are needed for each linear controller. In the design of the Robust Adaptive Backstepping Linear Controller (RABLIN) a transfer function from Δu to Δp_L is needed, and for the linear reference controller (LINREF) a transfer function from Δu to Δx_{CE} is needed.

First we derive the transfer function for the RABLIN controller, by re-arranging the block diagram seen in Figure B.2. The re-arranging is confirmed by calculations using Equation (B.5) and (B.25).

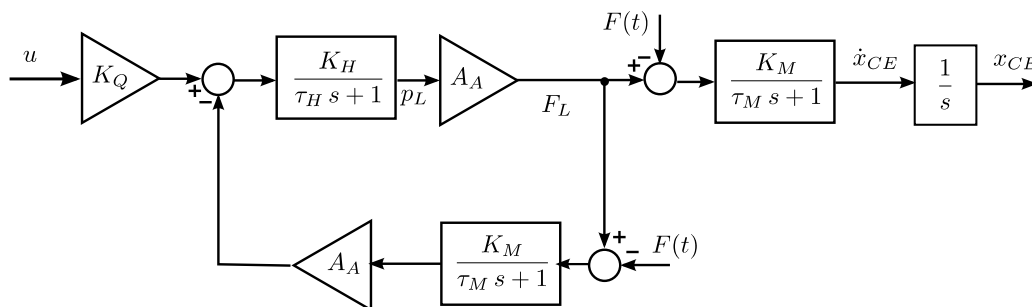


Figure B.3: Re-arranged version of the block diagram seen in Figure B.2.

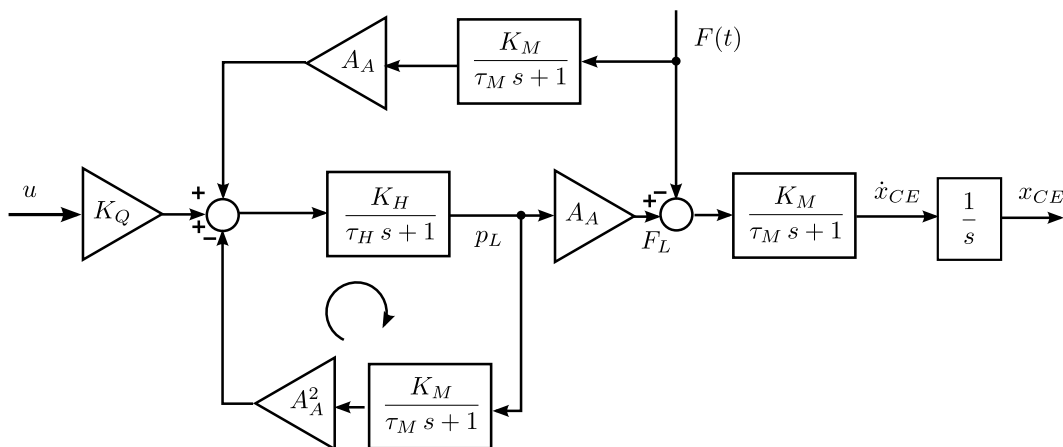


Figure B.4: Re-arranged version of the block diagram seen in Figure B.3.

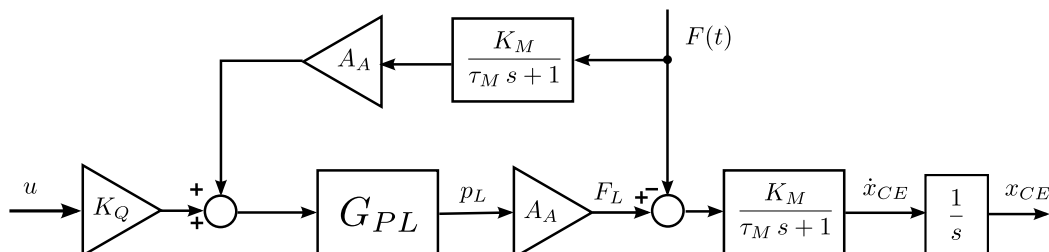


Figure B.5: Block diagram of system used for controller design.

Closing the loop indicated in Figure B.4 reveals the transfer function G_{PL} seen in Figure B.5.

The calculations for closing the loop in Figure B.5 are:

$$\begin{aligned}
G_{PL} &= \frac{\frac{K_H}{\tau_H s+1}}{1 + \frac{K_H}{\tau_H s+1} \frac{A_A^2 K_M}{\tau_M s+1}} \\
&= \frac{K_H(\tau_m s + 1)}{(\tau_H s + 1)(\tau_M s + 1) + K_H K_M A_A^2} \\
&= \frac{K_H(\tau_m s + 1)}{\tau_H \tau_M s^2 + (\tau_H + \tau_M)s + K_H K_M A_A^2 + 1} \\
&= \frac{\frac{K_H}{\tau_H \tau_M}(\tau_m s + 1)}{s^2 + \frac{\tau_H + \tau_M}{\tau_H \tau_M} s + \frac{K_H K_M A_A^2 + 1}{\tau_H \tau_M}} \\
&= \frac{K_H}{K_M K_H A_A^2 + 1} \frac{\frac{K_H K_M A_A^2 + 1}{\tau_H \tau_M}(\tau_m s + 1)}{s^2 + \frac{\tau_H + \tau_M}{\tau_H \tau_M} s + \frac{K_H K_M A_A^2 + 1}{\tau_H \tau_M}} \tag{B.31}
\end{aligned}$$

Comparing to a standard second order system, with a real zero at $\frac{1}{\tau_M}$,

$$G_{PL} = K_{PL} \frac{\omega_{PL}^2 (\tau_M s + 1)}{s^2 + 2\zeta_{PL} \omega_{PL} s + \omega_{PL}^2} \tag{B.32}$$

yields the coefficients:

$$K_{PL} = \frac{K_H}{K_M K_H A_A^2 + 1} \tag{B.33}$$

$$\omega_{PL} = \sqrt{\frac{K_H K_M A_A^2 + 1}{\tau_H \tau_M}} \tag{B.34}$$

$$\zeta_{PL} = \sqrt{\frac{(\tau_H + \tau_M)^2}{4\tau_H \tau_M (K_H K_M A_A^2 + 1)}} \tag{B.35}$$

The coefficients are calculated using K_H and τ_H from the linearized hydraulic model, and as these changes for positive (K_{HP} , τ_{HP}) and negative (K_{HN} , τ_{HN}) input signal u so does the coefficients. This is denoted with P and N in the suffix like for the linearized hydraulic model.

To confirm the derivation of the transfer functions G_M , G_H and G_{PL} the frequency response of the systems shown in Figure B.1 and B.5 are calculated and they yield the exact same response when shown in a bode plot.

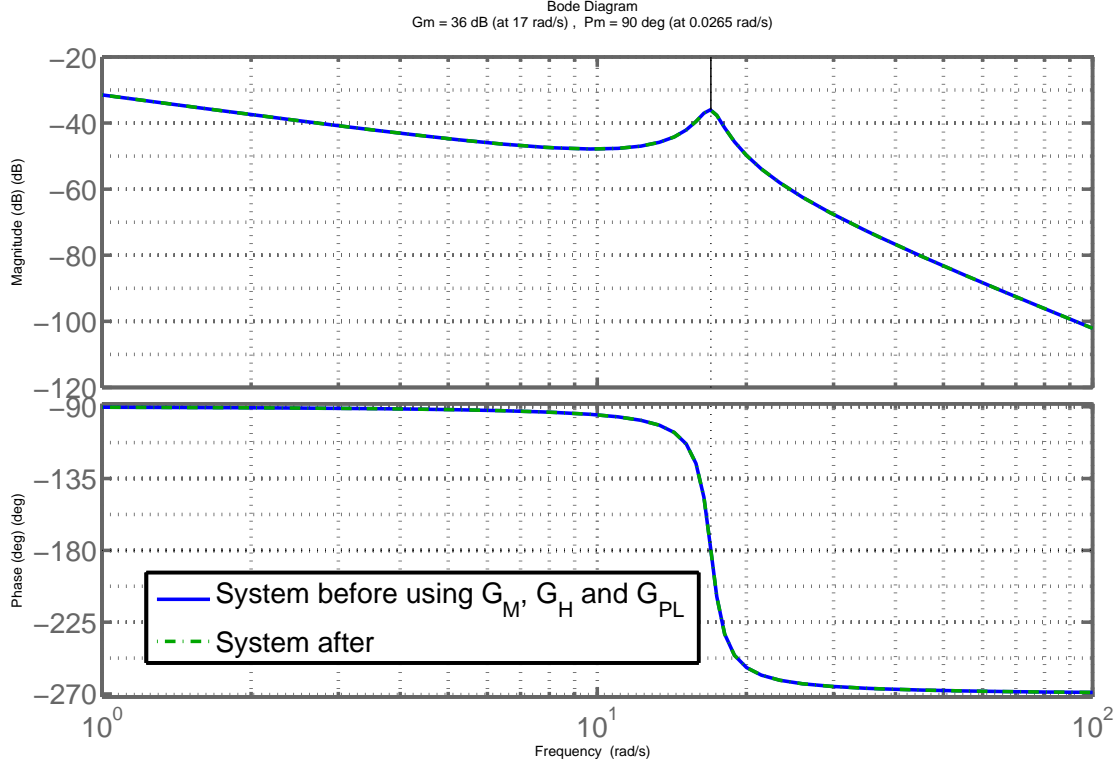


Figure B.6: Bode plot showing the frequency response of the system before introducing G_M , G_H and G_{PL} (Figure B.1) and after the response after (Figure B.5). The operating point is chosen different from zero so no coefficients cancels out.

The transfer function used in the design of the LINREF controller is the transfer function from Δu to Δx_{CE} . From Figure B.5:

$$G_{UX} = \underbrace{A_A K_Q K_{PL} K_M}_{K_{UX}} \frac{\omega_{PL}^2}{s(s^2 + 2\zeta_{PL} \omega_{PL} s + \omega_{PL}^2)} \quad (\text{B.36})$$

Where K_{UX} can be simplified by substituting expressions for K_{PL} and K_M :

$$K_{UX} = \frac{K_Q}{A_A} \quad (\text{B.37})$$

As we now have transfer function for the system we are able to find the operating point that should be used in the controller design. This is done in Appendix D, and the result obtained requires that the linearized model is altered.

B.4 System For Critical Operating Point

When the leakage coefficient $C_{LF} = 0$ and the linearization point for the input signal $u_0 = 0$ the linearized hydraulic model changes from a first order system to a simple integrator with a gain. A very small value for the leakage coefficient could be used to keep the first order system, or derive a new linearized hydraulic system. The last option is chosen.

From (B.23) we get:

$$G_H(s) = \frac{K_H}{s} \quad (\text{B.38})$$

$$K_H = \frac{\beta(\gamma + \alpha^2)}{\gamma V_{AL}} \quad (\text{B.39})$$

Deriving G_{PL} again using Figure B.4:

$$\begin{aligned} G_{PL} &= \frac{\frac{K_H}{s}}{1 + A_A^2 \frac{K_M K_H}{s(\tau_M s + 1)}} \\ &= \frac{K_H(\tau_M s + 1)}{s(\tau_M s + 1) + A_A^2 K_M K_H} \\ &= \frac{\frac{K_H}{\tau_M}(\tau_M s + 1)}{s^2 + \frac{1}{\tau_M} s + \frac{A_A^2 K_M K_H}{\tau_M}} \\ &= \frac{1}{A_A^2 K_M} \frac{\frac{A_A^2 K_M K_H}{\tau_M}(\tau_M s + 1)}{s^2 + \frac{1}{\tau_M} s + \frac{A_A^2 K_M K_H}{\tau_M}} \end{aligned} \quad (\text{B.40})$$

Comparing to a standard second order system, with a real zero at $\frac{1}{\tau_M}$,

$$G_{PL} = K_{PL} \frac{\omega_{PL}^2(\tau_M s + 1)}{s^2 + 2\zeta_{PL}\omega_{PL}s + \omega_{PL}^2} \quad (\text{B.41})$$

yields the coefficients:

$$K_{PL} = \frac{1}{A_A^2 K_M} \quad (\text{B.42})$$

$$\omega_{PL} = \sqrt{\frac{A_A^2 K_M K_H}{\tau_M}} \quad (\text{B.43})$$

$$\zeta_{PL} = \sqrt{\frac{1}{4 A_A^2 K_M K_H \tau_M}} \quad (\text{B.44})$$

If the DC-gains (K_M , K_H) and the time constants (τ_M , τ_H) are substituted we get:

$$K_{PL} = \frac{B}{A_A^2} \quad \omega_{PL} = \sqrt{\frac{A_A^2 \beta(\gamma + \alpha^2)}{M \gamma V_{AL}}} \quad \zeta_{PL} = \frac{B}{2 A_A} \sqrt{\frac{\gamma V_{AL}}{M \beta(\gamma + \alpha^2)}} \quad (\text{B.45})$$

This concludes the linearized model. A summary of the equations are given in Section 6.

Appendix C

Parameter Variations

This chapter presents the parameter variations of the hydraulic and mechanical part of the model. The variations are used in the controller design to determine operating points and parameter bounds.

C.1 Mechanical

The variations of the mechanical model is calculated using the non-linear expressions found in the model summary (4.43)-(4.47) page 30. In the physical setup the parameters might vary more than calculated so the parameter bounds have a safety margin of approximately 20% of the end values. The parameter

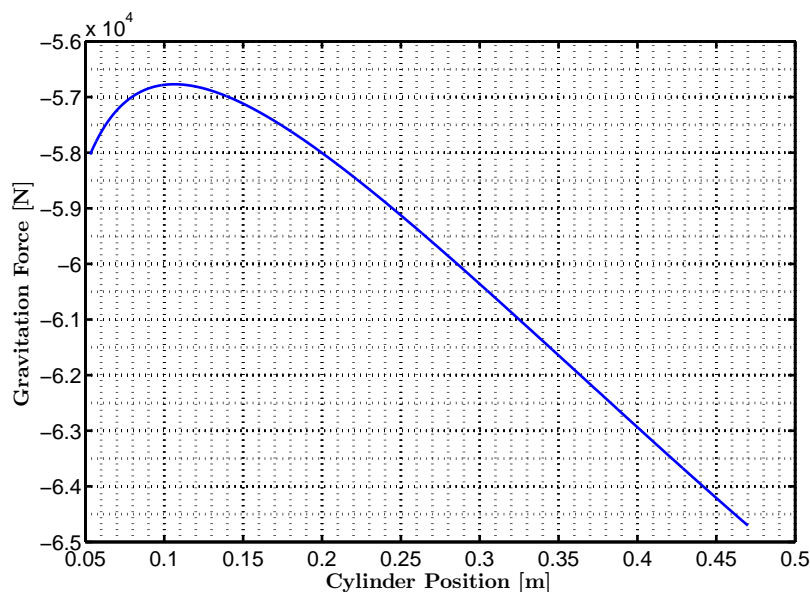


Figure C.1: Variation of the parameter F . From Equation: (4.45) page 30.

variation of the disturbance parameter F is seen in Figure C.1. In the figure it is calculated only on the gravitational force, but in reality it will also include stiction and coulomb friction. These however is assumed small compared to the gravitational force and assumed to stay within the 20% safety margin. Applying this margin to the maximum and minimum values seen in the figure, we obtain:

$$F_{MIN} = 48000 \text{ N} \quad F_{MAX} = 78000 \text{ N} \quad (\text{C.1})$$

The system is operated without applying extra mass to its own body weight, and the values seen in

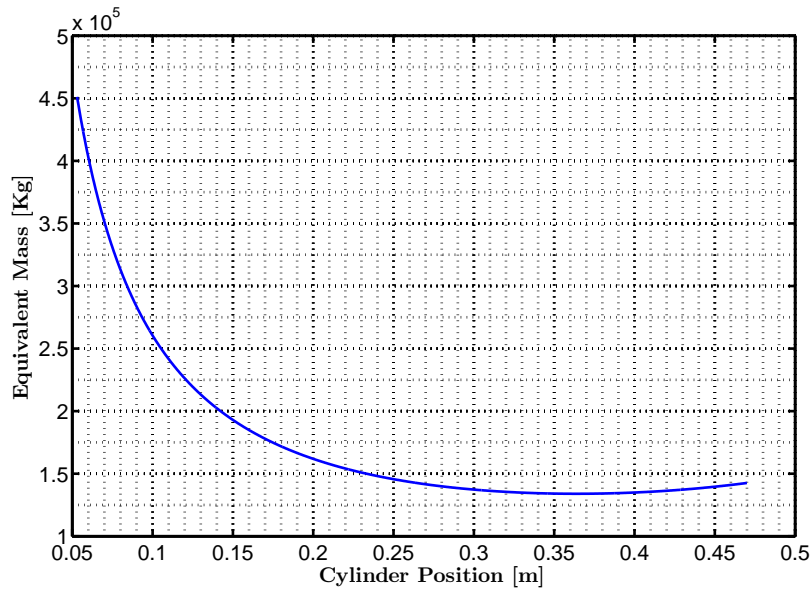


Figure C.2: Variation of the parameter M. From Equation: (4.43) page 30.

Figure C.2 is used to calculate the bounds with 20% safety margin:

$$M_{MIN} = 104,000 \text{ Kg} \quad M_{MAX} = 540,000 \text{ Kg} \quad (C.2)$$

The friction coefficient also yields some uncertainty. The parameter is seen to vary only little with

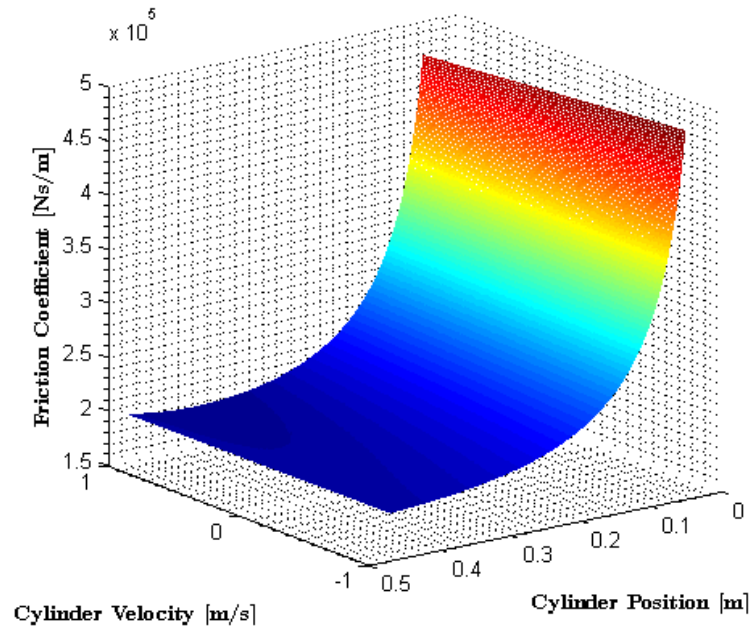


Figure C.3: Variation of the parameter B. From Equation: (4.44) page 30.

velocity but highly with position. Again, the 20% safety margin is calculated using the figure and the following bounds are obtained.

$$B_{MIN} = 160,000 \text{ kg/s} \quad B_{MAX} = 576,000 \text{ kg/s} \quad (C.3)$$

C.2 Hydraulic

It has not been prioritized to find precise bounds for the hydraulic part of the system as it is very time consuming compared to how much the controller design benefits from the improved accurateness. The resources are put elsewhere.

The initial volumes are determined quite accurately, but again the safety margin of 20% is used for these parameters.

$$V_{0AMIN} = 0.0013504 \text{ m}^3 \quad V_{0AMAX} = 0.0020256 \text{ m}^3 \quad (\text{C.4})$$

$$V_{0BMIN} = 0.0078930 \text{ m}^3 \quad V_{0BMAX} = 0.0118404 \text{ m}^3 \quad (\text{C.5})$$

Besides the initial volumes, the hydraulic parameters are: Bulk modulus β , cylinder leakage coefficient C_L and valve flow gain K_A . There is no model of the variations for these parameters so they are chosen with much uncertainty.

The mentioned parameters are all temperature dependent, but as the system is temperature controlled the change is ignored. However, all bounds have a safety margin to account for the small change there will be.

The leakage coefficient C_L will increase with wear and tear on the cylinder, so it is difficult to give an estimate of how much this parameter will change, and it would require extensive tests to give an indication. It should be noted that this parameter changes doing operation but mainly over longer time. So for controller evaluation purposes it is determined as $\pm 100\%$ which results in the following bounds:

$$C_{LMIN} = 0 \text{ m}^3/\text{sPa} \quad C_{LMAX} = 2.20\text{e-}12 \text{ m}^3/\text{sPa} \quad (\text{C.6})$$

Bulk modulus varies with pressure; how much is mainly determined by how much dissolved air the oil contains [Andersen and Hansen, 2007, p.141].

Based on the figure we define the following bounds for bulk modulus:

$$\beta_{MIN} = 1000\text{e}5 \text{ Pa} \quad \beta_{MAX} = 12000\text{e}5 \text{ Pa} \quad (\text{C.7})$$

Which allow it to change to 20% above the value found in the verification of the Simulation model (10.000 Bar) and 90% below.

The value K_A is a combined quantity. From (4.30) on page 27 we see that it is combined of the discharge coefficient C_D and the oil density ρ . The density is highly temperature dependent but only vary a small amount with pressure [Andersen and Hansen, 2007, p.141]. The discharge coefficient becomes small if the flow changes from turbulent to laminar over the valve, otherwise it is fairly constant. It is assumed that this will not happen. In (5.17) on page 44 we determined $K_A = 6.4974\text{e-}4 \frac{\text{m}^2}{\text{s}\sqrt{\text{Pa}}}$ and here we choose the bounds as $\pm 20\%$:

$$K_{AMIN} = 5.1979\text{e-}4 \frac{\text{m}^2}{\text{s}\sqrt{\text{Pa}}} \quad K_{AMAX} = 7.7969\text{e-}4 \frac{\text{m}^2}{\text{s}\sqrt{\text{Pa}}} \quad (\text{C.8})$$

This concludes the parameter variations. A more thorough discussion are made in the controller design part of the report.

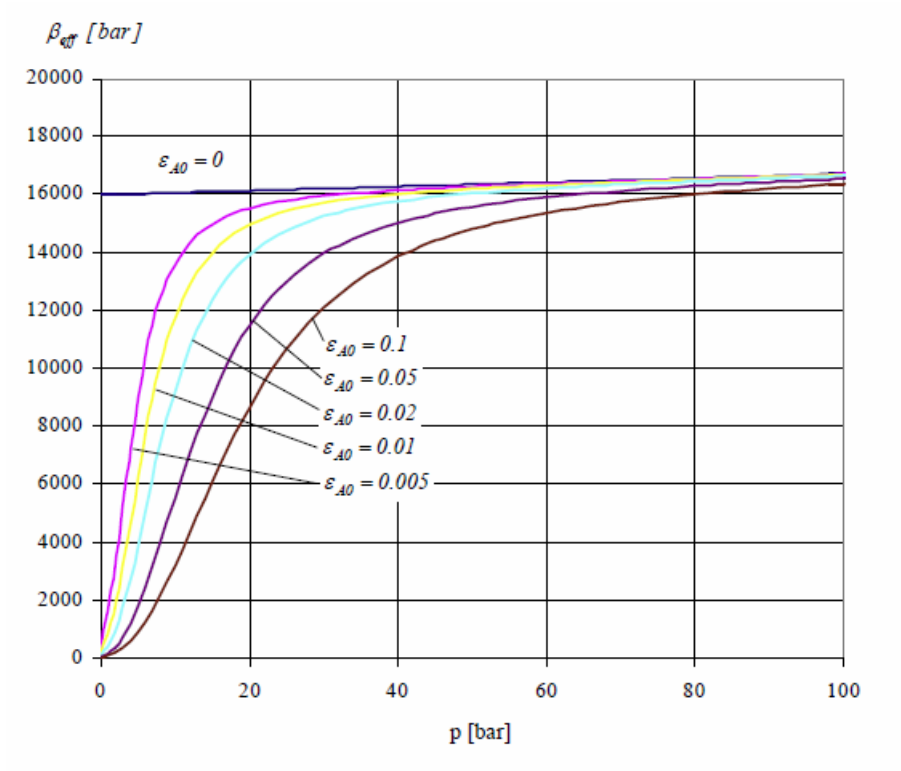


Fig. A6 Variation of effective stiffness of fluid-air mixture with respect to pressure and volume ratio of free air at atmospheric pressure. The temperature of the fluid is 40 °C and the compression of the free air is assumed adiabatic

Figure C.4: Variation of bulk modulus β as a function of pressure for different levels of dissolved air [Andersen and Hansen, 2007, p.141].

Appendix D

Operating Point and Parameter Values

In the design of the linear controllers we use a linearized model and therefore have to choose an operating point for the states. As the parameter variations of the hydraulic part is unmodeled these parameters should be determined as well. The parameters and the operating point should be the most critical with respect to design specifications, as the same controller should be able to operate in all operating points. How the critical operating point and critical parameter values are chosen is explained in the following section.

D.1 Choosing Critical Operating Point and Parameter Values

D.1.1 Defining Critical

The most important design specification is always *stability* as all other criteria require that the system is stable. Stability is therefore the first thing that defines a critical operating point. If more operating points are equally critical regarding stability, the second most important design criterion can be considered or a trade off between several criteria.

In general the most critical operating point depends on how we shape the loop, and how we shape the loop depends on the operating point. This a complex situation that makes the design process iterative. [Phillips and Harbor, 2000, p. 356].

D.1.2 Critical Indicators

We want to increase the open-loop gain over as wide band of frequencies as possible. The reason for this is: fast transient response, good tracking accuracy, good sensitivity and good disturbance rejection [Phillips and Harbor, 2000, p.351-356]. The trade off is lowered stability margins and possible reduced transient performance as low stability margins introduce resonance which result in overshoot and prolonged settling time. [Phillips and Harbor, 2000, p.356].

If we use pure gain compensation we increase the *gain* crossover frequency, but leaves the phase unaltered. Therefore we can expect the operating point yielding the **lowest gain margin** for the uncompensated system to be a critical operating point in the compensated system as well.

As the frequency where the phase margin is defined is changed the phase margin for the uncompensated

system cannot be used as an indicator, but one has to look at the **phase crossover frequency** or the **lowest eigenfrequency** to find a critical operating point.

In our case the phase crossover frequency happens at the resonance peak, which allows us to consider the resonance peak of the magnitude plot and choose the operating point and parameter values yielding the **highest magnitude at the lowest eigenfrequency**.

D.1.3 Systems

As mentioned before two linear controllers are designed, and their respective plant transfer functions are:

Plant for LINREF controller (from Equation (B.36)):

$$G_{UX} = \underbrace{A_A K_Q K_{PL} K_M}_{K_{UX}} \frac{\omega_{PL}^2}{s(s^2 + 2\zeta_{PL}\omega_{PL}s + \omega_{PL}^2)} \quad (D.1)$$

Plant for RABLIN controller (from Equation (D.2)):

$$G_{PL} = K_{PL} \frac{\omega_{PL}^2(\tau_M s + 1)}{s^2 + 2\zeta_{PL}\omega_{PL}s + \omega_{PL}^2} \quad (D.2)$$

First the plant for the LINREF controller is considered, and the obtained critical operating point is then evaluated for the RABLIN plant.

D.2 Parameter Values

First the parameter values are considered. The mechanical parameters are included in the model so these are determined indirectly through the operating point. The safety margin for these parameters is assumed satisfied through the stability margins of the final controller.

The hydraulic parameters are not modeled but vary within the safety margins defined in Section C and therefore we have to determine the critical values for these. The bodeplots for varying the hydraulic parameter values are seen in Figure D.1 to Figure D.4, and the chosen critical values are listed in table D.1.

Name	Symbol	Symbolic Value	Value	Unit
Initial Volume A	V_{A0}	V_{A0MAX}	2.0256 e-3	$[m^3]$
Flow Constant A	K_A	K_{AMAX}	7.7969 e-4	$[m^2/s\sqrt{Pa}]$
Bulk Modulus	β	β_{MIN}	1000 e5	$[Pa]$
Leakage Coefficient	C_{LF}	C_{LFMIN}	0e-12	$[m^3/sPa]$

Table D.1: Critical parameter values for G_{UX} and G_{PL} .

It is seen that the eigenfrequency of the control system depends heavily on the value of bulk modulus β of the oil. This parameter changes during operation with changing pressure and with dissolved air. Some systems are tuned without modeling, and a linear controller performing well at tuning time might get unstable later when bulk modulus changes.

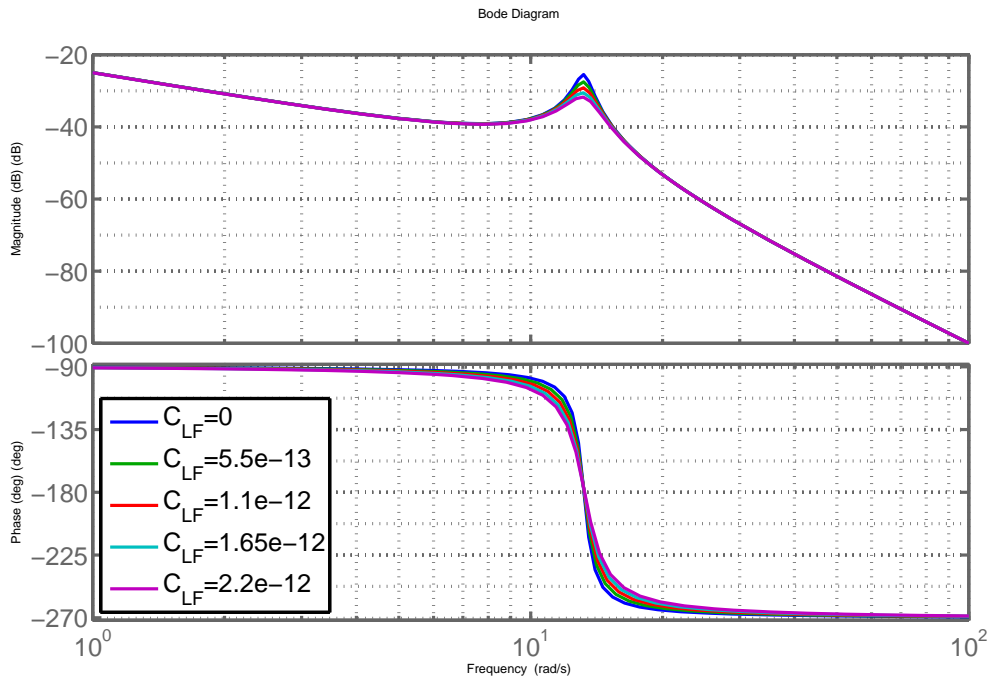


Figure D.1: Bodeplots of system dynamics with varying leakage coefficient.

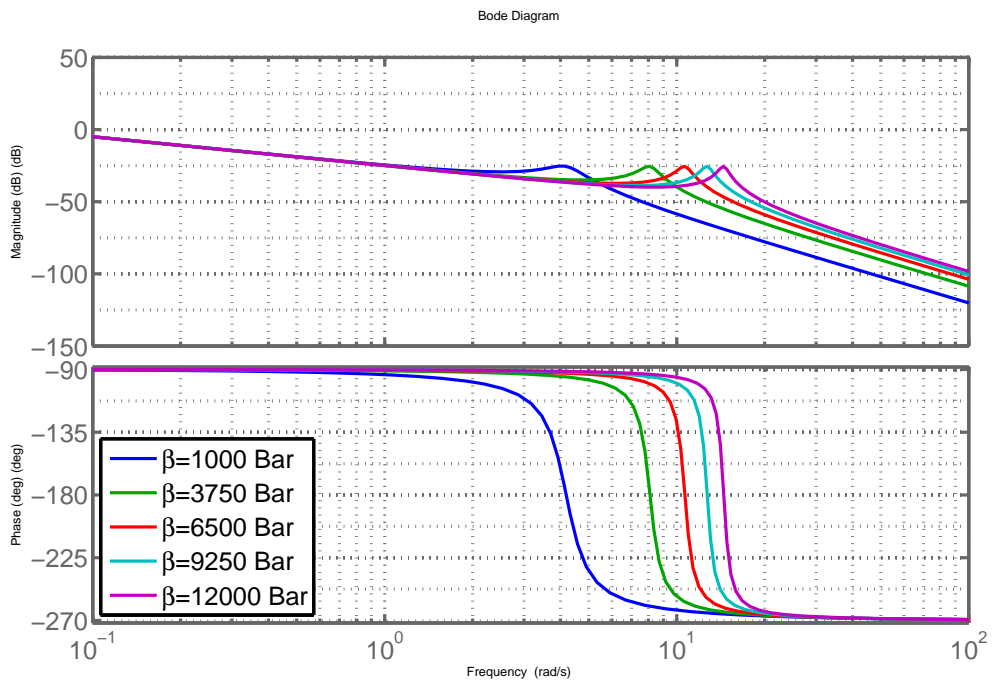


Figure D.2: Bodeplots of system dynamics with varying bulk modulus.

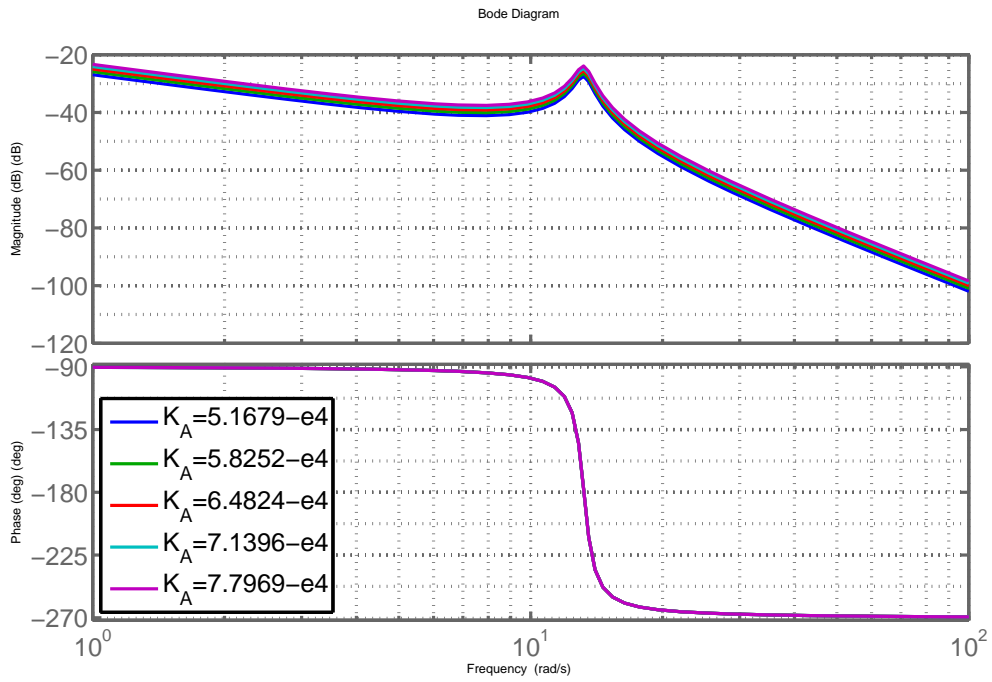


Figure D.3: Bodeplots of system dynamics with varying flow constant.

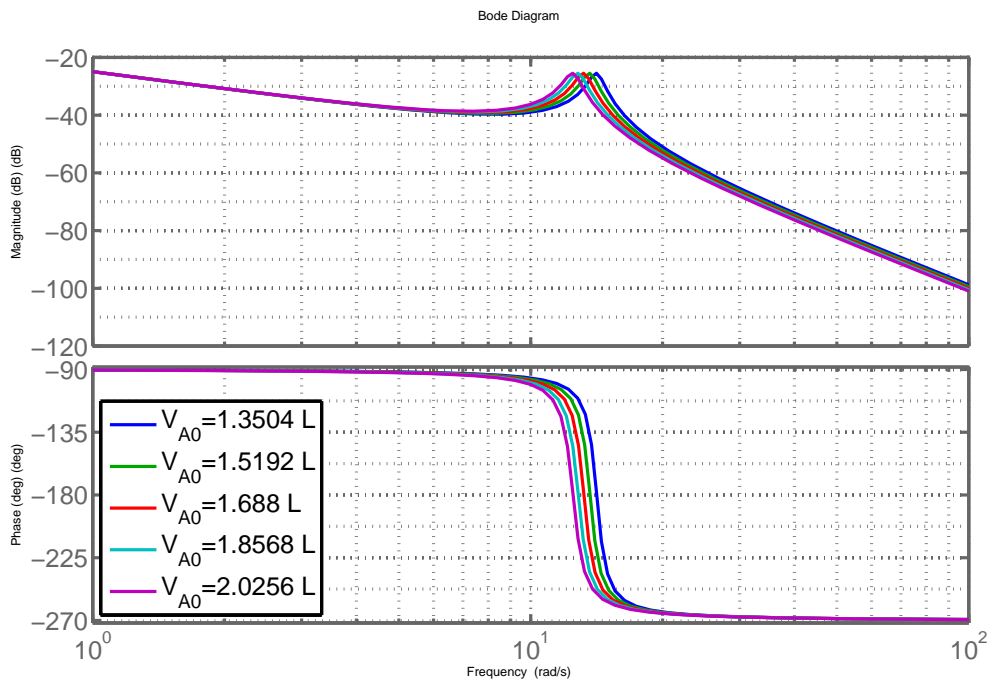


Figure D.4: Bodeplots of system dynamics with varying initial volume.

D.3 Operating Point

The same procedure we used to find the critical parameter values are used to find the critical operating point. The bode plots are shown in Figure D.5 to Figure D.8, and the result is shown in Table D.2.

Name	Symbol	Symbolic Value	Value	Unit
Input Signal	u_0	-	0.00	[V]
Cylinder Position	x_{CE0}	x_{CEMIN}	0.0530	[m]
Cylinder Velocity	\dot{x}_{CE0}	-	0.00	[m/s]
Load Pressure	p_{L0}	$p_T - \alpha p_P$	-119 e5	[Pa]

Table D.2: Critical operating point for the linearized system.

It is seen that the systems eigenfrequency is lowered considerable when the arm is in the upright position ($x_{CE} = x_{CEMIN}$), and when the valve is in middle position, equivalent of $u_0 = 0$. The velocity only affects the parameter B which is dominated by the viscous damping coefficient ν_X so the change in \dot{x}_{CE} do not change the response noticeable. The loop gain is highly affected by the load pressure and a design based on the critical operating point will result in a conservative controller, but is required as stability in all operating points are the most important design criterion.

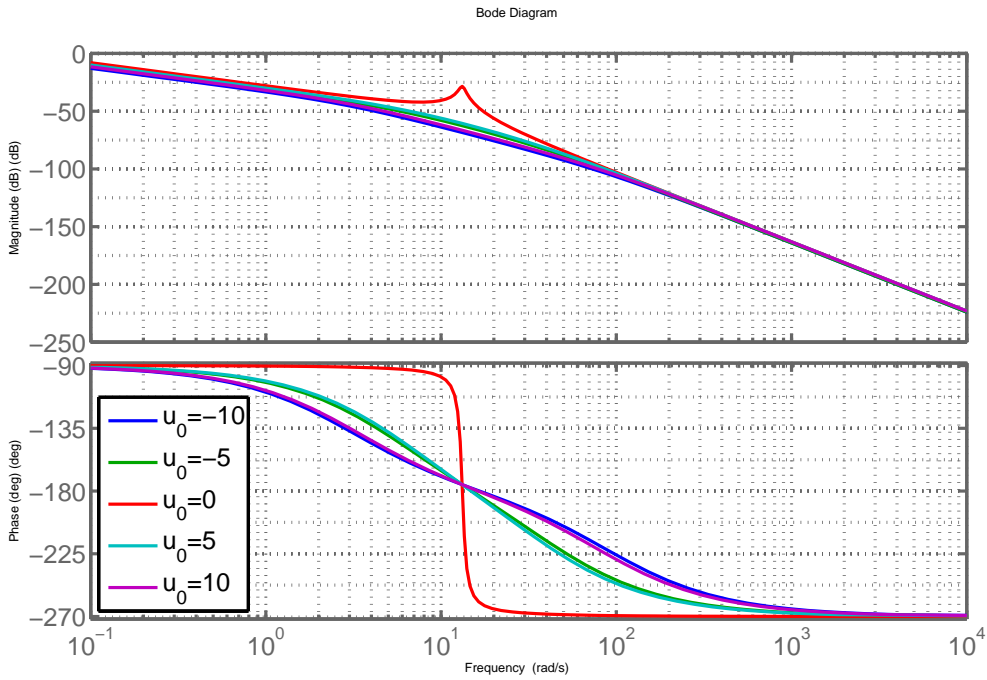


Figure D.5: Bodeplots of system dynamics with varying input signal.

The maximum and minimum values of the load-pressure is calculated as the situations where p_A and p_B attains the values of p_P and p_T . Which is calculated as:

$$\begin{aligned}
 p_{LMIN} &= p_T - \alpha p_P \approx -119 \text{ Bar} \\
 p_{LMAX} &= p_P - \alpha p_T \approx 149 \text{ Bar}
 \end{aligned}
 \tag{D.3}$$

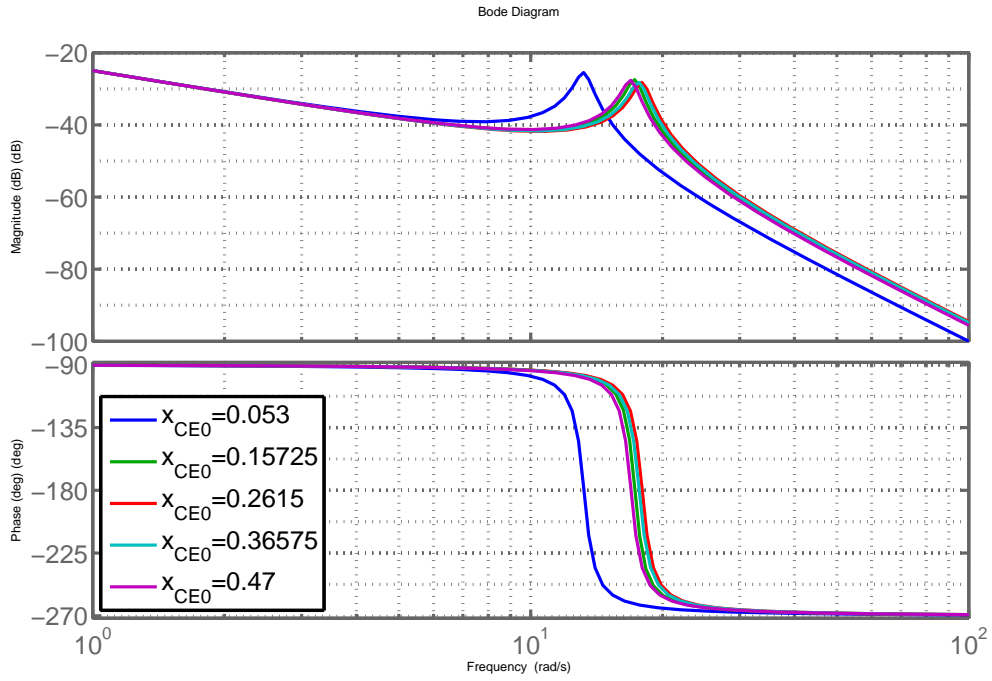


Figure D.6: Bodeplots of system dynamics with varying cylinder position.

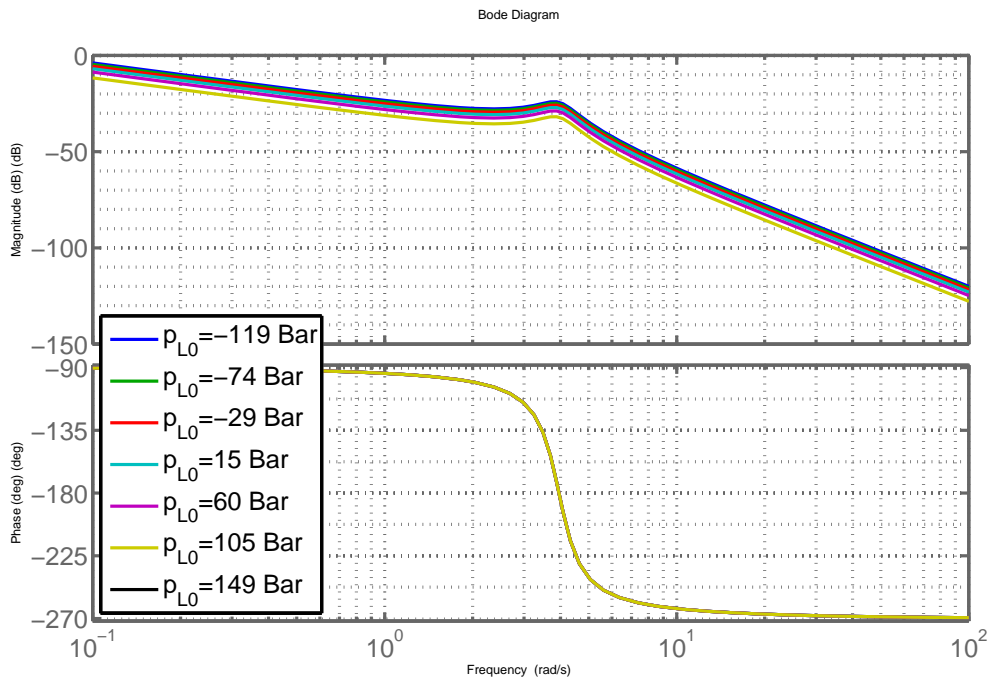


Figure D.7: Bodeplots of varying load pressure operating point. For positive spool displacement $u \geq 0$. The black line is not seen in the plot as it result in $K_Q = 0$.

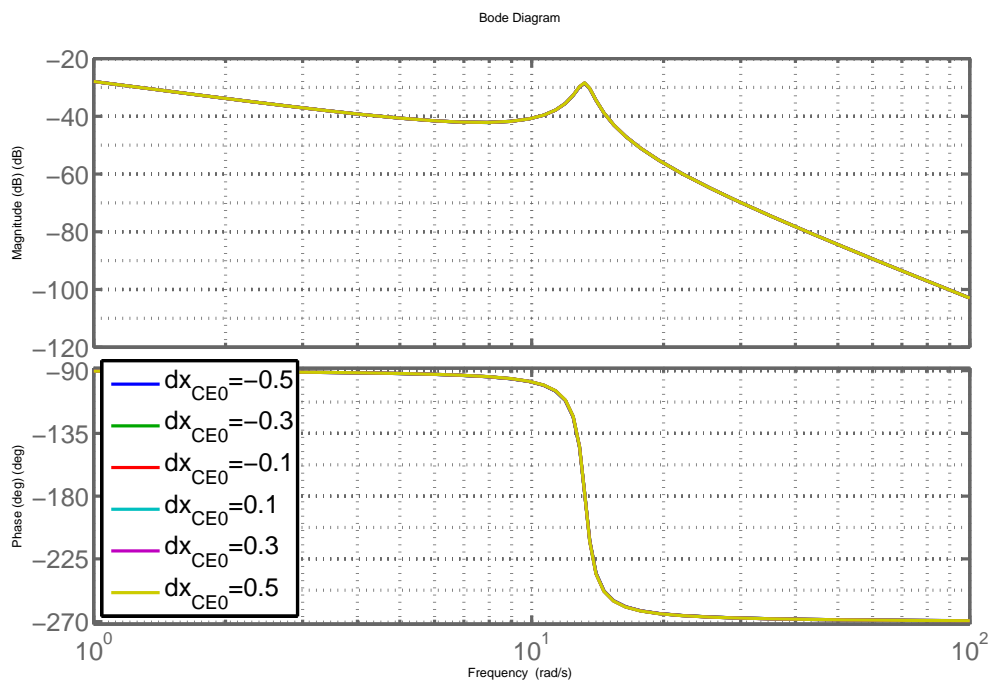


Figure D.8: Bodeplots of system dynamics with varying cylinder velocity.

D.4 Critical Point for RABLIN Control System

In Section D.1.2 we defined the indicator for a critical point as **highest magnitude at the lowest eigenfrequency**. For G_{UX} the definition lead to a unique definition of critical parameters and operating point. The same is the case for G_{PL} besides the value of V_{A0} and β . It is assumed that the critical operating point will be the same as that for G_{UX} , but the RABLIN controller design must be evaluated for the parameters $\beta = 12000$ Bar and $V_{A0} = 2.0256$ as well.

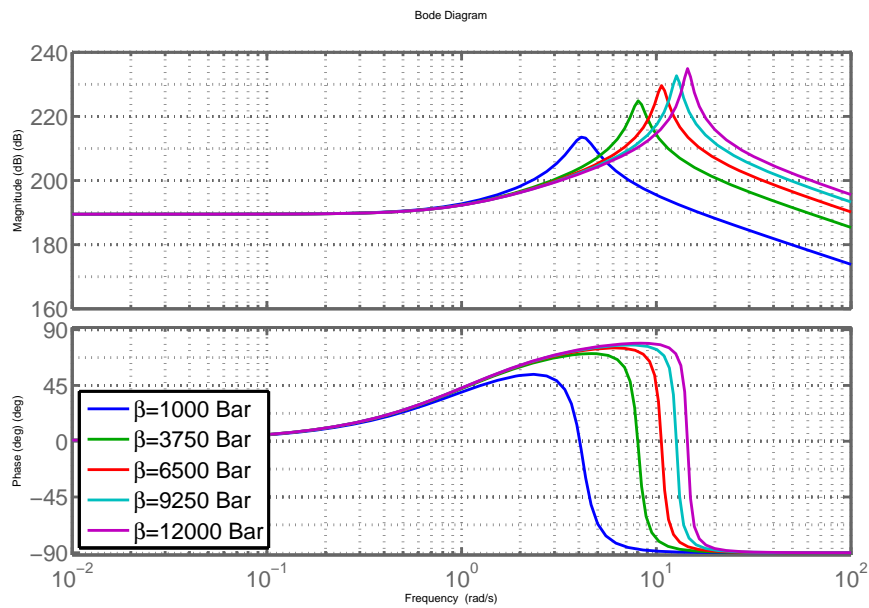


Figure D.9: Bodeplots of system dynamics with varying bulk modulus.

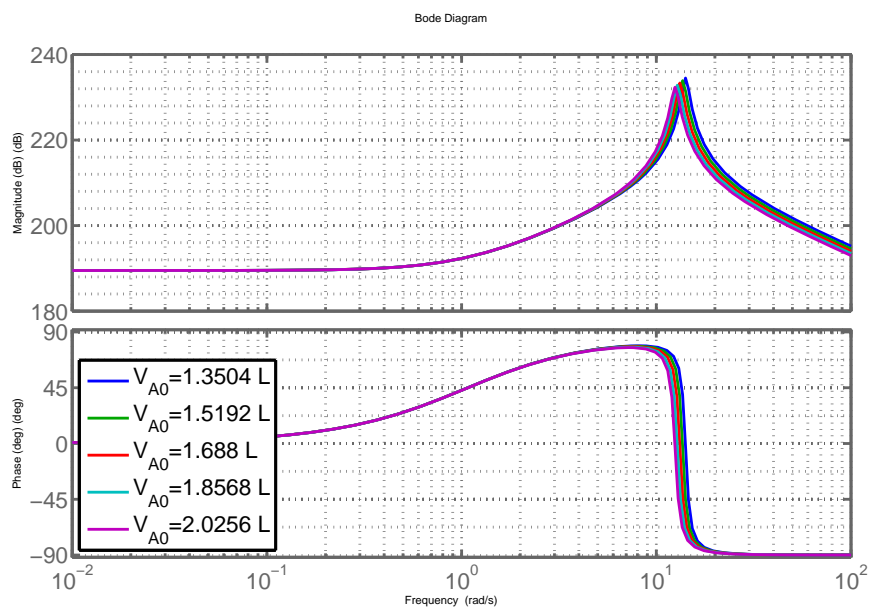


Figure D.10: Bodeplots of system dynamics with varying initial volumes.

D.5 Final Remark

Bodeplots are not the only way to evaluate for critical operating points. It is also possible to use root locus techniques. Plotting the closed loop poles of the transfer function in the S-plane. As an example the root locus for varying cylinder position is shown in Figure D.11, which show that the inner blue dot is the most critical position.

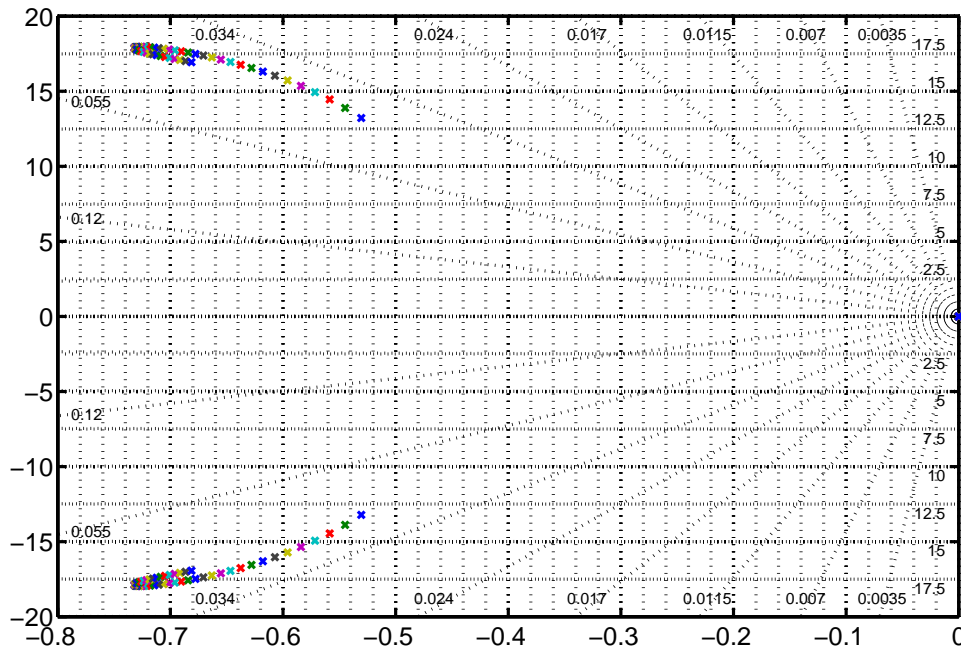


Figure D.11: Root locus of various operating points.

Appendix E

Data for Verification

To verify the model three trajectories have been used. The arguments for choosing these directories are given in Section 5 together with the result of the verification. This section contains additional data complementing the data presented in the verification chapter. More data than what is presented have been logged. However, the data shown are what have been used to obtain the parameter values and to verify the model.

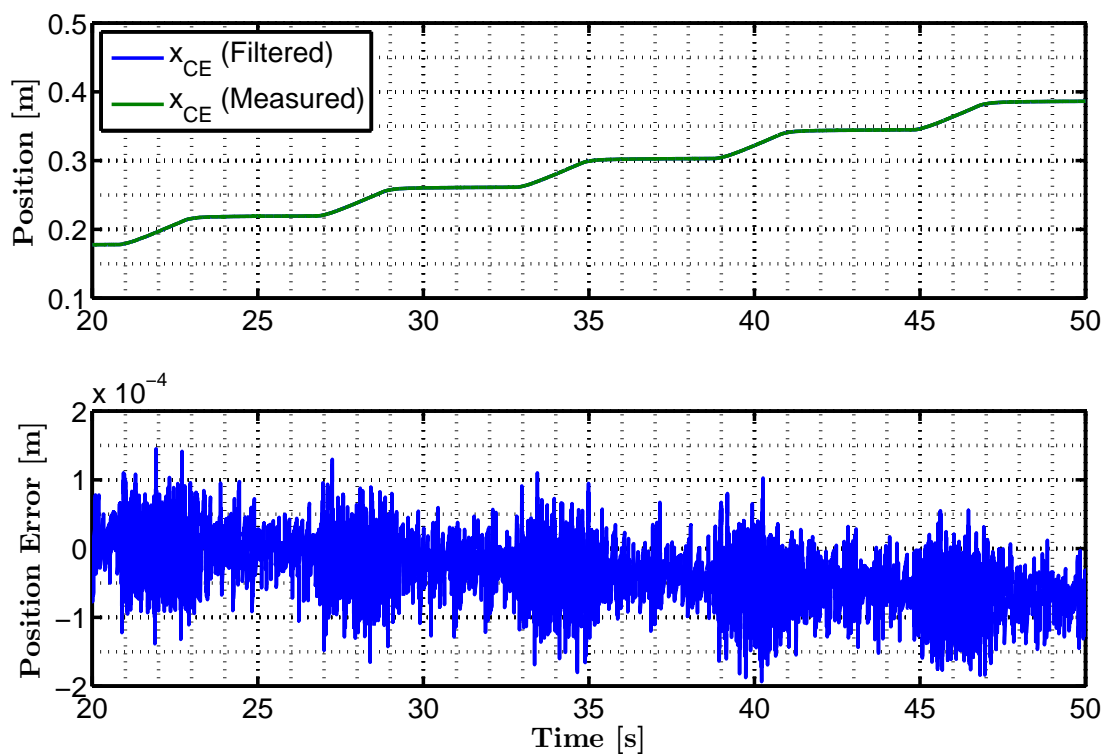


Figure E.1: Position error of **Stair** trajectory. The acceleration, obtained from differentiation and filtering, is integrated twice and compared to the original position signal.

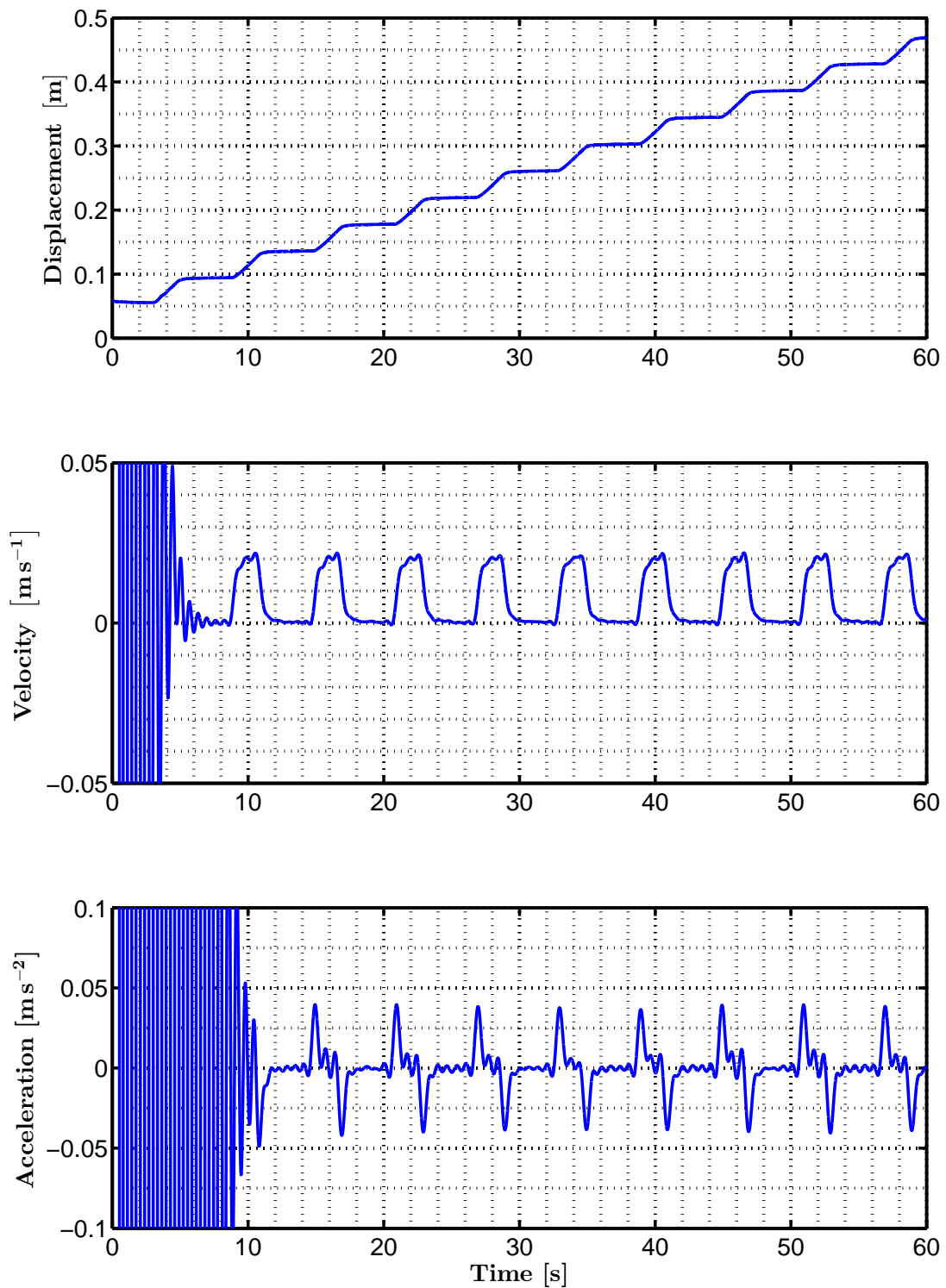


Figure E.2: Result of filtering of the **Stair** trajectory.

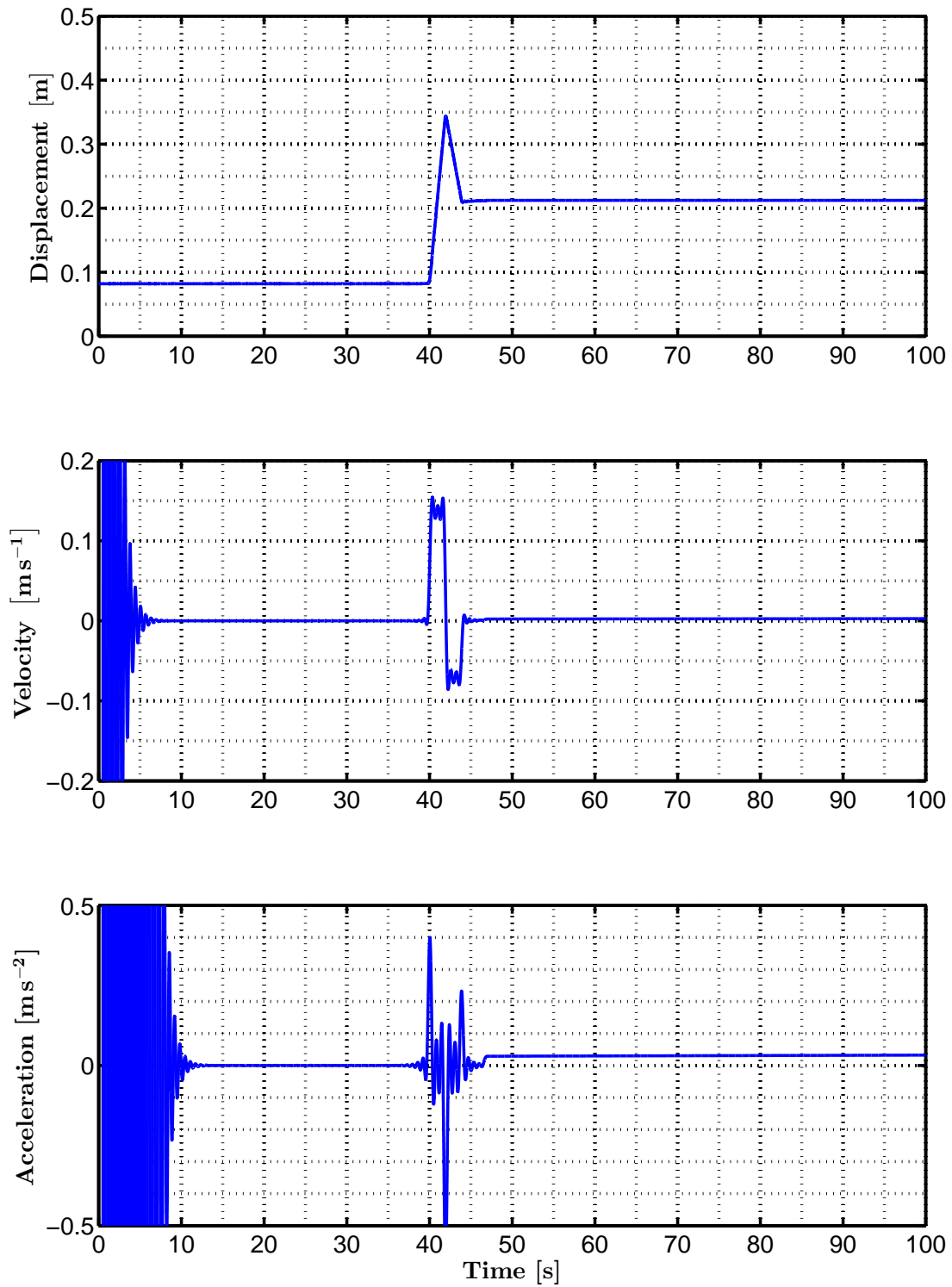


Figure E.3: Result of filtering of the **Step** trajectory.

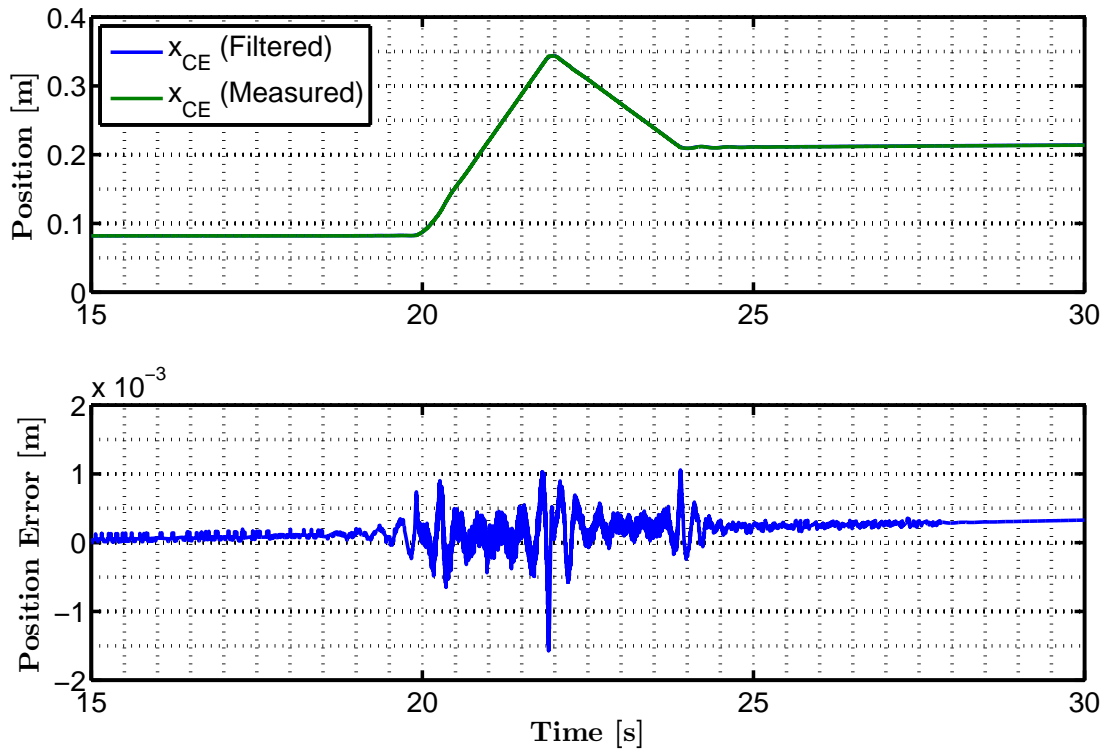


Figure E.4: Position error of **step** trajectory. The acceleration, obtained from differentiation and filtering, is integrated twice and compared to the original position signal. Time is shifted 20 s compared to Figure E.3.

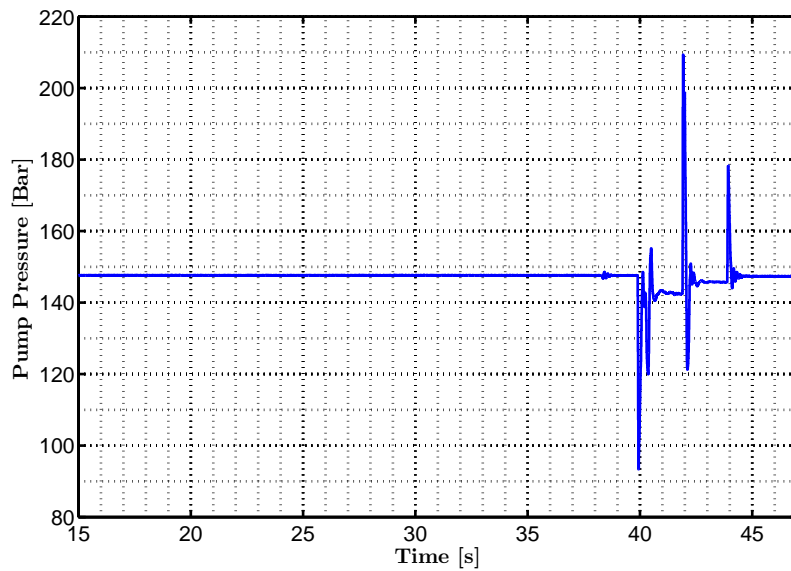


Figure E.5: Measured Pump pressure p_P doing the **Step** trajectory.

Appendix F

Stability Theorems and Lemmas

The theorems presented in this chapter makes up the theoretical background for the backstepping design procedure. In special cases, more tools might be needed, but for most systems, and the system considered in this report, the following theorems cover the mathematical foundation. Especially the Lyapunov-like LaSalle-Yoshizawa Theorem F.4.2 is important when guaranteeing global stability and asymptotically tracking of the developed controller.

F.1 Lyapunov's Stability Theorem (Direct Method)

The following theories apply to *autonomous systems* of the form

$$\dot{x} = f(x). \tag{F.1}$$

F.1.1 Local Stability

If, in a ball \mathbf{B}_{R_0} there exists a scalar function $V(\mathbf{x})$ with continuous first partial derivatives such that

- $V(\mathbf{x})$ is positive definite (locally in \mathbf{B}_{R_0})
- $\dot{V}(\mathbf{x})$ is negative semi-definite (locally in \mathbf{B}_{R_0})

then the equilibrium point $\mathbf{x} = \mathbf{0}$ is stable. If, actually, the derivative $\dot{V}(\mathbf{x})$ is locally negative definite in \mathbf{B}_{R_0} , then the stability is asymptotic. [Slotine and Li, 1991, p. 62].

F.1.2 Global Stability

Assume that there exists a scalar function V of the states \mathbf{x} with continuous first order derivatives such that

- $V(\mathbf{x})$ is positive definite
- $\dot{V}(\mathbf{x})$ is negative definite
- $V(\mathbf{x}) \rightarrow \infty$ for $|\mathbf{x}| \rightarrow \infty$

then the equilibrium at the origin is globally asymptotically stable. [Slotine and Li, 1991, p. 65].

For both local and global stability LaSalle's invariant set theorem F.2 might be applied to obtain convergence to the equilibrium, with a $\dot{V}(x)$ being only negative semi-definite.

F.2 LaSalle's Invariance Theorem

This theorem is of great importance in backstepping design for autonomous systems of form (F.2).

Definition Let Ω be a positively invariant set of the *autonomous system*

$$\dot{x} = f(x). \tag{F.2}$$

Let $V : \Omega \rightarrow \mathbb{R}_+$ be a continuously differentiable function $V(x)$ such that $\dot{V}(x) \leq 0, \forall x \in \Omega$. Let $E = \{x \in \Omega | \dot{V}(x) = 0\}$, and let M be the largest invariant set contained in E . Then, every bounded solution $x(t)$ starting in Ω converges to M as $t \rightarrow \infty$. [Miroslav Krstic and Kokotovic, 1995, p.25].

Interpretation When applying the traditional Lyapunov stability method (F.1) to a system and the derivative of the Lyapunov function $\dot{V}(x) \leq 0$ end up being only negative semi-definite, one can use LaSalle's invariant set theorem to find a set of points, M

$$M = \{x \in \mathbb{R}^n | \dot{V}(x) = 0 \wedge \dot{x} = 0\} \tag{F.3}$$

that the solution $x(t)$ will converge to when $t \rightarrow \infty$. If M happens to contain only the equilibrium point $x = 0$ of (F.2) then all trajectories $x(t)$ will converge to this equilibrium point when $t \rightarrow \infty$, and a result equivalent of having a negative definite ($\dot{V}(0) = 0$ and $\dot{V}(x) < 0$ for $x \neq 0$) is then obtained for the negative semi-definite $\dot{V} \leq 0$.

F.3 Raffoul's Boundedness of Solutions Theorem

This Theorem is presented in [Raffoul, 2012, p. 2].

Let D be a set in \mathbb{R}^n . Suppose there exist a continuously differentiable Lyapunov function $V : D \times \mathbb{R}^+ \rightarrow \mathbb{R}^+$ that satisfies

$$\lambda_1 \|x\|^p \leq V(x, t) \leq \lambda_2 \|x\|^q \tag{F.4}$$

and

$$V'(x, t) \leq -\lambda_3 \|x\|^r + L \tag{F.5}$$

for some positive constants $\lambda_1, \lambda_2, \lambda_3, p, q, r$ and L . Moreover, if for some constant $\gamma \geq 0$ the inequality

$$V(x, t) - V^{r/q}(x, t) \leq \gamma \tag{F.6}$$

holds, then all solutions of the system is uniformly bounded.

Interpretation: The norm is calculated as $\|x\| = \sqrt{x \bullet x} = \sqrt{x_1^2 + \dots + x_n^2}$. For the Lyapunov functions considered in this project $\lambda_1 = \lambda_2 = \frac{1}{2}, p = q = r = 2$ and $\gamma = 0$. Equation (F.4) is therefore satisfied when $V(x) = \frac{1}{2}(x_1^2 + \dots + x_n^2)$, and due to $r = q$ the inequality is satisfied as well. The statement says that if the derivative can be expressed as a negative semi-definite function of the states plus a positive constant L then all the states are bounded. The *semi*-definite part is not obvious from the statement, but is confirmed by the author of the paper [Raffoul, 2012] Youssef N. Raffoul.

At first the theory do not state if the property is also true when the derivative only includes some of the

F.4 LaSalle-Yoshizawa Theorem

The LaSalle-Yoshizawa Theorem is of great importance in backstepping design, as it allows the designer to establish convergence of the system states in cases where the derivative of a Lyapunov function is only negative semi-definite. It is similar to LaSalle's Invariance Theorem F.2, but LaSalle-Yoshizawa Theorem is also applicable to time-varying (non-autonomous) systems.

Another theorem, the "Lyapunov-Like Lemma" presented in [Slotine and Li, 1991, p. 125], and repeated in Section F.5, is also applicable to non-autonomous systems, and it is able to obtain the same result as the LaSalle-Yoshizawa Theorem. However, the two methods are distinct in the way the result is obtained, and a comparison is given in F.5.

In the first subsection the General LaSalle-Yoshizawa theorem is presented, and then a simplified version is given. It is the simplified version that is referenced in the report, but the general theorem is included in order to complete the picture for the reader.

F.4.1 General Theorem

The following theorem is presented and proven in: [Miroslav Krstic and Kokotovic, 1995, p.492].

Let $x = 0$ be an equilibrium point of

$$\dot{x} = f(x, t) \quad (\text{F.7})$$

and suppose f is locally Lipschitz in x uniformly in t .

Let $V : \mathbb{R}^n \times \mathbb{R}_+ \rightarrow \mathbb{R}_+$ be a continuously differentiable function such that

$$\gamma_1(|x|) \leq V(x, t) \leq \gamma_2(|x|) \quad (\text{F.8})$$

$$\dot{V} = \frac{\partial V}{\partial t} + \frac{\partial V}{\partial x} f(x, t) \leq -W(x) \leq 0 \quad (\text{F.9})$$

$\forall t \geq 0, \forall x \in \mathbb{R}^n$, where γ_1 and γ_2 are class \mathcal{K}_∞ functions and W is a continuous function.

Then, all solutions of (F.7) are globally uniformly bounded and satisfy:

$$\lim_{t \rightarrow \infty} W(x(t)) = 0 \quad (\text{F.10})$$

In addition, if $W(x)$ is positive definite, then the equilibrium $x = 0$ is globally uniformly asymptotically stable.

Definition of class \mathcal{K}_∞ A continuous function $\gamma : [0, a) \rightarrow \mathbb{R}_+$ is said to belong to class \mathcal{K} if it is strictly increasing and $\gamma(0) = 0$. It is said to belong to class \mathcal{K}_∞ if $a = \infty$ and $\gamma(r) \rightarrow \infty$ as $r \rightarrow \infty$ [Miroslav Krstic and Kokotovic, 1995, p. 489].

F.4.2 Lyapunov-Like LaSalle-Yoshizawa

The following theorem is presented in: [Miroslav Krstic and Kokotovic, 1995, p.24], and it is a less general version of the LaSalle-Yoshizawa Theorem.

Definition Let $x = 0$ be an equilibrium point of (F.7) and suppose f is locally Lipschitz in x uniformly in t . Let $V : \mathbb{R}^n \rightarrow \mathbb{R}_+$ be a continuously differentiable, positive definite and radially unbounded function

$V(x)$ such that

$$\dot{V} = \frac{\partial V}{\partial x} f(x, t) \leq -W(x) \leq 0, \quad \forall t \geq 0, \forall x \in \mathbb{R}^n, \quad (\text{F.11})$$

where W is a continuous function. Then, all solutions of (F.7) are globally uniformly bounded and satisfy

$$\lim_{t \rightarrow \infty} W(x(t)) = 0 \quad (\text{F.12})$$

In addition, if $W(x)$ is positive definite, then the equilibrium $x=0$ is globally uniformly asymptotically stable (GUAS).

F.4.3 Lipschitz Continuity

The mathematical definition and the remarks is from [Lakkis, 2006, p. 1-3]. The emphasize is on the interpretation and the remarks, the definition is included to complete the description.

Definition Lipschitz-continuity comes in three different flavours.

let $f : \mathbb{R}^m \rightarrow \mathbb{R}^m$.

- a) Given an open set $B \subseteq \mathbb{R}^m$, we say that f is *Lipschitz-continuous on the open subset B* if there exists a constant $\Lambda \in \mathbb{R}_0^+$ (called the *Lipschitz constant* of f on B) such that

$$\|f(x) - f(y)\| \leq \Lambda \|x - y\|, \quad \forall x, y \in B \quad (\text{F.13})$$

- b) The function f is called *locally Lipschitz-continuous*, if for each $z \in \mathbb{R}^n$ there exists an $L > 0$ such that f is Lipschitz-continuous on the open ball of center z and radius L

$$B_L(z) := \{y \in \mathbb{R}^m : \|y - z\| < L\}. \quad (\text{F.14})$$

- c) if f is continuous on all of the space \mathbb{R}^m (i.e. $B = \mathbb{R}^m$ in then f is called *globally Lipschitz-continuous*.

Remarks

- (*Lipschitz* \Rightarrow C^0) Every locally Lipschitz-continuous function is continuous.
- ($C^1 \Rightarrow$ *Lipschitz*) Every continuously differentiable function is locally Lipschitz.

Interpretation

- A continuously differentiable function is always Lipschitz-continuous, but a function can be locally Lipschitz without being differentiable. One such function is $f(x) = |x|$, which is Lipschitz-continuous but not differentiable.
- If a continuous function f has a maximum "slope" $|\Lambda| < \infty$, then f is said to be locally Lipschitz.
- "Lipschitz just means f can't be too steep, the bound on the difference quotient being the Lipschitz constant". [Lakkis, 2006, p. 1]

F.5 "Lyapunov-Like Lemma" (Based on Barbalat's Lemma)

When using Lyapunov stability analysis and the derivative of the Lyapunov function turns out to be only negative semi-definite, then in some cases this theorem can be applied to guarantee asymptotic stability of the equilibrium point, just like the LaSalle-Yoshizawa theorem F.4.2.

Definition The following is presented and proven in [Slotine and Li, 1991, p. 125].

If a scalar function $V(\mathbf{x}, t)$ satisfies the following conditions

- $V(\mathbf{x}, t)$ is lower bounded
- $\dot{V}(\mathbf{x}, t)$ is negative semi-definite
- $\dot{V}(\mathbf{x}, t)$ is uniformly continuous in time $\Leftrightarrow \ddot{V}(\mathbf{x}, t)$ is bounded.

then $\dot{V}(\mathbf{x}, t) \rightarrow 0$ as $t \rightarrow \infty$.

F.5.1 Comparison to LaSalle-Yoshizawa Theorem

The most important difference in the two Lyapunov-Like methods: "Lyapunov-Like Lemma based on Barbalat's Lemma (LB)" and "Lyapunov-Like LaSalle-Yoshizawa theorem (LY)", presented on page 154, is outlined here.

- When using (LB) on a system $\dot{x} = f(x, t)$ one has to prove that the derivative of the Lyapunov function $\dot{V}(x, t)$ is uniformly continuous in time, which is often done by verifying that its derivative $\ddot{V}(x, t)$ is bounded. When using (LY) one have to prove that the system $\dot{x} = f(x, t)$ is locally Lipschitz, and then find a negative semi-definite function $-W(x)$ such that

$$\dot{V} \leq -W(x) \leq 0, \quad \forall t \geq 0, \forall x \in \mathbb{R}^n, \quad (\text{F.15})$$

which means that the derivative of the Lyapunov function $\dot{V}(\mathbf{x}, t)$ has to be less than some time-invariant negative semi-definite function $-W(x)$.

- The result obtained in (LY) is that the *time-invariant* bounding function $W(x) \rightarrow 0$ and not the *time-dependent* $\dot{V}(\mathbf{x}, t) \rightarrow 0$ for $t \rightarrow \infty$.
- In (LB) the function $V(\mathbf{x}, t)$ just has to be lower bounded. This means that in (LB) the function $V(\mathbf{x}, t)$ can be negative, as long as it is lower bounded. In (LY) it has to be both positive definite and radially unbounded meaning that $V(0, t) = 0$, $V(\mathbf{x}, t) > 0$ for $x \neq 0$, and $V(\mathbf{x}, t) \rightarrow \infty$ for $|x| \rightarrow \infty$.

Appendix G

System Forms

Besides the two following classes of nonlinear systems: "*strict-feedback systems*" and "*pure-feedback systems*" the backstepping procedure can also be applied to systems on "*Block-strict-feedback form*" and "*parametric-strict-feedback systems*", but as the system considered in this project do not attend these forms, we do not consider them further. [Miroslav Krstic and Kokotovic, 1995, p. 58]

The difference between a strict-feedback system and a pure-feedback system, is that in the strict-feedback case both the control variable and all the intermediate control variables appear affine/linear in the state equations. Notice that both system forms are *time-invariant* and therefore apply to autonomous systems.

G.1 Strict Feedback Systems

Nonlinear *strict-feedback systems* are of the form

$$\begin{aligned}\dot{\mathbf{x}} &= \mathbf{f}(\mathbf{x}) + \mathbf{g}(\mathbf{x})\xi_1 \\ \dot{\xi}_1 &= f_1(\mathbf{x}, \xi_1) + g_1(\mathbf{x}, \xi_1)\xi_2 \\ \dot{\xi}_2 &= f_2(\mathbf{x}, \xi_1, \xi_2) + g_2(\mathbf{x}, \xi_1, \xi_2)\xi_3 \\ &\vdots \\ \dot{\xi}_{k-1} &= f_{k-1}(\mathbf{x}, \xi_1, \dots, \xi_{k-1}) + g_{k-1}(\mathbf{x}, \xi_1, \dots, \xi_{k-1})\xi_k \\ \dot{\xi}_k &= f_k(\mathbf{x}, \xi_1, \dots, \xi_k) + g_k(\mathbf{x}, \xi_1, \dots, \xi_k)u\end{aligned}\tag{G.1}$$

where $\mathbf{x} \in \mathbb{R}^n$ and $\xi_i, u \in \mathbb{R}$, and \dot{x} satisfy G.3 [Miroslav Krstic and Kokotovic, 1995, p. 58].

G.2 Pure Feedback Systems

A more general class of "triangular" systems comprises *pure-feedback-systems*.

$$\begin{aligned}\dot{\mathbf{x}} &= \mathbf{f}(\mathbf{x}) + \mathbf{g}(\mathbf{x})\xi_1 \\ \dot{\xi}_1 &= f_1(\mathbf{x}, \xi_1, \xi_2) \\ \dot{\xi}_2 &= f_2(\mathbf{x}, \xi_1, \xi_2, \xi_3) \\ &\vdots \\ \dot{\xi}_{k-1} &= f_{k-1}(\mathbf{x}, \xi_1, \dots, \xi_k) \\ \dot{\xi}_k &= f_k(\mathbf{x}, \xi_1, \dots, \xi_k, u)\end{aligned}\tag{G.2}$$

where $\mathbf{x} \in \mathbb{R}^n$ and $\xi_i, u \in \mathbb{R}$, and \dot{x} satisfy G.3. [Miroslav Krstic and Kokotovic, 1995, p. 61].

G.3 Assumption

The following assumption is from [Miroslav Krstic and Kokotovic, 1995, p. 33].

Consider the system

$$\dot{\mathbf{x}} = \mathbf{f}(\mathbf{x}) + \mathbf{g}(\mathbf{x})u, \quad \mathbf{f}(\mathbf{0}) = \mathbf{0} \quad (\text{G.3})$$

where $\mathbf{x} \in \mathbb{R}^n$ is the state and $u \in \mathbb{R}$ is the control input. There exist a continuously differentiable feedback control law

$$u = \alpha(\mathbf{x}), \quad \alpha(\mathbf{0}) = 0, \quad (\text{G.4})$$

and a smooth positive definite, radially unbounded function $V : \mathbb{R}^n \rightarrow \mathbb{R}$ such that

$$\frac{\partial V(\mathbf{x})}{\partial \mathbf{x}} [\mathbf{f}(\mathbf{x}) + \mathbf{g}(\mathbf{x})\alpha(\mathbf{x})] \leq -W(\mathbf{x}) \leq 0, \quad \forall \mathbf{x} \in \mathbb{R}^n, \quad (\text{G.5})$$

where $W : \mathbb{R}^n \rightarrow \mathbb{R}$ is positive semi-definite.

Remarks It is important to notice that:

- The assumption in (G.3) require that $\mathbf{x} = \mathbf{0}$ is an equilibrium point when $u = 0$, and that the control input, u , appear affine/linear in the state-space equation.
- The intermediate control $\alpha(\mathbf{x})$ must equal 0 when $\mathbf{x} = 0$, due to (G.4).

The reason for the assumption Under this assumption, using the intermediate control $\alpha(\mathbf{x})$ on the autonomous system G.3 global boundedness of $\mathbf{x}(t)$ is guaranteed, and according to LaSalle-Yoshizawa theorem F.4.2, the function $W(\mathbf{x}) \rightarrow 0$ for $t \rightarrow \infty$, and according to LaSalle's invariant set theorem F.2, the trajectories of $\mathbf{x}(t)$ converge to the set M defined as

$$M = \{x \in \mathbb{R}^n \mid \dot{V}(x) = 0 \wedge \dot{x} = 0\}. \quad (\text{G.6})$$

which is $M = \mathbf{0}$ if $W(\mathbf{x})$ is positive definite.

Bibliography

- [Alleyne and Hedrick, 1995] Alleyne and Hedrick (1995). Nonlinear adaptive control of active suspensions. *IEEE TRANSACTIONS ON CONTROL SYSTEMS TECHNOLOGY*, vol 3:94–101.
- [Alleyne and Liu, 2000a] Alleyne, A. and Liu, R. (2000a). Nonlinear force/pressure tracking of an electro-hydraulic actuator. *Journal of Dynamic Systems, Measurement and Control*, 122:pp. 232–237.
- [Alleyne and Liu, 2000b] Alleyne, A. and Liu, R. (2000b). A simplified approach to force control for electro-hydraulic systems. *Control Engineering Practice*, 8:1347 – 1356.
- [Andersen and Hansen, 2007] Andersen, T. O. and Hansen, M. R. (2007). *Fluid Power Circuits - System Design and Analysis*. Aalborg Universitet.
- [Bobrow and Lum, 1996] Bobrow and Lum (1996). Adaptive, high bandwidth control of a hydraulic actuator. *Journal of Dynamic Systems, Measurement and Control*.
- [Garagic and Srinivasan, 2004] Garagic and Srinivasan (2004). Application of nonlinear adaptive control techniques to an electrohydraulic velocity servomechanism. *IEEE TRANSACTIONS ON CONTROL SYSTEMS TECHNOLOGY*, 12:303–314.
- [Guan and Pan, 2008] Guan, C. and Pan, S. (2008). Nonlinear adaptive robust control of single-rod electro-hydraulic actuator with unknown nonlinear parameters. *IEEE Transactions on Control Systems Technology*, 16:434–445.
- [Lakkis, 2006] Lakkis, O. (2006). Lipschitz condition and lipschitz continuity. Handout / Internet.
- [Linköping University, 2008] Linköping University (2008). Formula book for hydraulics and pneumatics. Internet.
- [Mark W. Spong, 2005] Mark W. Spong, Seth Hutchinson, M. V. (2005). *Robot Modeling and Control*.
- [Matlab, 2012a] Matlab (2012a). `filtfilt` - zero-phase digital filtering. <http://www.mathworks.se/help/toolbox/signal/ref/filtfilt.html>.
- [Matlab, 2012b] Matlab (2012b). Nelder mead simplex algorithm `fminsearch`. <http://www.mathworks.se/help/techdoc/math/bsotu2d.html#bsgpq6p-11>.
- [Merritt, 1967] Merritt, H. E. (1967). *Hydraulic Control Systems*. John Wiley & Sons, Inc.
- [Miroslav Krstic and Kokotovic, 1995] Miroslav Krstic, I. K. and Kokotovic, P. (1995). *Nonlinear and Adaptive Control Design*. John Wiley & Sons, Inc.
- [Oppenheim and Willsky, 1998] Oppenheim, A. and Willsky, A. (1998). Signals and systems. Prentice-Hall International, Inc.
- [Phillips and Harbor, 2000] Phillips, C. L. and Harbor, R. D. (2000). *Feedback Control Systems*. Tom Robbins, 4th edition.
- [Plummer and Vaughan, 1996] Plummer and Vaughan (1996). Robust adaptive control for hydraulic servosystems.

- [Raffoul, 2012] Raffoul, Y. N. (2012). Boundedness in nonlinear differential equations. <http://academic.udayton.edu/yousseffraffoul/pdf/ExponentialBoundedness.pdf>.
- [Rexroth, 2012a] Rexroth (2012a). D & c system simulator. Not Published.
- [Rexroth, 2006] Rexroth, B. (2006). *Bosch-Rexroth, 4/3-way high response valve, pilot operated, with electrical position feedback and integrated electronics (OBE) specifications*. Bosch Rexroth AG Hydraulics, Zum Eisengießwerk 1 97816 Lohr am Main, Germany, re 29083 edition.
- [Rexroth, 2012b] Rexroth, B. (2012b). The company bosch-rexroth randers.
- [Rydberg, 2008] Rydberg, K.-E. (2008). Hydraulic servo systems - theory and applications.
- [Slotine and Li, 1991] Slotine, J.-J. E. and Li, W. (1991). *Applied nonlinear control*. Prentice-Hall.
- [Way-Con, 2012] Way-Con (2012). Drawwire sx50 1000 mm. <http://www.waycon.biz/drawwiresensor.html>.
- [Yao and Chiu, 1998] Yao and Chiu (1998). Nonlinear adaptive robust control of electro-hydraulic servo systems with discontinuous projections. *IEEE Conf. Decision Control*, pages pp. 2265–2270.
- [Yao and Chiu, 1999] Yao and Chiu (1999). Adaptive robust motion control of single-rod hydraulic actuators: Theory and experiments. *IEEE/ASME Transactions on Mechatronics*, 5:79–91.
- [Zhou and Wen, 2008] Zhou, J. and Wen, C. (2008). *Adaptive Backstepping Control of Uncertain Systems*. Springer.